Project No. NCHRP 12-79 **COPY NO. 1 of 20**

EVALUATION OF ANALYTICAL METHODS FOR CONSTRUCTION ENGINEERING OF CURVED AND SKEWED STEEL GIRDER BRIDGES

TASK 8 REPORT

Prepared for
NCHRP
Transportation Research Board
of
The National Academies

Donald W. White, Georgia Institute of Technology, Atlanta, GA
Andres Sanchez, HDR Engineering, Inc., Pittsburgh, PA
Cagri Ozgur, Paul C. Rizzo Associates, Inc., Pittsburgh, PA
Juan Manuel Jimenez Chong, Paul C. Rizzo Associates, Inc., Pittsburgh, PA

February 29, 2012

ACKNOWLEDGMENT OF SPONSORSHIP

This work was sponsored by one or more of the following as noted:

☑ American Association of State Highway and Transportation Officials, in cooperation with the Federal Highway Administration, and was conducted in the **National Cooperative Highway Research Program,**

☐ Federal Transit Administration and was conducted in the **Transit Cooperative Research Program**,

☐ American Association of State Highway and Transportation Officials, in cooperation with the Federal Motor Carriers Safety Administration, and was conducted in the **Commercial Truck and Bus Safety Synthesis Program,**

☐ Federal Aviation Administration and was conducted in the **Airports Cooperative Research Program,**

which is administered by the Transportation Research Board of the National Academies.

DISCLAIMER

Project No. NCHRP 12-79

EVALUATION OF ANALYTICAL METHODS FOR CONSTRUCTION ENGINEERING OF CURVED AND SKEWED STEEL GIRDER BRIDGES

TASK 8 REPORT

Prepared for
NCHRP
Transportation Research Board
of
The National Academies

Donald W. White, Georgia Institute of Technology, Atlanta, GA
Andres Sanchez, HDR Engineering, Inc., Pittsburgh, PA
Cagri Ozgur, Paul C. Rizzo Associates, Inc., Pittsburgh, PA
Juan Manuel Jimenez Chong, Paul C. Rizzo Associates, Inc., Pittsburgh, PA

February 29, 2012

Table of Contents

List of Figures

List of Tables

Executive Summary

In current practice (2012), the construction of curved and/or skewed steel girder bridges is sometimes hampered by misconceptions regarding the three-dimensional behavior of these structures. The deflections of curved and skewed girder bridges intrinsically involve torsion of the bridge cross-section and of the individual girders. The resulting 3D movements can affect the fit-up of cross-frames or diaphragms during the steel erection. Furthermore, they can influence the control of the deck thickness, the final deck slopes and superelevations, the dead load rotations at bearings, the alignment of units at deck joints, and the matching of stages in phased construction projects. Depending on the severity of the bridge geometric conditions and the specific needs regarding the geometry control, a simple analysis solution may be sufficient to assess these considerations or a more refined analysis may be necessary.

This document provides guidelines for the selection of analytical methods for the design of skewed and/or horizontally curved steel girder bridges for construction. Both steel I- and tub-girder bridges are addressed. Emphasis is placed on the assessment of when simplified 1D or 2D analysis methods are sufficient, and when 3D methods may be more appropriate for assessment of constructability demands and prediction of the constructed geometry of curved and/or skewed structures.

The report first scrutinizes a number of commonly used 1D, 2D and 3D analysis idealizations to provide a detailed understanding of the underlying assumptions and basic limits of applicability of the methods. A number of established extensions of typical 1D and 2D analyses are discussed that allow the engineer to obtain the broadest potential range of information with these methods when they are applicable. Secondly, several key geometry related bridge indices are identified that can be utilized as aids to identify when different simplified approximations may be suspect. These indices are then used as a part of guidelines for the selection of analytical methods.

Interestingly, although vertical deflections and girder major-axis bending stresses may be estimated with reasonable accuracy in a large number of situations, the cross-frame forces and girder flange lateral bending stresses in skewed I-girder bridges are essentially impossible to determine with any confidence using 1D line-girder and conventional 2D-grid analysis methods. The problems lie in general with the lack of any ability to capture transverse load paths using the 1D methods, and the gross errors associated with neglecting the true girder warping torsion stiffness and the cross-frame stiffness characteristics in conventional 2D-grid methods. Modifications to conventional 2D-grid analysis methods are provided, however, which result in reliable predictions over a wide range of I-girder bridges.

This study also addresses the difficult questions of what types of cross-frame detailing are most effective for different bridge geometries, and when should locked-in force effects due to the detailing of cross-frames be considered in the calculation of I-girder bridge responses. Recommended procedures are provided for determining locked-in force effects for cases in which these effects need to be included. In addition, guidelines are provided for the selection of cross-frame detailing methods as a function of the bridge geometry.

Lastly, the report discusses a number of design and construction considerations that can be implemented to alleviate the demands on the methods of structural analysis by improving the bridge behavior, various problematic physical characteristics, details and practices are outlined, and important potential pitfalls associated with 1D, 2D and 3D analysis techniques are highlighted.

1. Introduction

1.1 Problem Statement

Curved and/or skewed steel I- and tub-girder bridges can experience significant 3D deflections and rotations. In general, 3D deflections and rotations must be considered in the design, detailing and construction engineering of these bridge types. The 3D movements can affect the fit up of cross-frames or diaphragms during the steel erection. Furthermore, they can influence the control of the bridge geometry, including the deck thickness, the final deck slopes and superelevations, the dead load rotations at the bearings, the alignment of units at deck joints, and the matching of stages in phased construction projects. Depending on the severity of the bridge geometric conditions and the specific needs regarding the geometry control, a simple analysis solution may be sufficient or a more refined analysis may be necessary.

Longer span bridges tend to be affected more substantially by dead load effects, potentially resulting in more significant stability considerations during construction. In curved and/or skewed structures, these effects are manifested predominantly in the second-order amplification of the deflections and internal stresses. During intermediate erection stages, it is important that the physical component stresses are limited, including any significant second-order effects, such that there is no significant onset of inelastic deformations and no component strength limits are exceeded. Conversely, shorter span bridges tend to be dominated more by live load effects; thus, these bridges tend to be less affected by construction loading conditions.

Longer span bridges generally exhibit larger deflections; hence, the accuracy of the deflection predictions can be more critical. Shorter span bridges have smaller deflections and are thus less apt to experience problems due to the movements of the structure during construction. One of the key instances where the deflections during construction can be a factor is during the placement of the deck. Inaccurate prediction of the system deflections can result in over-run or under-run of the deck thickness, deviations from intended deck slopes and superelevations, local dips in deck elevation that are susceptible to ponding, unintended bearing rotations, misalignment of units at deck joints, and/or mismatched stages in phased construction projects. Since the overall deflections are larger in longer span bridges, the relative deflections that drive the above concerns are also larger. Control of the geometry during the placement of the deck is an essential consideration in the construction of curved and skewed girder bridges, particularly for bridges with longer spans.

Structural engineers currently have a wide array of approximate and refined analysis and design tools at their disposal. It is important that the right tool is selected for a given bridge. In addition, there are a number of specific cross-frame detailing practices typically used to economically control, i.e., to compensate for, the 3D deflections and rotations in curved and skewed I-girder bridges. The application of and the implications of these practices need to be better understood so that they can be applied in the most effective ways.

Bridges with significant span lengths, curvature and skew generally require careful planning of the erection procedures and sequences such that lifting and fit-up of their spatially deformed components and subassemblies is achievable. Longer and/or wider bridges also may require placement of the deck in multiple stages. Setup of the concrete from prior stages, and in some cases during the current stage, can have a significant influence on the final geometry and on the ultimate performance of the deck. Some wide bridges may require construction in multiple longitudinal phases, with the corresponding problems of connecting new steel to a completed structure, and the matching of deck elevations between adjacent phases. On the other hand, shorter bridges with minor curvature and skew often can be built with less attention to the construction engineering. With respect to all the above considerations, it is important that the appropriate level of effort is applied for the task at hand.

1.2 Objectives

This document outlines the key characteristics of various simplified 1D and 2D analysis methods. It provides guidelines for when these methods are sufficient as well as recommendations for when more sophisticated 3D analysis capabilities may be warranted for assessment of the constructability and prediction of the final constructed geometry of curved and/or skewed steel girder bridges. Both I-girder and tub-girder bridges are addressed. These guidelines are based on extensive information collected from prior and current research, input from bridge owner and consultant policies and practices, and fundamental studies of the accuracy of the simplified methods of analysis conducted by NCHRP Project 12-79, "Guidelines for Analytical Methods and Erection Engineering of Curved and Skewed Steel Deck-Girder Bridges." This report focuses on the accuracy of analysis methods commonly used to determine the strength, stability, and constructability of curved and/or skewed steel girder bridges under the action of their self-weight and various loads imposed during construction operations. In addition, a number of improvements are recommended to conventional analysis techniques that are necessary to eliminate several critical flaws identified by the NCHRP Project 12-79 research.

1.3 Organization

This report is subdivided into eleven main chapters. Chapter 2 aims to establish the framework for the discussions in the other chapters by providing an overview of the common structural analysis tools available in current (2012) practice for analysis of curved and/or skewed steel girder bridges. Namely, these are:

1) Line-girder (1D) methods,
2) 2D-grid methods,
3) 2D-frame methods,
4) Plate and eccentric beam methods,
5) Conventional 3D-frame methods,
6) Thin-walled open-section (TWOS) 3D-frame methods, and
7) 3D Finite Element Analysis (FEA) methods.

The essential idealizations and approximations are summarized for each of these methods. In addition, Chapter 2 discusses specific hand calculation equations commonly used with the 1D and 2D methods, second-order amplification estimates for displacements and stresses in cases where stability effects may be important, and analysis of composite action between the bridge deck and the steel structure, including staged deck placement and consideration of early stiffness and strength gains of the concrete. Chapter

2 closes with a discussion of response attributes that generally cannot be captured by 1D and 2D methods. Of course, in cases where these attributes are not an important factor in the response of the structure, these limitations do not significantly impact the accuracy of the analysis. However, clearly if any of these attributes is expected to be an important contributor to particular structural actions, the engineer must utilize an analysis method capable of capturing the contribution when evaluating these actions.

Chapter 3 defines several key indices identified by NCHRP 12-79 as the most useful for characterizing the importance of curvature and skew on the accuracy of analysis methods for steel girder bridges. Subsequently, these indices are employed as aids to identify when simpler methods of analysis are sufficient as well as when more sophisticated methods should be applied. In addition, this chapter comments on the broad range of factors that generally can influence the detailed behavior of these types of structures.

Chapter 4 provides an overview of the NCHRP 12-79 studies leading to the recommendations of this report. The emphasis of this chapter is on the design and development of a large parametric study of curved and skewed I- and tub-girder bridge systems conducted in the NCHRP research.

Chapter 5 summarizes the core results of the parametric studies conducted by NCHRP 12-79. A scoring method is introduced and utilized to quantify the ability of the different methods of analysis for predicting essential responses. Unfortunately, for a number of responses pertaining to I-girder bridges, the accuracy of commonly used (conventional) simplified methods is essentially binary. That is, either a given method works well or its usage is very suspect. The reasons for this behavior are explained in Chapter 6. Chapter 6 also recommends specific improvements to conventional 2D-grid methods for the analysis of I-girder bridges developed in the NCHRP 12-79 research.

Chapter 7 addresses the consideration of locked-in force effects associated with cross-frame detailing methods commonly used to achieve approximately plumb girder webs at targeted stages of I-girder bridge construction. The highly complex bridge behavior associated with these relatively simple cross-frame detailing practices is explained through a series of examples. Specific conditions are shown where the locked-in forces from cross-frame detailing should be considered in the design. In addition, specific analysis procedures for determining the locked-in force effects are presented. It is emphasized that these locked-in forces are beneficial in that they provide a simple and cost-effective means of achieving plumb webs under a given dead load condition. However, in certain cases, these effects need to be considered in determining vertical deflections and setting cambers, and in evaluating the structural resistances. Lastly, Chapter 7 discusses several special cases where a 1D (line-girder) analysis (with proper extensions where needed) tends to produce sufficiently accurate results for all the essential response quantities (including locked-in forces), as well as when an accurate structural analysis without including the locked-in forces potentially can be used to estimate the maximum cross-frame forces and girder flange lateral bending stresses in I-girder bridges.

In many situations, the need for a more sophisticated type of analysis can be reduced or eliminated by intelligent and prudent decisions made during the design and construction engineering. Chapter 8 discusses a number of considerations that can ease the demands on the structural analysis via improved structural behavior.

Chapter 9 discusses specific characteristics, practices and details that can lead to major difficulties in the ability to predict the response of the structure during construction, and therefore should be used very carefully or sparingly if they are used at all. Lastly, Chapter 10 summarizes key pitfalls in 1D, 2D and 3D methods of analysis for construction engineering of curved and/or skewed girder bridges. Chapter 11 summarizes the recommendations of this report in a concise form.

1.4 Scope and Intended Audience of this Report

This report presents the results of the NCHRP 12-79 research on methods of analysis in a summary form for engineers interested in accessing the details of the research behind the subject recommendations. Readers interested in a concise implementation of the NCHRP 12-79 recommendations in a code-type format oriented toward current practice should first view the companion Task 9 report “Recommendations for Construction Plan Details and Level of Construction Analysis.” Readers interested in a concise summary of the improvements to simplified methods of analysis and their application, should first consult the NCHRP 12-79 Final Report.

2. Overview of Methods (Types) of Analysis

2.1 Line-Girder (1D) Analysis

Line-girder analysis is the most basic method used in the engineering of girder bridges. In this method, the bridge girders are analyzed individually, and their interaction with the bracing system is ignored or accounted for only in a coarse fashion. The loads during steel erection are commonly taken as those acting directly on each girder, but various approaches are used for distributing the subsequent dead loads. NHI (2007) suggests that when the width of the deck is constant, the girders are parallel and have approximately the same stiffness, and the number of girders is not less than four, the permanent load of the wet concrete deck may be distributed equally to each of the girders in the cross-section. Article 4.6.2.2.4 of (AASHTO, 2010) indicates that wearing surface and other distributed loads may be assumed uniformly distributed to each girder in the cross-section of curved steel bridges. However, (NHI, 2011) emphasizes that heavier DC_2 line loads such as parapets, barriers, sidewalks or sound walls should not be distributed equally to all the girders. If the overhang widths and/or the concrete barrier loads are large, engineers commonly use the lever rule (AASHTO, 2010) to distribute the overhang and barrier loads to the girders. Alternatively, some state DOTs assign 60 % of the barrier weight to the exterior girders and 40 % to the adjacent interior girders (NHI, 2007). If the lever rule is used, the portion of the dead load assigned to the fascia girders is increased, while the loads on the interior girders are reduced. NHI (2010) points out that estimating the distribution of DC_2 line loads to the individual girders for line girder analysis is particularly difficult in skewed bridges since the loads may only be on one side of the bridge over significant portions of the span. In addition, NHI (2007) indicates equal distribution of distributed loads can be suspect for skews larger than 10 degrees. Considering all these factors, the distributed dead loads were assigned to the girders based on tributary area in the 1D analyses conducted by the NCHRP 12-79 project team. Parapet loads were considered in the design of parametric study bridges in the NCHRP 12-79 research, but these bridge designs were conducted using 2D-grid and Plate-eccentric beam analysis procedures discussed subsequently.

Typically, various other supplementary calculations are added to the basic line-girder estimates to account for important effects not inherently included in the 1D idealization. The next two sections summarize calculations commonly utilized to extend the line-girder method to the analysis and design of horizontally curved I- and tub-girder bridges. Section 2.1.3 then summarizes equations for estimating flange lateral bending stresses in I-girders and in the top flange of tub girders due to eccentric overhang bracket loads on fascia girders, and due to horizontal curvature effects. Section 2.1.4 addresses the estimation of girder layovers, and Section 2.1.5 recommends a procedure for estimating the torques due to skew effects in tub girders when a line-girder analysis is used.

2.1.1 V-Load Method

The V-load method extends the capabilities of a 1D line-girder analysis to address horizontal curvature effects in I-girder bridges. The method was originally developed by Richardson, Gordon, and Associates (presently the Pittsburgh office of HDR Engineering, Inc.) and was published in the *"USS Structural Report, Analysis and Design of Horizontally Curved Steel Bridge Girders"* (USS, 1965). The V-load method has been used for more than four decades in the preliminary and final design of curved I-girder bridges. This section discusses the background of the method to highlight its attributes and applicability for the analysis of I-girder bridges. The derivations are based on the work presented in Grubb (1984) and Poellot (1987).

Consider the simply-supported curved I-girder shown in Figure 2.1a, which is subjected to a major-axis uniform bending moment, M, via forces applied at its ends. The corresponding flange axial forces, T, are approximately equal to M/h, where h is the distance between the flange centroids. A differential element of the top flange with an arc length $ds = R\, d\theta$ is extracted from the girder, where R is the horizontal radius of curvature of the girder. Figure 2.1b shows a free body diagram (FBD) of this flange segment. The longitudinal components of the forces, T_x, cancel each other. However, the radial components

$$T_y = \frac{M}{h}\frac{d\theta}{2} \tag{2.1}$$

are additive. Therefore, a uniformly distributed internal force

$$q = \frac{2T_y}{ds} = \frac{M}{Rh} \tag{2.2}$$

transferred via the web, is necessary to balance these components. Upon multiplying both sides of this equation by the radius R, one can observe that the flange axial force, T, is equal to qR.

(a) Axial forces in the top flange due to uniform moment

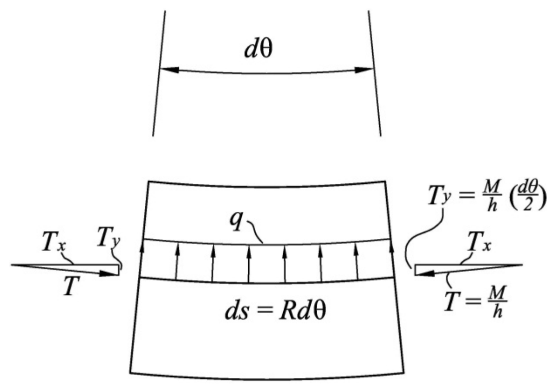

(b) Free body diagram of the flange segment

Figure 2.1. Curved girder subjected to a uniform major-axis bending moment.

The above uniformly distributed force, q, subjects the flanges to lateral bending. Hence, in a two-girder system such as the one depicted in Figure 2.2a, the flanges behave like continuous-span beams in the lateral direction, while the cross-frames act like the continuous-span beam supports. The girders G1 and G2 in this figure are subjected to major-axis bending moments $M_1(x)$ and $M_2(x)$, respectively, where x is the coordinate measured along the arc length of the girders. For equilibrium of the exterior girder at the first intermediate cross-frame in Figure 2.2b the reaction at the level of the cross-frame chords, H_1, must be approximately equal to $q_1 L_{b1} h / h_{CF}$, where h_{CF} is the depth between the centerline of the cross-frame chords and L_{b1} is the distance between cross-frames measured along the centerline of G1 (assumed constant). By substituting $q_1 = M_1/R_1h$, one obtains

$$H_1 = \frac{M_1 L_{b1}}{R_1 h_{CF}} \tag{2.3}$$

where R_1 is taken as the radius of curvature of the girder at location 1. The moment in this equation, M_1, is taken as the value at the cross-frame position, i.e., $M_1 = M_1(L_{b1})$.

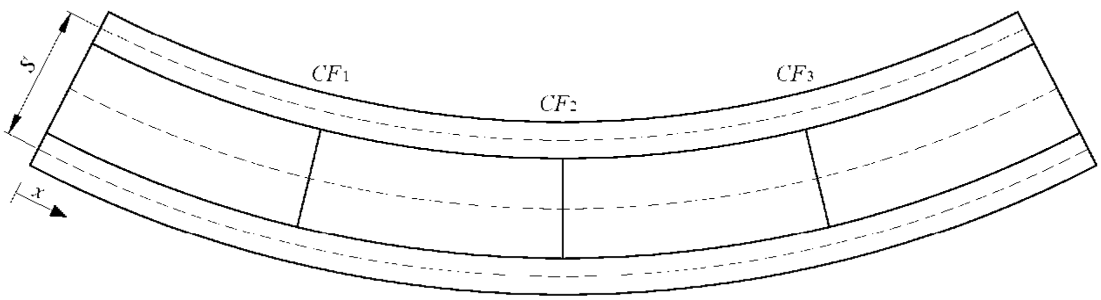

(a) Plan view of the two-girder system

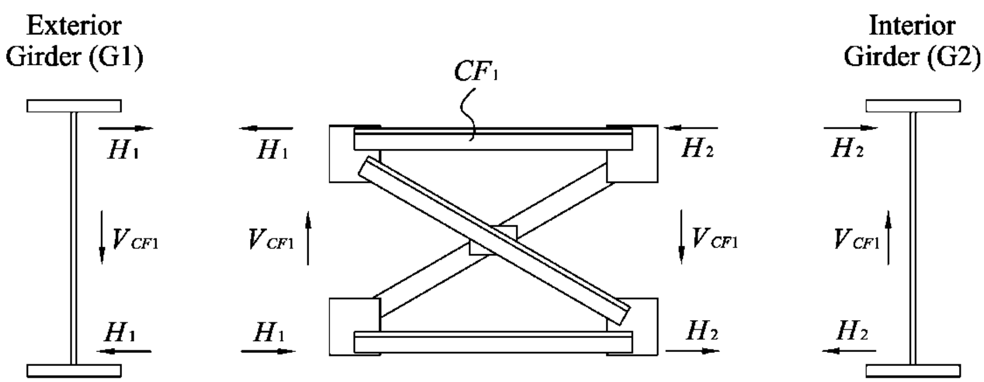

(b) Free body diagram of the first intermediate cross-frame

Figure 2.2. Interaction of forces in a curved girder system.

The reaction at the bottom chord level is the same as H_1, but is in the opposite direction, since the moment causes compression in the top flange and is assumed to cause an equal tension in the bottom flange. Similarly, for the interior girder, G2, the reaction, H_2, may be written as

$$H_2 = q_2 L_{b2} = \frac{M_2 L_{b2}}{R_2 h_{CF}} \tag{2.4}$$

where $M_2 = M_2(L_{b2})$. Note that $L_{b1}/R_1 = L_{b2}/R_2$ may be written as a common value L_b/R, such that $H_1 = M_1 L_b/Rh_{CF}$ and $H_2 = M_2 L_b/Rh_{CF}$.

In the cross-frame shown in Figure 2.2b, moment equilibrium requires that

$$V_{CF\mathbf{1}} = \frac{(H_\mathbf{1} + H_\mathbf{2})h_{CF}}{S} = \frac{M_\mathbf{1} + M_\mathbf{2}}{RS/L_b} \tag{2.5}$$

These vertical forces are a direct effect of the horizontal curvature, and are known as the V-loads. In Eq. 2.5, the subscript $CF1$ is used to emphasize that this is a load at the first intermediate cross-frame position. Similarly, the loads at the other cross-frame positions can be found by substituting the corresponding moments M_1 and M_2, accordingly. In the exterior girder, G1, the additional moments caused by the downward action of the V-loads, M_{1s}, add to the moments produced directly by the gravity loads, M_{1p}. In the interior girder, G2, these loads are in opposite directions, so the resulting moments are subtracted from the gravity load moments. Therefore, the total moment in a particular cross-section of girder G1, M_1, is equal to $M_{1p} + M_{1s}$. Likewise, for the interior girder, $M_2 = M_{2p} + M_{2s}$. Moreover, at any cross-frame position, $M_{1s} \cong -M_{2s} (L_1/L_2)$, where L_1 and L_2 are the arc-span lengths of G1 and G2, respectively. For practical cases, the term (L_1/L_2) is close to one, so $M_{1s} \approx -M_{2s}$. Given this approximation, the sum of the total moments in G1 and G2, $M_1 + M_2$, may be taken as $M_{1p} + M_{2p}$. Substituting this result into Eq. 2.5, one has

$$V_{CF1} = \frac{M_{1p} + M_{2p}}{RS/L_b} \tag{2.6}$$

Given the above approximations, the girders can be analyzed independently using a line-girder analysis. The curved girders are represented with equivalent straight girders of length L_1 and L_2, and they are subjected to the gravity loads plus the V-loads.

The above development can be extended to consider cases with more than two girders. As explained by Poellot (1987), the V-loads in a multi-girder system are the total vertical loads delivered to the girders from the cross-frames (equal to the difference in the cross-frame shear forces on the interior girders). The V-load delivered to the girder farthest from the bridge centerline is calculated as

$$V = \frac{\sum M_p}{CRS/L_b} \tag{2.7}$$

The V-loads delivered to the other girders are assumed to vary linearly between a value of zero for any girder at the bridge centerline to the maximum value predicted by Eq. 2.7 for the girder(s) farthest from the centerline. The constant *C* in this equation depends on the number of girders in the structure. Table 2.1 shows the values of *C* for systems with up to ten girders. These constants are derived based on the above assumption.

Table 2.1. Values of the *C* coefficient.

Girders	Coefficient
2	1
3	1
4	10/9
5	5/4
6	7/5
7	14/9
8	12/7
9	15/8
10	165/81

The V-load idealization basically assumes: (1) approximately equal vertical stiffness of all the girders (defined by a unit load applied at a given cross-frame location, divided by the vertical deflection at that location due to the unit load), and (2) a linear variation in vertical displacements across the bridge cross-section due to overall torsion. In general, the V-load method is reasonably accurate for cases that closely satisfy the above assumptions used in its derivation. However, for bridges with skewed supports, staggered cross-frame patterns, etc., a line-girder analysis based on the V-load method may not be sufficient. For those cases, a 3D FEA model, or 2D-grid model with the recommended improvements discussed in Chapter 6 (which captures the interaction between the structural components more accurately than conventional 2D-grid methods), may be required. These aspects are discussed in the subsequent sections of this report.

2.1.2 M/R Method

The M/R method is a simplified tool for estimating the torsional effects due to curvature in general box girders. This method, which was first introduced by Tung and Fountain (1970), applies an equivalent distributed torsional moment M/R to an individual girder, where M is the major-axis bending moment and R is the radius of curvature. This method assumes that each of the box-girders in the bridge cross-section deforms independently from the other girders for a given span. That is, any interaction between the girders due to their interconnection via the bridge deck and/or intermediate external diaphragms is neglected. The assumptions behind the method are explained by Figure 2.3, which shows a free-body diagram for a box girder differential segment *ds*. The equivalent force at the flange levels, *M/h*, is the same as the force *T* in Figure 2.1.

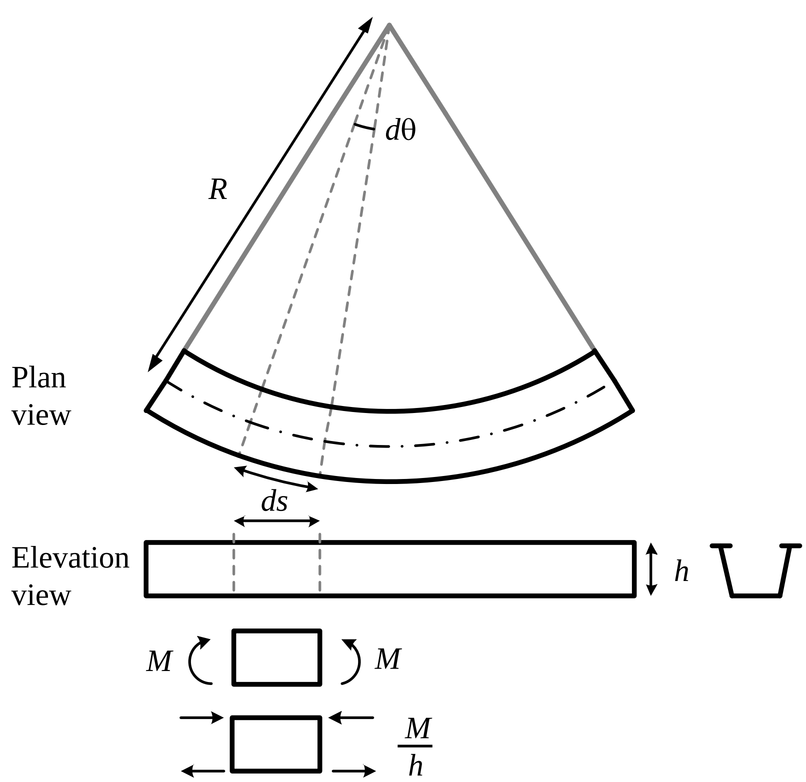

Figure 2.3. Force equilibrium in a segment of a box girder.

As in the V-load method developments explained in Section 2.1.1, the unbalanced flange-level lateral force due to the curvature at the given segment $ds = R\,d\theta$ is obtained as

$$T_y = 2\left(\frac{M}{h}\frac{d\theta}{2}\right) = \frac{M}{h}\frac{ds}{R} \tag{2.8}$$

By dividing both sides of this equation by *ds*, one obtains the equivalent distributed lateral loads at the top and bottom of the section

$$q = \frac{H}{ds} = \frac{M}{h}\frac{ds}{R}\frac{1}{ds} = \frac{M}{Rh} \tag{2.9}$$

These loads produce an equivalent distributed torsional moment *M/R* shown in Figure 2.4, which is identical to the effect of the flange-level distributed lateral load shown in the previous section.

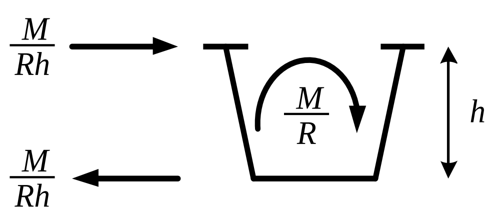

Figure 2.4. M/R torsional moment.

Next, given the specific *M/R* method assumption of no interactions between the girders along the span length, the internal torsional moment at a given position *s* can be found, considering a free body diagram of the girder segment from zero to *s*, and assuming cos(*L*/*R*) = 1.0 (i.e., assuming a small subtended angle over the length *s*), as

$$T(s) = T_{\text{support}} - \int_0^s \frac{M(s)}{R}\,ds \tag{2.10}$$

where $M(s)$ is the distribution of the major-axis bending moment along the length. In addition, the contribution from the span to the end torsional reaction at $s = 0$ may be determined as

$$T_{\text{support}} = \frac{1}{L}\int_0^L \frac{M(s)}{R}(L-s)ds \tag{2.11}$$

by solving the statically indeterminate problem of a span subjected to a distributed torque with twisting fully restrained at each end. The contribution to the torsional reaction at the other end of the span is determined by placing the origin for s at that end.

For a simple span bridge subjected to uniformly distributed vertical load w, the corresponding internal torsional moment from Eq. (2.11) is

$$T(s) = \frac{wL^3}{24R} - \frac{ws^2(3L-2s)}{12R} \tag{2.12}$$

For continuous span bridges, the M/R procedure requires the assumption that the torsion in each span is independent of the other adjacent spans. The above equations are then applied to each span of the bridge. The integration in Eqs. (2.10) and (2.11) is commonly carried out numerically.

2.1.3 Calculation of Flange Lateral Bending Stresses, f_ℓ

Torsion induces girder flange lateral bending stresses, f_ℓ, in the top flanges of tub-girders and in both flanges of I-girders. Several primary sources of girder torsion in I-girder bridges are:

- Eccentric overhang bracket loads
- Horizontal curvature effects
- Support skew effects

In tub-girders, two additional sources of top flange lateral bending are:

- The continuity effects between single-diagonal top flange lateral bracing and the girder top flanges, and
- The lateral component of transverse compression stresses in inclined girder webs.

The AASHTO Specifications require the consideration of these stresses in construction checks. Methods commonly used to estimate the first set of these stresses in design are discussed next. The additional tub-girder stress estimates are addressed subsequently in Section 2.7.

2.1.3.1 Flange Lateral Bending due to Overhang Bracket Loads

The maximum flange lateral bending stress due to overhang bracket loads can be estimated in a given unbraced length of fascia girders as

$$f_\ell = \frac{w_\ell L_b^{\,2} / 12}{S_{yf}} \tag{2.13}$$

where w_ℓ is a lateral uniformly distributed load imposed on the flange by the overhangs, calculated by dividing the moment from the distributed loads on the overhang by the depth of the overhang brackets (see Figure 2.5), L_b is the distance between cross-frames, and S_{yf} is the elastic section modulus of the flange. The above equation is based on the assumption of approximate symmetry boundary conditions for the flange lateral bending at the cross-frame locations. Correspondingly, the term in the numerator is basically the end moment for a fixed-fixed beam. In Eq. (2.13), the value 12 is sometimes changed to 10, to recognize the fact that the flange may not be fully fixed (per symmetry boundary conditions) at the cross-frame locations (the value 12 is used in all the NCHRP 12-79 calculations). In many situations, the highest levels of flange lateral bending stress occur at the cross-frame positions; therefore, the stresses calculated with Eq. 2.13 represent reasonable estimates for design.

When considering concentrated loads on the overhangs (P_ℓ), for example from the wheel loads of a screed rail, one may wish to use the equation

$$f_\ell = \frac{P_\ell L_b / 8}{S_{yf}} \tag{2.14}$$

where $P_\ell = P(e/h)$, and e is the eccentricity of the concentrated load.

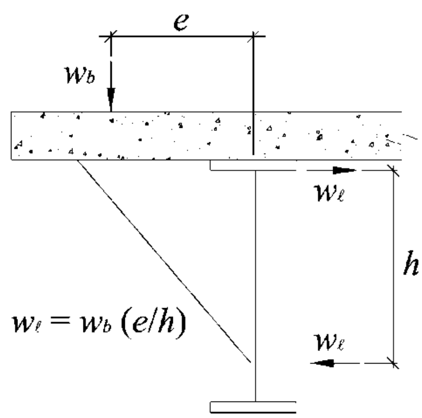

Figure 2.5. Determination of the uniformly distributed load w_ℓ.

It is important generally to ensure that the bracket loads applied to the I-girder web are sufficiently close to the bottom flange such that there is negligible distortion of the web from the reaction at the bottom of the overhang bracket (Ohio DOT, 2008; Roddis et al., 2005). Note that if the bracket cannot be located close to the bottom flange (approximately 6 inches), then it may be necessary to verify that the bracket load will not distort the web, or some type of additional bracing support may be required.

2.1.3.2 Flange Lateral Bending due to Horizontal Curvature

The flange lateral bending stresses due to horizontal curvature can be estimated at the cross-frame locations using the formula

$$f_\ell = \frac{M L_b^{\,2} / 12\,Rh}{S_{yf}} \tag{2.15}$$

This equation is essentially the same form as Eq. 2.13, but with an assumed uniformly distributed lateral load, $q = M/Rh$, derived from the V-load method, and substituted for w_ℓ (see Section 2.1.1). In Eq. 2.15, the moment M typically is taken as the total major-axis bending moment at a particular cross-frame location resulting from the action of the gravity loads and the V-loads, i.e., $M = M_p + M_s$. In the fascia girder on the outside of the curve, the combined effects of the horizontal curvature and the overhang bracket loads are considered simultaneously by adding the results of Eqs. (2.13) and (2.15). Similar to the application of Eq. (2.13), engineers sometimes use a coefficient of 10 rather than 12 in Eq. (2.15), as an attempt to ensure a conservative estimate of the flange lateral bending stress. The coefficient 12 is used in all the NCHRP 12-79 studies,

In Eq. 2.15, the elastic section modulus for a typical rectangular flange, S_{yf}, is equal to $(t_f\, b_f^3/12)/(b_f/2)$, where b_f and t_f are the flange width and thickness, respectively. Since the flange area, A_f, is equal to $b_f\, t_f$, the section modulus can be expressed as $S_y = A_f b_f/6$. In addition, the moment, M, is equal to $f_b\, S_x$, where f_b is the major-axis bending stress and S_x is the strong-axis elastic section modulus to the flange under consideration. Substituting these parameters into Eq. 2.15, the flange lateral bending stress can be expressed as

$$f_\ell = \frac{f_b}{2}\frac{S_x}{A_f h_o}\frac{L_b}{R}\frac{L_b}{b_f} \tag{2.16}$$

This form of the equation for f_ℓ highlights the fundamental factors influencing the flange lateral bending stresses induced by the horizontal curvature (in the context of the above idealizations). Note that if the girder is doubly-symmetric and the contribution of the web to the girder moment of inertia is relatively small, $S_x/(A_f\, h_o) \approx 1$. In this case, the f_ℓ stress is simply equal to one-half of the product of the major-axis bending stress f_b, the sub-tended angle between the cross-frames L_b/R, and the flange length-to-width ratio L_b/b_f.

2.1.3.3 Flange Lateral Bending due to Skew Effects

There is limited guidance in current practice on how to calculate the f_ℓ stresses resulting from skew effects when an I-girder bridge is evaluated using a line-girder or a conventional 2D-grid analysis. In lieu of providing a predictor method, AASHTO LRFD Article C6.10.1 states:

"In the absence of calculated values of f_ℓ from a refined analysis, a suggested estimate for the total f_ℓ in a flange at a cross-frame or diaphragm due to the use of discontinuous cross-frame or diaphragm lines is 10.0 ksi for interior girders and 7.5 ksi for exterior girders. These estimates are based on a limited examination of refined analysis results for bridges with skews approaching 60 degrees from normal and an average D/b_f ratio of approximately 4.0. In regions of the girders with contiguous cross-frames or diaphragms, these values need not be considered. Lateral flange bending in the exterior girders is substantially reduced when cross-frames or diaphragms are placed in discontinuous lines over the entire bridge due to the reduced cross-frame or diaphragm forces. A value of 2.0 ksi is suggested for f_ℓ, for the exterior girders in such cases, with the suggested value of 10 ksi retained for the interior girders. In all cases, it is suggested that the recommended values of f_ℓ be proportioned [apportioned] to dead and live load in the same proportion as the unfactored major-axis dead and live load stresses at the section under consideration. An examination of cross-frame or diaphragm forces is also considered prudent in all bridges with skew angles exceeding 20 degrees."

The above recommendations are intended as coarse estimates of the total *unfactored* stresses associated with the controlling Strength load condition. Hence, for an example location in a straight skewed bridge governed by the STRENGTH I load combination, with discontinuous cross-frames over only a portion of the bridge and with a ratio of dead load stress to total stress (dead plus live load) of 1/3, the nominal total *dead load* flange lateral bending stress in the exterior girders may be taken as 7.5 ksi x 1/3 = 2.5 ksi. If discontinuous cross-frame lines are used throughout the entire bridge, then using this same example dead-to-live load ratio, f_ℓ may be taken equal to 2.0 ksi x 1/3 = 0.7 ksi. In both of these cases, the dead load f_ℓ values may be taken as 10.0/3 = 3.3 ksi on the interior girders.

In the case that a more rational method of determining the flange lateral bending effects is not used (the subsequent Section 6.4 of this report provides a more rational method that can be used as part of an improved 2D-grid analysis), the NCHRP 12-79 research recommends that the value of f_ℓ from the above AASHTO (2010) provisions should be combined additively with the results from Eqs. (2.13) and/or (2.15) to account for the effects of overhang bracket loads and horizontal curvature. However, the variety of geometries and framing conditions in highway bridges is extensive, involving a large range of skew, length, width, number of span, and curvature combinations. Therefore, the above recommendations are very coarse estimates. The subsequent Section 6.4 introduces a 2D-grid approach to more closely predict the f_ℓ stresses caused by skew effects.

2.1.3.4 Local Amplification of Flange Lateral Bending between Cross-Frames

The f_ℓ stress estimates discussed in the above sections are based on a first-order analysis. They do not consider any potential amplification that may occur between cross-frames due to second-order effects. That is, they do not consider equilibrium on the deflected geometry of the structure in the evaluation of the stresses. The corresponding second-order response amplification can be estimated by multiplying the first-order f_ℓ stresses by the amplification factor discussed in Article 6.10.1.6 of the AAHSTO LRFD Specifications,

$$AF = \frac{0.85}{1 - f_b / F_{cr}} \geq 1.0 \tag{2.17}$$

where F_{cr} is the elastic buckling stress for the compression flange, based on lateral-torsional buckling of the unbraced length L_b between the cross-frames, and f_b is the maximum major-axis bending stress in the compression flange within the targeted unbraced length. It should be noted that when Eq. (2.17) gives a value less than 1.0, AF must be taken equal to 1.0; in this case, the second-order amplification of the flange lateral bending is considered negligible.

When determining the amplification of f_ℓ in horizontally curved I-girders, White et al. (2001) indicate that for girders with $L_b/R \geq 0.05$, F_{cr} in Eq. (2.17) may be determined using $KL_b = 0.5L_b$. For girders with L_b/R < 0.05, they recommend using the actual unsupported length L_b in Eq. (2.17). The use of $KL_b = 0.5L_b$ for $L_b/R \geq 0.05$ better approximates the amplification of the bending deformations associated with the approximate symmetry boundary conditions for the flange lateral bending at the cross-frame locations, and assumes that an unwinding stability failure of the compression flange is unlikely for this magnitude of the girder horizontal curvature. Figure 2.6 illustrates the flange lateral deflection mode associated with the horizontal curvature effects as well as the unwinding stability failure mode for a straight elastic member.

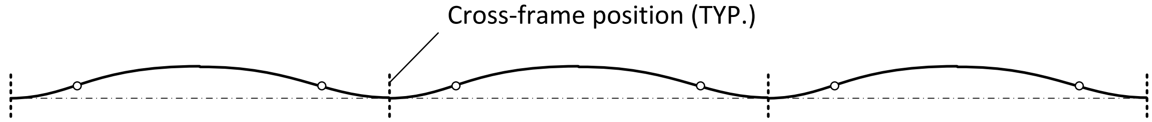

(a) Flange lateral deflection mode associated with horizontal curvature effects

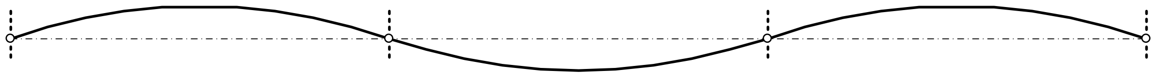

(b) "Unwinding" elastic stability failure mode for straight members

Figure 2.6. Elastic deflection mode of a horizontally curved flange and unwinding stability failure mode of the compression flange in a straight member.

The use of $KL_b = L_b$ for L_b/R < 0.05 guards against the amplification of flange deformation modes that are affine to the simply-supported flange buckling condition (shown in Figure 2.6b) in less highly curved flanges, and guards against a potential unwinding stability failure of the compression flange in these cases.

2.1.4 Estimation of Girder Layovers

The cross-frames at skewed bearing lines tend to rotate about their own skewed axis and warp (twist) out of their plane due to the girder rotations. However, typically the cross-frames are relatively rigid compared to the girders in their own plane. Figure 2.7 shows representative I-girder top flange deflections and rotations at a hypothetical fixed bearing location along a skewed bearing line, where θ is the skew angle (taken as the angle between the normal to the girders at their ends and the tangent to the skewed bearing line, thus θ = 0 for zero skew), ϕ_z is the girder torsional rotation at the skewed bearing line, ϕ_x is the major-axis bending rotation at the skewed bearing line, Δ_z is the longitudinal deflection of the top flange due to the major-axis bending rotation, Δ_x is the girder layover due to the torsional rotation, and *h* may be approximated as the distance between the centroids of the flanges.

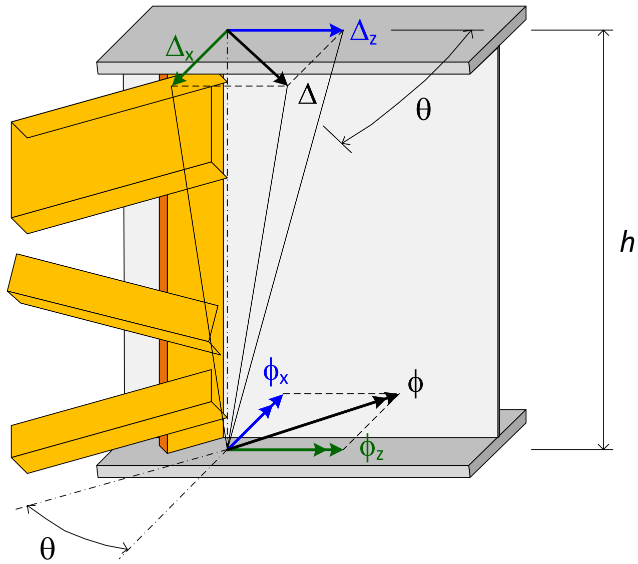

Figure 2.7. Girder top flange deflections and rotations at a fixed bearing location along a skewed bearing line.

The skewed orientation of the cross-frame forces the major-axis bending rotation and the torsional rotation of the girder to be coupled at the bearing, based on the assumption that the in-plane cross-frame deformations are small compared to the displacements. As shown in Ozgur and White (2007), by assuming small rotations such that $\tan(\phi) \cong \sin(\phi) \cong \phi$, the longitudinal deflection of the top flange due to the major-axis bending rotation can be derived from the geometry as

$$\Delta_z = h\phi_x \tag{2.18}$$

where ϕ_x is measured in radians. Also, the layover of the girders at the skewed bearing due to the torsional rotations can be expressed as

$$\Delta_x = h\phi_z \tag{2.19}$$

where ϕ_z is measured in radians. Furthermore, because of the kinematic constraint induced by the in-plane rigidity of the cross-frames, the coupling relationship between the twist and the major-axis bending rotations is

$$\phi_z = \phi_x \tan(\theta) \tag{2.20}$$

Therefore, the layover of the girder at the skewed bearing line (i.e., the lateral displacement of the top flange relative to the bottom flange) is forced to be

$$\Delta_x = h\phi_x \tan(\theta) = \Delta_z \tan(\theta) \qquad (2.21)$$

to maintain compatibility between the girders and cross-frames.

In the case of a non-fixed bearing, Eq. (2.21) still gives the girder layover at the bearing, i.e., the relative lateral displacement of the top and bottom flanges. However, the bottom flange is able to translate based on the degrees of freedom of the bearing.

It is emphasized that properly designed cross-frames often are relatively rigid compared to the girders in I-girder bridges. Taking advantage of this assumption, also the layovers of the girders along the spans may be estimated. Figure 2.8 shows representative girder deflections and rotations for an intermediate cross-frame location where Δ_y is the differential vertical displacement between the girders due to dead loads and *s* is the girder spacing.

The layovers within the span can be estimated from the line-girder analysis vertical displacements, assuming negligible cross-frame in-plane deformations and cross-frames framed normal to the girders, as (Sanchez, 2011)

$$\Delta_x = h \ \Delta_y / s \qquad (2.22)$$

Figure 2.8 illustrates the definitions of the variables in Eq. (2.22).

Although the above kinematics is illustrated in the context of an I-girder bridge in this figure, the above equations also can be applied similarly to tub-girders to estimate the relative lateral displacements between their top and bottom flanges at skewed bearing lines (Eq. 2.21) and at external intermediate diaphragm locations (Eq. 2.22). In addition, these results may be divided by the depth *h* to estimate the girder twist rotations (Eq. 2.20).

The next section takes advantage of these developments to estimate tub-girder torques.

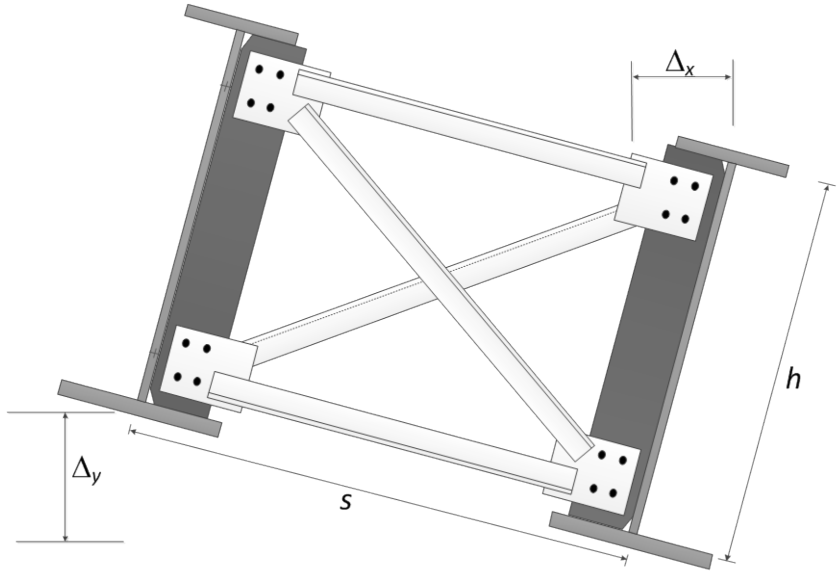

Figure 2.8. Magnified girder deflections and rotations at an intermediate cross-frame location.

2.1.5 Estimation of Tub-Girder Torques due to Skew Effects

The effect of skewed supports on the girder torques in tub-girder bridges can be explained by a few simple mechanistic models. The basic kinematic assumption is the one discussed in the previous section, i.e., the external diaphragms at the supports are effectively rigid in their own plane, while they provide relatively little restraint to the tub girders in their out-of-plane direction. Such assumptions are reasonable approximations since the external diaphragms are usually solid stiffened plates of relatively small length compared to the length of the girders, leading to relatively large in-plane stiffness. Furthermore, the diaphragms are typically I-sections and therefore their torsional stiffness is relatively small compared to that of the tub girders.

As the girders deflect vertically, they rotate about the line between the bearings at the supports. Similarly, the diaphragms, acting approximately as rigid plates in their own plane, rotate about the lines connecting the bearings. When the support line is skewed, the diaphragm thus forces the girders to twist to maintain compatibility (see Figure 2.9).

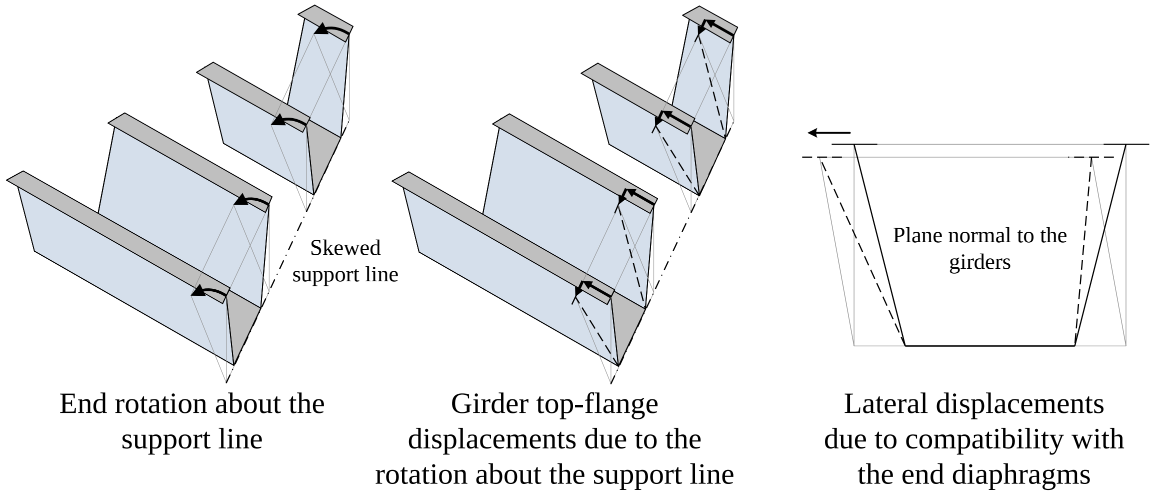

Figure 2.9. Lateral displacements due to rotation about the line of the support in a tub-girder bridge.

The above behavior is essentially the same as that described in Figure 2.7, and its basic overall impact on the tub girders can be understood by modeling a straight bridge composed of two tub girders with end diaphragms and no intermediate internal diaphragms in a 2D-grid analysis. The support diaphragms are modeled effectively as rigid components in their own plane and as highly flexible components out of their plane. Given the rigid in-plane assumption, the diaphragms have two rotation components relative to the axis of the girders, one corresponding to the major-axis bending rotation of the girders and one corresponding to twist rotation of the girders (see Figure 2.10).

When the corresponding model at the opposite end of the girders is considered, it can be observed that the girder ends can twist by equal or different amounts and in the same or opposite direction depending on the relative skew angle of the bearing lines at the girder ends. Figure 2.11 shows two configurations, one with parallel skew and one with an equal but opposite skew angle. Figure 2.11a illustrates the behavior for the parallel skew case. In this situation the girders experience equal twist but in opposite directions at their ends. This produces a constant torque in the girders. Figure 2.11b illustrates the case when the skew angles are equal but opposite in sign. In this special case, the girder ends twist the same amount and in the same direction. This results in a rigid body girder rotation and zero internal torque in the girders. Other skew configurations would result in unequal twist of the ends resulting in a constant torque proportional to the relative angle of twist between the girder ends.

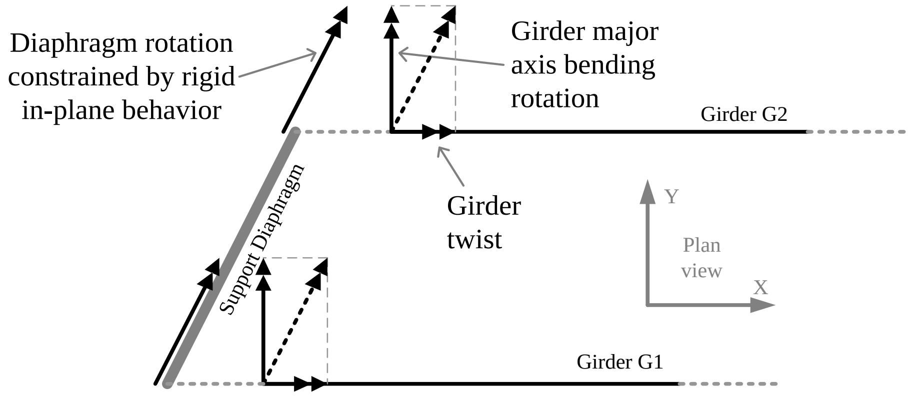

Figure 2.10. Rigid diaphragm rotation mechanism at a skewed support of a tub-girder bridge.

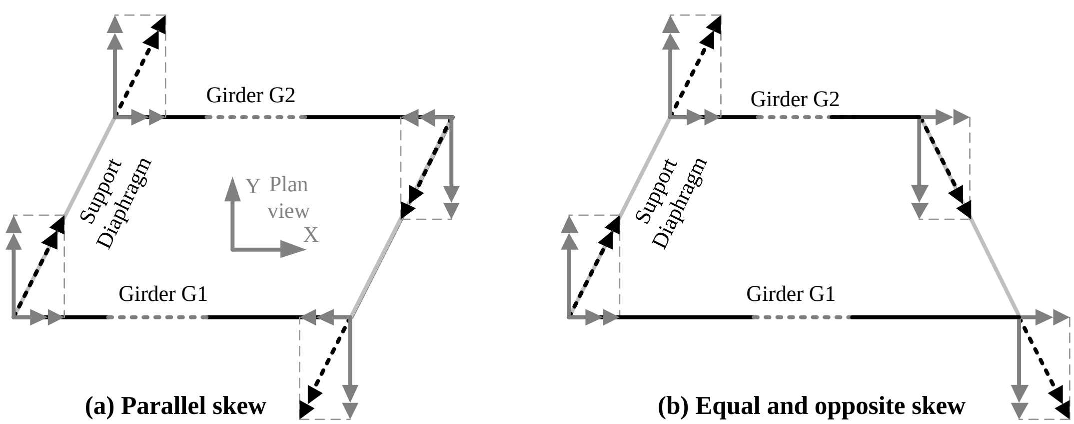

Figure 2.11. Girder end rotations in a tub-girder bridge with parallel skew of the bearing lines and with equal and opposite skew of the bearing lines.

The assumption that the end diaphragms are rigid in their own plane, produces an upper-bound estimate of the relative angle of twist between the girder ends. This can be used with a torsional model of the individual girders, in a line-girder analysis, to obtain an upper-bound estimate of the tub-girder torques due to the skew (Jimenez Chong, 2012).

As an example application, the above procedure is used to estimate the torsional moments in the simple-span curved and skewed tub-girder bridge NTSCS29 studied in NCHRP 12-79 (the bridge name designations are explained in Chapter 4). The bridge is a twin tub-girder system with a span of L = 225 ft. and a skewed support at its left-hand end with θ = 15.7°. The bridge framing plan is shown in Figure 2.12.

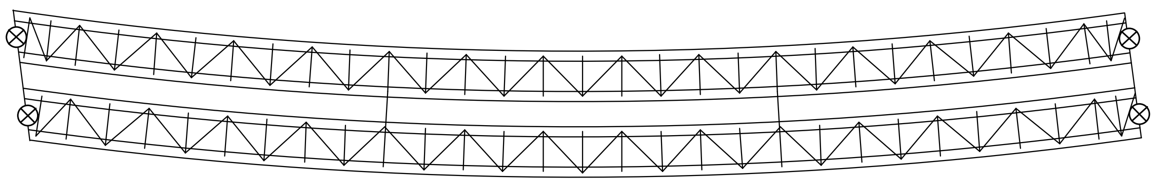

Figure 2.12. Plan view of NTSCS29.

The girder torsional moments are estimated by multiplying the girder torsional stiffness GJ/L by the girder twist rotation at the left-hand bearing line ϕ_z (since the right-hand abutment does not have any skew). The girder end twist rotation can be estimated from the end major-axis bending rotation ϕ_x and the support skew angle θ, using Eq. (2.20). By substituting the simply-supported end major-axis bending rotation, $\phi_x = wL^3/(24EI)$ into Eq. (2.20) and then substituting Eq. (2.20) into the stiffness equation $T = GJ\phi_z/L$, the upper-bound estimate of the torsional moment due to skew is obtained as $T = wL^2GJ \tan\theta /(24EI)$, where w is the vertical distributed load, I and J are the bending and torsional properties of the tub girder and E and G are the material elastic properties. By using the ratio E/G=2.6, the torsional moment in the simple-span single tub-girder is then estimated as

$$T = \frac{wL^2 J}{64.2I} \tan\theta \tag{2.23}$$

Figure 2.13 illustrates the torsional moments in the exterior girder of bridge NTSCS29, obtained from the integration of the 3D FEA stresses on the girder cross-section, as well as the M/R Method estimates with and without the torsional moment T due to the skew. The results from a 3D FEA model without the two intermediate external diaphragms shown in Figure 2.12 are also included in the plot. Jimenez Chong (2012) studies the evaluation of the internal torques in curved and/or skewed tub-girder bridges by the different methods in detail for a relatively wide range of tub-girder bridges.

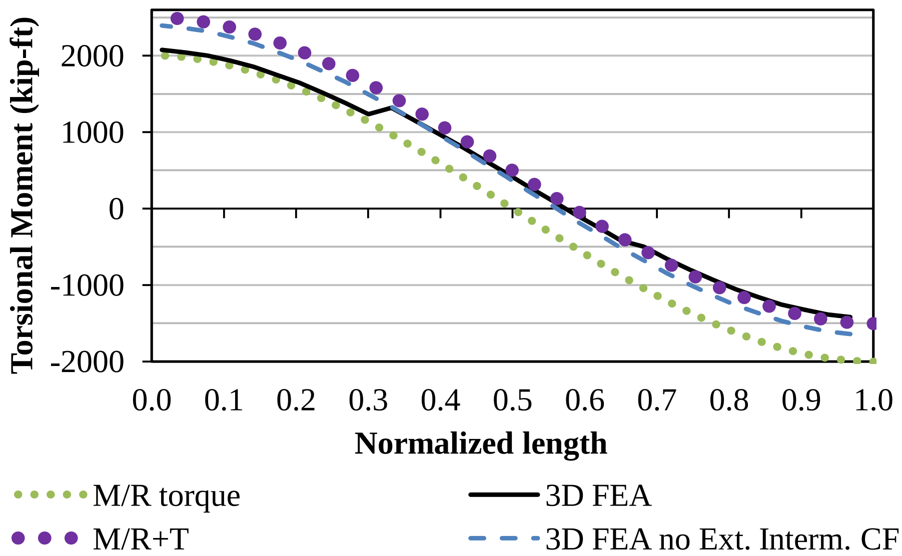

Figure 2.13. Comparison of torsional moments in the exterior girder of Bridge NTSCS29 predicted using refined and approximate analysis methods.

The above bridge has two intermediate external diaphragms as illustrated in Figure 2.12. These diaphragms influence the torsional response due to the shear and moment that they transmit between the girders. The plot in Figure 2.13 shows that the estimated girder torque is very close to the torque from the 3D FEA if the bridge is modeled without any intermediate external diaphragms. In the case with the external intermediate diaphragms, the approximate equations still give a conservative estimate of the maximum girder torque. Furthermore, the maximum errors in the predictions by the simplified calculations are very similar to the estimated additional torque generated by the skew effects. It can be observed that the intermediate external cross-frames assist in activating another source of torque in the overall bridge cross-section, i.e., a torsional couple developed by equal and opposite shear forces in the adjacent girders.

Given the above estimate of the tub girder torques, one must generally consider the moment equilibrium between the tub girder and the support diaphragm as shown in Figure 2.14. If the diaphragm is assumed to have negligible torsional stiffness, the tub girder torque must be balanced by an internal major-axis bending moment in the tub-girder, in addition to the moment restraint provided by the in-plane stiffness of the diaphragm. This in turn influences the overall vertical bending deflections of the tub girder. This additional effect on the vertical bending deflections typically is neglected in the above type of hand estimate and the results at this stage are taken as a coarse line-girder estimate of the tub-girder bridge response.

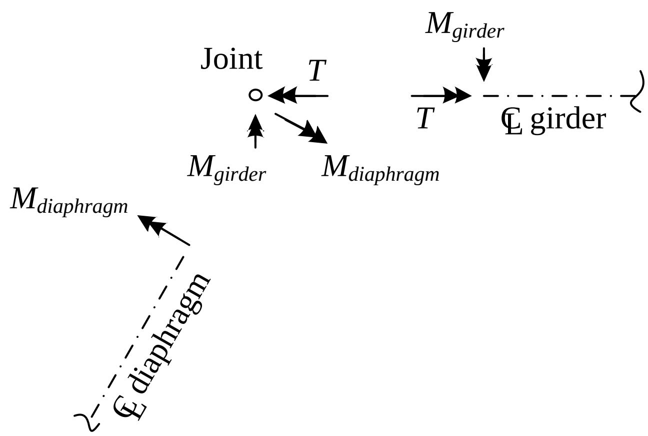

Figure 2.14. Idealization of moment equilibrium at the joint between a tub girder and its support diaphragm.

In bridges that contain intermediate external diaphragms, the behavior is more complex. External intermediate diaphragms typically are provided to control the specific differential displacements between the girders that can affect the transverse bending of the deck and the deck thickness profile (see Figure 2.15). Tub-girder bridges with external intermediate diaphragms generally require a more refined model than a line-girder analysis to properly account for the coupling of the tub-girders by the intermediate diaphragms. However, Helwig et al. suggest an approach that accommodates the use of a line girder analysis. For simplicity, Helwig et al. (2007) recommend the design of tub-girder bridges for their final constructed condition assuming no intermediate external diaphragms or cross-frames. This is followed by the provision of external cross-frames solely to control the profile of the slab thickness during the placement of the concrete deck. They give expressions for sizing the external intermediate cross-frames based on the criterion of controlling the girder differential deflections that influence the deck thickness profile.

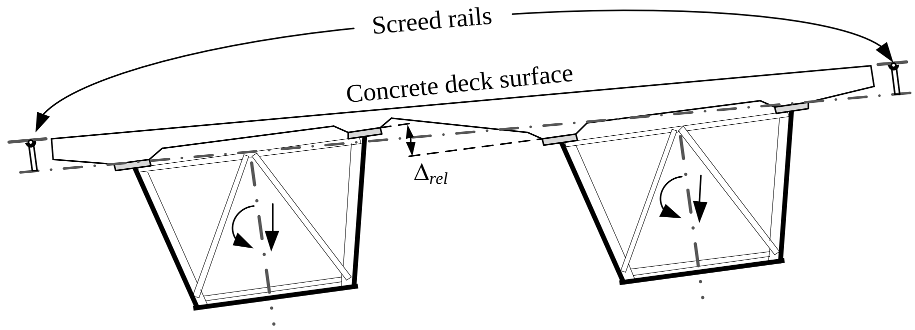

Figure 2.15. Exaggerated deck profile in a tub-girder bridge due to independent deflections of two tub-girders.

2.2 2D-Grid Analysis

The 2D-grid method is an approximate analysis technique commonly used in the design of steel I- and tub-girder bridges. In the most basic and common 2D-grid approach, the girders and cross-frames are modeled as line elements that have three degrees-of-freedom (dofs) per node, two rotational and one translational (see Figure 2.16). The rotational dofs capture the girder major-axis bending and torsional response, and the translational dof corresponds to the vertical displacements. Figure 2.17 shows a perspective view of bridge XICCS7 to illustrate the characteristics of the 2D-grid models (see Chapter 4 for a discussion of the various bridges studied in the NCHRP 12-79 research).

The vertical depth of the superstructure is not considered at all in the 2D-grid models. The girders and their cross-frames or diaphragms are theoretically connected together at a single common elevation, implicitly taken as the centroidal axis of girders (i.e., the axes of all the girders are assumed to bend without any longitudinal or lateral displacement at the connections with the axes of the diaphragms or cross-frames, even if the centroids of the different girders, cross-frames and diaphragms are at different depths). All the bearings and all of the diaphragms and cross-frames theoretically are located at this same elevation in the model. The software calculates only the vertical displacements and the rotations within the plan of the bridge. The popular software packages DESCUS I and II (Best Center, 2011) and MDX (MDX Software, 2011) both utilize these idealizations. In the NCHRP 12-79 research, the MDX as well as the LARSA 4D software (LARSA, 2010) are used for the analysis studies conducted using 2D-grid models. In the remainder of this report, the LARSA and MDX programs are referred to as program P1 and program P2, respectively.

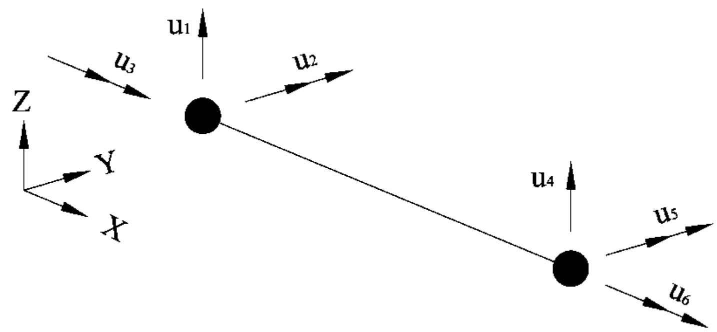

Figure 2.16. Schematic representation of the general two-node element implemented in computer programs for 2D-grid analysis of I-girder bridges.

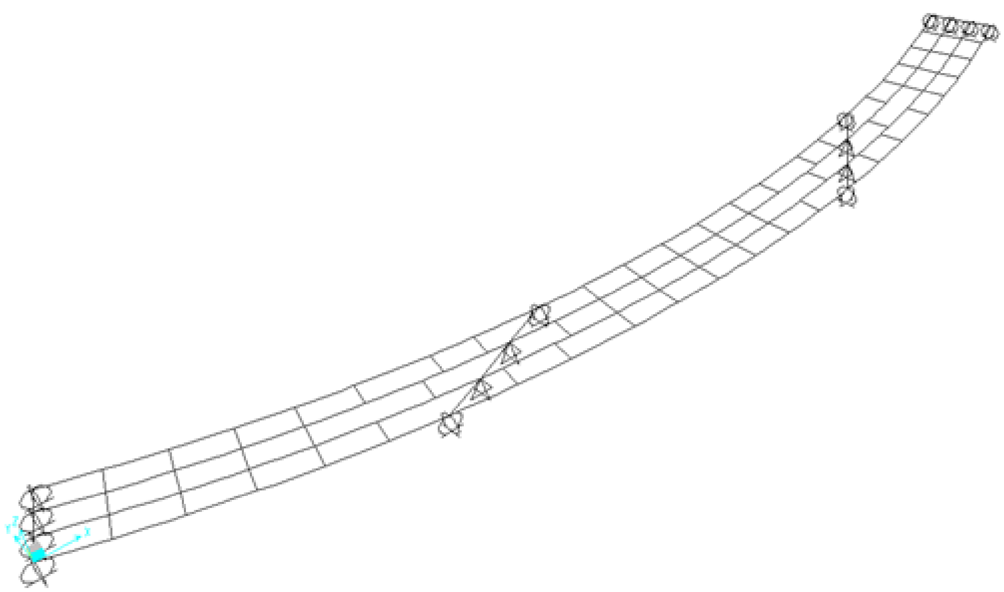

Figure 2.17. 2D-grid model of Bridge XICCS7.

It should be noted that all conventional 2D-grid analyses evaluated in the NCHRP 12-79 research involved the use of the physical girder St. Venant torsion constant, *J*, in setting the torsional properties of the girders, as well as the shear analogy method discussed subsequently in Section 6.2.1 for determining the cross-frame stiffnesses unless noted otherwise.

2.3 2D-Frame Analysis

When using general-purpose software packages, 2D-grid models typically are constructed using beam or frame elements that have six dofs per node. As shown in Figure 2.18, these elements have three translational and three rotational dofs at each node. In this figure, the dofs that are essential to construct a 2D-grid model are u_3, u_4, u_5, u_9, u_{10}, and u_{11}. These implementations are distinguished from the analysis types discussed in Section 2.2 by referring to them as 2D-frame methods.

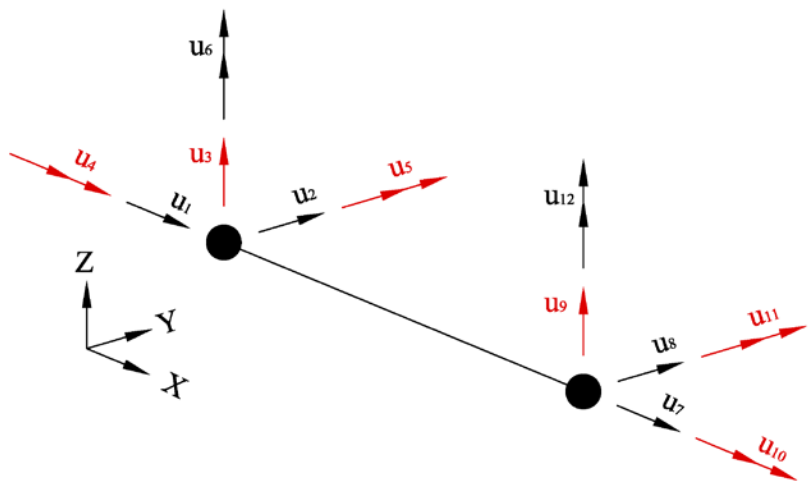

Figure 2.18. Schematic representation of the general two-node element implemented in computer programs for 2D-frame analysis of I-girder bridges.

If the structural model is constructed all in one plane, with no depth information being represented, and if the element formulations do not include any coupling between the conventional 2D-grid dofs and the additional dofs (which is practically always the case), 2D-frame models actually do not provide any additional information beyond the ordinary 2D-grid solutions. Assuming gravity loading normal to the plane of the structure, all the displacements at the three additional nodal dofs will be zero. Therefore, *for purposes of discussion in this report, 2D-frame models are also referred to as 2D-grid*. Nevertheless, the 2D-grid implementation in LARSA 4D discussed in this report is specifically a 2D-frame model.

2.4 Plate and Eccentric Beam Analysis

The MDX Software system implements a second type of model for the analysis of I- and tub-girder bridges that is commonly referred to as a plate and eccentric beam model. In this idealization, the composite bridge deck is modeled using flat shell (or plate) finite elements and the girders are modeled using 6 dof per node frame elements (total of 12 dofs per element, see Figure 2.18) with an offset relative to the slab (see Figure 2.19).

The plate and eccentric beam model is used typically for analysis of composite bridge structures in their final constructed configuration. In the NCHRP 12-79 research, this type of modeling approach was used in the design of various parametric study bridges. Specifically, it was used for the design analysis of the bridges in their final constructed condition. The reader is referred to Chapter 4 for an overview of the various bridges considered in the NCHRP research.

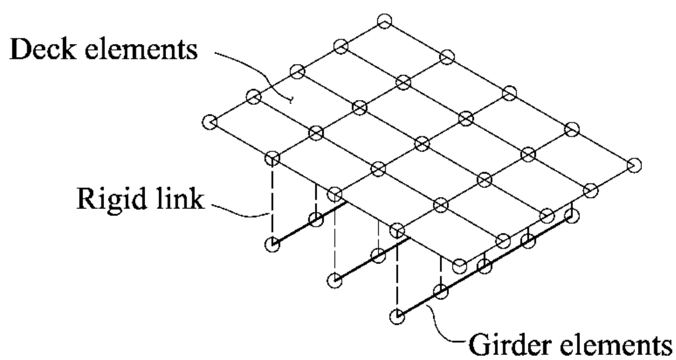

Figure 2.19. Schematic representation of the plate-and-eccentric-beam model.

2.5 Conventional 3D-Frame Analysis

An analysis model may be referred to as a conventional 3D-frame if:

- The structure is modeled using the above 3D frame elements and the centroid and shear center of the girders are modeled at their actual spatial locations,
- The actual location of the cross-frames or diaphragms through the depth is modeled (typically using a single frame element to represent each entire cross-frame or diaphragm between the points of connection to the other components)

- Rigid offsets are used to represent the differences in the depths between the girders, the cross-frames, and the bridge bearings.

It is important to note that this type of model generally provides little to no additional accuracy in representing the bridge responses for I-girder bridges, unless accurate girder torsional stiffnesses and accurate cross-frame generalized stiffnesses are employed. This is because the typical torsional stiffness used by the elements shown in Figure 2.18 is simply GJ/L. However, it is well known that the physical I-girder stiffnesses are dominated by the nonuniform torsion associated with warping of the cross-section (i.e., lateral bending of the flanges). In most situations with I-girder bridges, the St. Venant torsional stiffness GJ/L is so small, compared to the physical torsional stiffness, any results influenced by torsion have essentially no resemblance to the true physical responses if only the St. Venant torsional response is included. Adjustments to rectify this problem are addressed subsequently in Section 6.1 of this report.

For tub-girder bridges, the torsional response of the semi-closed section tends to be captured relatively well by conventional 3D-frame elements. Therefore, the 3D-frame method is reasonably accurate provided that the tub-girder bracing systems are properly designed. However, there are a number of common approximations in 3D-frame models that can potentially lead to some loss of accuracy. These include:

- Conventional 3D-frame elements typically do not account for differences between the shear center axis and the centroidal axis in their formulation, and
- The width and depth of the tub-girder cross-sections are typically very similar to the length and depth of the external cross-frames. However, the 3D-frame model represents all of these elements as lines.

With respect to the second point, the transfer of shear and moment from the external cross-frames or diaphragms to the tub-girders involves internal diaphragms or cross-frames in the cross-section, as shown in Figure 2.20. The detailed force transfer between the external and internal cross-frames, the webs, the top flanges and the bottom flanges involves more degrees of freedom than included in the 3D-frame models. Therefore, some type of simplified idealization is necessary for 3D-frame models to represent the detailed responses in these regions. Furthermore, it should be noted that, if the internal cross-frames or diaphragms at these locations have any significant flexibility within their plane, the resulting deformations cause distortion of the tub-girder cross-section.

In many situations where the width of the structure is relatively small compared to the span lengths, the internal and external cross-frames or diaphragms are likely to be sufficiently stiff relative to the girders such that they perform essentially as rigid components in their plane with respect to the overall response of the bridge.

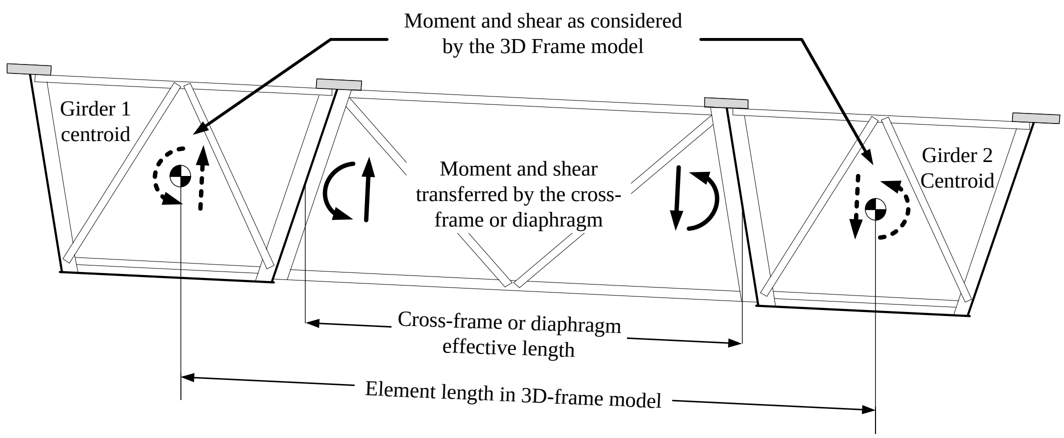

Figure 2.20. Moment and shear force transfer from the external cross-frames or diaphragm to the tub-girders.

2.6 Thin-Walled Open-Section (TWOS) 3D-Frame Analysis

The most accurate frame (i.e., line) element model for I-girder bridges is designated here as a Thin-Walled Open-Section (TWOS) 3D-frame model. This name is used to refer to bridge models constructed with a frame element having seven dofs per node, three translations, three rotations and one warping dof. A schematic representation of a line element having these characteristics is shown in Figure 2.21. The warping degrees of freedom are numbered 7 and 14 in the sketch. This type of element can be utilized to provide a highly accurate characterization of bridge I-girder torsional responses. Typically, this type of element has been used along with comprehensive modeling of the depth information throughout the structure, i.e., representation of the girder shear center and centroidal axes, modeling of the cross-frames, and representation of bearings all at their corresponding depths (Chang, 2006; Huang, 1996). Selected studies have been conducted in the NCHRP 12-79 research using this type of element as implemented by Chang (2006) in the program GT-Sabre. GT-Sabre not only includes a refined open-section thin-walled beam theory representation of the I-girders, but it also includes the modeling of all the individual cross-frame components (i.e., the separate modeling of the cross-frame chords and diagonals using individual frame elements). In GT-Sabre, the individual elements representing the cross-frame members are tied to the girder nodes by rigid offsets.

The TWOS 3D-frame modeling approach is capable of matching the results of 3D FEA quite closely, with the exception that it is not able to capture the influence of I-girder web distortion on the physical responses. Web distortion can be an important factor when modeling composite I-girder torsional responses (Chang, 2006; Chang and White, 2008), but otherwise, its effect is typically inconsequential. In basic terms, if a TWOS element is tied to a slab via a rigid link, similar to the plate and eccentric beam modeling approach, the slab will incorrectly restrain the lateral bending of the bottom flange unless special modeling procedures, such as those discussed by Chang (2006), are invoked.

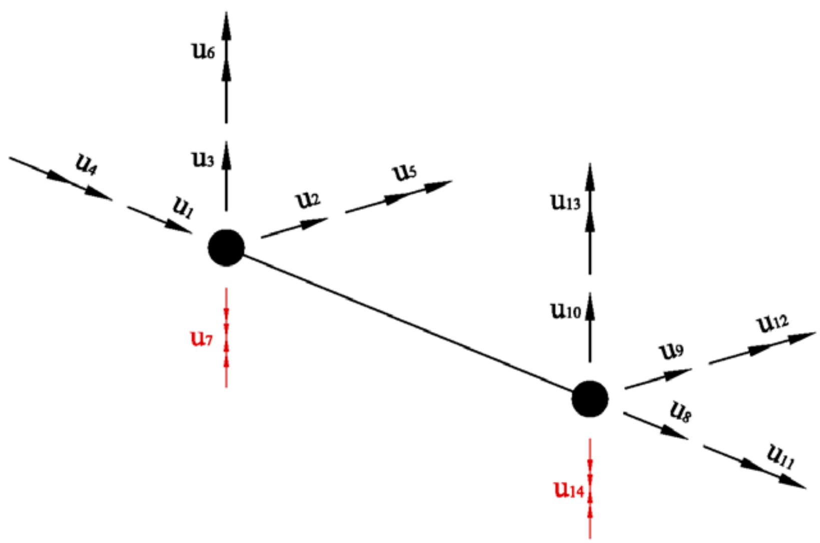

Figure 2.21. Schematic representation of a general two-node 3D TWOS frame element implemented in computer programs of I-girder bridges.

As discussed by Chang (2006), there are a number of other complexities that are difficult to handle in the implementation of 3D TWOS frame elements. These include the modeling of continuity conditions at cross-section transitions (e.g., changes in flange thickness and/or width), and the modeling of the continuity conditions for bifurcated girders (three girder elements framing into a common node). In addition, GT-Sabre (Chang, 2006) is the only known software that correctly displays the detailed three-dimensional deformed geometry from a TWOS 3D-frame analysis. Most TWOS 3D-frame elements have been implemented only in a structural engineering research setting, and either do not include any capability for graphical display of the deflected geometry at all, or display the deformed geometry only as the deformed centroidal axis of the member. Although advanced simulation software systems such as ABAQUS (Simulia, 2010), typically can graphically render the 3D I-section geometry, they do not graphically display the detailed warping deformations of 3D TWOS frame elements when they render the displaced geometry of the structure. As a result of the above complexities, as well as the fact that with increasing computer speeds, large degree of freedom 3D FEA computations can be conducted in a small amount of time, 3D FEA generally is preferred over TWOS 3D-frame analysis for design of steel girder bridges when line-girder or 2D-grid methods do not suffice.

2.7 Calculation of Component Forces Given the Line-Girder or 2D-Grid Analysis Results for Tub-Girder Bridges

Due to the idealization of the tub-girders, cross-frames and diaphragms as “line” elements in the above line-girder, 2D-grid, or 3D-frame approaches, the analysis of tub-girder bridges by any of these methods requires additional calculations to estimate the forces in the bracing components, as well as the stresses in the tub-girders. The bracing components include the top horizontal truss, also known as the top flange lateral bracing (TFLB) system, and the different components of the internal and external cross-frames and diaphragms at intermediate locations and at the supports.

To ensure good accuracy in the evaluation of the component forces in curved and skewed tub-girder bridges, the overall analysis must accurately capture the effects of curvature and skew. In general, conventional line-girder analysis calculations do not include skewed support effects. However, they include a separate torsional analysis of the individual girders, via the M/R method discussed previously in Section 2.1.2, to account for the influence of horizontal curvature on the girder torques. As shown in Section 2.1.5, reasonable 1D analysis approximations can be obtained for the influence of the skew on the girder torques, particularly when there are no intermediate external diaphragms and the tub girders deflect independently of one another within each span length. 2D-grid methods directly include the effect of the curvature and skew, as well as the influence of intermediate external cross-frames or diaphragms, provided that the external intermediate and support diaphragms and cross-frames are accurately represented in the model.

Estimates of the vertical displacements can be obtained directly from 1D line-girder, 2D-grid and 3D-frame analyses. However, to obtain the girder stresses and the forces in the bracing components, additional calculations are needed.

The TFLB system in tub-girders creates a quasi-closed box section which significantly increases the girder torsional stiffness and strength. To estimate this behavior in a simplified way, Kollbrunner (1966) developed the Equivalent Plate Method (EPM) in which the top truss is replaced by an equivalent plate of a given thickness depending on the top truss characteristics. EPM expressions exist for Warren, Pratt and X-type top truss configurations (Helwig et al., 2007).

In the NCHRP 12-79 studies, the tub-girder top flange lateral bending response as well as all the bracing element forces are calculated using component force equations summarized in (Helwig et al., 2007), supplemented by a small number of additional calculations recommended by (Jimenez Chong, 2012). In broad conceptual terms, these equations address the following:

- The girder top flange major-axis bending stresses are calculated from two contributions: (1) the "average" major-axis bending stress, $f_b = M/S_{x,top},$ where $S_{x,top}$ is the elastic section modules of the girder calculated neglecting any contribution from the TFLB system, plus (2) a "saw-tooth" stress effect due to the local effects of the longitudinal forces transferred to the top flanges from the TFLB system (Jimenez Chong, 2012).

- The TFLB diagonal forces, D_{tot}, are determined from the girder torques and the girder major-axis bending moments as the sum of two contributions, D_{EPM} and D_{Bend}. The contribution D_{EPM} is obtained from a girder pseudo closed-section torsional analysis, and the contribution D_{Bend} is obtained by considering the axial deformations of the girder top flanges due to flexure and the continuity of the TFLB struts and diagonals with the top flanges.
- The TFLB transverse strut force S_{tot} is obtained from two contributions: (1) the force S_{Bend} required to equilibrate the lateral component of the diagonal forces at the joints of the TFLB system, and (2) the force S_{Lat} caused by the lateral component of the transverse normal forces in the sloping webs required to resist the distributed vertical loads applied to the top flanges of the tub girder.
- The lateral bending stresses in the tub-girder top flanges, $f_{\ell\ Tot}$, are calculated generally from three effects: (1) the effect of the lateral forces S_{Bend} coming from the TFLB struts, $f_{\ell\ Bend}$ (this effect is zero for X-type TFLB systems, but is non-zero due to the “back-and-forth” loading effects on the flanges from the deformations of the top flange truss in Warren-type TFLB systems), (2) the effect of the lateral component of the transverse normal forces in the tub-girder sloping webs required to resist the distributed vertical loads applied to the girder top flanges, $f_{\ell p}$, and (3) the influence of the horizontal curvature of the top flanges $f_{\ell M/Rh}$ from Eq. (2.15). In addition, the influence of overhang bracket loads per Eqs. (2.13) and (2.14) is included on the outside flanges of fascia girders.
- The forces in the internal cross-frame diagonals D and the forces in the internal cross-frame top chords S are obtained from tub-girder cross-section distortional force equations developed by (Fan and Helwig, 2002). These forces depend upon the spacing between the internal cross-frames measured along the girder length, s_K, and they are driven by the effects from the equivalent distributed torque M/R associated with the horizontal curvature as well as an eccentricity effect of the vertical loads w, which are assumed to be applied to the top flanges.
- The forces in the intermediate external cross-frame diagonals F_D, the top chord, F_T, and the bottom chord, F_B, are determined based on the spacing between the

external cross-frames along the length of the bridge, as well as the exterior and interior girder rotations and vertical displacements at the external cross-frame locations, obtained from an analysis neglecting the intermediate external cross-frames. These equations were developed by Li (2004) specifically to control the relative deformations shown in Figure 2.15 for two-girder systems.

Jimenez Chong (2012) provides a detailed overview of the background and development of the various component force equations. The following sections document all the specific component force calculations utilized in the NCHRP 12-79 studies. Section 2.7.8 provides a definition of all the variables used in the equations.

2.7.1 Input

2.7.1.1 Major-Axis Bending Moment, M

The girder major-axis bending moment distribution is directly obtained from a 1D or 2D analysis.

2.7.1.2 Torque, T

The girder torsional moment is directly obtained from a 2D-grid analysis. With a 1D line-girder analysis, the torsional moment distribution is calculated independently for each girder and each span as follows. At a location *s*, the torsional moment due to curvature is given by:

$$T_{C0} = \frac{1}{L}\int_0^L \frac{M(s)}{R}(L-s)\,ds \tag{2.24}$$

$$T_C(s) = T_{C0} - \int_0^s \frac{M(s)}{R}\,ds \tag{2.25}$$

Concentrated torques are applied to the girders from the skewed supports. The girder internal torque from the skew in each span is obtained by determining a twist rotation at each end of the span (ends 1 and 2) and then multiplying the total relative twist between the two ends by the St. Venant torsional stiffness GJ/L. The resulting constant torque in a given span due to skewed supports is given by:

$$T_S = -\frac{GJ}{L}(\phi_{y1} \tan\theta_1 + \phi_{y2} \tan\theta_2) \tag{2.26}$$

The total torque is equal to the sum of the torque due to curvature and due to skew:

$$T(s) = T_C(s) + T_S \tag{2.27}$$

2.7.1.3 Average Major-Axis Bending Stress

The top flange "average" major-axis bending stress is calculated as

$$f_b = \frac{M}{S_{x,top}} \tag{2.28}$$

where $S_{x,top}$ does not include any contribution from the TFLB system.

2.7.1.4 Vertical Displacements, Δ

The vertical displacements are directly obtained from the 1D or 2D analysis.

2.7.1.5 Girder Twist Rotations, ϕ

The girder twist rotations for 2D analysis are directly obtained from the analysis. For 1D analysis the twist rotations are estimated as follows. At a location *s*, the twist rotation due to curvature is given by:

$$\phi_{x,C}(s) = \frac{1}{R}\left(1 + \frac{EI}{GJ}\right)\Delta(s) \tag{2.29}$$

The twist rotation due to skew is calculated at each support by the equation

$$\phi_{xi} = -\phi_{yi} \tan(\theta_i) \tag{2.30}$$

and the distribution along the span length is assumed to vary linearly as

$$\phi_{x,S}(s) = \phi_{x1} - (\phi_{x1} - \phi_{x2})\frac{s}{L} \tag{2.31}$$

The total girder twist rotations are equal to the sum of those due to curvature and those due to skew:

$$\phi_x(s) = \phi_{x,C}(s) + \phi_{x,S}(s) \tag{2.32}$$

2.7.2 Equivalent Plate Method

The Equivalent Plate Method allows the estimation of the girder torsional constant as

$$J = \frac{4A_0^2}{\sum_i b_i/t_i} \tag{2.33}$$

The top truss contribution to the system torsional behavior is estimated by replacing the truss by a fictitious equivalent plate. The equivalent plate thickness t^* can be determined for different truss layouts and cross-sectional areas of the diagonals and struts.

2.7.3 Warren TFLB Systems

The following sketch illustrates the general layout of a Warren TFLB System.

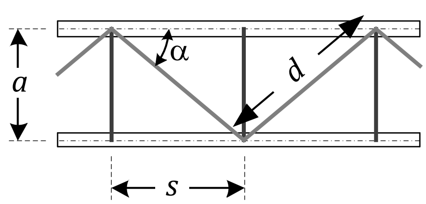

Figure 2.22. Warren TFLB system.

2.7.3.1 Equivalent Plate Thickness

The equivalent plate thickness for a Warren TFLB system is calculated using

$$t^* = \frac{E}{G} \frac{sa}{\left[\frac{d^3}{A_d} + \frac{2s^3}{3A_f} \right]} \tag{2.34}$$

2.7.3.2 TFLB Diagonal Forces

The separate contributions to the TFLB diagonal forces in a Warren TFLB system are determined as follows.

Torsion contribution

$$q = \frac{T}{2A_0} \tag{2.35}$$

$$D_{Torsion} = \frac{qa}{\sin\alpha} \tag{2.36}$$

Bending contribution

$$K_1 = \frac{d}{A_d} + \frac{a}{A_s}\sin^2\alpha + \frac{s^2}{2b_f^2 t_f}\sin^2\alpha \tag{2.37}$$

$$D_{Bend} = \frac{f_b s\cos\alpha}{K_1} \tag{2.38}$$

Other contributions

The lateral components of the transverse forces in the inclined girder webs are assumed to be developed entirely by the TFLB struts.

The influence of distortion on the TFLB diagonal forces is assumed to be negligible.

Total TFLB diagonal forces

$$D_{Tot} = D_{Torsion} + D_{Bend} \tag{2.39}$$

2.7.3.3 TFLB Strut Forces

The transverse strut forces in a Warren TFLB system are determined using the following equations.

Torsion contribution

$$S_{Torsion} = D_{Tot,i}\sin\alpha_i + D_{Tot,j}\sin\alpha_j \tag{2.40}$$

This is typically neglected, and is not considered in the base calculations employed in the NCHRP 12-79 research.

Bending contribution

$$S_{Bend} = -D_{Bend}\sin\alpha \tag{2.41}$$

Transverse load contribution

$$p = \frac{w}{2} \tan \phi \tag{2.42}$$

$$S_{Lat} = ps \tag{2.43}$$

Girder distortional contribution

$$S_{Dist} = \pm \frac{s_K b}{4A_0} \left(\frac{b}{a} ew - \frac{M}{R} \right) \tag{2.44}$$

S_{Dist} affects only the struts that also serve as internal cross-frame top chords.

The only significant girder distortions are assumed to be due to eccentricity of the vertical load *w*, and due to the horizontal curvature effects.

Other contributions

At external cross-frame locations, significant TFLB strut forces may be developed. These forces should be estimated by basic principles considering the overall force paths and joint equilibrium for the bracing components.

Total TFLB strut forces

$$S_{Tot} = S_{Bend} + S_{Lat} + S_{Torsion} + S_{Dist} \tag{2.45}$$

2.7.3.4 Intermediate Internal Cross-Frame Diagonals

Distortion effects due to eccentric vertical load and due to horizontal curvature are assumed to be the only contributor to the internal cross-frame diagonal forces,

$$D = \pm \frac{s_K L_{DK}}{2A_0} \left(\frac{M}{R} - \frac{b}{a} ew \right) \tag{2.46}$$

2.7.3.5 Top Flange Lateral Bending

The tub-girder top flange lateral bending stresses are determined using the following equations.

Major-axis bending contribution (from interaction with TFLB system)

$$f_{\ell,Bend} = \frac{1.5s}{b_f^2 t_f} S_{Bend} \tag{2.47}$$

Horizontal curvature contribution

$$f_{\ell,M/Rh} = \frac{0.6Ms^2}{Rhb_f^2 t_f} \tag{2.48}$$

Transverse load contribution

$$f_{\ell,p} = \frac{0.6ps^2}{b_f^2 t_f} \tag{2.49}$$

Total top flange lateral bending stresses

$$f_{\ell,Tot} = f_{\ell,p} + f_{\ell,M/Rh} + f_{\ell,Bend} \tag{2.50}$$

2.7.3.6 Top Flange Major-Axis Bending Stresses

The top flange major-axis bending stresses are determined generally as follows. The longitudinal force transferred to the top flange at the panel points of the Warren TFLB system may be calculated as

$$P = D_{Tot,i} \cos\alpha_i - D_{Tot,j} \cos\alpha_j \tag{2.51}$$

The corresponding "jump" in the flange major-axis bending stress at these locations is taken as

$$f_{b,TFLB} = f_b \pm \frac{P}{2b_f t_f} \tag{2.52}$$

The $P/2b_f t_f$ stress causes a reduction of the axial stress on one side of the top truss panel point and an increase at the other side. Between the panel points the stress is assumed to vary linearly, causing a saw-tooth distribution of the flange major-axis bending stresses along the length of a tub-girder.

It should be noted that the saw-tooth portion of the flange major-axis bending stresses is not included in the error assessment for f_b conducted in the NCHRP 12-79 research. This is because conventional software, such as MDX, does not include this contribution to the major-axis bending stress in its calculations.

2.7.4 X-Type TFLB Systems

The following sketch shows the general configuration of an X-type TFLB system

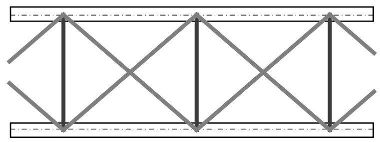

Figure 2.23. X-type TFLB system.

2.7.4.1 Equivalent Plate Thickness

The equivalent plate thickness for an X-type TFLB system is calculated using

$$t^* = \frac{E}{G} \frac{sa}{\left[\dfrac{d^3}{2A_d} + \dfrac{s^3}{6A_f} \right]} \tag{2.53}$$

2.7.4.2 TFLB Diagonal Forces

The separate contributions to the TFLB diagonal forces in an X-type TFLB system are determined as follows.

Torsion contribution

$$q = \frac{T}{2A_0} \tag{2.54}$$

$$D_{Torsion} = \frac{qa}{2\sin\alpha} \tag{2.55}$$

Bending contribution

$$K_2 = \frac{d}{A_d} + \frac{2a}{A_s}\sin^2\alpha \tag{2.56}$$

$$D_{Bend} = \frac{f_b s \cos\alpha}{K_2} \tag{2.57}$$

Other contributions

The lateral components of the transverse forces in the inclined girder webs are assumed to be developed entirely by the TFLB struts.

The influence of distortion on the TFLB diagonal forces is assumed to be negligible.

Total TFLB Diagonal Forces

$$D_{Tot} = D_{Torsion} + D_{Bend} \tag{2.58}$$

2.7.4.3 TFLB Strut Forces

The transverse strut forces in a Warren TFLB system are determined using the following equations.

Torsion contribution

$$S_{Torsion} = D_{Tot,i} \sin \alpha_i + D_{Tot,j} \sin \alpha_j \tag{2.59}$$

This is typically neglected, and is not considered in the base calculations.

Bending contribution

$$S_{Bend} = -2D_{Bend} \sin \alpha \tag{2.60}$$

Transverse load contribution

$$p = \frac{w}{2} \tan \phi \tag{2.61}$$

$$S_{Lat} = ps \tag{2.62}$$

Girder distortional contribution

$$S_{Dist} = \pm \frac{s_K b}{4A_0}\left(\frac{b}{a}ew - \frac{M}{R}\right) \tag{2.63}$$

S_{Dist} is assumed to affect the struts that also serve as internal cross-frame top chords.

The only significant girder distortions are assumed to be due to eccentricity of the vertical load w, and due to the horizontal curvature effects.

Other contributions

At external cross-frame locations, significant TFLB strut forces may be developed. These forces should be estimated by basic principles considering the overall force paths and joint equilibrium for the bracing components.

Total

$$S_{Tot} = S_{Bend} + S_{Lat} + S_{Torsion} + S_{Dist} \tag{2.64}$$

2.7.4.4 Intermediate Internal Cross-Frame Diagonal Forces

Distortion effects due to eccentric vertical load and due to horizontal curvature are assumed to be the only contributor to the internal cross-frame diagonal forces.

$$D = \pm \frac{s_K L_{DK}}{2A_0}\left(\frac{M}{R} - \frac{b}{a}ew\right) \tag{2.65}$$

2.7.4.5 Top Flange Lateral Bending

The tub-girder top flange lateral bending stresses in X-type TFLB systems are determined using the following equations.

Major-axis bending contribution (from interaction with TFLB system)

$$f_{\ell,Bend} = 0 \tag{2.66}$$

Horizontal curvature contribution

$$f_{\ell,M/Rh} = \frac{0.6Ms^2}{Rhb_f^2 t_f} \tag{2.67}$$

Transverse load contribution:

$$f_{\ell,p} = \frac{0.6ps^2}{b_f^2 t_f} \tag{2.68}$$

Total

$$f_{\ell,Tot} = f_{\ell,p} + f_{\ell,M/Rh} + f_{\ell,Bend} \tag{2.69}$$

2.7.4.6 Top Flange Major-Axis Bending Stresses

The top flange major-axis bending stresses are determined generally as follows. The longitudinal force transferred to the top flange at the panel points of the X-type TFLB system may be calculated as

$$P = D_{Tot,i} \cos\alpha_i - D_{Tot,j} \cos\alpha_j \tag{2.70}$$

The corresponding "jump" in the flange major-axis bending stress at these locations is taken as

$$f_{b,TFLB} = f_b \pm \frac{P}{2b_f t_f} \tag{2.71}$$

The $P/2b_f t_f$ stress causes a reduction of the axial stress at one side of the top truss work point and an increase at the other side. Between the work points, the stress is assumed to vary linearly causing a saw-tooth distribution of the flange major-axis bending stresses along the length of a tub-girder.

It should be noted that the saw-tooth portion of the flange major-axis bending stresses is not included in the error assessment for f_b conducted in the NCHRP 12-79 research. This is because conventional software, such as MDX, does not include this contribution to the major-axis bending stress in its calculations.

2.7.5 Pratt TFLB Systems

The following sketch illustrates the general layout of a Pratt TFLB System.

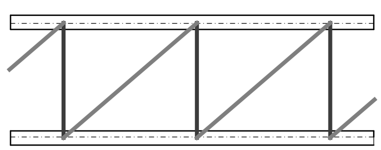

Figure 2.24. Pratt TFLB system.

2.7.5.1 Equivalent Plate Thickness

The equivalent plate thickness for a Pratt TFLB system is calculated using

$$t^* = \frac{E}{G}\frac{sa}{\left[\frac{d^3}{2A_d} + \frac{s^3}{6A_f}\right]} \tag{2.72}$$

2.7.5.2 TFLB Diagonal Forces

The separate contributions to the TFLB diagonal forces in a Pratt TFLB system are determined as follows.

Torsion contribution

$$q = \frac{T}{2A_0} \tag{2.73}$$

$$D_{Torsion} = \frac{qa}{\sin\alpha} \tag{2.74}$$

Bending contribution

$$K_1 = \frac{d}{A_d} + \frac{a}{A_s}\sin^2\alpha + \frac{s^2}{2b_f^2 t_f}\sin^2\alpha \tag{2.75}$$

$$D_{Bend} = \frac{f_b s\cos\alpha}{K_1} \tag{2.76}$$

Other contributions

The lateral components of the transverse forces in the inclined girder webs are assumed to be developed entirely by the TFLB struts.

The influence of distortion on the TFLB diagonal forces is assumed to be negligible.

Total

$$D_{Tot} = D_{Torsion} + D_{Bend} \tag{2.77}$$

2.7.5.3 TFLB Strut Forces

The transverse strut forces in a Pratt TFLB system are determined using the following equations.

Torsion contribution

$$S_{Torsion} = qa \tag{2.78}$$

Bending contribution

$$S_{Bend} = -D_{Bend} \sin \alpha \tag{2.79}$$

Transverse load contribution

$$p = \frac{w}{2} \tan \phi \tag{2.80}$$

$$S_{Lat} = ps \tag{2.81}$$

Girder distortional contribution

$$S_{Dist} = \pm \frac{s_K b}{4A_0} \left(\frac{b}{a} ew - \frac{M}{R} \right) \tag{2.82}$$

S_{Dist} is assumed to affect the struts that also serve as internal cross-frame top chords.

The only significant girder distortions are assumed to be due to eccentricity of the vertical load *w*, and due to the horizontal curvature effects.

Other contributions

At external cross-frame locations, significant TFLB strut forces may be developed. These forces are not considered in the base calculations.

Total

$$S_{Tot} = S_{Bend} + S_{Lat} + S_{Torsion} + S_{Dist} \tag{2.83}$$

2.7.5.4 Intermediate Internal Cross-Frame Diagonals

Distortion effects due to eccentric vertical load and due to horizontal curvature are assumed to be the only contributor to the internal cross-frame diagonal forces.

$$D = \pm \frac{s_K L_{DK}}{2A_0} \left(\frac{M}{R} - \frac{b}{a} ew \right) \tag{2.84}$$

2.7.5.5 Top Flange Lateral Bending

The tub-girder top flange lateral bending stresses in Pratt TFLB systems are determined using the following equations.

Major-axis bending contribution (from interaction with TFLB system):

$$f_{\ell,Bend} = \frac{1.5s}{b_f^2 t_f} S_{Bend} \tag{2.85}$$

Horizontal curvature contribution

$$f_{\ell,M/Rh} = \frac{0.6Ms^2}{Rhb_f^2 t_f} \tag{2.86}$$

Transverse load contribution

$$f_{\ell,p} = \frac{0.6ps^2}{b_f^2 t_f} \tag{2.87}$$

Total

$$f_{\ell,Tot} = f_{\ell,p} + f_{\ell,M/Rh} + f_{\ell,Bend} \tag{2.88}$$

2.7.5.6 Top Flange Major-Axis Bending Stresses

The top flange major-axis bending stresses are determined generally as follows. The longitudinal force transferred to the top flange at the panel points of the X-type TFLB system may be calculated as

$$P_{Pratt} = D_{Tot} \cos\alpha \tag{2.89}$$

$$f_{b,TFLB} = f_b \pm \frac{P_{Pratt}}{2b_f t_f} \tag{2.90}$$

The $P_{Pratt}/2b_f t_f$ stress causes a reduction of the axial stress at one side of the top truss work point and an increase at the other side. Between the work points, the stress is assumed to vary linearly causing a saw-tooth stress distribution of the flange major-axis bending stresses along the length of a tub-girder.

2.7.6 External Intermediate Cross-Frame Forces

The forces in the diagonals of external intermediate cross-frames are calculated using the equation

$$F_D = 4GJ\,\frac{\left(L_i\phi_{w,ext} + L_e\phi_{w,\text{int}} - K_{e1}\Delta_{w,rel}\right)}{K_{e2}} \tag{2.91}$$

whereas the forces in the top and bottom chords are obtained using

$$F_T = \frac{4GJ\left(\phi_{w,ext} - \phi_{w,\text{int}}\right) - F_D L_K\left(L_e - L_i\right)}{h_k\left(L_i + L_e\right)} \tag{2.92}$$

$$F_B = \pm F_D \cos\psi - F_T \tag{2.93}$$

where the variables in these equations are

$$L_K = h_K \cos\psi + L_T \sin\psi \tag{2.94}$$

$$K_{e0} = 1 + \left(1 + \frac{EI}{GJ}\right)\left(1 - \cos\frac{\beta_0}{2}\right) \tag{2.95}$$

$$K_{e1} = \frac{L_i + L_e}{a + c} \tag{2.96}$$

$$K_{e2} = K_{e0}K_{e1}\frac{L_i^3 + L_e^3}{12\left(EI/GJ\right)}\sin\psi + 2L_iL_eL_K \tag{2.97}$$

2.7.7 Support Diaphragms

The following equations from Helwig et al. (2007) are used for as a basic strength and stiffness criterion for the support diaphragms in the NCHRP 12-79 project research.

Strength requirement

$$A_{d,strength} = \frac{T_1 + T_2}{L_d\left(0.58F_y\right)} \tag{2.98}$$

Stiffness requirement

$$x_r = \left(a + b_f\right)/2 \tag{2.99}$$

$$A_{d,stiffness} = \frac{(T_1 + T_2)x_r}{0.0125GL_d} \tag{2.100}$$

2.7.8 Variables Used in the Equations

The definitions of the variables used in the tub-girder bridge component force equations are as follows. Figure 2.25 illustrates several of the key variables.

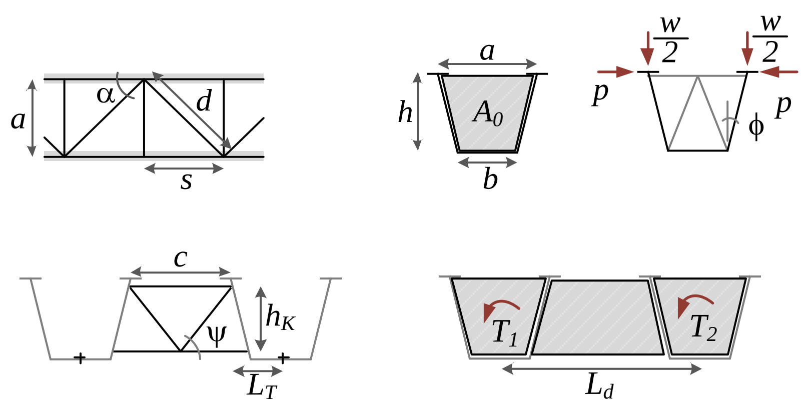

Figure 2.25. Illustration of the displacement, force and stress variables for tub-girder components (two girder systems).

A_0 = area enclosed by box.

$A_{D,stiffness}$ = external end diaphragm cross section area stiffness requirement.

$A_{D,strength}$ = external end diaphragm cross section area strength requirement.

A_d, A_s = cross section area of TFLB diagonal and strut.

D = internal CF diagonal axial force.

$D_{Torsion}, D_{Bend}$ = TFLB diagonals torsional and bending force components.

D_{Tot} = TFLB diagonal axial forces.

$D_{Tot,i}, D_{Tot,j}$ = TFLB diagonal axial forces in two consecutive panels.

E = steel elasticity modulus.

F_D, F_T, F_B = external CF diagonal, top and bottom chord axial forces.

F_y = steel yield strength.

G = steel shear modulus.

I = tub-girder cross-section moment of inertia.

J = St Venant tub-girder torsional constant.

K_1, K_2 = EPM constants for TFLB force calculation.

K_{e0}, K_{e1}, K_{e2} = constants for external intermediate CF force calculation.

L_d = diaphragm length between supports.

L_{DK} = length of internal CF diagonal.

L_i, L_e = internal and external girder CL lengths.

L_K = constant for external intermediate CF force calculation.

L_T = external CF top chord distance to tub centerline.

M = girder bending moment.

R = radius of horizontal curvature of girder.

$S_{Lat}, S_{Bend}, S_{Dist}, S_{Torsion}$ = TFLB struts lateral, bending, distortional and torsion force components.

S_{Tot} = TFLB strut axial forces.

$S_{x,top}$ = top flange section modulus.

T = total girder torsional moment

T_C, T_S = girder torsional moments due to curvature and skew.

T_1, T_2 = girder end torques.

a = box girder top width.

b = bottom flange width.

b_f = top flange width.

c = external CF top chord length.

d = TFLB diagonal length.

e = effective eccentricity of resultant distributed load.

f_b = average top flange major-axis bending stress.

$f_{b,TFLB}$ = top flange major-axis bending stress including the TFLB interaction.

$f_{\ell,Bend}, f_{\ell,p}$ = lateral force and major-axis bending components of lateral bending.

$f_{\ell,M/Rh}$ = influence of the horizontal curvature of the top flanges lateral force to lateral bending.

$f_{\ell,Tot}$ = total top flange lateral bending stress.

h = box girder depth.

h_d = end diaphragm depth.

h_K = external CF chords distance.

p = lateral component of the normal force *w* due the sloping webs.

q = torsion shear flow.

s = TFLB panel length.

s_K = spacing between internal CF measured along the girder length.

t_d = end diaphragm thickness.

t_f = top flange thickness.

x_r = constant for diaphragm force calculation.

w = distributed vertical load per unit length assumed to be applied at the top flange.

α = TFLB diagonal angle.

α_i, α_j = TFLB diagonal angles in two consecutive panels.

β_0 = subtended angle.

$\Delta_{w,rel}$ = relative vertical displacement between girders at external CF location.

$\phi_{w,ext}, \phi_{w,\text{int}}$ = interior and exterior girder twist rotations at CF location.

ϕ = web slope.

ψ = external CF diagonal angle.

2.8 3D Finite Element Analysis (FEA)

2.8.1 3D FEA Procedures for Design Analysis

Generally speaking, any matrix analysis software where the structure is modeled in three dimensions may be referred to as a three-dimensional finite element analysis (3D FEA). This report adopts the more restrictive definition of 3D FEA stated by

AASHTO/NSBA G13.1 (2011). According to G13.1, an analysis method is classified as a 3D FEA if:

1) The superstructure is modeled fully in three dimensions,
2) The individual girder flanges are modeled using beam, shell or solid type elements,
3) The girder webs are modeled using shell or solid type elements,
4) The cross-frames or diaphragms are modeled using truss, beam, shell or solid type elements as appropriate, and
5) The concrete deck is modeled using shell or solid elements (when considering the response of the composite structure).

It is important to recognize that the finite element method generally entails the use of a large number "elements" that are small in dimension compared to the structural dimensions that influence the responses to be evaluated. Furthermore, there are many detailed decisions that either explicitly or implicitly can impact the results, and therefore it is important to recognize that not all 3D FEA models are the same. When creating a 3D FEA model, the engineer (explicitly, or implicitly) selects a theoretical representation for the various parts of the structure (e.g., 3D solid, thick shell, thin shell, Timoshenko beam, Euler-Bernoulli beam, etc.), a mesh density sufficient to ensure convergence of the FEA numerical approximations within an acceptable tolerance, an element formulation type such as a displacement-based, flexibility-based or mixed formulation, an interpolation order for the different element response quantities (e.g., linear or quadratic order interpolation of the element internal displacements), a numerical integration scheme for evaluation of the element nodal forces and stiffnesses (e.g., standard Gauss quadrature, Gauss-Lobatto integration, etc.), and procedures for calculating, extrapolating, and smoothing or averaging of element internal stresses and strains.

The handling of the above attributes, as well as various other important analytical and numerical considerations, is beyond the scope of this document. However, with the exception of the first two of the above considerations, these decisions are more within the realm of finite element software development rather than the domain of engineering design and analysis. The engineer generally should understand the broad aspects of the assumptions and limitations of the 3D FEA procedures, to ensure their proper application. Furthermore, generally he or she should conduct testing and validation studies with the software to ensure that the methods work as intended and that they provide correct answers for relevant benchmark problems.

Different analysis objectives, although they may be applied to the same structure, generally require different finite element models. For example, 3D FEA can be very useful for performing refined local stress analysis of complex structural details. This is not the objective within the context of this report. The recommendations in this report address the calculation of accurate:

- Elastic girder vertical deflections, lateral deflections, and rotations,
- Elastic girder major-axis bending stresses, or the corresponding bending moments, flange lateral bending stresses, web shear forces, and for tub girders, bottom flange shear stresses,
- Elastic cross-frame component axial forces,
- Elastic diaphragm major-axis bending stresses and web shear stresses, or the corresponding bending moments, and web shear forces, and
- Where composite action is considered, elastic slab normal and shear stresses and strains.

Basically, the objective of the 3D FEA models targeted in this report is the accurate calculation of all the bridge responses utilized by the AASHTO LRFD Specifications for the *overall* design of curved and/or skewed steel I- and tub-girder bridge structures.

There are various 3D FEA modeling strategies that can accomplish this objective. The approach recommended by the NCHRP 12-79 research, and utilized by the project team for their three-dimensional elastic finite element design analyses (i.e., 3D FEA analyses conducted for the purpose of design or design checking) entails the use of:

- A general-purpose 4-node quadrilateral Reissner-Mindin (shear-deformable) shell element for modeling I- and tub-girder webs, tub-girder bottom flanges, and the concrete deck slab, as well as a compatible 3-node triangular shell element, used sparingly for modeling of the concrete deck at skewed bearing lines (tub-girder webs and bottom flanges are modeled at skewed bearing lines by "fanning" the geometry of the quadrilateral elements).
- A compatible 2-node shear-deformable beam element for modeling I-girder flanges, tub-girder top flanges, bearing stiffeners, connection plates, intermediate transverse stiffeners, longitudinal stiffeners, and the "lips" of tub-girder bottom flanges extending outside of the webs.
- A 2-node shear-deformable beam element for modeling of cross-frame chords. The cross-frame chords are modeled at their physical location through the depth of the structure. Their connections into the girders are modeled generally using multi-point constraints so that the FEA discretization through the depth of the webs does not have to be adjusted to place nodes at the specific cross-frame chord depths. In effect, this rigidly connects the cross-frame chords at the location where they intersect the mid-thickness of the girder webs without the need for a web node at that location.
- A 2-node truss element for modeling of cross-frame diagonals, and for modeling of flange-level lateral bracing.
- Connector elements, if desired, to model the interconnection between the slab and the steel girders, but otherwise, rigid multi-point constraints (effectively acting as rigid beam elements) between the top flanges of the girders and the mid-thickness of the slab.

Figure 2.26 shows a segment of a three I-girder bridge unit illustrating the finite element representations of the various structural steel components.

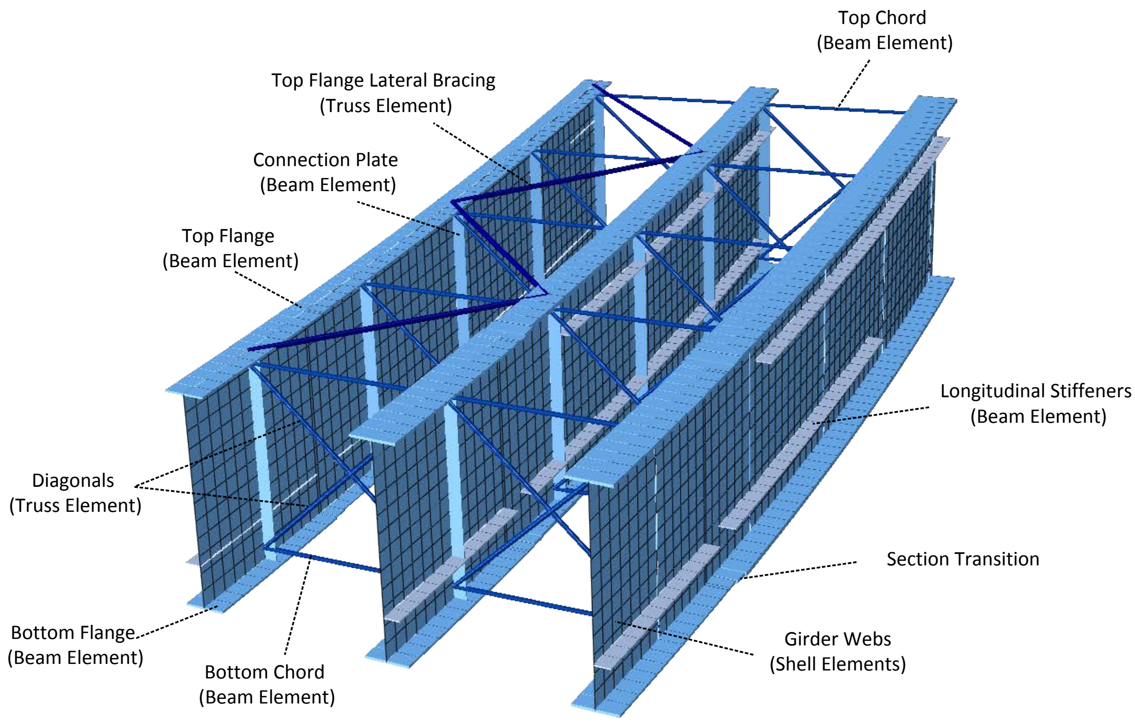

Figure 2.26. Example of recommended 3D FEA modeling approach on a segment of a three-I-girder bridge unit.

All of the bridge components are modeled at their physical geometric locations using the nominal dimensions, with the exception that the girder webs are modeled between the centerlines of the girder flanges. Therefore, the flanges are at the correct physical depth in all cases, and the model of the web has an overlap of t_f /2 with the flange areas. This is comparable to the manner in which joint size often is neglected in the modeling of frame structures; the resulting additional web area is on the order of the steel area from web-flange fillet welds, while the web-flange fillet welds are not explicitly included in the model.

At transitions in girder flange thickness, the centerline of the flange elements shifts with the change in thickness as shown in Figure 2.27. Therefore, the depth of the girder web also shifts with changes in the flange thickness in the FEA model. The average of the two flange areas is used within a one-element transition length along the flange at these locations. The transition element is located on the side of the transition with the larger flange area.

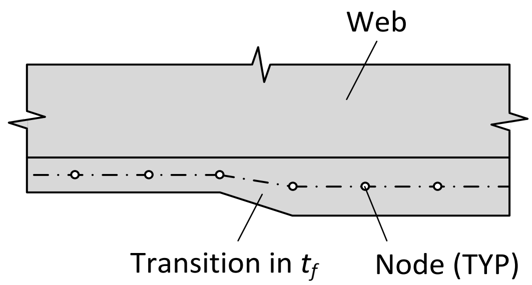

Figure 2.27. FEA Model at a flange thickness transition.

In addition to the above, the recommended 3D FEA modeling approach invokes the following idealizations:

- Similar to the above modeling idealizations, all beam and truss elements representing bracing members are connected directly into the work point locations at the mid-thickness of the girder webs, or in the case of flange-level lateral bracing, at the web-flange juncture.
- In I-girders, the support bearings are modeled as a point vertical support at the web-flange juncture, whereas in tub-girders, they are modeled as a point vertical support at the intersection of the bottom flange and an end diaphragm. At the bearing location, the beam element representations of the flange and of the bearing stiffeners enforce plane sections to remain plane across the width of the flange and distribute the point reaction into the web. In addition, for the tub-girders, a rigid rectangular patch with dimensions equal to those of the sole plate is modeled on the bottom flange. The girder model is generally free to rotate about the point support location, and horizontal displacement constraints representing guided bearings are placed at the point support where applicable.
- The substructure is modeled as a rigid support, including any temporary towers for construction. (This is an idealization in the NCHRP 12-79 research targeted at simplifying the scope of the studies, and is not believed to be a factor affecting the assessment of the accuracy of simplified models of the superstructure.)
- Uplift at bearings is modeled, where desired (or necessary), by using a "one-directional" support.

- The girder cambers are included explicitly for I-girder bridges. Practically speaking, this can be important in some cases where the second-order amplification becomes significant. In addition, it can aid the understanding of the calculations in cases where lack-of-fit effects are included to model the influence of the detailing of the cross-frames in I-girder bridges. Otherwise, the explicit modeling of the girder cambers is not believed to be an important consideration.
- Both geometrically linear (linear elastic) and geometrically nonlinear (second-order elastic) behavior of the elements are considered.
- Any superelevation, grade and vertical curve are not included in the models. It is believed that in most situations in practice, the bridge response to vertical (gravity) loads during construction is not significantly influenced by these attributes.
- The weights of the structural steel components are modeled as distributed body loads of 490 pcf in all of the finite elements. If necessary, additional concentrated loads are applied at cross-frame end nodes to represent the additional weight of connection elements and miscellaneous steel.
- The weights of formwork (10 psf) and the concrete slab including the reinforcing steel (150 pcf) are modeled using equivalent vertical line loads at the middle of the top flanges of the girders. The influence of eccentric loads on the slab overhangs, supported by overhang brackets, is modeled as a force couple composed of equal and opposite horizontal distributed loads, one at the level of the top flange and one at the level of the bottom of the overhang brackets. (Unless noted otherwise, the bottom of the overhang brackets is assumed to frame in at the bottom flange in the NCHRP 12-79 studies).
- The weight of construction equipment is neglected in most cases in the NCHRP 12-79 studies since the accuracy of the simplified methods can be assessed without including these loads.
- When and where the girders are composite, the concrete slab is modeled at its nominal physical location, including the depth of the haunch (i.e., the depth of the bolsters) over the girder flanges. If the slab overhang is tapered, the overhang is

modeled using the average slab thickness within the overhang region. The nominal thickness of the slab at the haunch is included in the FEA models.

- Steel erection stages are modeled by activating the portion of the steel structure for that stage and "turning on" the corresponding gravity loads.
- Holding cranes are modeled as a rigid vertical point support with no horizontal restraint at the hold location.
- Tie downs are modeled as rigid point supports.
- Staged deck placement and/or early stiffness gain of the concrete are modeled, where desired, by incrementally "turning on" and subsequently increasing the stiffness of the concrete as appropriate from stage to stage.

One of the important considerations in conducting a 3D FEA is the discretization of the various structural components into a sufficiently dense mesh to ensure acceptable convergence of the FEA approximations. The required mesh density generally varies with the FEA element theory, formulation and implementation. However, the best performing elements in various software packages usually tend to have roughly similar mesh density requirements (in terms of number of nodes) for a given theory and formulation type.

ABAQUS 6.10 (Simulia, 2010) is the specific software utilized for all the NCHRP 12-79 3D FEA studies. This software was selected because of its acclaim as one of the premier platforms for sophisticated physical test simulation. Model generators were developed by the NCHRP 12-79 researchers that permitted a streamlined comprehensive description of complete I- and tub-girder bridge structures for the above purpose. That is, for the purposes of the NCHRP 12-79 research, it was desired to be able to conduct comprehensive strength test simulations, where needed, including stability effects, the onset of distributed yielding in the steel components due to the combination of the applied stresses and initial residual stresses, and the strength of the concrete slab in tension and compression. Given the development of these capabilities, obviously the same general tools can be used to create elastic FEA design-analysis models. The specific ABAQUS elements utilized and the corresponding FEA discretization selected for the design analyses were as follows:

- For the I- and tub-girders, generally 12 S4R shell elements were utilized through the web depth. The S4R element is a linear-order (i.e., linear displacement field) 4-node quadrilateral Reissner-Mindlin displacement-based shell element with reduced integration. For geometric nonlinear analysis, the element is formulated for large strain. The number of shell elements along the girder lengths was selected such that all the shell elements in the web have an aspect ratio close to 1.0.
- The flanges of the I-girders, the top flanges of the tub girders, the various stiffeners, and the cross-frame connection plates were modeled using the B31 element, which is a two-node beam element compatible with the S4R shell element.
- The bottom flanges of the tub-girders were modeled generally using 20 S4R elements through their width. One B31 element was used on each side of the bottom flange to model the "lips" of the bottom flange that project beyond the intersection of the flange with the webs.
- The solid plate diaphragms in tub-girder bridges were modeled using S4R elements for their web and B31 elements for their flanges. The trapezoidal geometry of the diaphragm webs was represented by "fanning out" the S4R element geometries.
- The cross-frame chords also were modeled using B31 elements.
- The cross-frame diagonals as well as any flange-level lateral bracing were modeled using the T31 truss element.
- Where composite action was considered, the deck was modeled using S4R shell elements, and where needed at skewed bearing lines, the compatible 3-node triangular S3R shell element. The FEA mesh discretization utilized for the slab was generally coarser than the FEA mesh discretization utilized for the steel girders. The slab was modeled by one shell element along the bridge length for every two shell elements in the top flanges in the NCHRP 12-79 studies. Correspondingly, the slab discretization was set in the transverse direction of the bridge so that the slab elements have an aspect ratio approximately equal to 1.0.

The above FEA discretization is relatively dense compared to the coarser mesh requirements (i.e., minimum number of elements) expected to be sufficient for convergence of the elastic stresses in the majority of problems. Based on benchmark testing with the ABAQUS software, the use of 8 S4R elements through the web depth is expected to be sufficient in most problems for elastic analysis.

It should be noted generally that geometric nonlinear elastic FEA solutions, using the above models, were utilized as the primary standard for assessment of the different simplified 1D and 2D models in the NCHRP 12-79 research.

2.8.2 3D FEA for Physical Test Simulation

In recent years, the capabilities for simulation of physical tests using advanced 3D finite element analysis (FEA) has progressed to the point that, in numerous areas, the results from physical experiments can be reproduced readily and quite reliably. However, similar to successful experimental testing, the execution of test simulations requires great care. This is particularly the case where advanced simulation capabilities are not facilitated well by the software user interfaces. It should be noted that the results from an FEA test simulation are only as good as the accuracy of:

- The detailed geometry (e.g., plate thicknesses, deck-slab thicknesses, haunch depths, girder web depths, bearing heights, bearing plan locations, etc.),
- The load and displacement boundary conditions,
- The assumed (or nominal) initial conditions (e.g., initial internal residual stresses, geometric imperfections, any lack-of-fit between components in their unloaded condition, etc.),
- The constitutive relationships for the various constituent materials,
- The kinematic assumptions and/or constraints imposed by the structural theories.

The consideration of the above attributes should not detract from the use of advanced 3D FEA test simulations. In many respects, the above attributes are more easily specified, controlled and quantified in sophisticated 3D FEA models than in physical experiments.

In the NCHRP 12-79 research, 3D nonlinear FEA test simulations were conducted, where needed, using ABAQUS (Simulia, 2010). These simulations generally include realistic modeling of the steel three-dimensional stress-strain response and the modeling of initial residual stresses due to the manufacturing and fabrication of the steel. In these FEA solutions, 20 S4R shell elements were employed through the depth of the webs, primarily to capture the spread of yielding through the web depth, and the other finite element discretizations were refined accordingly. In addition, the I-girder flanges and the top flanges of the tub girders were modeled using 12 S4R shell finite elements in these studies. The modeling of the flanges with shell finite elements for the test simulation studies is primarily for two purposes:

1) The refined shell element discretization across the flange width facilitates the modeling of flange longitudinal residual stresses, and
2) The shell elements allow the consideration of multi-dimensional plasticity effects, although it is expected that the inelastic response of the flanges is associated predominantly with the longitudinal normal stress and strain.

The reader is referred to (Jimenez Chong, 2012; Ozgur, 2011; and Sanchez, 2011) for detailed discussions of inelastic test simulation analyses.

2.9 Global Second-Order Amplification Estimates

In certain situations, steel I-girder bridges can be vulnerable to stability related failures during their construction. The noncomposite dead loads must be resisted by the steel structure prior to hardening of the concrete deck. I-girder bridge units with large span-to-width ratios may be susceptible to global stability problems rather than cross-section or individual unbraced length strength limit states (Yura et al., 2008). In fact, due to second-order lateral-torsional amplification of the displacements and stresses, the limit of the structural resistance may be reached well before the theoretical elastic buckling load. Therefore, in structures sensitive to second-order effects, simply ensuring that the loads for a given configuration are below estimated global elastic buckling level is not sufficient. Furthermore, large displacement amplifications can make it difficult to predict and control the structure's geometry during construction. Possible situations with these characteristics include widening projects of existing bridges, pedestrian bridges with twin girders, phased construction, and erection stages where only a few girders of a bridge unit are in place, and thus the unit is relatively long and narrow.

Bridge EISCS4 (see Figure 2.28) is an existing structure with these characteristics studied in NCHRP 12-79 (see Chapter 4 for a discussion of the bridges considered in this project and their naming). This structure had a three-girder unit with a span of 256 ft. that experienced large second-order amplifications during its construction. This unit, composed of girders G15 to G17, was the third phase of a construction project erected next to Phases I and II consisting of 14 girders that had been previously constructed.

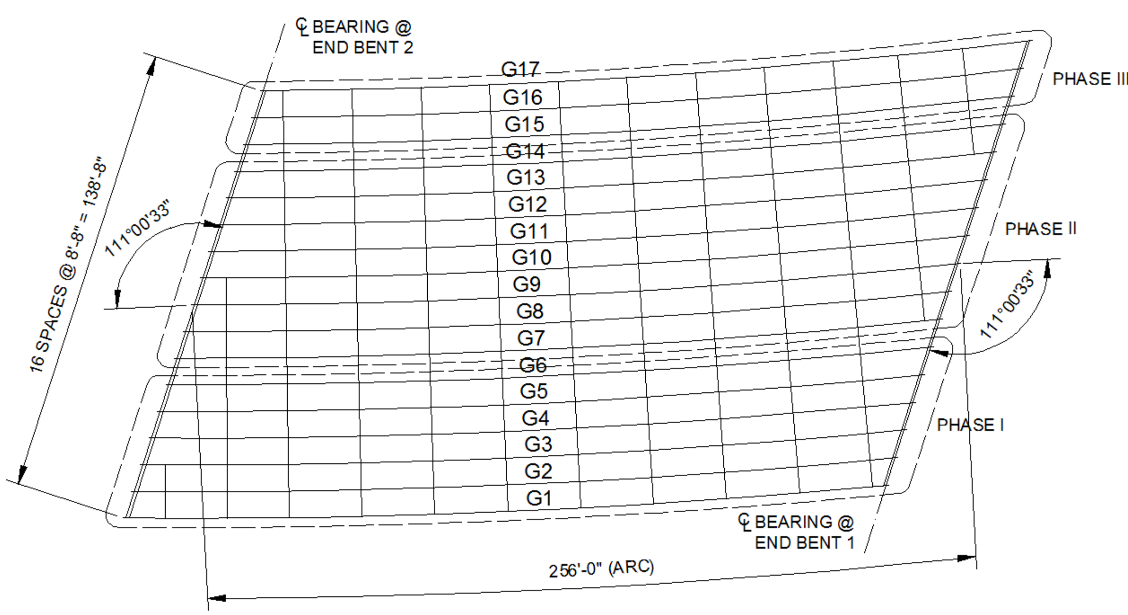

Figure 2.28. Plan view of EISCS4.

The concrete deck in the three-girder unit was placed starting at Bent 1 and moving toward Bent 2. By the time approximately two-thirds of the deck had been placed, the vertical deflections in girder G15 were considerably larger than in girder G14. As a result, there was a significant difference between the slab elevations for Phases II and III. At this point, it was decided to halt the concrete placement. The three-girder unit had deflected more than anticipated, and the structure was potentially at the point of incipient collapse. More detailed descriptions of the bridge and the studies conducted to assess its performance are presented in (Sanchez, 2011) and in Appendices E and I of the NCHRP 12-79 Final Report.

To accurately capture the behavior of a long-and-narrow bridge unit with these characteristics, a geometric nonlinear (i.e., second-order) 3D FEA is generally required. Figures 2.29 and 2.30 show the major-axis bending stress response, f_b, and the vertical displacements for girder G15 (the girder farthest from the center of curvature) obtained from a second-order (nonlinear) and first-order (linear) elastic 3D FEA of the above Phase III unit. In addition, these figures show the predictions obtained from a line-girder analysis (1D model) conducted using the V-load method, as well as the results from a 2D-grid analysis. These figures show that the simplified solutions provide a close estimate of the first-order 3D FEA predictions. However, the second-order amplification of the responses is not captured by any of these analyses, since all of these analyses are first-order. The first-order analyses are conducted at the Total Dead Load (TDL) level, which is equal to the sum of the structure's self-weight (SDL), the additional dead load due to the weight of the metal deck forms (ADL), and the concrete load (CDL). The responses obtained from the second-order analysis are shown at a lower load level (75 % of the CDL). This is because the geometrically nonlinear 3D FEA predicts that the structure becomes unstable at 75 % of the CDL.

A simple method that can be used to alert the engineer to these potential undesired response amplifications due to second-order effects is recommended in the NCHRP 12-79 research. The linear response prediction obtained from any of the first-order analyses can be multiplied by the following amplification factor:

$$AF_G = \frac{1}{1 - \dfrac{M_{maxG}}{M_{crG}}} \tag{2.101}$$

where M_{maxG} is the maximum total moment supported by the bridge unit for the loading under consideration, equal to the sum of all the girder moments, and

$$M_{crG} = C_b \frac{\pi^2 s E}{L_s^2} \sqrt{I_{ye} I_x} \tag{2.102}$$

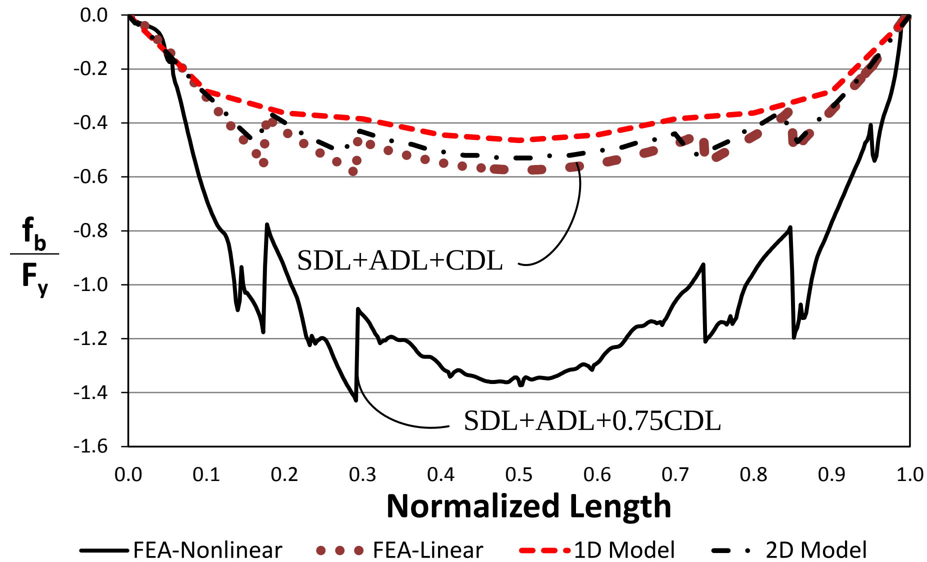

Figure 2.29. Comparison of major-axis bending stresses in girder G15 predicted using refined and approximate analysis methods (SDL = Steel Dead Load; ADL = Additional Dead Load due to metal deck forms; CDL = Concrete Dead Load).

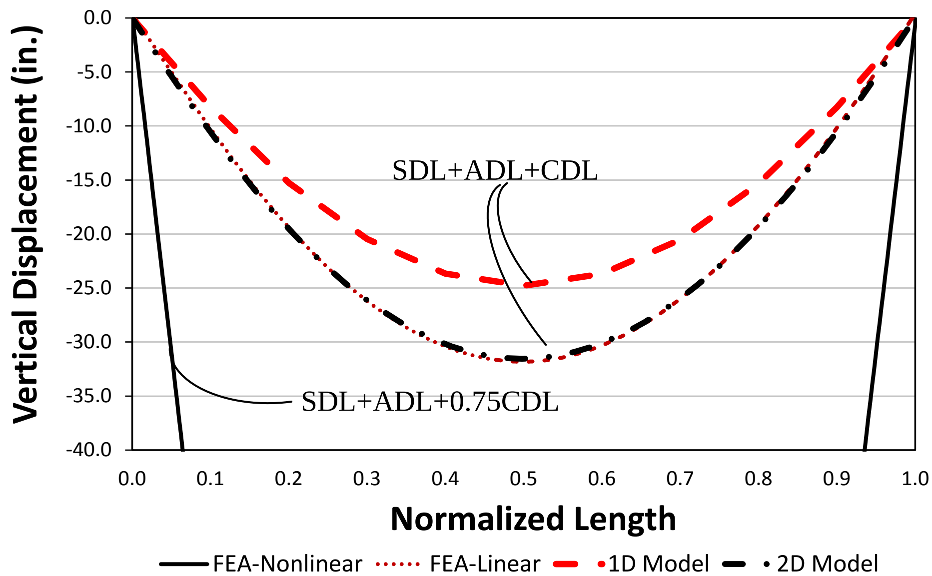

Figure 2.30. Comparison of vertical displacements in girder G15 predicted using refined and approximate analysis methods.

is the elastic global buckling moment of the bridge unit (Yura et al., 2008). In Eq. (2.102), C_b is the moment gradient modification factor applied to the full bridge cross-section moment diagram, s is the spacing between the two outside girders of the unit, E is the modulus of elasticity of steel,

$$I_{ye} = I_{yc} + (b/c)I_{yt} \tag{2.103}$$

is the effective moment of inertia of the individual I-girders about their weak axis, where I_{yc} and I_{yt} are the moments of inertia of the compression and tension flanges about the weak-axis of the girder cross-section respectively, b and c are the distances from the mid-thickness of the tension and compression flanges to the centroidal axis of the cross-section, and I_x is the moment of inertia of the individual girders about their major-axis of bending.

Yura et al. (2008) developed Eq. (2.102) considering multiple girder systems with up to four girders in the cross-section of the bridge unit. The individual girders are assumed to be prismatic and all the girders are assumed to have the same cross-section. For Phase III of EISCR4, $\gamma_{crG} = M_{crG} / M_{maxG} = 0.60$ corresponding to the nominal (unfactored) total dead load, using the sum of the maximum mid-span moments for the three girders for the calculation of M_{maxG}, and using the largest girder cross-section for the calculation of M_{crG}. Even when the largest mid-span cross-section (girder G15) is used for the calculation, Eq. (2.102) still provides a conservative prediction of the rigorous global buckling load level of $\gamma_{crG} = 0.85$ obtained from a 3D FEA eigenvalue buckling analysis. The use of the largest cross-section in Eq. (2.102) can be justified in this problem based on the logic that:

- G15 is the girder farthest from the center of curvature, and therefore, this girder has a greater influence on the global buckling resistance, and
- The mid-span cross-section of the girders provides the dominant contribution to the global elastic LTB resistance.

A global buckling load level of $\gamma_{crG} = M_{crG} / M_{maxG} = 0.24$ is obtained relative to the nominal (unfactored) total dead load if the smallest cross-section at the mid-span of the girders is used, and $\gamma_{crG} = 0.40$ is obtained if the average girder cross-section dimensions are used to determine I_x and I_{ye} in Eq. (2.103).

Figure 2.31 shows the vertical displacements at the mid-span of girder G15 vs. the fraction of the TDL obtained from the linear and nonlinear FEA models. In addition, a response curve obtained by multiplying the first-order response by the amplification factor of Eq. (2.101), using γ_{crG} = 0.85, is shown in the figure. This calculation generally provides a conservative estimate of the amplified responses. Clearly, the vertical deflection of girder G15 is excessive well before the elastic buckling load level of γ_{crG} = 0.85 is reached.

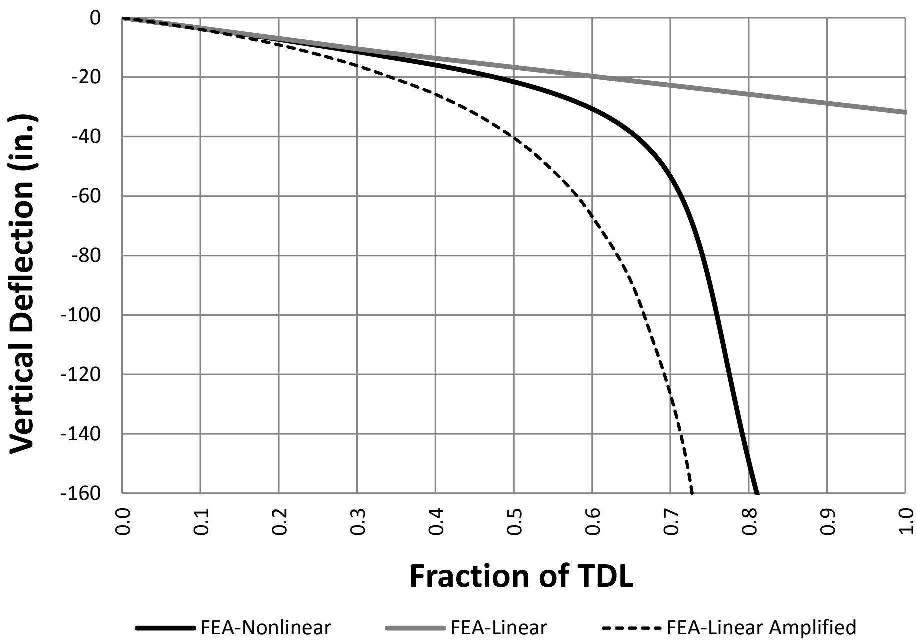

Figure 2.31. Vertical deflection at mid-span of girder G15 vs. the fraction of the TDL.

In addition to providing an estimate of the second-order effects on the girder displacements, the above amplification factor equation also can be used to predict the corresponding amplification of the girder stresses. Hence, the results of an approximate 1D or 2D analysis can be amplified, using Eq. (2.101), to conduct the constructability checks required by AASHTO LRFD Article 6.10.3. These checks are:

- Nominal initial yielding due to combined major-axis bending and flange lateral bending,
- Strength under combined major-axis and flange lateral bending (referred to as the 1/3 rule),
- Web bend buckling, and

- A maximum limit on the flange lateral bending stress of $0.6F_y$.

To illustrate the method, the load level at which the above three-girder unit violates the AASHTO constructability checks is determined using two different approaches:

- A “rigorous” solution in which 3D FEA is used to determine the global eigenvalue buckling resistance (γ_{crG} = 0.85) as well as to solve directly for the second-order load-deflection response in the critical girder G15, and
- The combined use of the global elastic buckling resistance computed using Eq. (2.102) (γ_{crG} = 0.60), the use of the 1D V-load method to estimate the girder G15 linear elastic responses, and the use of Eq. (2.101) to amplify these responses.

The results from these two sets of calculations are then substituted into the AASHTO constructability checks to determine the fraction of the TDL at which the different checks are violated. Table 2.2 summarizes the results. The check associated with web bend buckling is not included here since it does not govern for this bridge. The terms f_{bu} and f_ℓ in the table are the major-axis bending and flange lateral bending stresses predicted by the *second-order (geometric nonlinear)* 3D FEA in the first set of analysis and by the *first-order (linear) elastic* line-girder analysis with the V-load extensions in the second set of analyses. As shown in the table, the checks conducted using the simplified manual equations provide a conservative estimate of the nonlinear FEA predictions. For the case study bridge unit, both procedures predict that the 1/3 rule strength check using the girder G15 elastic global buckling stress for ϕF_{nc}, is the controlling limit state check.

Table 2.2 shows that the simplified analysis can be used to obtain a conservative estimate that this bridge unit is approaching a dangerous condition. That is, the simplified analysis predicts a lower fraction of the TDL at which the checks are breached, compared to the 3D FEA solution. Although the results may be judged to be too conservative for final design, the approximate calculations provide a warning of the magnitude of the amplifications expected in the system due to the nonlinear response.

Table 2.2. AASHTO constructability checks using simplified line-girder (V-load) analysis with global amplification factor and refined 3D FE analysis results.

Limit State	Analysis Type	AF_G	TDL fraction	f_{bu} (ksi)	f_ℓ (ksi)
Nominal yielding AASHTO Eq. 6.10.3.2.1-1	Nonlinear FEA	NA	0.560	39.90	30.10
	Simplified	3.736	0.440	17.52	1.16
1/3 rule strength based on elastic global buckling, AASHTO Eq. 6.10.3.2.1-2	Nonlinear FEA	NA	0.540	33.00	21.00
	Simplified	2.132	0.319	12.70	0.84
$f_\ell \leq 0.6F_y$ AASHTO Eq. 6.10.1.6-1	Nonlinear FEA	NA	0.615	NA	42.00
	Simplified	27.54	0.579	NA	1.52

Regarding the specific case study bridge unit, one can observe from the nonlinear 3D FEA that the structure experiences substantial second-order amplification of the girder G15 major-axis bending stress in addition to the flange lateral bending stress. In fact, because of the relatively large radius of curvature and the relatively minor effects of skew on this narrow and long bridge unit, the first-order flange lateral bending stresses are particularly small. This causes the one-third rule strength interaction check to be more critical than the flange nominal yielding check.

Lastly, it should be noted that although a second-order analysis could be conducted using the 2D-frame model described in Section 2.3, this does not provide any useful results since the corresponding girder torsional stiffness representation (i.e., GJ/L) is poor. Only the 3D FEA provides an accurate analysis of the girder 3D lateral-torsional responses. (This limitation of the conventional 2D-grid procedures is addressed further in Section 6.1, although second-order analysis with the improved 2D-grid method is not recommended either. As the global buckling load level is approached, the approximations associated with the improved 2D-grid calculations are amplified; hence, although the improved 2D-grid methods work well for linear elastic analysis, they do not have sufficient resolution for reliable second-order analysis.)

The NCHRP 12-79 research suggests that Eq. (2.101) can be used to detect possible large response amplifications during preliminary construction engineering. If the amplifier shows that a structure will exhibit significant nonlinear behavior during the deck placement, the scheme adopted for the construction should be revisited. By providing additional shoring or by bracing off of adjacent units, the system response amplifications can be reduced. If it is found necessary to construct a structure that has potentially large response amplification during the deck placement, the engineer should perform a final check of the suspect conditions using a second-order (geometric nonlinear) 3D FEA. In addition, the construction processes must be monitored carefully, since the structure will be sensitive to any changes in the structural conditions, to ensure that the construction proceeds as assumed.

Substantial nonlinearity during the steel erection may be a concern in some situations; however, if the steel stresses are small and if the influence of the displacements on fit-up is not a factor, large second-order amplification of the deformations may not present any issue during the steel erection. These considerations are discussed further in Section 3.1.1.

2.10 Analysis Including the Effects of Early Concrete Stiffness and Staged Deck Placement

The application of a concrete slab to a steel girder bridge is a complex analysis problem, particularly on longer and/or wider bridges. When initially placed on the steel girders, the wet concrete offers no structural capacity or stiffness to the system and represents nothing more than a gravity load. However, as the concrete begins to cure it develops stiffness and affects the overall stiffness of the structure. Topkaya et al. (2003; 2004a & b) have evaluated the effects of early stiffness gain of the deck concrete for steel girder bridges. These investigators have shown that the interface between shear studs and the deck concrete can transfer considerable force only a few hours after the start of the concrete placement. In addition, they have shown that significant local crushing may occur if the studs are highly loaded at early ages, resulting in a loss of stiffness in the final constructed condition.

In most cases involving reasonable size deck casting stages, the job parameters are set such that early stiffness gain can be neglected within a given stage. In addition, for most simple-span bridges, the job parameters are commonly set such that the concrete can be placed in a single stage, without any significant stiffness gain of the concrete prior to the completion of the stage. In some cases, the construction specifications may require the use of set-retarding concrete additives to keep the concrete fluid longer and avoid the need to consider early concrete stiffness. Nevertheless, in situations such as continuous placement of a large bridge deck, it may be prudent to investigate the effects of the onset of early composite action.

In continuous-span steel bridges, it is common that the deck will be placed in multiple stages. The main goal of this technique of using separate stages is to minimize deck cracking over the piers. As such, a typical sequence requires that the positive moment regions be placed first, followed by the negative moment zones (days later, after the positive moment regions have sufficiently cured). The variation in the concrete stiffness properties from stage-to-stage needs to be accounted for when computing stresses or resistances, and it can be of substantial importance to the control of the bridge geometry, when determining deflections and girder cambers. The eventual accumulated moments, shears and deflections at a given location generally are different from a staged analysis than from an analysis assuming simultaneous placement. In addition, the maximum flexural demands may be reached at some sections at an intermediate stage of the construction rather than in the final constructed condition when staged deck placement is considered. Uplift can be a concern and should be checked when evaluating deck placement sequences, particularly for relatively light continuous-span framing with heavy concrete loads in adjacent spans.

The above considerations also apply to steel girder bridges built using phased construction. In addition, for phased construction, some girders in a given construction stage may have a reduced composite section due to the proximity of a longitudinal construction joint in the deck. The different section properties that these girders have, as the construction progresses, must be accounted for when evaluating strength and serviceability, and also, when estimating girder deflections and cambers.

The modeling of staged deck placement and incremental (stage-to-stage) increases in the concrete stiffness is possible in numerous 3D FEA software systems used in current practice (2012), and is also available in some 2D-grid software packages. For example, the MDX platform (MDX, 2011) has the ability to incrementally include slab segments in the analysis model, within a 2D-grid idealization. In addition, the program settings allow the user to set full, partial or non-composite action to simulate the effects of early concrete stiffness. Recent work by Stith (2010) includes the consideration of staged concrete deck placement via 3D FEA in the program UT-Bridge.

In the NCHRP 12-79 research, a limited number of studies of staged concrete deck placement focused on comparisons of solutions obtained using MDX to 3D-FEA results using the ABAQUS software system. The primary focus of the Project 12-79 studies was on the prediction of the bridge responses prior to the participation of the concrete deck.

2.11 Analysis of I-Girders During Lifting

Straight I-girders may be susceptible to buckling and curved I-girders may be susceptible to excessive deflection during lifting operations. Essa and Kennedy (1993) provide recommendations to maximize the buckling capacity of doubly-symmetric prismatic I-section members based on the position of the lift clamps along the length of the field section. Their recommendations are developed for cases involving a single spreader beam. Essa and Kennedy observe that the buckling capacity is largest when the lift clamps are placed near the quarter points. However, the buckling capacity is most sensitive to the position of the lift clamps when they are placed in these positions. If the lift clamps are moved either toward the middle or the ends of the member, the buckling capacity sharply decreases.

For the lifting of more general singly-symmetric horizontally-curved non-prismatic I-girders, the software UT Lift (Farris, 2008) is available to evaluate the girder pick locations. UT Lift calculates both the girder rigid body rotation as well as the deformations under self-weight for the lifted girder. The program also reports major-axis bending, flange lateral bending and warping normal stresses, as well as the critical buckling load of the lifted girder. The program's analysis calculations are based on a Thin-Walled Open-Section (TWOS) 3D-Frame model.

The analysis of I-girders during lifting is not addressed in this report. The focus of this report is on analysis of bridge systems in their partially or fully erected construction conditions.

2.12 Responses that a Line-Girder Analysis Cannot Model

In line-girder models, the girders in the system are analyzed independently. For the noncomposite structure, the loadings acting on each individual girder are determined based on tributary area or by other simplified lateral distribution assumptions. The V-load method extends the capabilities of a line-girder analysis to include horizontal curvature effects in I-girder bridges. However, this method does not include any information about skew, and therefore, it is not able to accurately capture the effects of skewed supports. The software VANCK (used for the V-load calculations in the NCHRP 12-79 research), may be applied to a skewed bridge, but inherently, this program does not address skew effects. This highlights the following important question that the engineer should always raise before utilizing a particular software system or set of calculation equations: Does the software or do the equations account for the important characteristics of the problem at hand? Just because a software package accepts the input parameters for a given structure does not make it applicable for the problem at hand.

For tub-girder bridges, the M/R method provides a way to include the torsional moments due to curvature in a 1D line-girder analysis; however, this method cannot model the effect of external intermediate diaphragms, which potentially can introduce large forces and cause significant differences in the physical response (see Figure 2.13) when the external diaphragms are used to control the girder relative displacements as shown in Figure 2.15.

Support skews generally introduce a transverse load path in the structure. In I-girder bridges, loads are transferred laterally from girder to girder through the cross-frames, subjecting the system to torsion. Since the line-girder analysis does not contain any information regarding the cross-frame contributions to the system response, it cannot predict the collateral effects of skew. In particular, the cross-frame forces and flange lateral bending stresses associated with the skew are responses that cannot be captured with this method. In addition, Sanchez (2011) shows that in some cases, the major-axis bending stresses and the vertical displacements also can be influenced significantly by the skew effects. Furthermore, it is important to note that if the accuracy of the simplified vertical deflection estimates is degraded, the estimates of the girder layovers also is affected. For tub-girder bridges a traditional line-girder analysis does not include the skew effects; however, these effects can be included with reasonable accuracy when there are no external intermediate diaphragm, as explained in Sections 2.1.4 and 2.1.5.

Fortunately, in many structures the effects of skew are minor. Limits for when it is necessary to capture the skew effects in the analysis of I-girder bridges are proposed in Chapters 3 and 5 of this report. In Section 3.1.2, a "skew index" that relates the skew angle with the width and the span length of the bridge is introduced. For I-girder bridges, the collateral skew effects are observed to be relatively small when the skew index is less than 0.30. This is shown in the quantitative assessment of the approximate analysis methods discussed in Section 5.1. Hence, even though a line-girder analysis is not able to capture the responses mentioned previously, this inaccuracy does not have an important effect on the structural behavior in bridges having indices below this limit. For structures with indices above this limit, the skew effects generally have a significant influence on the system responses. For these structures, a more refined method of analysis should be considered.

2.13 Responses that a 2D-Grid Analysis Cannot Model

In 2D-grid analyses, most of the overall structural components of the bridge are included in the model. Specifically, 2D-grid models are capable of representing the girders and the cross-frames and/or diaphragms. In many cases, all the cross-frames, diaphragms and girders are modeled with elements that are based on Euler-Bernoulli beam theory. In some situations, models are created based on Timoshenko beam theory to consider shear deformations. The capabilities of an element formulated with these theories generally are not sufficient to represent the physical behavior of the structural components. In particular, the poor representation of the torsional stiffnesses of the I-girders, as well as the poor representation of the cross-frame generalized flexural-shear stiffnesses results in an inaccurate prediction of the bridge responses in certain cases.

Tub-girder bridges are in some respects more easily modeled by 2D-grid methods than I-girder bridges. This is because the tubs act as pseudo-closed sections. As such, warping torsion typically does not need to be considered (assuming an adequate top-flange lateral bracing system and adequate restraint of cross-section distortion by the internal cross-frames). Tub-girder bridges, however, experience modeling difficulties due to the finite size of the cross section relative to the external diaphragms and cross-frames. In 2D-grid analyses, the tub-girders are represented as line elements at their centroid but the offset from the support to the girder centroid is ignored. Similarly, the girder rotations are estimated about the girder centroid but the actual center of rotation can be offset from this location. For multiple girder systems, the external intermediate diaphragm lengths are modeled from the girder centerlines. In cases where the flexibility of the external and/or internal diaphragms or cross-frames has a significant effect on the system response, the force transfer and the deformations within the vicinity of these components are more complex than can be represented accurately by traditional 2D-grid or 3D-frame elements.

Section 5.1 shows quantitatively the results obtained for 58 I-girder bridges studied in NCHRP 12-79 and the influence of the simplifications used in the 2D- grid models on the prediction of the structural behavior. The studies conducted in this research show that, for I-girder bridges, the basic beam or frame elements commonly available in analysis and design software packages can give poor predictions of the displacements in cases involving the following attributes, or certain combinations of these attributes:

- The bridge is highly curved,
- The girders are connected by only a few cross-frames,
- There is a small number of girders in the bridge cross-section (final or during an intermediate stage of construction).

The poor predictions are tied largely to a poor characterization of the true girder torsional stiffnesses by the common St. Venant torsional stiffness idealization, *GJ*/*L*. The analysis models in common software packages do not include the torsional stiffness associated with the warping (or lateral bending) of the I-girder flanges. However, the girder warping response dominates the girder torsional stiffness for essentially all practical geometries. This can be understood by considering a basic I-section member subjected to an end torque, as shown in Figure 2.32. The majority of the torsional stiffness comes from the cross-bending of the flanges for essentially all practical lengths when one considers bridge girder type I-sections. The girder torsional stiffness is even larger if the warping of the flanges is restrained at both ends of the member.

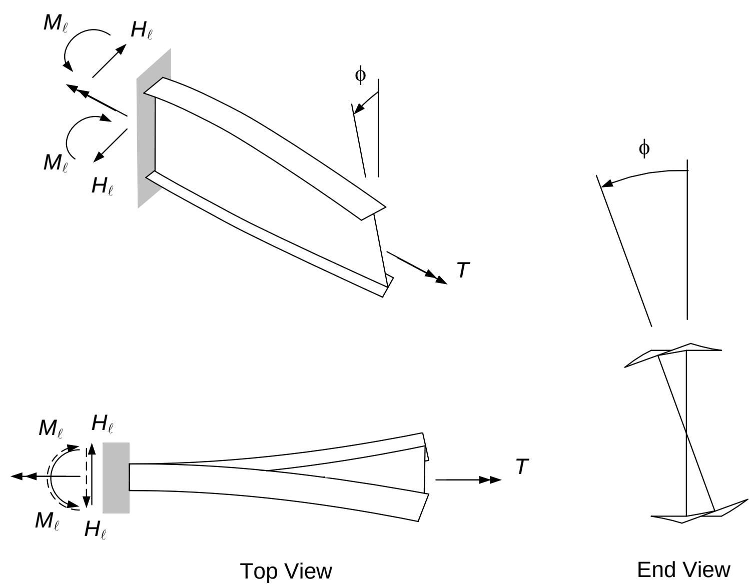

Figure 2.32. Example I-section member subjected to torsion.

It is important to note that horizontal curvature significantly influences the impact of the poor representation of the girder torsional response, and that horizontal curvature can have a dominant effect on the overall analysis accuracy. However, horizontal curvature is not the only factor that can influence the accuracy of 2D-grid methods. Straight skewed bridges having multiple lines of discontinuous (staggered) cross-frames also can be sensitive to the girder torsional stiffnesses used in the analysis models versus the physical torsional stiffness of the girders. Since the skew induces torsion in the I-girders, the predictions obtained from the 2D-grid model of a straight-skewed I-girder system can be inaccurate for bridges having a skew index equal or larger than 0.30.

Specifically, the cross-frame forces and the resulting f_ℓ stresses can be severely underpredicted. For bridges below this limit, the skew effects are relatively minor. Hence, although a conventional 2D-grid analysis may not be able to capture the distribution of transverse forces that result from skew, these effects may be neglected in the design.

The investigations conducted for the bridges studied in NCHRP 12-79 (see Chapter 4) show that the inaccurate representation of the torsional properties of the I-girders can have a minor effect on the major-axis bending stress responses. As shown in the quantitative assessment of the 58 I-girder and 18 tub-girder bridges considered in these studies, the major-axis bending stresses are less sensitive to poor torsion models than the vertical displacements. On the other hand, the torsion model has a significant influence on the vertical displacement predictions in curved I-girder bridges. Due to the lack of consideration of warping torsion in the conventional 2D-grid element formulations, the vertical displacements are commonly over-predicted in curved structures.

Another response of interest for the design of steel girder bridges is the cross-frame forces resulting from horizontal curvature and support skew. When conducting a 2D-grid analysis of a bridge structure, there are two particular practices that can affect the accuracy of the internal force predictions. The first practice is the modeling of the cross-frames. In grid analyses, the cross-frames are typically represented by an equivalent prismatic beam element. In conventional practice, the cross-section properties of the beam element are determined typically by equating either the flexural or the shear stiffness of an explicit model of the cross-frame to the corresponding beam element stiffness (Coletti and Yadlosky, 2007; AASHTO-NSBA, 2011). Some of the subtle attributes of the equivalent beam cross-frame modeling can be understood by considering the three in-plane co-rotational (i.e., deformational) degrees of freedom (dofs) at the ends of a cross-frame. As shown in Figure 2.33, one possible set of these co-rotational dofs involves the rotations at the connection plates on each side of the cross-frame as well as the relative axial extension of the cross-frame between the connection plates at say the mid-depth of the girders. The element equations for the full set of six dofs in the plane of the cross-frame are obtained from the co-rotational set by fundamental rigid-body kinematics and beam element equilibrium (Sanchez, 2011). If one uses an equivalent prismatic Euler-Bernoulli beam element to represent the cross-frame, the corresponding co-rotational stiffness terms are

$$\begin{bmatrix} EA/L & 0 & 0 \\ 0 & 4EI/L & 2EI/L \\ 0 & 2EI/L & 4EI/L \end{bmatrix} \tag{2.104}$$

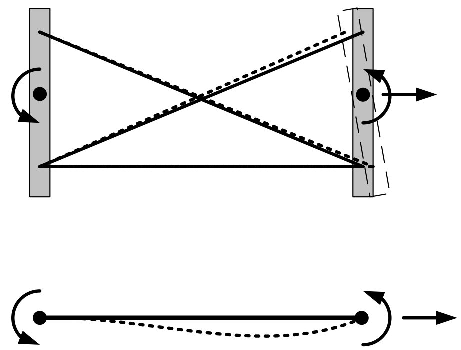

Figure 2.33. Typical cross-frame and equivalent beam element shown with their co-rotational (i.e., deformational) dofs.

If a Timoshenko beam or Reissner-Mindlin beam formulation is used, additional terms will appear in the bending stiffness coefficients that account for the beam shear deformations. In either case, each of the columns in the stiffness matrix gives the forces due to unit displacement at one of the dofs with the other dofs held fixed at zero displacement. If one imposes a unit relative displacement at the axial dof on the X-type frame in Figure 2.33, one will obtain bending moments at the two rotational dofs. This is because the center of axial stiffness of the cross-frames and the mid-height of the girders are not at the same elevation. Consequently, axial lengthening or shortening of the cross-frame between the girders is coupled with the cross-frame bending rotations at the centerline of the connection to the girders. Physically, the ends of the cross-frame cannot rotate relative to one another without some spreading apart or pulling together of the girders. In addition, if one considers the rotational degrees of freedom, it should be recognized that even if the primary rotational stiffness (4*EI*/*L* in the Euler-Bernoulli beam element) is matched to the corresponding "true" cross-frame stiffness, the ratio of the off-diagonal rotational stiffness term to the primary rotational stiffness in the true cross-frame generally will not be the same as the ratio of these terms in the equivalent beam element (e.g., $(4EI/L)/(2EI/L) = 2$ to 1 in the Euler-Bernoulli beam formulation).

The second practice that has an important role in the prediction of the cross-frame forces, as well as potentially the prediction of the behavior of the entire bridge structure, is the representation of the torsional rigidity of the I-girders. As previously stated, the formulation of the element used to represent the I-girders in 2D-grid models typically considers only the St. Venant or pure torsion contribution to the stiffness (GJ/L) and neglects the contribution from flange warping stiffness. In general, this limitation not only has a considerable influence in the prediction of the girder responses; also, it can have a substantial impact on the prediction of the cross-frame forces.

Figure 2.34 shows that the bending dofs for the cross-frames correspond to the torsional dofs of the girders. Only these dofs are shown in the figure to simplify the sketch. In the figure, Nodes 2 and 3 are connected; therefore, the bending moments in the cross-frames, $M_{1\text{-}CF}$, and the torsional moments in the girders, $T_{2\text{-}G}$, generally must balance with one another at this common joint (note that this figure could represent the behavior at the end bearing-line cross-frames of a bridge, but in general, other girder and/or cross-frame elements may frame into this common joint).

Generally, due to the limited capabilities of 2D-grid models to represent the actual torsional stiffness of the girders, the results obtained for $T_{2\text{-}G}$ and $M_{1\text{-}CF}$, will be severely underestimated. The neglect of the flange warping contributions to the stiffness results in a girder torsion model that is considerably more flexible than the physical girders. This means that even though the cross-frames are included in a 2D-grid analysis model, the girders respond as if they were disconnected since they do not have any torsional stiffness to react the cross-frame forces. This is observed particularly in straight and skewed I-girder bridges where the cross-frames are perpendicular to the girders. Since the *torsional* dofs of the girders are connected to *bending* dofs of the cross-frames, the cross-frame forces predicted from a 2D model also will be underpredicted. In fact, the cross-frame forces obtained from refined 3D FEA in straight-skewed with skew indices larger than

0.3 are often considerable, whereas conventional 2D-grid analyses indicate that these forces are essentially zero.

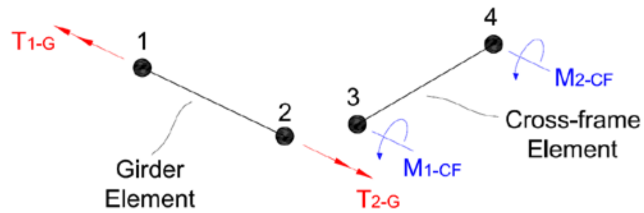

Figure 2.34. Interaction of girder and cross-frame stiffnesses.

Given that the cross-frame forces cause lateral bending in the girder flanges, it is necessary to have an accurate prediction of the cross-frame forces to compute the expected levels of the girder flange f_ℓ stress. Hence, conventional 2D-grid models are not able to predict the flange lateral bending responses with reasonable accuracy. However, as in the case of the cross-frame forces, the flange lateral bending stresses in skewed bridges with a skew index less than 0.30 may be neglected for design purposes.

Sections 6.1 and 6.2 explain the development of modeling techniques that improve the accuracy of the conventional 2D-grid models and extend their applicability to structures with complex geometries. As shown in these sections, a better representation of the cross-frames and of the torsional properties of the I-girders can significantly increase the accuracy of a 2D-grid analysis.

3. Bridge Characterization with Respect to Curvature and Skew

This chapter discusses five key indices identified by NCHRP 12-79 as being the most useful for characterizing the importance of skew and curvature on the response of steel girder bridges and the ability of simplified methods to capture this response. The first index is an estimate of the global second-order amplification of the bridge displacements and stresses, AF_G. This index should be checked to determine whether the stability effects are significant in cases such as relatively narrow and/or long units with a small number of girders. The second two indices are termed the skew index, I_S, and the connectivity index, I_C, and are used in Chapter 5 as an aid to identify when the simpler methods of analysis are sufficient and when more sophisticated methods should be applied for the construction engineering of curved and/or skewed I-girder bridges. The last two indices are termed the torsion index, I_T, and the girder length index, I_L. These indices are used in Chapter 4 as part of the characterization of curved and/or skewed bridges for the design of the project analytical studies. Section 3.2 provides an overview of broad factors that generally can influence the detailed behavior of curved and/or skewed steel girder bridges. These factors were considered in the development of a wide range of bridge geometries and configurations studied within the NCHRP 12-79 research. Chapter 4 discusses these factors and provides an overview of the NCHRP 12-79 studies that serve as input for the guidelines provided in this report.

3.1 Key Bridge Response Indices

3.1.1 Global Second-Order Amplification Factor, AF_G

The potential importance of the global second-order amplification of the vertical and lateral displacements, and of the corresponding girder major-axis and flange lateral bending stresses, is emphasized in Section 2.9. In that section, an equation for AF_G is recommended for making a basic conservative estimate of the second-order amplification. If the corresponding amplified major-axis bending and flange lateral bending stresses do not violate the required AASHTO Article 6.10.3 constructability checks, then strictly speaking, the AASHTO constructability requirements are satisfied. However, one should note that as the physical second-order amplification becomes large, the structural response becomes sensitive to minor variations in the load and support conditions, as well as any other characteristics that influence the stiffness. Therefore, for construction stages such as the placement of the concrete deck, it is advisable to restrict the estimated AF_G (Eq. 2.101) to a maximum value of approximately 1.25, or perform a 3D FEA of the structure to assess the second-order amplification more carefully. It is recommended that if AF_G from Eq. (2.101) is smaller than 1.10, the global second-order amplification of the structural responses may be neglected. If the designer is concerned about the potential underestimation of design stresses or forces, the design can be conducted using a capacity ratio of 0.9. However, it should be noted that there is no such thing as a conservative prediction of deflections in the context of the control of the constructed geometry of a bridge.

For intermediate steel erection stages, larger values of AF_G should be acceptable as long as the amplified stresses are sufficiently low. The AASHTO Article 6.10.3 yielding and one-third rule strength checks are expected to provide sufficient constructability limits in these cases, without the need to directly assess the structure's amplified deflections. It is important to note that in typical intermediate erection stages, the girder stresses are well below the AASHTO constructability limits.

There are various precedents for the above limits of AF_G = 1.10 and AF_G = 1.25 in the literature, but the rationale for these types of limits hinges largely on ones confidence in not overpredicting the ratio of the theoretical elastic buckling load of the structure to the design load under consideration, $\gamma_{crG} = M_{crG} / M_{maxG}$. At AF_G = 1.10, an underprediction of 10 % for γ_{crG} results in an underestimate in AF_G of approximately 2 %. At AF_G = 1.25, an underprediction of 10 % for γ_{crG} results in an underestimate in AF_G of approximately 3 %. At AF_G = 2.0, an underproduction of 10 % for γ_{crG} results in an underestimate in AF_G of approximately 12 %.

3.1.2 Skew Index, I_S

The skew index, I_S differentiates bridges where the skew effects are expected to be more significant from those where the collateral effects of skew are relatively small. This index is defined as

$$I_S = \frac{w_g \tan\theta}{L_s} \tag{3.1}$$

where w_g is the width of the bridge measured between the centerline of the fascia girders, θ is the skew angle, and L_s is the span length. In bridge spans with unequal skew of the bearing lines, θ is taken as the largest skew angle of the supports. In continuous-span bridges, one index is determined for each span. Figure 3.1 illustrates the variables required to calculate the skew index.

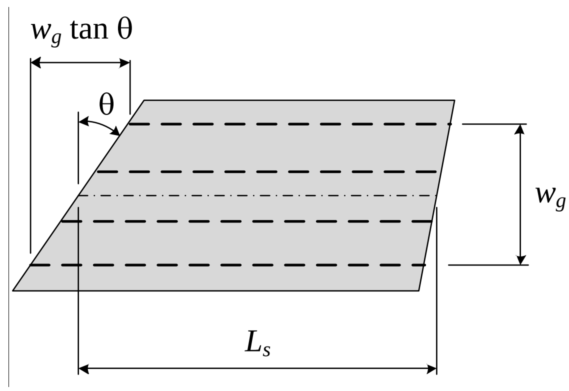

Figure 3.1. Parameters for the definition of the skew index.

The studies conducted in the NCHRP 12-79 research show that the effects of skew, which are largely related to the bridge transverse stiffness and transverse load paths, tend to increase with a larger skew index. Specifically, the levels of flange lateral bending stresses, cross-frame forces, and girder layovers tend to increase with increases in the skew index. The results obtained from 24 straight and skewed I-girder bridges studied in the project show that a value of the skew index of 0.30 differentiates bridges that are more sensitive to the skew from the ones that are less influenced by skew. For most of the structures above this limit, the stress ratio f_ℓ / f_b, which is one of the most suitable parameters to characterize the skew effects, is more than 0.3 in regions of the bridge where the cross-frames are staggered. That is, in these bridges, the levels of flange lateral bending stress are more than 30 % of the major-axis bending stresses, f_b, which may be considered as a large flange lateral bending effect. This limit parallels the limit suggested in the Commentary to Article 6.7.4.2 of AASHTO (2010), which states that for curved bridges, “A maximum value of 0.3 may be used for the bending stress ratio (i.e., f_ℓ / f_b).”

A second limit on the skew index, where the skew effects not only cause large values in the responses associated with the lateral bending of the girder flanges, but also can significantly influence the major-axis bending responses is 0.65. In bridges where I_S is above this limit, the influence of the skew on the girder major-axis bending stresses, f_b, as well as the girder vertical displacements can be significant. Below this limit, the influence of skew on these quantities tends to be small.

To illustrate the use of the skew index, the construction sequence of bridge NISSS14 is discussed (see Chapter 4 for a description of the NCHRP 12-79 studies and bridge naming conventions). Figure 3.2 shows three of the four stages of this bridge's construction considered below. Stage 3, not shown, corresponds to the condition where three girders have been erected and the cross-frames have been installed between the girders.

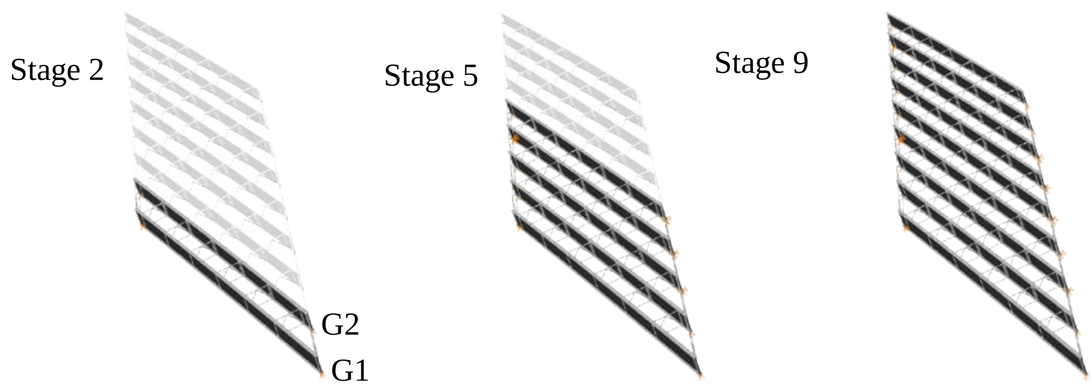

Figure 3.2. Erection stages investigated in bridge NISSS14.

In this bridge, the spacing between the girders is 9.25 ft., the span length is 150 ft., and the skew angle is 70 degrees. Hence, the skew index for Stage 2 is

$$I_S = \frac{9.25\,\text{ft} \times \tan 70^{\circ}}{150\,\text{ft}} = 0.17$$

Similarly, for Stages 3, 5, and 9 the skew index is 0.34, 0.68, and 1.36, respectively.

Figure 3.3 shows the f_b and f_ℓ plots of girders G1 and G2 for each of the stages. The plots contain three responses: the f_b and f_ℓ stresses obtained from the 3D FEA and the f_b stress obtained from a 1D line girder analysis. The bending stresses from the 1D analyses are based only on the individual weights of the girders. These analyses do not consider the influence of the internal forces in the cross-frames resulting from the skew effects. Since the cross-section dimensions of G1 and G2 are the same and the only loading considered is the structure's self-weight, the line girder analysis predictions for G1 and G2 are also the same and do not change during the construction simulation.

From these plots, it is evident that as the construction progresses and the geometry of the bridge changes, the skew effects become more important. It is observed that in Stage 2, the influence of the skew is negligible, since the horizontal components of the cross-frame forces do not cause considerable levels of f_ℓ. Also, the f_b stresses associated with major-axis bending are dominated by the gravity load effects on each girder. The vertical components of the forces from the cross-frames are too small to influence the response. Hence, the 1D line-girder analysis is a good match to the benchmark. As more girders are erected, the influence of the skew is more noticeable. In Stage 5 for example, when five girders have been erected, the level of the f_ℓ stresses is significant compared to the f_b stresses. Furthermore, the effect of the cross-frame shear forces is particularly noticeable since the line girder analysis prediction of f_b deviates considerably from the benchmark response. In the 1D analysis, the participation of the cross-frames is not included, so the forces transferred by the bracing system do not contribute to the predictions. A similar trend is observed for Stage 9, when the structure's erection is completed. The plots show that the forces transferred through the cross-frames have a considerable impact in the performance of the structure at this stage.

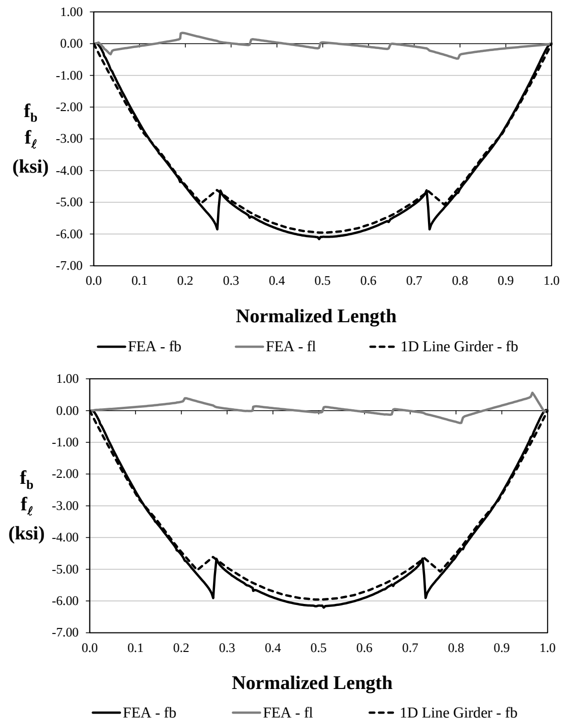

Girder G1 Girder G2

(a) Stage 2 (I_{SE} = 0.17)

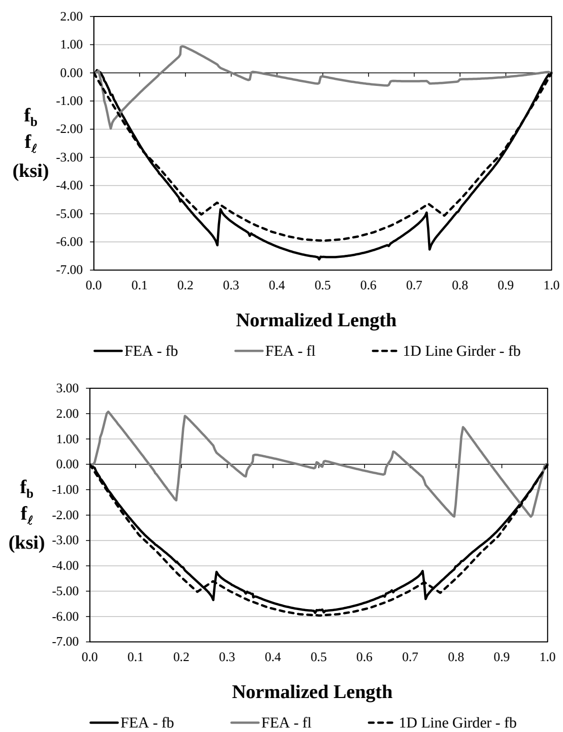

Girder G1 Girder G2

(b) Stage 3 (I_{SE} = 0.34)

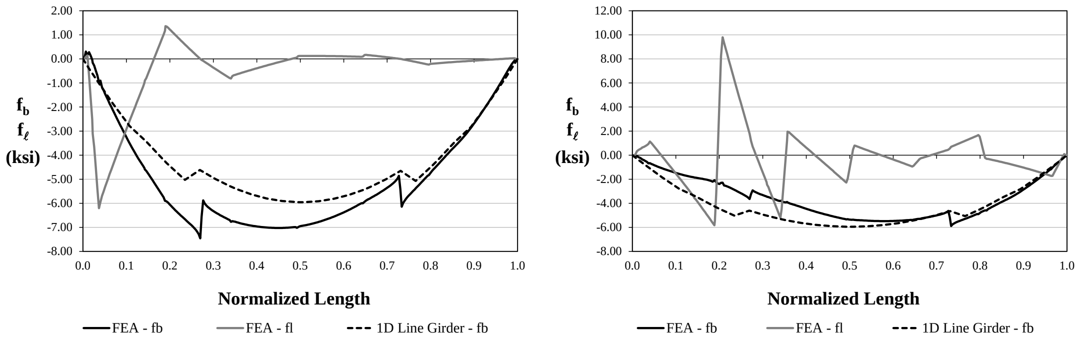

Girder G1 Girder G2

(a) Stage 5 (I_{SE} = 0.68)

Figure 3.3. Stress responses in the top flanges of girders G1 and G2 of bridge NISSS14 during four construction stages.

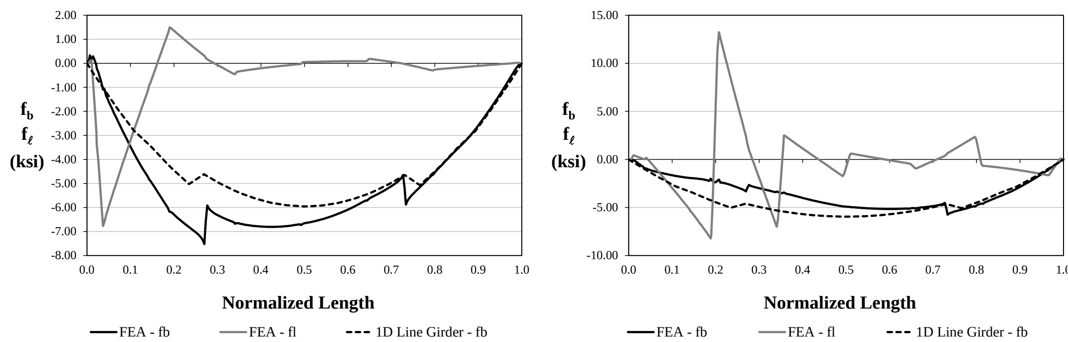

Girder G1 Girder G2

(b) Stage 9 (I_{SE} = 1.36)

Figure 3.3 (continued). Stress responses in the top flanges of girders G1 and G2 of bridge NISSS14 during four construction stages.

The above analyses also demonstrate that the behavior of a skewed bridge depends on more than just the severity of the skew. The skew angle by itself does not determine the magnitude of the collateral skew effects. Instead, it is the combination of the span length, the bridge width (between the fascia girders), the skew angle, and the distribution of the cross-frames in the bridge layout that determines the structural behavior. The proposed skew index relates the first three of these parameters, which define the geometry of the bridge. As discussed, as the index increases, so does the influence of the skew on the system response. Also, it should be noted that in the construction stages investigated for this bridge, the responses in Stages 5 and 9, which have indexes of 0.68 and 1.36, are more significantly affected by the skew compared to Stages 2 and 3, where the index is close to and less than 0.30.

The above construction simulation also highlights an important aspect regarding the accuracy of the 1D model predictions. By comparing the predictions obtained from the 1D and 3D analyses, it is observed that even when the line girder solution deviates from the physical response, in general, the difference in the major-axis bending stress magnitudes tends to be minor. For example, at the mid-span of girder G1, Stage 9, the f_b stress obtained from the 3D model is -6.65 ksi. At the same position, the 1D model predicts a stress of -5.96 ksi, resulting in a difference of 0.69 ksi. For design purposes, this difference is negligible. Therefore, many engineers would conclude that the 1D model is sufficient to represent the expected structural behavior of this bridge. However, it is important to notice that the 1D model does not provide any information regarding the cross-frame forces and girder flange lateral bending stresses, which according to the AASHTO Specifications must be included in the construction checks when the lateral bending is significant. Hence, although the 1D analysis may capture approximately the major-axis bending response of the girders, it does not provide the information needed to design all the structural components. Additional studies that show the validity of the skew index as a method used to characterize the influence of skew on the structural behavior are provided in Sanchez (2011).

3.1.3 Connectivity Index, I_C

The studies conducted in the NCHRP 12-79 research show that in curved radially supported I-girder bridges, the cross-frame spacing (or the number of intermediate cross-frames within the span) is a key indicator of the accuracy of the results obtained from 2D-grid analyses. In conventional 2D-grid models, the representation of the torsional stiffness of the I-girders is dramatically underestimated since the contributions of warping to the girder stiffness are neglected. If the bridge is significantly curved and/or the girders are not closely connected by cross-frames, the results obtained from these 2D-grid models do not properly represent the structural behavior of the curved bridge during construction. Chapter 6 provides an extensive discussion regarding this topic. The errors are tied largely to the coupling between major-axis bending and torsion in curved girders.

A trend that is noticeable in curved radially supported bridges is that the accuracy of the analysis is roughly proportional to the radius of curvature, R, and to the span length to unbraced length ratio, L_s / L_b. In a straight bridge connected with a typical number of cross-frames needed to make the structure behave as a unit, $R = \infty$ and the L_s / L_b ratio is large. Also, the accuracy of the results obtained from 2D-grid models should be within acceptable limits. On the other hand, if the structure has a tight radius of curvature and/or is connected with a small number of cross-frames, giving a smaller L_s / L_b ratio, the results of the conventional 2D-grid models may be suspect. In addition, continuous-span I-girder bridges tend to be able to tolerate smaller values of R and L_s / L_b for a given error tolerance.

Based on the above observations, the following ad hoc connectivity index is proposed to characterize when the results from a 2D-grid analysis may not be sufficiently accurate:

$$I_C = 15{,}000 \frac{1}{R} \frac{1}{m} \frac{L_{b.avg}}{L_s} = \frac{15{,}000}{R(n_{cf} + 1)m} \tag{3.2}$$

where R is the radius of curvature of the bridge centerline in units of ft., m is a constant equal to 1 for simple-span bridges and 2 for continuous-span bridges, $L_{b.avg}$ is the average unbraced length between the cross-frames within the span, L_s is the span length at the bridge centerline, and n_{cf} is the number of intermediate cross-frames within the span. In continuous-span bridges, R and n_{cf} can vary from span to span. Therefore, I_C is calculated for each span, and the largest value is taken as the index for the full bridge.

In the NCHRP 12-79 studies, 14 curved radially-supported I-girder bridges were studied to determine the ability of the simplified methods to capture the responses predicted by refined 3D models (see Chapter 4 of this report, and Appendices E and I of the NCHRP 12-79 Final Report). From the results of this study it was determined that bridges with $I_C > 1$ tend to exhibit large errors from conventional 2D-grid analyses, while for $I_C \leq 1$, the 2D-grid analysis predictions are significantly better. Chapter 5 discusses the categorization of the curved and radial bridges as function of I_C in further detail.

To illustrate the use of this index, consider Bridge EISCR1 depicted in Figure 3.4a. This is a simple-span bridge with a radius of curvature equal to 200 ft. The girders are connected with five cross-frames. For this structure, I_C = 15,000/200/(3+1) = 18.75; therefore a conventional 2D-grid analysis may not be sufficient to capture the expected behavior. Conversely, Figure 3.4b shows the plan view of Bridge EICCR15, a two-span structure with 10 intermediate cross-frames in the first span and 13 intermediate cross-frames in the second. For this bridge, I_{C1} = 15,000/1,921/2/(10+1) = 0.35 and I_{C2} = 15,000/1,921/2/(13+1) = 0.28. Therefore, I_C = 0.35 < 1.0. Hence, the results obtained from the 2D-grid analyses should closely represent the benchmark responses.

The connectivity index is determined empirically based on the NCHRP 12-79 studies. In essence, this index evaluates "how curved is the bridge?" and "how well connected are the girders?" for conventional 2D-grid analysis purposes. It should not be used for any other purpose than identifying I-girder bridges where the results of a conventional 2D-grid analysis may or may not be reliable. It is not intended to be used in design to determine the number of cross-frames or the cross-frame spacing, for example, since it applies only to assessment of the inadequacies of the traditional 2D-grid calculations. It is emphasized that if a 3D analysis (or a 2D-grid analysis including the recommendations of Chapter 6) is conducted, the engineer will have the required information to dimension the structural members and check the different strength and serviceability limit states according to the requirements of the AASHTO LRFD Specifications, regardless of whether I_C is above or below 1.0.

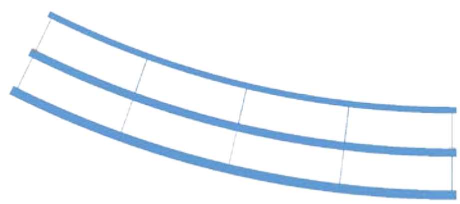

L_1 = 90 ft. / R = 200 ft. / *w* = 23.5 ft.

(a) Bridge EISCR1

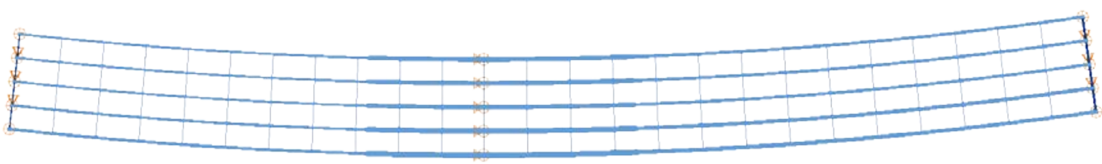

L1 = 210 ft., L2 = 271 ft. / R = 1921 ft. / w = 48.9 ft.

(b) Bridge EICCR15

Figure 3.4. Examples for the calculation of I_C in curved and radial bridges.

3.1.4 Torsion Index, I_T

Regarding the characterization of horizontal curvature effects on the bridge behavior and the corresponding analysis accuracy, the non-dimensional factor L_s/R, which is the subtended angle of a span's centerline expressed in radians, is important (see Figure 3.5). However, the maximum practical values of L_s/R can vary substantially as a function of the width of the structural system. The maximum L_s/R is more limited in relatively narrow bridges because of the greater tendency for overall overturning of the structure (or structural unit). This characteristic is illustrated by the plan sketches of the two hypothetical simple-span bridges shown in Figure 3.6. Both bridges have span lengths of L_s = 300 ft. and a constant horizontal radius of curvature R. However, one bridge has a 30 ft. wide deck while the other has an 80 ft. wide deck. The deck overhang width is 3 ft. on each side for both bridges. If one considers a representative uniformly distributed deck weight loading on these two structures, the subtended angle between the supports L_s/R needs to be much smaller for the narrower structure to avoid uplift at the inside fascia girder supports, i.e., the supports closer to the center of curvature.

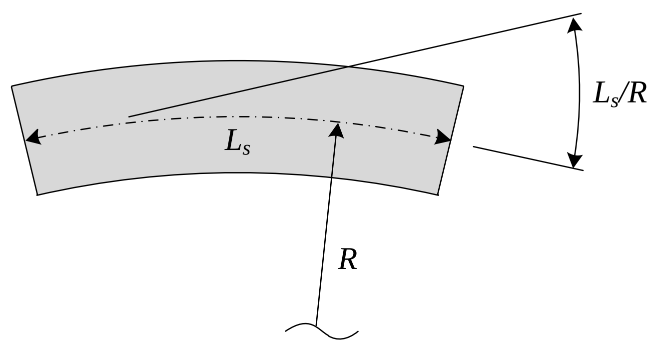

Figure 3.5. Subtended angle of a span's centerline, L_s/R.

Two straight dashed lines are drawn along the length direction of the plan sketches in Figure 3.6. One of the dashed lines is the chord between the fascia girder bearings on the outside of the curve. The other is the chord between the fascia girder bearings on the inside of the curve. Also shown on the plan sketches is the symbol "x", which indicates the centroid of the deck area (and hence the approximate centroid of dead weight of the structure). For bridges that are more highly curved (smaller R), the centroid (x) is closer to the outside chord line. If the curvature is such that the centroid (x) is positioned directly over the outside chord line, then all the bridge reactions have to be zero except for the reactions at the outside bearings. That is, the bridge unit is at the verge of tipping about its outside bearings (assuming a single span, simply-supported ends, and no hold-downs at the other bearings). This is obviously an extreme condition. Even a bridge with a much smaller curvature (larger radius of curvature) would require hold downs at bearings closer to the center of curvature to equilibrate (or balance) the structure weight assuming a uniform distribution over the deck area.

The following “torsion index” is an indicator of the overall magnitude of the torsion within a bridge (or bridge unit) span, and is a strong indicator of the tendency for uplift at the bearings:

$$I_T = \frac{s_{ci}}{s_{ci} + s_{co}} \tag{3.3}$$

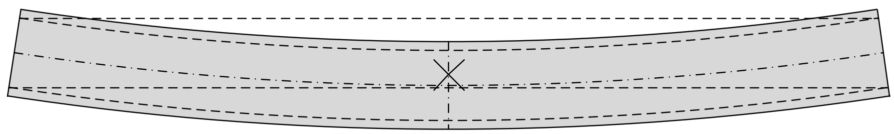

L_s = 300 ft, w = 30 ft, w_g = 24 ft, R = 1000 ft, L_s/R = 0.30

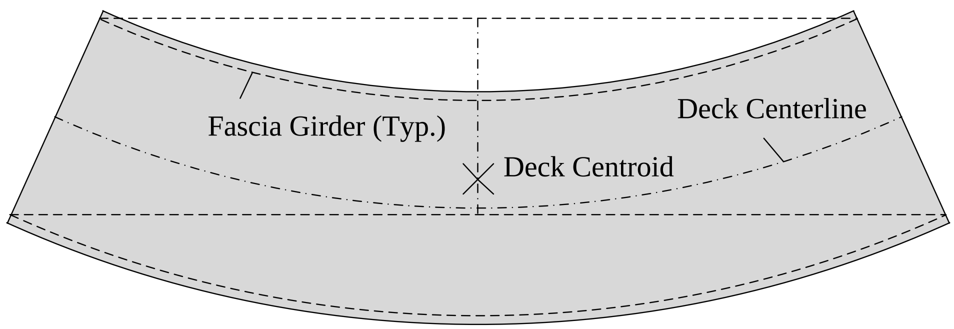

L_s = 300 ft, w = 80 ft, w_g = 74 ft, R = 353 ft, L_s/R = 0.85

Figure 3.6. Plan geometries of two representative simple-span horizontally-curved bridges with L_s = 300 ft.

The terms in this equation, illustrated in Figure 3.7, are:

- s_{ci}, the distance between the centroid of the deck and the chord between the inside fascia girder bearing locations, measured at the bridge mid-span perpendicular to a chord between the intersections of the deck centerline with the bearing lines, and
- s_{co}, the distance between the centroid of the deck and the chord between the outside fascia girder bearing locations, measured at the bridge mid-span perpendicular to a chord between the intersections of the deck centerline with the bearing lines.

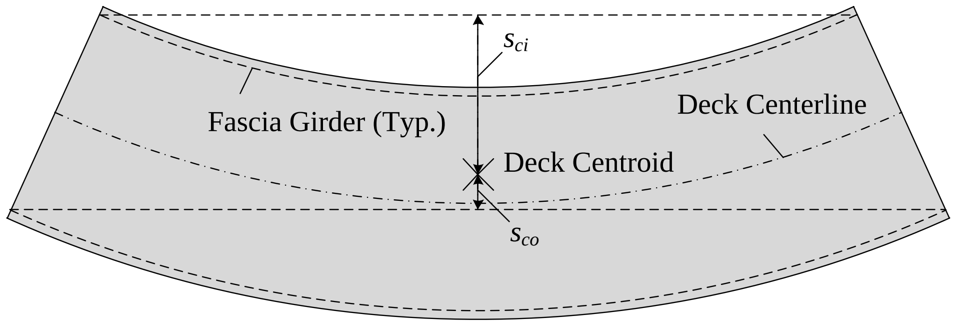

Figure 3.7. Illustration of terms in the equation for I_T.

A value of I_T = 0.5 means that the centroid of the deck area is mid-way between the chords intersecting the outside and inside end bearings. This is the ideal case where the radius of curvature is equal to infinity and the skew is zero, i.e., a straight tangent bridge. A value of I_T = 1.0 means that the centroid of the deck area is located at the chord line between the outside bearings. This implies that the bridge is at incipient overturning instability, by rocking about its outside bearings under uniform self-weight. For a curved radially-supported span, the denominator in Eq. (3.3), $s_{ci} + s_{co}$, is equal to $w_g \cos(L_s/2R)$.

As noted above, the torsion index is related to the magnitude of the overall torsion that exists in the bridge (or bridge unit) span, due to the eccentricity of its self-weight. Furthermore, it is a strong indicator of the potential for uplift at the inside bearings. In the NCHRP 12-79 research, it has been observed that simple-span I-girder bridges with a torsion index of 0.65 and higher are susceptible to uplift at the bearings (Ozgur, 2011). Continuous-span bridges can tolerate higher indices due to the stabilizing effect of the continuity with the adjacent spans. However, the continuity with the adjacent spans generally varies during the steel erection. The torsion index can be calculated for an intermediate steel erection stage using the width between the outside and inside girders during that stage. $I_T > 0.65$ can serve as a rough indicator of when the engineer should check carefully for uplift during the stage.

Tub-girder bridge bearings are typically closer to the bridge centerline and also tub girders are more efficient at resisting overall torsion; therefore, the torsion index in tub-girder bridges tends to be larger than that for an I-girder bridge with the same deck geometry.

3.1.5 Girder Length Index, I_L

The last key index recommended in the NCHRP 12-79 research for characterizing the demands on the methods of analysis with respect to the handling of curvature and skew effects is the girder length index, I_L. This index is usually expressed as

$$I_L = \frac{L_L}{L_S} \tag{3.4}$$

where L_L is the span length of the longest fascia girder and L_S is the span length of the shortest fascia girder within each span. For the curved and skewed bridges considered in the NCHRP 12-79 project research, this definition is modified to

$$I_L = \frac{L_1}{L_{ng}} \tag{3.5}$$

where L_1 is the span length of fascia girder number 1, and L_{ng} is the span length of the highest numbered fascia girder. In the NCHRP 12-79 research, all the curved bridges are displayed in a "concave up" orientation with girder G1 located on the outside of the curve at the bottom of the sketch. Therefore, for the curved radially-supported bridges, I_L is generally somewhat larger than 1.0. If a bridge is curved and skewed, I_L is increased from this value if the skew increases the length of the outside fascia girder. Correspondingly, I_L is decreased and may be less than 1.0 if the fascia girder on the outside of the curve is decreased in length by the skew.

In continuous-span bridges, one index is determined for each span, and the value most different from 1.0 is used to represent the bridge.

The NCHRP 12-79 studies actually indicate that the previous four indices are sufficient to form decisions about the selection of the different methods of analysis. However, the girder length index I_L is an additional parameter indicative of the tendency for differential vertical deflections across the bridge width. The value of I_L is 1.0 for straight bridges with parallel bearing lines, whereas it can be a relatively large number if the bridge is wide and has a significant difference between the skew of adjacent bearing lines. Therefore, one might expect that of two bridges with a large skew index, I_S, the demands on the analysis may be greater if the index I_L is larger. This trend is not borne out in the NCHRP project studies however. It is believed that the satisfaction of the AASHTO Specification requirements in the bridge designs diminishes the importance of I_L.

3.2 Other Factors

The second and third indices discussed in Section 3.1 (I_S and I_C) are the basis of the scoring system presented in Chapter 5 to assess the ability of the approximate methods to capture the structural responses during the construction of steel I-girder bridges. The first index, AF_G, is used as an indicator of when second-order amplification of the responses may be significant, and the fourth index, (I_T) is used as an indicator of when bearing uplift considerations may be particularly significant. In addition to these indices, NCHRP 12-79 investigated the influence of various other factors that may affect the structural behavior and the analysis accuracy during construction. Span length, radius of curvature, support skew, number of spans and other parameters were variables considered to assess the geometry of the bridges included in the research studies. Chapter 4 discusses these parameters in detail along with criteria for the selection of the bridge geometries that were studied.

4. Design of NCHRP 12-79 Analytical Studies

4.1 Introduction

Curved and/or skewed bridge structures with different geometries can respond in dramatically different ways during their various stages of construction; therefore, extensive studies of a wide range of bridge structures are necessary to gain a true understanding of the accuracy of different analysis methods and the effect of this accuracy on the structural performance.

It should be emphasized that both over-prediction and underprediction of displacements can be equally bad in cases where certain relative deflections are critical. Furthermore, one should not specify a simple blanket accuracy requirement on all the analysis deflections. Specific deflections should be considered, and in cases where the deflections are sufficiently small, larger inaccuracies can be tolerated.

It is important that the accuracy of simplified analysis methods be evaluated using actual bridge designs that satisfy either prior and/or current AASHTO design criteria. The results of simply varying bridge parameters without checking Specification requirements can be misleading. AASHTO requirements must be satisfied for the study bridges to allow the research to establish appropriate relationships between bridge design variables and recommended levels of analysis and construction engineering effort.

One of the early tasks of NCHRP 12-79 was to identify existing bridges representing a spectrum of various combinations of span arrangement, span length, curvature, bridge widths and skew. It was desired to consider both simple and continuous-spans, and that preference would be given to bridges that had:

- Good instrumented field data or at least good field observations, particularly data and observations during intermediate stages of construction and
- Detailed construction plans,

and in which

- The design and construction satisfied prior and/or current AASHTO Specifications and established recommendations, yet construction challenges were encountered or certain attributes resulted in concerns about the final state of stress in the girders, etc.

Bridges where technical challenges were addressed very successfully as well as cases where there were some significant problems were sought. However bridges involving generally acknowledged poor practices, e.g., inappropriate use of oversize or slotted holes, inadequate attachment of cross-frames during construction, etc., were not considered. The focus of Project 12-79 was on analysis and design using appropriate practices. Analysis requirements for forensic investigation of bridges with faulty details were not addressed. However, it was desired for the studies to shed light on the ability of analysis methods to highlight faulty erection schemes, etc., given appropriate design details.

Once the above existing bridge collection effort was completed, then the geometric factors influencing the analysis, design and construction of the bridges were identified. Finally, the ranges and number of levels of these factors were selected for subsequent analytical study.

The following sections provide a detailed description of each of the above steps.

4.2 Identification and Collection of Existing Bridges

Figures 4.1 through 4.6 summarize the overall characteristics of the existing I-girder bridges contributed to NCHRP 12-79 from various owners and consultants. These figures show sketches of the overall plan geometry of the deck and of the bearing lines. Although the number of pages used to illustrate the various geometries is relatively large, these sketches convey a great deal of useful information in a succinct fashion. All the linear dimensions indicated in the sketches are provided in units of feet and all the angular dimensions are provided in degrees. These figures subdivide the collected existing I-girder bridges into the following categories:

- Simple-span, Straight, with Skewed supports (ISSS),
- Continuous-span, Straight, with Skewed supports (ICSS),
- Simple-span, Curved, with Radial supports (ISCR),
- Continuous-span, Curved, with Radial supports (ICCR),
- Simple-span, Curved, with Skewed supports (ISCS), and
- Continuous-span, Curved, with Skewed supports (ICCS).

Each of the bridge sketches in Figures 4.1 through 4.6 has a title block containing the following information:

1. An identification label, composed of the letter “E” for “Existing” followed by the above symbols indicating the bridge category, and ending with the bridge number for that category, e.g., bridge “EISCR1” in Figure 4.3.
2. A description of the structure, composed of the bridge name and/or location.
3. A summary of the basic geometry information about the bridge, enclosed in parentheses. For instance, in Figure 4.3, the basic geometry information for the single EISCR bridge includes:
    - The span length of the bridge centerline (measured along the horizontal curve),
    - The horizontal radius of curvature of the bridge centerline, and
    - The out-to-out width of the bridge deck perpendicular to the bridge centerline.

   This information is conveyed symbolically in the figure caption as “(LENGTH/RADIUS/WIDTH).” The other categories have similar but different basic geometry information. This information is summarized symbolically in each of their figure captions. The skew angle of the bearing lines is represented by the symbol θ. This angle is taken as zero when a bearing line is perpendicular to the centerline of the structure, that is, when the bearing line does not have any skew.
4. The symbol “*”, at the end of the parentheses delimiting the basic geometry information, if the bridge has erection plans. No symbol is shown if the bridge does not have erection plans.

5. The organization that provided the drawings for each bridge. This information is delimited by square brackets, i.e., “[FHWA]” in Figure 4.3.

Other pertinent information is provided underneath the plan sketch of each of the bridges. This information includes data such as the number of girders in the bridge cross-section, whether test or field data is available for the structure, references to papers or reports containing test data or documentation of previous research on the bridge, and brief notes regarding successes or difficulties for certain bridges. Note that one scale is utilized for all the simple-span bridges, whereas a slightly smaller scale is used for all the continuous-span bridges.

Figures 4.7 through 4.12 summarize the overall characteristics of the existing tub-girder bridges. These figures are organized in a similar fashion to Figures 4.1 through 4.6.

The various existing bridges shown in Figures 4.1 through 4.12 served two purposes:

1. The composite of all the existing bridges was an aid to the project team in gauging the range and level of geometries that should be considered within the main parametric studies of the Project.

2. A number of the existing bridges that best fit the Project’s criteria for the analytical studies, discussed in Section 4.1, were selected for detailed study and inserted into the complete parametric study matrix, discussed subsequently in this chapter.

One can observe that there is a significant diversity of geometries among the existing bridges. This is particularly true for the skewed bridges. It was clear from these sketches that both the skew angle and the skew pattern (i.e., radial, non-radial, parallel and non-parallel bearing arrangements) must be studied. It was not sufficient to focus solely on bridges with parallel bearing lines if the complete implications of skew were to be addressed.

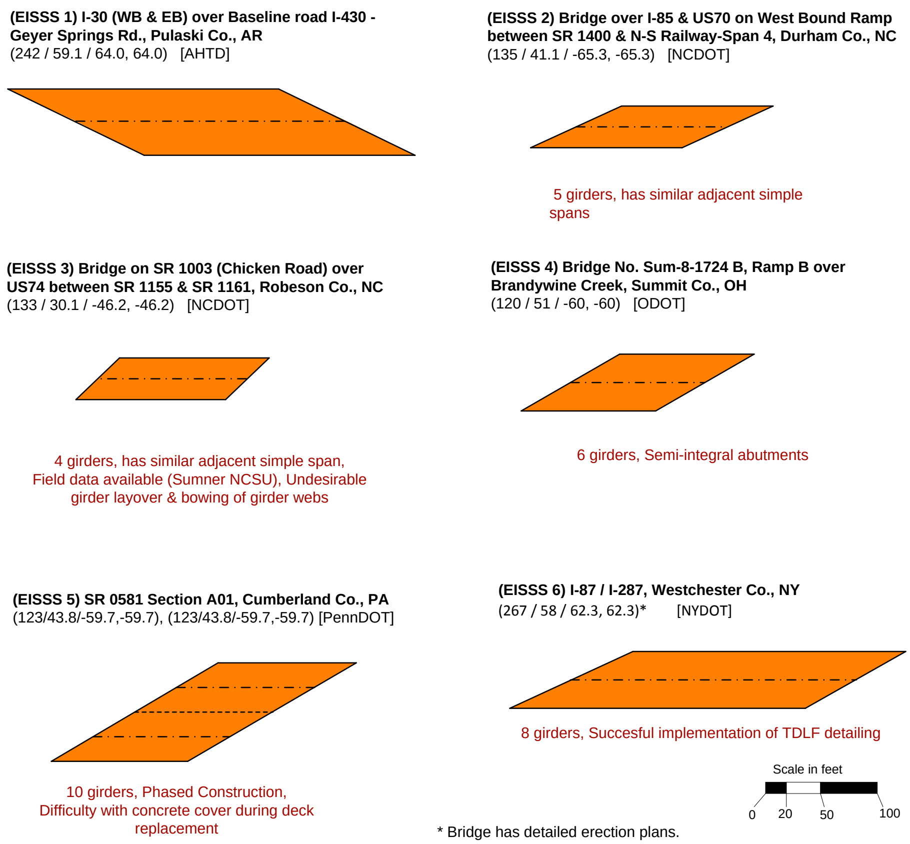

Figure 4.1. Existing I-girder bridges, Simple-span, Straight with Skewed supports, (EISSS #) Description (LENGTH / WIDTH / θ_{Left}, θ_{Right}) [Source].

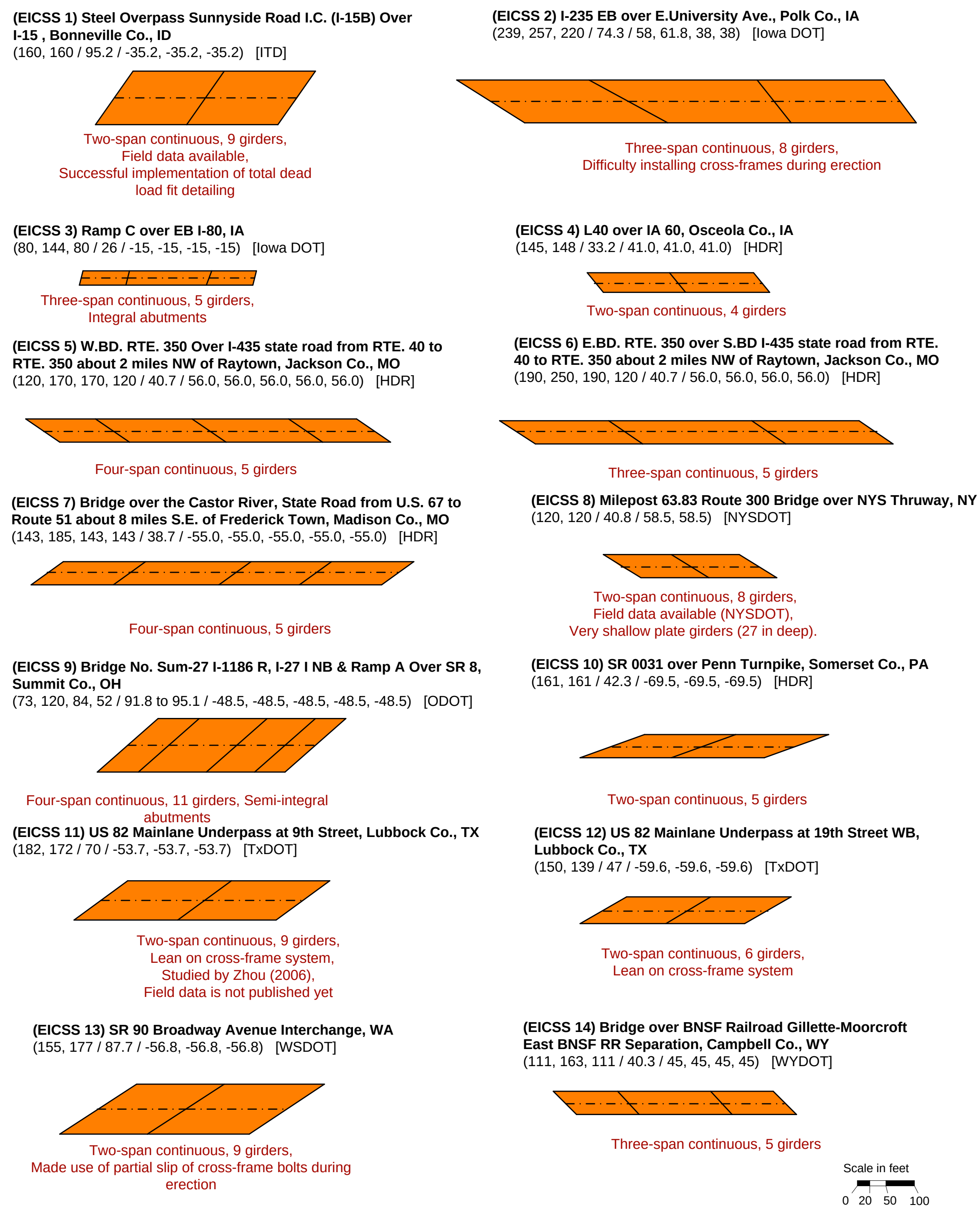

Figure 4.2. Existing I-girder bridges, Continuous-span, Straight with Skewed supports, (EICSS #) Description (LENGTH1, LENGTH2, ... / WIDTH / θ_{Left}, ..., θ_{Right}) [Source].

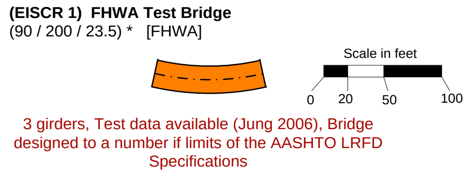

Figure 4.3. Existing I-girder bridges, Simple-span, Curved with Radial supports, (EISCR #) Description (LENGTH / RADIUS / WIDTH) [Source].

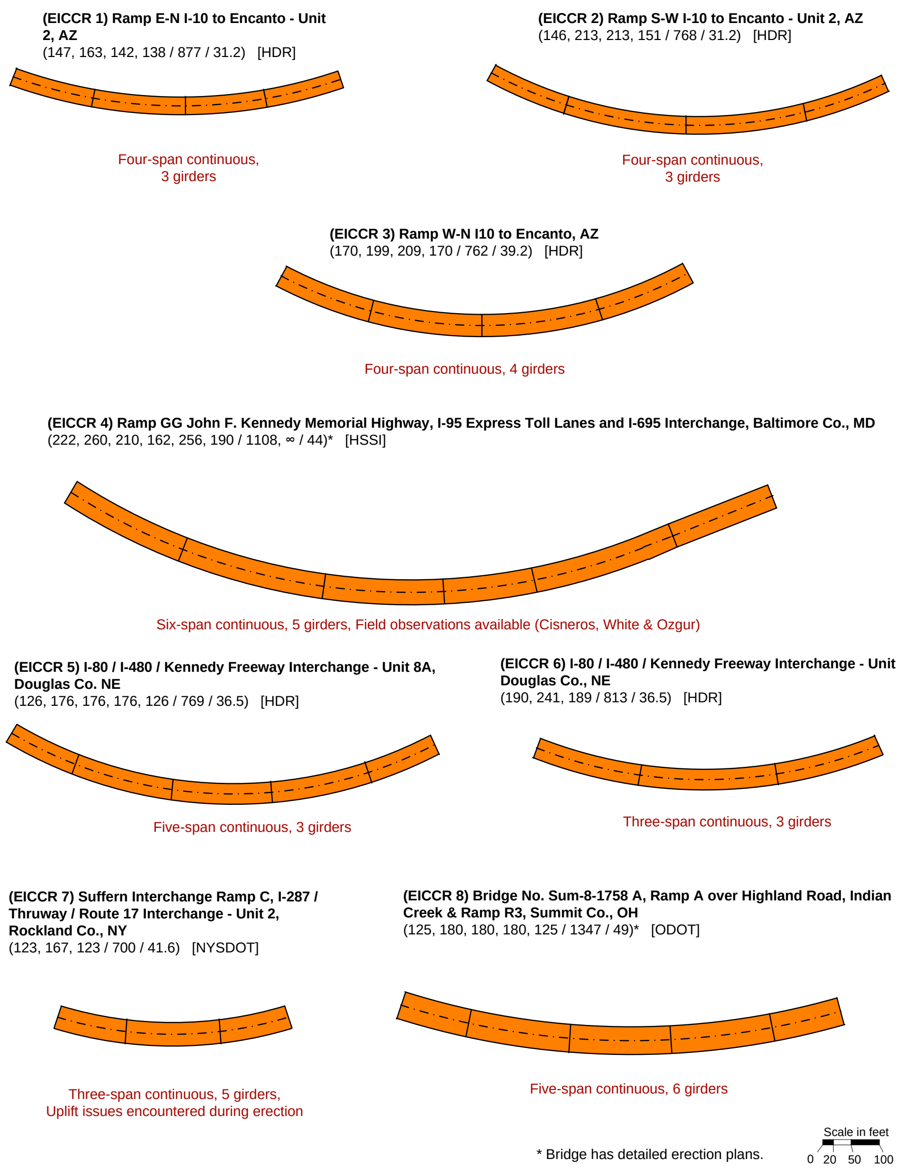

Figure 4.4. Existing I-girder bridges, Continuous-span, Curved with Radial supports, (EICCR #) Description (LENGTH1, LENGTH2, ... / RADIUS1, RADIUS2, .../ WIDTH) [Source].

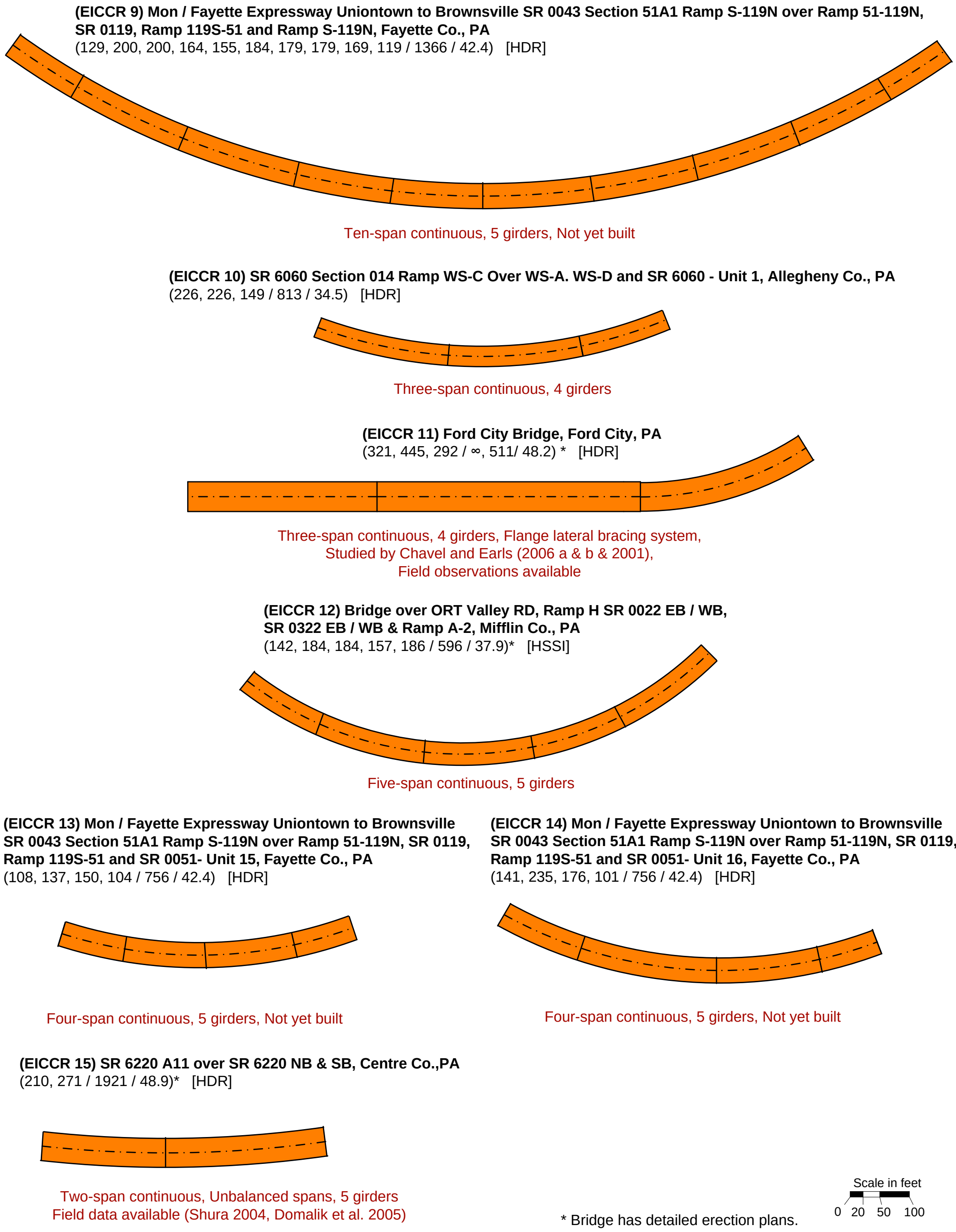

Figure 4.4. (continued). Existing I-girder bridges, Continuous-span, Curved with Radial supports, (EICCR #) Description (LENGTH1, LENGTH2, ... / RADIUS1, RADIUS2, .../ WIDTH) [Source].

(EICCR 16) SR 6026 Section CO2 over SR 0322 WB, Ramp N-W, SR 3007 & Ramp W-S- Unit 1, Centre Co., PA
(238, 334, 298 / 1940 / 46.9) [PennDOT]

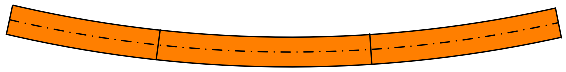

Three-span continuous, 5 girders,
Flange lateral bracing system, Study in progress (Linzell)

(EICCR 17) SR 6026 Section CO2 over SR 0322 WB, Ramp N-W, SR 3007 & Ramp W-S - Unit 2, Centre Co., PA
(298, 333, 266 / 1940 / 46.9) [PennDOT]

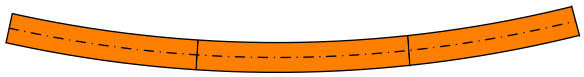

Three-span continuous, 5 girders,
Flange lateral bracing system, Study in Progress (Linzell)

(EICCR 18) Ramp G Over SR 0022, SR 0079, Campbells Run Road & Ramp F - Unit 1, Allegheny Co., PA
(182, 286, 236, 181 / 830 / 32.4)* [PennDOT]

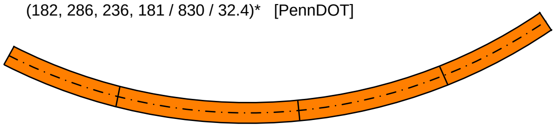

Four-span continuous, 5 girders,
Study in progress (Linzell)

(EICCR 19) Ramp G Over SR 0022, SR 0079, Campbells Run Road & Ramp F - Unit 2, Allegheny Co., PA
(206, 225, 208 / 830 / 32.4)* [PennDOT]

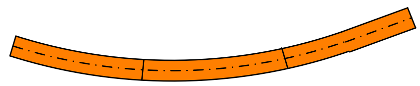

Three-span continuous, 5 girders,
Study in progress (Linzell)

(EICCR 20) PennDOT Structure #22737 (Structure #7A in construction documentation) at I-99 interchange, State College, PA
(296, 333, 266 / 1940 / 45.8)* [Linzell]

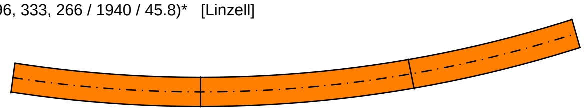

Three-span continuous, 5 girders,
Flange lateral bracing System, Field data available (Bell 2002)

(EICCR 21) SR 386 over Shute Lane, SR 6 and CSX Railroad, Sumner Co., TN
(237, 296, 237 / 1741 / 43.7) [TDOT]

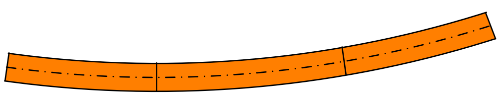

Three-span continuous, 5 girders

(EICCR 22) Ramp B over Briley Parkway and Ramp A, Davidson Co., TN
(141, 188, 188, 208, 157 / 449 / 44) [TDOT]

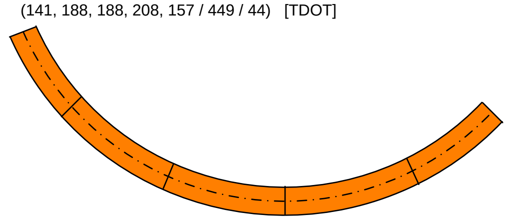

Five-span continuous, 5 girders,
Significantly curved

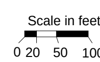

* Bridge has detailed erection plans.

Figure 4.4. (continued). Existing I-girder bridges, Continuous-span, Curved with Radial supports, (EICCR #) Description (LENGTH1, LENGTH2, ... / RADIUS1, RADIUS2, .../ WIDTH) [Source].

Figure 4.4. (continued). Existing I-girder bridges, Continuous-span, Curved with Radial supports, (EICCR #) Description (LENGTH1, LENGTH2, ... / RADIUS1, RADIUS2, .../ WIDTH) [Source].

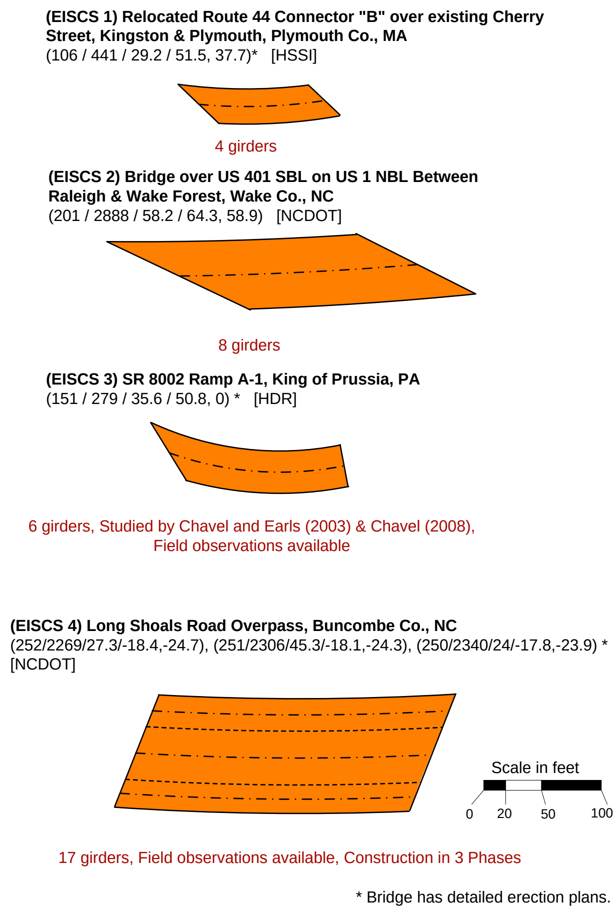

Figure 4.5. Existing I-girder bridges, Simple-span, Curved with Skewed supports, (EISCS #) Description (LENGTH / RADIUS / WIDTH / θ_{Left}, θ_{Right}) [Source].

Figure 4.6. Existing I-girder bridges, Continuous-span, Curved with Skewed supports, (EICCS #) Description (LENGTH1, LENGTH2, ... / RADIUS / WIDTH / θ_{Left}, ..., θ_{Right}) [Source].

(EICCS 12) SNI-A-BAR Rd. Over I-435 state road from RTE. 40 to RTE. 350 about 3.6 miles NW of Raytown, Jackson Co., MO
(60, 102, 92, 50 / 881 / 50.2 / -2.4, -6.4, -13.0, -18.9, -22.3)   [HDR]

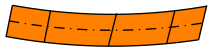

Four-span continuous, 5 girders

(EICCS 13) Bridge 5, West Dodge. 129th St. to I-680, Douglas Co., NE
(118, 128, 145 / 712, ∞, 699 / 32.7 / 0, 18.4, 18.8, 0)   [HDR]

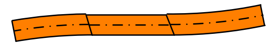

Three-span continuous, 4 girders

(EICCS 14) Abbott Drive Bridge, Abbott Drive over UPRR, Douglas Co., NE
(179, 168 / 1125, ∞ / 85.2 / -38, -42, -42)   [HDR]

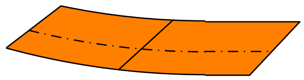

Two-span continuous, 8 girders,
Two different depths of cross-frames and girders

(EICCS 15) Suffern Interchange Ramp C, I-287 / Thruway / Route 17 Interchange - Unit 1, Rockland Co., NY
(148, 158 / 700 / 41.6 / 0, -49.5, -31.8)   [NYSDOT]

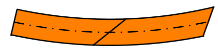

Two-span continuous, 5 girders,
Uplift issues encountered during erection

(EICCS 16) Bridge on Ramp BD over Greensboro Western Urban Loop, -RPCA-, and -CD- Between Bryan Blvd & US 220, Guilford Co., NC
(173, 171, 170 / 754 / 48.4 / 5.6, -2.6, 0, 0)   [HDR]

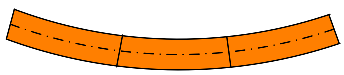

Three-span continuous, 5 girders

(EICCS 17) Bridge on Ramp BD over Bryan Blvd. and -RPD- between US 220 and Bryan Blvd, Guilford Co., NC
(117, 159 / 1574 / 48.4 / 0, 1.1, 0)   [HDR]

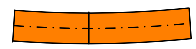

Two-span continuous, 5 girders

(EICCS 18) Bridge on Ramp CA over Bryan Blvd, and Ramp D between I-40 and Bryan Blvd, Guilford Co., NC
(107, 100, 110 / 754 / 48.4 / 0, -0.5, 0, 0)   [HDR]

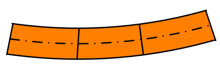

Three-span continuous, 5 girders

(EICCS 19) Bridge on Ramp CA over, Greensboro Western Urban loop, -RPD-, and -CD- BTN I-40 and Bryan Blvd, Guilford Co., NC
(100, 94, 82, 86 / 754 / 48.4 / 0, 0, 8.8, 2.6, 0)   [HDR]

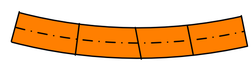

Four-span continuous, 5 girders

(EICCS 20) Bridge No. Sum-8-1757 B, Ramp B over Highland Road, Indian Creek & Ramp R3 & I-271, Summit Co., OH
(115, 170, 151, 182, 146 / 1347 / 49 / 0, 0, -20.7, 0, 0, 0)*   [ODOT]

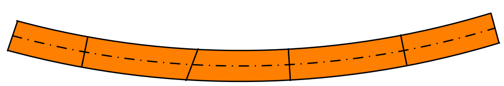

Five-span continuous, 6 girders

(EICCS 21) Grande Ronde River Bridge, Westbound Grande Ronde River Bridge Sec. Old Oregon Trail Hwy., Union Co., OR
(253, 177 / 951 / 50.9 / -31.1, -19.4, -27)   [ODOT]

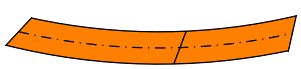

Two-span continuous,5 girders,
Stage 1, independent bridge structure in a phased construction

(EICCS 22) Grande Ronde River Bridge, Eastbound Grande Ronde River (Upper Perry) Bridge Sec. Old Oregon Trail Hwy., Union Co., OR
(240, 177 / 951 / 42.9 / -6.7, -20.4, -28.7)   [ODOT]

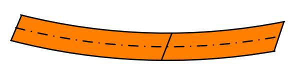

Two-span continuous, 4 girders

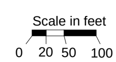

* Bridge has detailed erection plans.

Figure 4.6. (continued). Existing I-girder bridges, Continuous-span, Curved with Skewed supports, (EICCS #) Description (LENGTH1, LENGTH2, ... / RADIUS / WIDTH / θ_{Left}, ..., θ_{Right}) [Source].

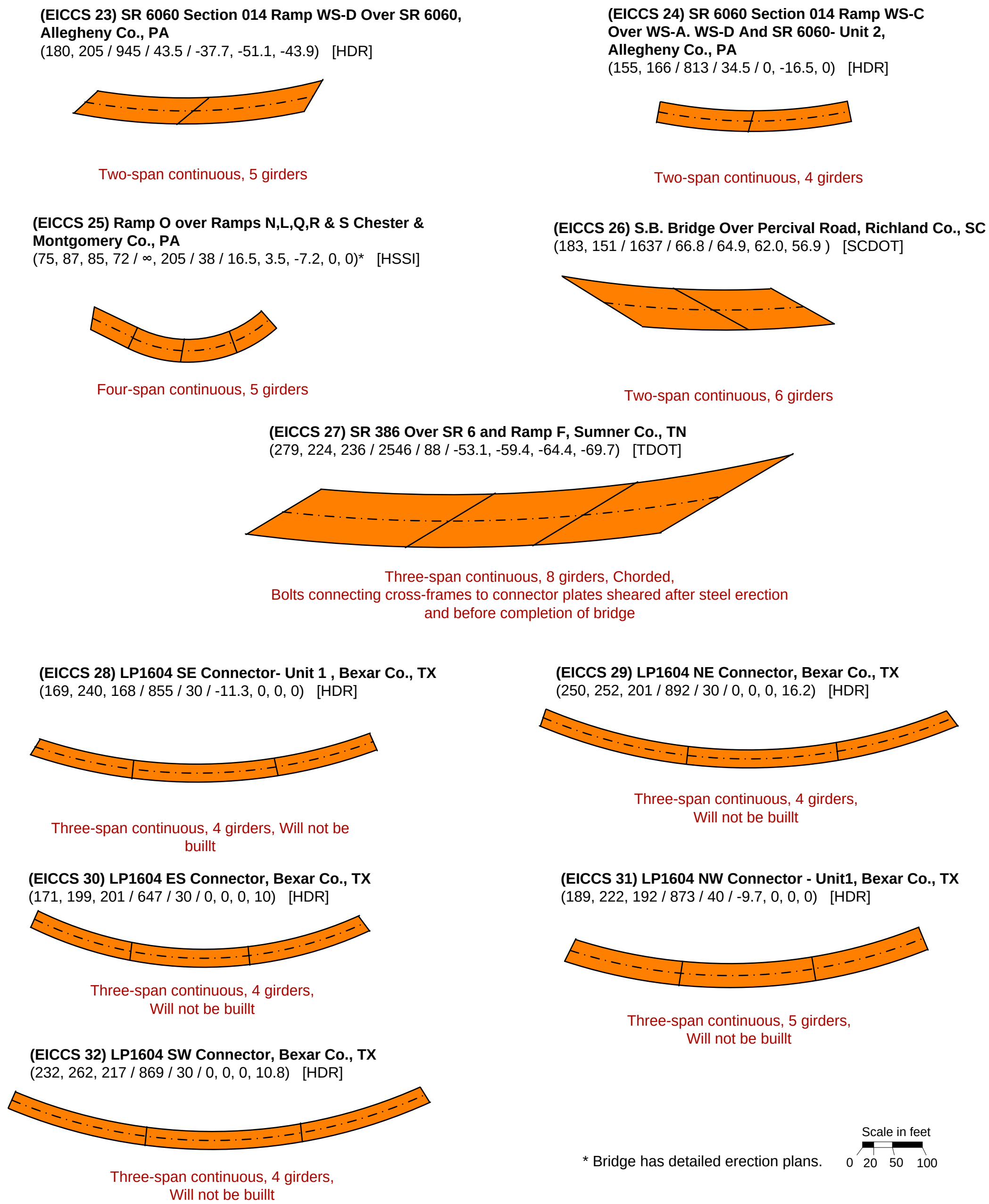

Figure 4.6. (continued). Existing I-girder bridges, Continuous-span, Curved with Skewed supports, (EICCS #) Description (LENGTH1, LENGTH2, ... / RADIUS / WIDTH / θ_{Left}, ..., θ_{Right}) [Source].

(EICCS 33) I-95 Southbound (Bridge B610) I95 / I-395 / I-495 Interchange, Fairfax Co., VA
(223, 273, 271 / 1308 / 59.5 / 0, -20.1, 0, 0)* [HSSI]

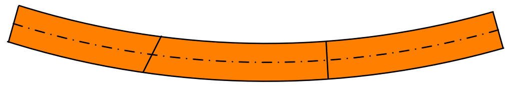

Three-span continuous, 6 girders

(EICCS 34) B-40-1111 Marquette Interchange - Unit 2, Milwaukee Co., WI
(116, 132, 144, 172, 170, 175, 110 / 1410, ∞, / 58.9 / -4.31, 0, 0, -10.7, -28.1, -28.1, -28.1, -28.1)***** [WisDOT]

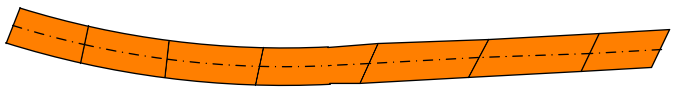

Seven span continuous, 5 I-girders

(EICCS 35) B-40-1211 Marquette Interchange - Unit 2, Milwaukee Co., WI
(119, 137, 188, 171, 195, 150 / 1450, ∞ / 58.9 / 8.54, 0, 0, -11.5, -27.5, -27.5, -27.5)* [WisDOT]

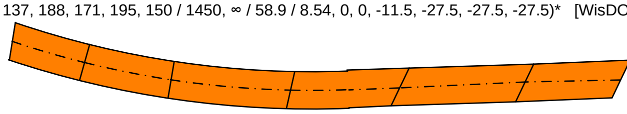

Six span continuous, 5 I-girders

* Bridge has detailed erection plans.

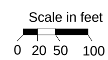

Figure 4.6. (continued). Existing I-girder bridges, Continuous-span, Curved with Skewed supports, (EICCS #) Description (LENGTH1, LENGTH2, ... / RADIUS / WIDTH / θ_{Left}, ..., θ_{Right}) [Source].

(ETSSS 1) Sheffield Rd. Over The Green River, Great Barrington, MA
(139 / 49.6 / -15, -15) [Tensor]

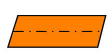

Simple span, Three tub-girders

(ETSSS 2) Sylvan Bridge over Sunset Hwy, Multnomah Co. OR
(205/58.7/33.4,33.4), (205/58.7/33.4,33.4) [ODOT]

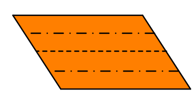

Simple span, Six tub-girders
Phased Construction

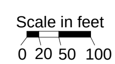

Figure 4.7. Existing Tub-girder bridges, Simple-span, Straight with Skewed supports, (ETSSS #) Description (LENGTH / WIDTH / θ_{Left}, θ_{Right}) [Source].

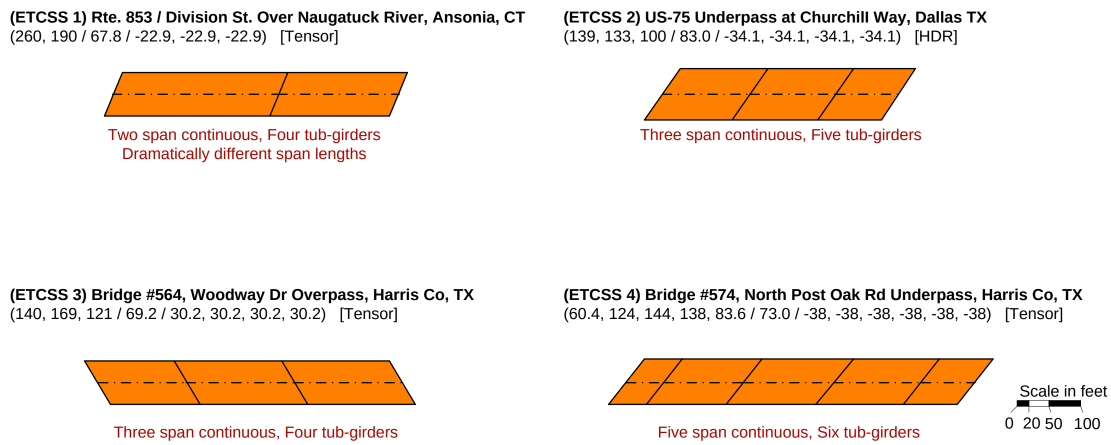

Figure 4.8. Existing Tub-girder bridges, Continuous-span, Straight with Skewed supports, (ETCSS #) Description (LENGTH1, LENGTH2, … / WIDTH / θ_{Left}, …, θ_{Right}) [Source].

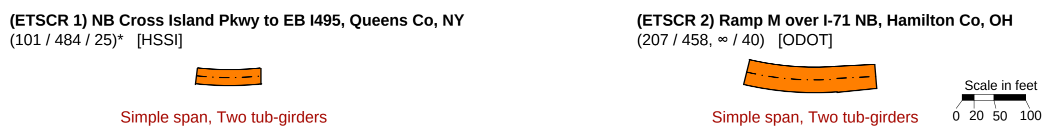

Figure 4.9. Existing Tub-girder bridges, Simple-span, Curved with Radial supports, (ETSCR #) Description (LENGTH / RADIUS / WIDTH) [Source].

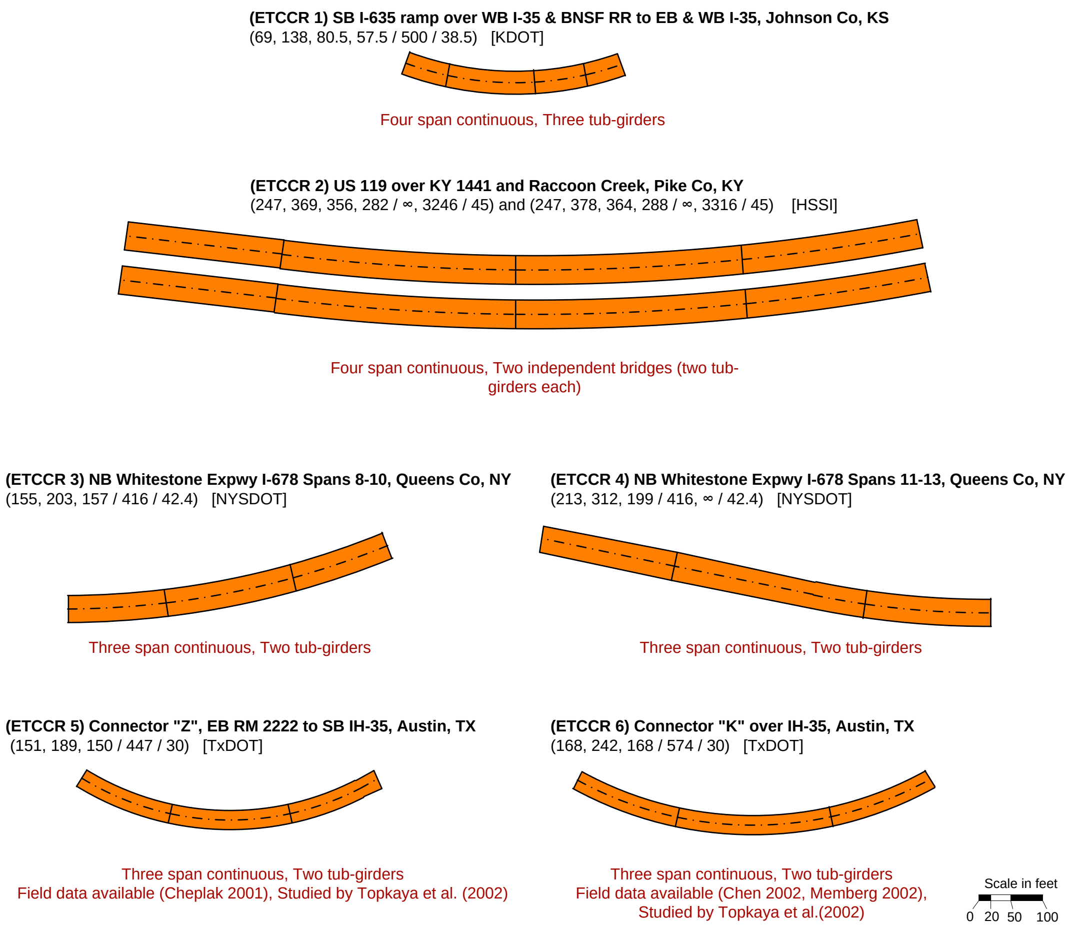

Figure 4.10. Existing Tub-girder bridges, Continuous-span, Curved with Radial supports, (ETCCR #) Description (LENGTH1, LENGTH2, … / RADIUS1, RADIUS2, … / WIDTH) [Source].

(ETCCR 7) DC02 Spans 1&2 IH-30 PGBT Interchange, Dallas, TX
(164, 164 / 895 / 29) [HDR]

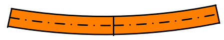

Two span continuous, Two tub-girders

(ETCCR 8) DC03 Spans 13&14 IH-30 PGBT Interchange, Dallas, TX
(155, 155 / 1010 / 29) [HDR]

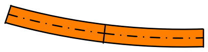

Two span continuous, Two tub-girders

(ETCCR 9) DC03 Spans 15&16 IH-30 PGBT Interchange, Dallas, TX
(170, 170 / 1010 / 29) [HDR]

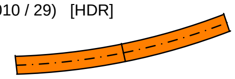

Two span continuous, Two tub-girders

(ETCCR 10) DC03 Spans 1, 2&3 IH-30 PGBT Interchange, Dallas, TX
(149, 189, 149 / 1010 / 29) [HDR]

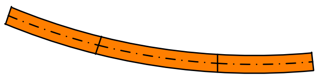

Three span continuous, Two tub-girders

(ETCCR 11) DC03 Spans 4&5 IH-30 PGBT Interchange, Dallas, TX
(167, 191 / 1010 / 29) [HDR]

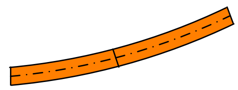

Two span continuous, Two tub-girders

(ETCCR 12) DC04 Spans 22&23 IH-30 PGBT Interchange, Dallas, TX
(165, 165 / 2060 / 29) [HDR]

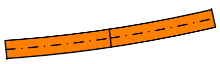

Two span continuous, Two tub-girders

(ETCCR 13) DC04 Spans 24, 25&26 IH-30 PGBT Interchange, Dallas, TX
(204, 254, 204 / 2060 / 29) [HDR]

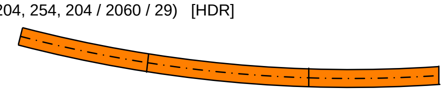

Three span continuous, Two tub-girders

(ETCCR 14) Connector EB North Beltway 8 to NB I-45, Houston, TX
(186, 286, 180 / 895 / 40.8) [TxDOT]

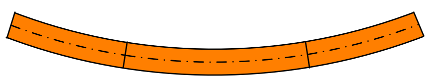

Three span continuous, Two tub-girders
Field data available (Fan 1999)

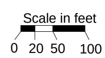

Figure 4.10. (continued). Existing Tub-girder bridges, Continuous-span, Curved with Radial supports, (ETCCR #) Description (LENGTH1, LENGTH2, … / RADIUS1, RADIUS2, … / WIDTH) [Source].

Figure 4.10. (continued). Existing Tub-girder bridges, Continuous-span, Curved with Radial supports, (ETCCR #) Description (LENGTH1, LENGTH2, … / RADIUS1, RADIUS2, … / WIDTH) [Source].

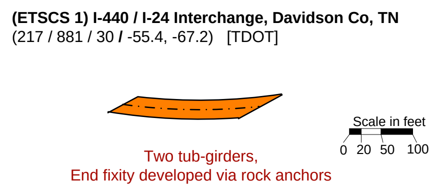

Figure 4.11. Existing Tub-girder bridges, Single-span, Curved with Skewed supports, (ETSCS #) Description (LENGTH / RADIUS / WIDTH / θ_{Left}, θ_{Right}) [Source].

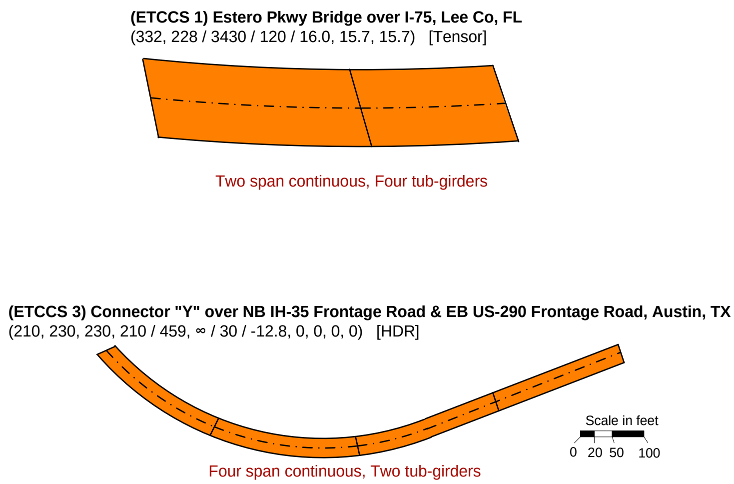

Figure 4.12. Existing Tub-girder bridges, Continuous-span, Curved with Skewed supports, (ETCCS #) Description (LENGTH1, LENGTH2, … / RADIUS1, RADIUS2, … / WIDTH / θ_{Left}, …, θ_{Right}) [Source].

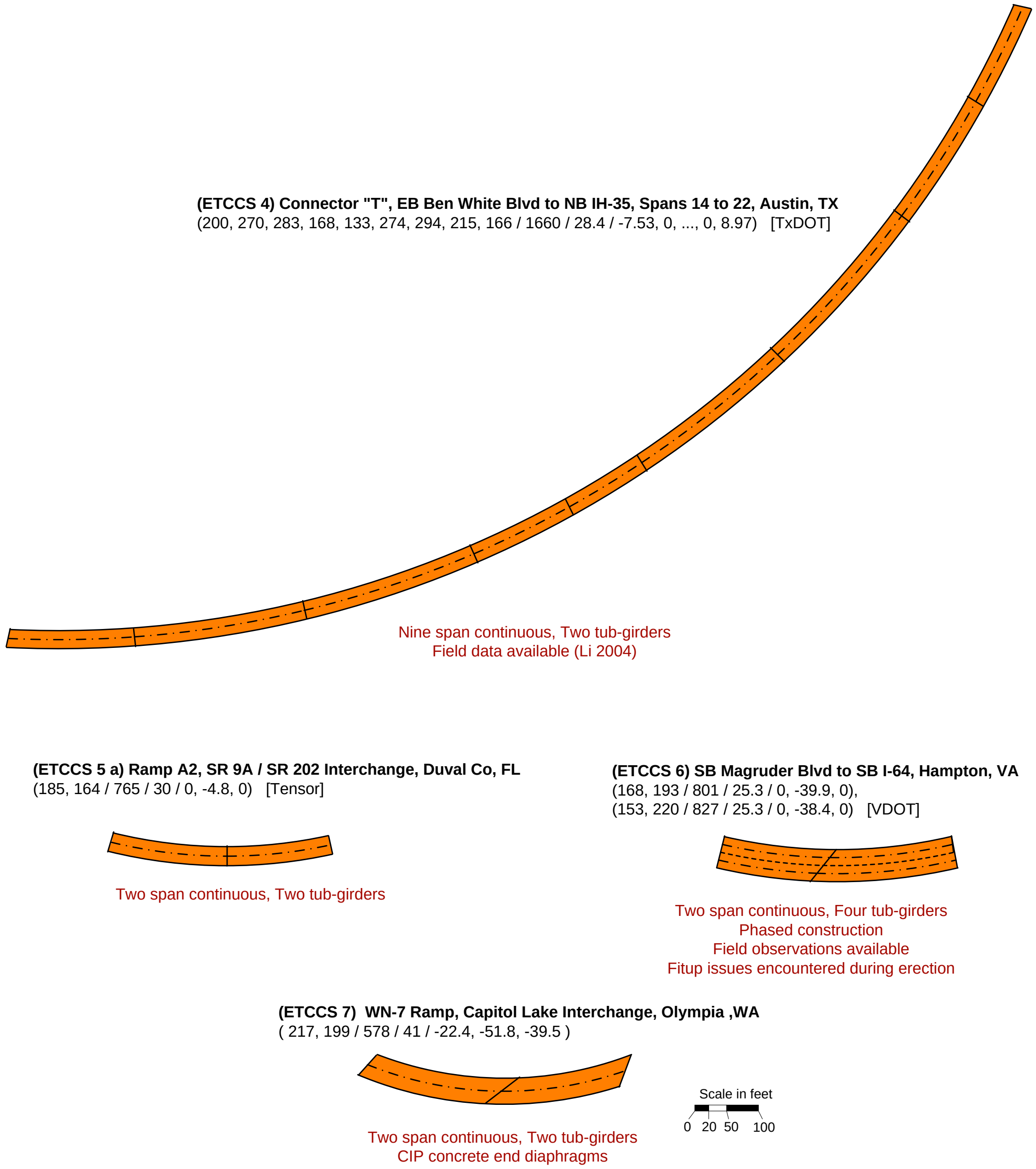

Figure 4.12. (continued). Existing Tub-girder bridges, Continuous-span, Curved with Skewed supports, (ETCCS #) Description (LENGTH1, LENGTH2, … / RADIUS1, RADIUS2, … / WIDTH / θ_{Left}, …, θ_{Right}) [Source].

Only twelve of the I-girder bridges in the above figures had both (1) measurements or field observations of some type during construction as well as (2) detailed construction plans. Four tub-girder bridges had measurements or field observations of some type during construction and six tub-girder bridges had detailed construction plans. Furthermore, the extent of the field measurements was generally limited. Detailed field measurements and observations were taken for the bridge EICCR22a by the NCHRP 12-79 project team during the course of the NCHRP 12-79 research (Leon, 2011). A number of the bridges were indicated as being very successful projects, with the bridge responding as predicted with respect to aspects such as initial layover of the webs but with the girders approaching a plumb condition under total dead load. A number of cases were cited as having a range of field problems including difficulty of fit-up, or unexpected final geometries.

In addition to the above existing bridges, a number of useful detailed LRFD example bridge designs have been published in the recent literature. Figure 4.13 summarizes the plan geometries of several of these hypothetical bridges. The straight, non-skewed bridges in these examples were selected as base-line problems for the project calculations. That is, they were selected to gage the accuracy of the analysis methods for bridges without any curvature or skew. The results for these cases serve as useful base-line benchmarks for decisions about the levels of accuracy sufficient for bridges with more complex geometries.

The selection of the existing and example bridges for inclusion in the Project overall parametric study is addressed subsequently in the discussion of the main analytical studies.

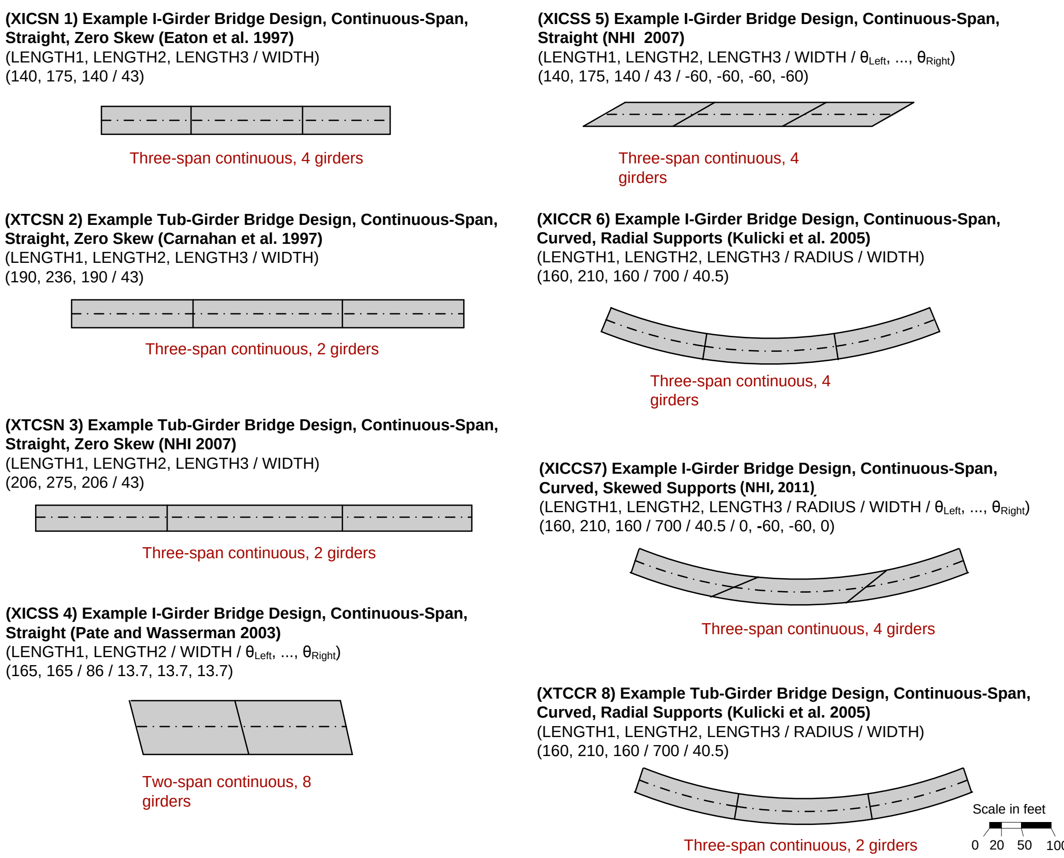

Figure 4.13. AASHTO LRFD example bridge designs.

4.3 Selection of Geometric Factors

4.3.1 Identification of Primary Geometric Factors

It was clear that if NCHRP 12-79 was to consider analysis accuracy for curved and/or skewed steel I- and tub-girder bridges, then the project would need to consider the following factors in the design of its parametric studies:

- Some measure of the horizontal curvature and
- Some quantification of the skew magnitude and pattern.

Furthermore, it was apparent that the bridge responses, and hence the analysis accuracy, can be affected significantly by the magnitude of the span lengths as well as the span length-to-width ratios. Longer span bridges tend to be affected more substantially by dead load effects, potentially resulting in more significant stability considerations during construction. In addition, beyond a certain span length, I-girder bridges are more likely to need partial or full-span horizontal flange-level bracing systems to ensure adequate stability and sufficient resistance to lateral loads during construction. Flange lateral bracing systems cause portions of the structure to act as “pseudo-box girders,” fundamentally changing the behavior of the structural system. Furthermore, longer bridges generally exhibit larger overall deflections. These larger overall deflections can lead to larger relative deflections at certain locations in the structural system, which can sometimes be problematic during construction. Longer span bridges often have a smaller ratio of the girder spacing relative to the girder depths, and typically have larger girder depth-to-flange-width ratios. These attributes can fundamentally affect various relative deflections in the structure as well as local and overall behavior and analysis accuracy at the different stages of construction.

In addition, the bridge span length-to-width ratios can significantly impact the influence of skew. Skewed bridges with smaller span length-to-width ratios tend to have more significant load transfer to the bearing lines across the width of the structure, and hence more significant “nuisance stiffness” effects that need to be addressed in the design. Furthermore, relatively narrow horizontally curved bridges experience a greater torsional “overturning component” of the reactions, which tends to increase the vertical reactions on the girders further from the center of curvature and decrease the vertical reactions on the girders closer to the center of curvature. In addition, relatively wide horizontally-curved bridges can have more substantial concerns related to overturning at intermediate stages of the steel erection, prior to assembly of the girders across the full width of the bridge cross-section. These spans become more stable as additional girders are erected and connected by cross-frames across the width of the bridge. Wide horizontally-curved bridges also can have greater concerns associated with overturning forces during deck placement.

Lastly, it was apparent that the bridge responses (and the analysis accuracy) can be significantly affected by whether the spans are simply-supported or continuous. Simple-span bridges tend to have larger deflections for a given geometry, and potentially can be more difficult to handle during construction. Although simple-span girders can see negative bending during erection (due to lifting or temporary support from holding cranes, etc.), continuous-spans have more significant negative bending considerations. Furthermore, particularly in I-girder bridges, continuous-span bridges can have significant interactions between adjacent spans with respect to both major-axis bending as well as the overall torsional response.

All of the above factors can have a substantial influence on the many detailed structural attributes of steel I-girder and tub-girder bridges. Also, there can be significant interactions between these factors in terms of their influence on the bridge responses, as well as the accuracy of different bridge analysis methods.

If one considers the many detailed attributes of steel I- and tub-girder bridge structural systems and their members and components addressed subsequently, the combinations and permutations of potential bridge designs become endless. Hence, it was decided that the most practical way of covering the design space of curved and/or skewed I-girder and tub-girder bridges was to consider a range of practical combinations and permutations of the following primary factors:

- Span length of the bridge centerline, L_s,
- Deck width normal to the girders, w, (in phased construction projects, w is determined separately for each bridge unit)
- Horizontal curvature, of which the most appropriate characterization is discussed below,
- Skew angle of the bearing lines relative to the bridge centerline, θ,
- Skew pattern of the bearing lines, of which the most appropriate characterization is discussed below, and
- Span type, simple and various types of continuous-spans.

4.3.1.1 Characterization of Horizontal Curvature

The NCHRP 12-79 project team identified the torsion index, I_T, discussed in Section 3.1.4 as a useful measure of the degree of curvature of the bridge spans at an early stage of the project. This parameter is closely related to the magnitude of the overall torsion that exists in the bridge (or bridge unit).

For curved simple-span radially supported I-girder bridges, the NCHRP 12-79 project team selected horizontal curvature values by first conducting basic estimates to determine the largest curvature (smallest *R*) that could be tolerated without having uplift at the most critical bearing location(s) under nominal dead plus live loads. This value of *R* was used as the most extreme value for the horizontal curvature. This radius of curvature then was increased 1.5 times to obtain cases with smaller curvature (larger *R*). This approach produced lower- and upper-bound values of I_T equal to 0.58 and 0.71 respectively. Continuous-span bridges can tolerate higher torsion indices due to continuity with the adjacent spans. Therefore, for curved continuous-span radially supported I-girder bridges, lower and upper bound values of I_T were obtained as 0.66 and 0.88 respectively.

Similarly, for curved simple-span radially supported tub-girder bridges, the smallest radius of curvature was estimated to avoid uplift at the supports under nominal dead load plus live loads. Tub-girder bridges tend to have relatively high torsion indices compared to I-girder bridges with similar deck geometry due to the shorter length between the fascia girder bearings. The estimated minimum radius of curvature was then increased 1.5 times. This resulted in lower and upper bound values of I_T equal to 0.72 and 0.87 respectively. For continuous-span radially supported tub-girder bridges, the lower and upper bound values of I_T were obtained as 0.69 and 1.14 respectively.

4.3.1.2 Characterization of Skew Pattern

There are a number of factors related to the representation of the skew pattern for practical designs. Figure 4.14 shows a number of possible combinations of θ values and skew patterns on individual straight I-girder bridge spans with w = 80 ft. and L = 250 ft. In general, various combinations of these arrangements are practical for continuous-span bridges. The first four cases in the figure have parallel bearing lines, that is, equal skew of the end supports. The four values of skew shown are 20, 35, 50 and 70^o. The 20^o skew case is significant since the AASHTO LRFD Specifications permit the cross-frames to be oriented parallel to the bearing lines up to this limit. The 70^o skew case is the maximum skew angle considered in prior NCHRP studies on deck effective widths (Chen, 2005). In addition, as summarized subsequently, this is the maximum value of the skew encountered in the existing I-girder bridges shown in the previous section. The 35^o skew is considered as a practical median skew value between zero and 70^o, and 50^o was selected as an appropriate large skew angle between 35^o and the relatively extreme value of 70^o.

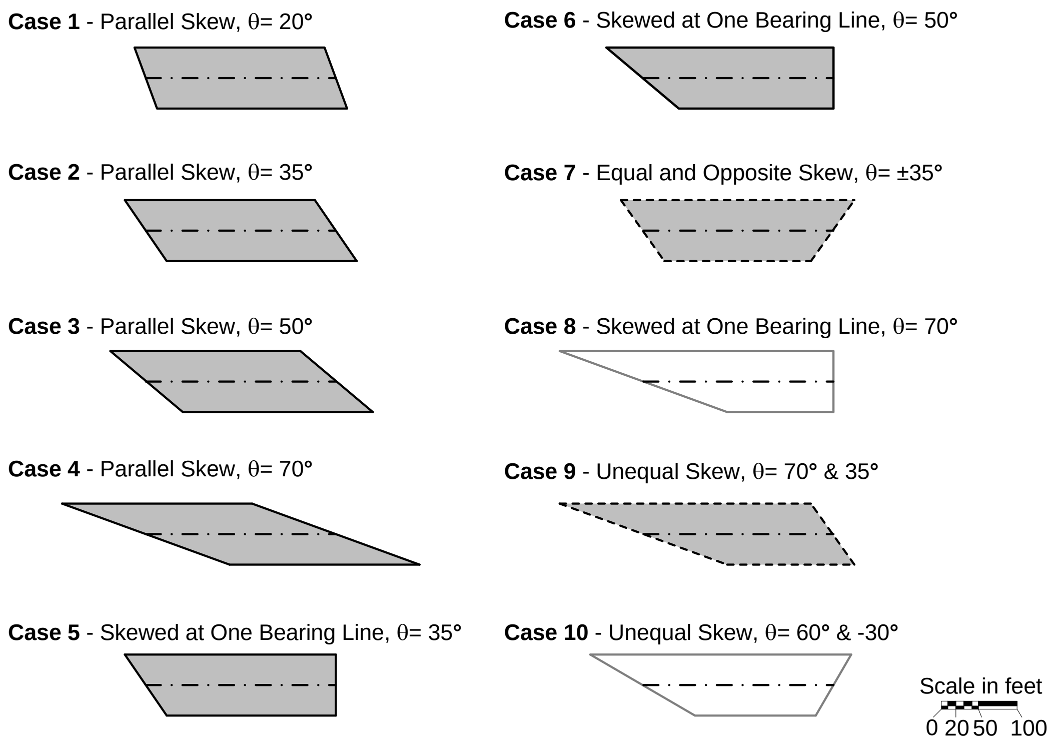

Figure 4.14. Potential skew combinations for straight I-girder bridge spans with *w*=80 ft. and L_s=250 ft.

The other sketches in Figure 4.14 show a number of representative unequal skew arrangements on individual straight spans in I-girder bridges. Cases 5 and 6 in the figure entail a situation where, due to a site geometry constraint existing at only one position, only one of the bearing lines is skewed. Case 7 shows a possible case where the bearing lines are skewed equally but in opposite directions. This case is considered to be more unusual, or exceptional. However, interestingly, the bearing line orientations for this case are exactly what one would encounter with a curved radially-supported span and L_s/R = 0.70. The outline of the deck is dashed in this case to highlight the fact that this geometry is considered exceptional. Case 8 is similar to Cases 5 and 6, but with a 70^o skew. This case illustrates a situation where, due to the extreme skew of the left-hand bearing line, the span length on one side of the deck is more than two times that on the other side of the deck, i.e., $L_2/L_1 > 2$. A value of $L_2/L_1 = 2$ was considered to be a practical maximum limit by the NCHRP 12-79 project team. It should be noted that if the span length of the centerline were larger, or if the deck width w were smaller for this case, this L_2/L_1 limit would not be exceeded. The outline of the deck geometry for Case 8 is shown as a grey line and the deck plan is shaded white to emphasize that this deck geometry is considered impractical. The above L_2/L_1 limit can be satisfied with $\theta = 70^o$ if the bearing lines are parallel as in Case 4, or if the bearing lines are unequally skewed such as in Case 9. Lastly, Case 10 shows an extreme situation of unequal skew in opposite directions for the two bearing lines. In this case, the bearing lines are oriented at 90^o relative to one another. The project team decided that one would practically never encounter a relative angle between adjacent bearing lines of more than 90^o. This type of bearing arrangement could occur for example if the span were crossing the corner of a rectangular lot and the bearing lines had to be placed parallel to the sides of the lot. Note that $L_2/L_1 > 2$ for Case 10; however, if the span is larger or the deck width is smaller, the $L_2/L_1 \leq 2$ limit could be satisfied.

The skew arrangements on straight tub-girder bridges can be similar to those considered in Figure 4.14. However, tub-girder bridges generally tend to have smaller skew values, due to the expected sensitivity of these types of bridges to skew effects as well as the fabrication difficulties and increased cost associated with complex skewed diaphragm connection details.

Figure 4.15 shows the various possible combinations of horizontal curvature and approximately $\pm$ 15 and 30^o skew on individual tub-girder bridge spans with $L_s = 150$ ft., $w = 30$ ft. and $R = 400$ ft. Again, various combinations of these arrangements are possible for continuous-span bridges. The skew and horizontal curvature combinations in Figure 4.15 are similar to those shown for the straight bridge spans in Figure 4.14. However, whereas a number of patterns with positive and negative skew produce the same net geometry in straight bridges, these positive and negative skew values give different geometries in similar curved bridges, due to the horizontal curvature. Fourteen total combinations are shown in Figure 4.15 that need to be considered in general. A large number of these combinations may be considered as exceptional cases and are drawn with dashed lines. Note that for Cases 2, 5 and 9 in Figure 4.15, the magnitudes of the skew angles are modified slightly to make the bearing lines parallel.

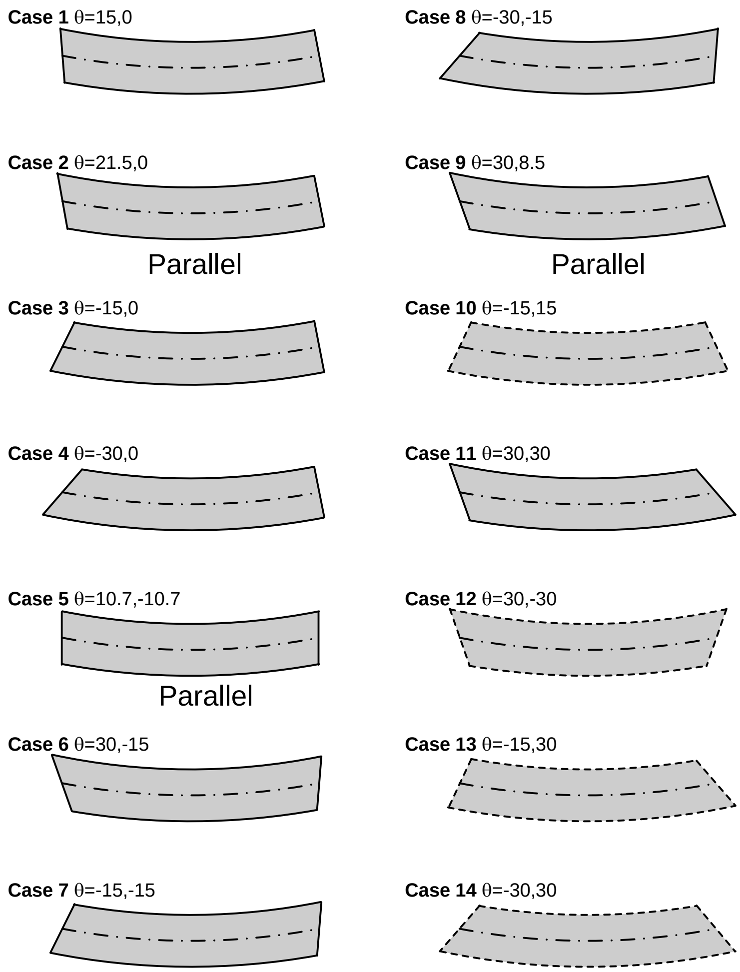

Figure 4.15. Example potential skew and horizontal curvature combinations for curved tub-girder bridge spans with w = 30 ft., L_s = 150 ft. and R = 400 ft.

The possible combinations of skew and horizontal curvature for I-girder bridges are similar to those shown in Figure 4.15, except that as noted previously, somewhat larger skew values can be accommodated generally in I-girder bridges. However, the extent of these patterns is limited by:

- A maximum limit on the ratio of the span lengths of the outside and inside edges of the deck, L_{so}/L_{si}, of 2, and
- A maximum limit on the orientation of adjacent bearing lines of 90^o

similar to the limits discussed previously for the straight skewed bridges. Lastly, for highly-curved spans, the Project team recognized that the skew angle at the inside edge of the deck can be substantially larger than that at the deck centerline. This is illustrated by Figure 4.16. It was decided that it is not practical for the skew angle at the inside edge of the deck to be greater than 70° in these cases.

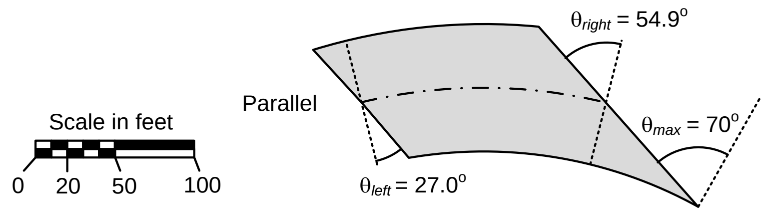

Figure 4.16. Highly-curved span with a skew angle of 70° at the inside edge of the deck and 54.9° at the centerline of the deck, w = 80 ft., L_s = 150 ft., R = 308 ft.

All of the above factors can have a substantial influence on the many detailed structural attributes of steel I-girder and tub-girder bridges. Also, there can be significant interactions between these factors in terms of their influence on the bridge responses, as well as the accuracy of different bridge analysis methods.

4.3.2 Synthesis of Primary Factor Ranges from the Collected Bridges

Upon synthesis of the primary factors from the existing bridges collected by NCHRP 12-79, the following ranges of these factors were observed:

- Span length, L_s
  - I-Girder
    - 120 to 254 ft. (straight simple-spans with skewed supports)
    - 90 ft. (curved simple-spans with radial supports)
    - Only one bridge was identified as curved simple-span with radial supports; this was the FHWA Test bridge, EISCR1.
    - 106 to 252 ft. (curved simple-spans with skewed supports)
    - 119 to 445 ft. (straight continuous-spans with zero skew)
    - 73 to 257 ft. (straight continuous-spans with skewed supports)
    - 101 to 334 ft. (curved continuous-spans with radial supports)
    - 50 to 279 ft. (curved continuous-spans with skewed supports)

- Tub-Girder
  - 139 to 205 ft. (straight simple-spans with skewed supports)
  - 101 to 207 ft. (curved simple-spans with radial supports)
  - 217 ft. (curved simple-spans with skewed supports)
  - Only one bridge was identified as curved simple-span with skewed supports; this was the bridge ETSCS1.
  - 57.5 to 373 ft. (curved continuous-spans with radial supports)
  - 153 to 332 ft. (curved continuous-spans with skewed supports)

- Deck width (per unit in cases involving phased construction), *w*
  - I-Girder
    - 24 to 87.5 ft. (spans with skew)
    - 30 to 71 ft. (spans with radial supports, with the exception of the EISCR1 FHWA test bridge, which was 23.5 ft.)
  - Tub-Girder
    - 25 to 45 ft. (spans with two tub-girders)
    - 36 ft. to 120 ft. (spans with more than two tub-girders)
- Torsion Index, I_T
  - I-Girder
    - 0.48 to 0.87
  - Tub-Girder
    - 0.50 to 1.14 (spans with two tub-girders; an I_T larger than 1.0 is possible due to continuity with adjacent spans)
    - 0.50 to 0.84 (spans with more than two tub-girders)
- Skew angle of the bearing lines relative to a tangent to the bridge centerline, θ
  - I-Girder
    - 0 to 69.5^o (straight bridges)
    - 0 to 64.3^o (curved bridges)
  - Tub-Girder
    - 0 to 12.8^o (spans with two tub-girders, excluding the ETCCS7 bridge, which had CIP concrete end diaphragms and non-typical bearing details)
    - 0 to 38.9^o (spans with more than two tub-girders)
- Skew pattern
  - I-Girder
    - The bearing lines were parallel in most of the collected I-girder bridges.
    - One straight bridge (EICSS2) has $\theta = 61.8^o$ & 38^o in one span.
    - One curved bridge (EICCS15) has $\theta = 0^o$ & 49.5^o resulting in a 19.8^o differ-ence in orientation between the bearing lines in one span.
    - One curved bridge (EICCS5) has $\theta = 0^o$ & 60.2^o resulting in a 72^o difference in orientation between the bearing lines in one span.

- Tub-Girder
  - All the skewed spans have non-parallel bearing lines for the collected bridges that are composed of two tub-girders.
  - One curved bridge with two tub-girders (ETCCS3) has $\theta = 0^o$ & 12.8^o and a 39.0^o difference in orientation between the bearing lines.
  - One curved bridge with two tub-girders (ETCCS7) has $\theta = 51.8^o$ & 39.5^o and a 32.0^o difference in orientation between the bearing lines; however, this bridge has cast-in-place (CIP) concrete end diaphragms and non-typical bearing details.
  - Most of the skewed spans with more than two tub-girders have parallel bearing lines.
  - One two-span continuous curved bridge with four tub-girders (ETCCS6), constructed in two phases with two girders in each phase, has $\theta = 0^o$ & 38.9^o and a difference in orientation of 53.8^o between the bearing lines in one span. However, no cross-frames or diaphragms are placed between the girders at the interior bearing line on this bridge, and this bridge does not contain any internal intermediate cross-frames or diaphragms.

- Type-of-span
  - I-Girder
    - Most of the collected I-girder bridges are continuous-span.
    - Ratio of exterior-to-interior span lengths: 0.56 to 1.25
    - Ratio of adjacent interior span lengths: 0.63 to 1.0
    - Ratio of span lengths, 2-span continuous: 0.77 to 1.0
  - Tub-Girder
    - Most of the collected tub-girder bridges are continuous-span.
    - Ratio of exterior-to-interior span lengths: 0.49 to 1.0
    - Ratio of adjacent interior span lengths: 0.49 to 1.0
    - Ratio of span lengths, 2-span continuous: 0.69 to 1.0
    - A fraction of the bridges with more than two tub-girders are simple-span.

The values for several additional "secondary" parameters discussed in the above, but not selected as primary factors were:

- Span length to deck width ratio, L_s/w (per unit in phased construction jobs)
  - I-Girder
    - 0.55 to 14.77 (spans with skew)
    - 1.67 to 8.83 (curved spans with radial supports)
  - Tub-Girder
    - 2.80 to 8.76 (radially-supported spans with two tub-girders)
    - 4.66 to 10.35 (skewed spans with two tub-girders)
    - 0.83 to 3.83 (skewed spans with more than two tub-girders)

- Subtended angle of the span's centerline, L_s/R
  - I-Girder
    - 0.0 to 0.57 radians (32.6^o)
  - Tub-Girder

0.0 to 0.68 radians (39.0°) (spans with two tub-girders)
0.07 to 0.28 radians (16.0°) (spans with more than two tub-girders)

In addition to the above parameters, several additional key indices that correlate with the accuracy of different simplified analysis methods were identified during the course of the NCHRP 12-79 research. These indices are discussed in Chapter 3. The ranges of values among the collected bridges for these indices are as follows.

- Skew index, I_S
  - I-Girder
    - 0.05 to 1.93
  - Tub-Girder
    - 0.08 to 0.77 (spans with two tub-girders)
    - 0.01 to 0.18 (spans with more than two tub-girders)
- Connectivity index, I_C
  - I-Girder
    - 0.35 to 18.75
  - Tub-Girder
    - The connectivity index is not applicable to tub-girder bridges
- Girder length index, I_L
  - I-Girder
    - 1.0 to 1.51
  - Tub-Girder
    - 1.0 to 1.09

4.3.3 Selection of Primary Factor Ranges and Levels

Table 4.1 shows the ranges and levels of the primary factors that were selected for the main analytical study of NCHRP 12-79. These primary factors are discussed in detail in the preceding sections.

The first row of Table 4.1 addresses the type of span. This factor is addressed in a similar fashion for both the I- and tub-girder bridges. Three-span continuous designs with one balanced end span and one end span of equal length to the main span capture both the behavior associated with drop-in spans as well as the interactions between balanced and unbalanced continuous-spans. However, two-span continuous bridges are apt to be more sensitive to skew effects. Also, the potential combinations of skew arrangements become large as the number of spans is increased. Many of these combinations would have a minor effect on the final analysis accuracy assessments though, due to the fact that the influence of the skew at a particular bearing line tends to die out as one moves several spans away from this bearing line. Furthermore, long multi-span curved bridges often may have only a few skewed bearing lines because of geometry constraints at a particular location, whereas it may be possible to orient other bearing lines radially. This can be understood by considering cases such as EICCS1 and EICCS5 in Figure 4.6. In these structures, one would quickly reach the maximum practical θ value of approximately 70^{o} if, for instance, all the bearing lines were parallel.

It was desired to study several continuous-span bridges that had significant unbalanced span lengths. This consideration was addressed by inserting selected existing bridges into the matrix of parametric study bridges. Also, bridges with more than three spans were considered by insertion of a number of existing bridges into the overall parametric study matrix.

The second row of Table 4.1 shows the values selected for the span length. For both I- and tub-girder bridges, the selected lengths for simple-spans were 150, 225 and 300 ft. and the selected lengths for continuous-spans were 150, 250 and 350 ft. The maximum span length of L_s = 350 ft. was selected to match the maximum value targeted by the AASHTO (2010) Specifications. All but one span of one of the existing I-girder bridges had span lengths smaller than 350 ft., although three of the existing I-girder bridge units had spans larger than 300 ft. The span larger than 350 ft. is one of the straight spans of the Ford City bridge (EICCR 11). In current (2012) practice, horizontal flange lateral bracing systems often are considered for span lengths of 250 ft. or more, but spans of 250 ft. may be acceptable without flange level lateral bracing systems in certain cases. A span length of L_s = 150 ft. is a rough lower-bound value at which welded girders are generally required.

Table 4.1. Primary factor ranges and levels for the NCHRP 12-79 main analytical study.

Factor	I-girder bridges	Tub-girder bridges
Type of span	Simple, 2-span continuous, and 3-span continuous with one balanced end span and one end span equal in length to the main center span. Use the above 3-span continuous bridges as base ICCR & TCCR cases. Consider both 2- and 3-span continuous bridges for the ICSS and TCSS. Consider only 2-span continuous cases for the ICCS and TCCS designs. Consider at least one 2-span continuous bridge with a significant unbalance between the span lengths.	
Maximum span length of bridge centerline, L_s	150, 225 & 300 ft. for simple-spans 150, 250 & 350 ft. for continuous-spans (measured along the curve)	
Deck width, *w*	30 ft. (1 to 2 traffic lanes + shoulders & barriers) 80 ft. (4 to 5 traffic lanes + shoulders & barriers	30 ft. (1 to 2 traffic lanes + shoulders & barriers)
Torsion Index, I_T	0.58 to 0.71 for ISCR bridges 0.66 to 0.88 for ICCR bridges	0.72 to 0.87 for TSCR bridges 0.69 to 1.14 for TCCR bridges
Skew angle relative to the bridge centerline, θ	20^o, 35^o, 50^o & 70^0 but with θ at the inside edge of the deck $\leq 70^o$ in curved spans	15^o & 30^o, plus additional sensitivity studies with variations up to ±15° from zero skew
Skew pattern	Consider the $\pm$ combinations of skew angles shown in Figure 4.14 (for straight bridges) and Figure 4.15 (for curved bridges), but using θ = 35 & 70^o for I-girder bridges and θ = 15 & 30^o for tub-girder bridges. Limit the ratio of the span lengths along the edges of the deck, L_2/L_1, to a maximum value of 2.0 in all cases. Limit the difference in orientation of adjacent bearing lines to a maximum of 90^o in all cases. Give preference to typical (i.e., non-exceptional) bridge geometries.	

Of the existing tub-girder bridges, only the two interior spans of the parallel US 119 bridges over KY 1441 and Raccoon Creek in Pike Co., KY (bridge ETCCR 2) have span lengths greater than 350 ft., although there are two other tub-girder bridges with spans larger than 300 ft.

The third row of Table 4.1 shows the selected deck widths for the parametric study bridges. For the I-girder bridge parametric designs, deck widths of 30 ft. and 80 ft. were selected by the project team. Only 30 ft. deck widths were considered in the new parametric designs for the tub-girder bridges. This smaller 30 ft. width is representative of one- to two-lane bridges, whereas the larger 80 ft. width is representative of structures with four to five lanes. A large number of the existing tub-girder bridges are one to two lane ramp type structures. Therefore, it was recommended that the Project should focus predominantly on these types of structures in its studies of tub-girder bridge system behavior and analysis accuracy. The less common tub-girder bridges having more than two girders were addressed by including one of these existing bridge cases in the overall parametric study matrix. However, this bridge involved phased construction, with each of the phases having two tub girders.

The combinations of L_s from 150 to 350 ft. with w from 30 to 80 ft. give span length to the bridge width, L_s/w, ranging from 150/80 = 1.88 to 350/30 = 11.7. The maximum value for this range is slightly larger than the maximum L_s/w of 7.90 and 8.29 for the existing I- and tub-girder bridges. It was believed that these larger values should be studied to fully address the bridge responses and analysis accuracies for these practical but more extreme geometry conditions.

The fourth row of Table 4.1 gives the selected ranges and levels for the torsion index I_T. The implications of I_T ranging from 0.5 to 1.0 have been discussed in Section 3.1.4. This parameter was used in establishing the horizontal radius of curvature R for the ISCR/TSCR and ICCR/TCCR designs, given the span length L_s and the deck width w. The horizontal radius of curvature obtained for the ISCR/TSCR designs was then employed for other new curved ISCS/TSCS parametric bridge designs. Similarly, the horizontal radius of curvature obtained for the ICCR/TCCR designs was employed for the other new curved ICCS/TCCS parametric bridge designs. A maximum limit on L_s/R

of 1.0 was imposed on the parametric designs. This limit can govern for shorter spans with wide decks and is somewhat larger than the maximum L_s/R of 0.57 and 0.68 radians for the collected existing I- and twin tub-girder bridges. Nevertheless, it was believed that $L_s/R = 1.0$ is a practical extreme that should be addressed in the parametric study design. Wide bridges with these larger L_s/R values may require special handling during the steel erection and/or deck placement.

The fifth row of Table 4.1 shows the selected ranges and levels of the skew angle θ. As noted previously, AASHTO (2010) allows the cross-frames to be framed parallel to the bearing lines in I-girder bridges with $\theta \leq 20^o$. Furthermore, it was expected that the effects of skew may be sufficiently small such that a line girder analysis may work quite adequately for certain cases at this skew level. A value of 70^o is a reasonable maximum limit for θ in I-girder bridges. This value was the maximum considered in studies of deck effective widths by Chen (2005), and represents roughly the largest skew angle encountered in the existing bridges. Smaller skew angles of 15 and 30^o were targeted for the tub-girder parametric study designs. In addition, a range of skew angles of $\pm 15^o$ from zero skew were considered in separate 3D FEA studies (with no separate consideration of the simplified analysis methods) to understand the influence of skew on the tub-girder bridge responses in greater detail.

Lastly, the sixth row of Table 4.1 explains the recommended variations of the skew pattern considered. These variations are understood most easily by viewing the actual deck plan geometries for various hypothetical new bridge designs. The reader is referred to Section 4.3.4 for these illustrations.

4.3.4 Selection of the Analytical Study Bridges

The following sub-sections summarize the key characteristics of the I- and tub-girder bridges selected for the NCHRP 12-79 analytical studies, given the ranges and levels of the primary factors identified in Section 4.3.3. To arrive at the analytical study design, the research team first developed a full factorial design matrix involving all the above factors and levels. This led to more than 500 I-girder bridges and more than 250 tub-girder bridges that would need to be studied. Fortunately, a number of these combinations and permutations could be considered impractical or unbuildable. However, even after the impractical and unbuildable cases were eliminated, the total number of bridges arrived at in the study design was relatively large. Therefore, some prioritization of the bridges was necessary within the full range of practical designs. As noted by Montgomery (2004), “If the experimenter can reasonably assume that certain high-order interactions are negligible, information on the main effects and low-order interactions may be obtained by running only a fraction of the complete factorial experiment. These fractional factorial designs are among the most widely used types of designs for product and process design and for process improvement.” In the context of the Project 12-79 analytical study design, this involved the elimination of individual bridges or groups of bridges where the interaction between the primary factor effects was expected to be relatively small. Furthermore, a number of bridges in which the combination of factors led to:

- Exceptional (i.e., particularly unusual) structures, or
- Designs that were very similar in one or more characteristics to other designs

were eliminated.

Once these selections were completed, the library of existing bridges summarized in Figures 4.1 through 4.12 was searched for bridges that:

- Matched closely with the analytical study design selections, and
- Satisfied the criteria described in Section 4.1.

In a few cases, modifications were made to the analytical study design to include existing bridges that were particularly good candidates based on the criteria specified in Section 4.1. In addition, several of the Example bridges from Figure 4.13 that matched closely with the analytical study design selections were selected for inclusion in the analytical study. The remaining bridges in the study design were targeted as “New” bridges, indicating that they were to be fully designed by the project team using the AASHTO LRFD Specifications and current common standards of care.

The initial design of the suite of bridges arrived at, based on the above process, involved approximately 100 bridges. The bridges were then subdivided into smaller suites for execution of the analytical studies. Various milestones were identified at which the study bridge selections were reevaluated based on what was learned from the completed studies. The resulting final study targeted 58 I-girder bridges and 18 tub-girder bridges in total.

The following sections first discuss several base straight, non-skewed study bridges considered at the beginning of the Project, followed by straight skewed simple and continuous-span cases, then simple and continuous-span curved bridges with radial supports, and finally curved and skewed simple- and continuous-span bridges. Each of these sections includes summary sketches of the bridge deck plans and bearing-line geometries corresponding to the designs along with a title block for each of the bridges containing:

1) An identification label, composed of the letter “X” for the “eXample” bridge designs, followed by the symbols explained at the beginning of Section 4.2, indicating the bridge category (e.g., ISSS, ICSS, etc.), and ending with the bridge number for that category. Two additional categories, ICSN and TCSN, are introduced in Figure 4.17. The “CSN” designation stands for Continuous-span, Straight, with Non-skewed supports. For example, the first eXample bridge in Figure 4.17 is labeled “XICSN 1.”
2) An identification label, composed of the letter “E” for the “Existing” bridges, followed by the above symbols indicating the bridge category, and ending with the bridge number for that category, e.g., bridge “EISSS 3” in Figure 4.18.
3) An identification label, composed of the letter “N” for the “New” bridge designs, followed by the above symbols indicating the bridge category, and ending with the bridge number for that category, e.g., bridge “NISSS 1” in Figure 4.18.
4) A summary of the basic geometry information about the bridge, enclosed in parentheses. For instance, in Figure 4.18, the basic geometry information includes:

- The span length of the bridge centerline,
- The out-to-out width of the bridge deck perpendicular to the bridge centerline (provided for each unit in phased construction jobs), and
- The skew angle with respect to centerline of the bridge for both bearing lines.

This information is conveyed symbolically in the figure caption as "(LENGTH/WIDTH/θ_1, θ_2)." The other categories have similar but different basic geometry information. This information is summarized symbolically in each of the figure captions. The skew angle of the bearing lines is represented by the symbol θ. This angle is taken as zero when a bearing line is perpendicular to the centerline of the structure, that is, when the bearing line does not have any skew.

All of the figures referenced in the following sub-sections adopt the following conventions:

- Typical or common geometries are sketched using a solid black outline,
- Geometries considered unusual or exceptional are sketched using a black dashed outline,
- A few bridge geometries that are considered impractical or unbuildable are sketched using a solid light-grey outline. (The only cases shown that are impractical or unbuildable are a few bridges with high skew and relatively small length-to-width ratios, where if the bridge span was longer or the deck was narrower, the geometry would indeed be possible.)
- The deck plans for the selected eXample bridges are shaded and cross-hatched,
- The deck plans for the selected Existing bridges are shaded with a textured background,
- The deck plans for the selected New bridges are shaded with a solid background,
- The deck plans of bridges that were not selected for study are white or unshaded,
- The bridge unit centerlines are indicated by a "dot-dash" line, and
- The different phases in phased construction bridges (i.e., bridges constructed as a number of separate longitudinal units) are delineated by dashed lines.

4.3.4.1 Straight Non-skewed Base-Line Comparison Cases (XITSN 1 and XTCSN 3)

The straight non-skewed "base-line" bridges are illustrated in Figure 4.17. The analysis accuracy results for these cases serve as useful indicators or benchmarks for decisions about the levels of accuracy sufficient for bridges with more complex geometries. Both of these bridges are carefully documented example designs.

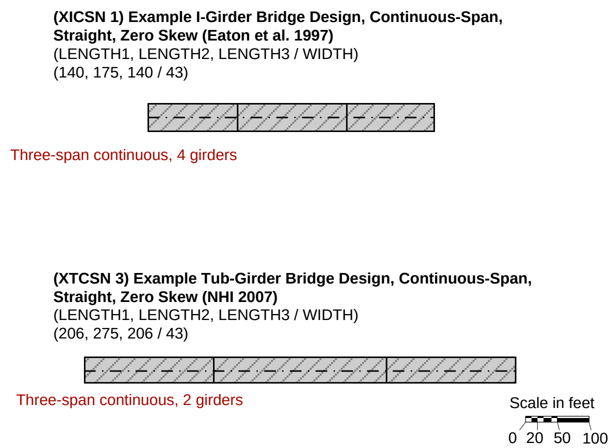

Figure 4.17. eXample Straight Non-skewed bridges used as base comparison cases, (LENGTH1, LENGTH2, LENGTH3 / WIDTH).

4.3.4.2 Simple-Span Bridges, Straight, with Skewed Supports (ISSS and TSSS)

Figure 4.18 shows the 60 total combinations and permutations for the ISSS bridges obtained considering:

- The ten combinations of skew magnitude and pattern for the straight bridges illustrated previously in Figure 4.14, $\{(\theta_{Left}, \theta_{Right}) = (20^o,20^o), (35^o,35^o), (50^o,50^o), (70^o,70^o), (35^o,0^o), (50^o,0^o), (35^o,-35^o), (70^o,0^o), (70^o,35^o), (60^o,-30^o)\}$,
- The three values for the length L_s (L_s = 150, 225 and 300 ft.), and
- The two values for the deck width w (w = 30 and 80 ft.)

Figure 4.18. Existing and New I-Girder bridges, Simple-span, Straight with Skewed Supports, EISSS or NISSS (LENGTH / WIDTH / θ_{Left}, θ_{Right}).

In Figure 4.18, one can observe that the selected ISSS bridges emphasize smaller L_s/w and larger θ. The influence of the skew is expected to be significant for the bridges in the 3rd and 4th rows. The selected unequal skew cases in the 6th row parallels the selections in the 3rd row, except for NISSS33 and NISSS36. Bridge NISSS37, in the 7th row, is an interesting case in that the orientation of its bearing lines is the same as in the curved design NISCR10 (shown subsequently). The inclusion of this bridge allows for a comparison of the effects of bearing orientation alone in NISSS37 versus the effects of horizontal curvature in NISCR10. In addition, several parallel skew cases are considered in Figure 4.18, with an emphasis on the bridges with larger L_s/w and moderate skew angle (e.g. NISSS2), as well as a wider bridge with a 20 degrees of skew (NISSS11).

EISSS3 is one of two adjacent simple-span highly-skewed grade separation structures on SR 10003 (Chicken Road) over US 74 in Robeson County, NC. This bridge was closely monitored during construction, and field data relating to undesirable girder layover and bowing of the girder webs has been collected by Morera (2010). The availability of the field data and the successful construction, but with some concerns about the state of the girders, made this bridge a worthwhile candidate for study. Figure 4.19 shows several photos of this bridge.

Figure 4.19. EISSS3, Bridge on SR 1003 (Chicken Road) over US74 between SR 1155 and SR 1161, Robeson Co., NC (Morera, 2010).

EISSS5 is selected due to its large skew angle and short span length. Moreover, EISSS6 is selected since this bridge is constructed with TDLF detailing and provides extensive information about the erection practices to eliminate the fit-up problems. This bridge was provided by High Steel Structures, Inc. Figure 4.20 shows a photo of EISSS6 during steel erection.

Figure 4.20. EISSS6, Bridge on Westchester Co., NY (courtesy of R. Cisneros, High Steel Structures, Inc.).

Figure 4.21 shows the 24 total combinations and permutations for the TSSS (tub-girder) bridges obtained considering:

- Eight combinations of skew magnitude and pattern for the straight bridges are: $\{(\theta_{Left}, \theta_{Right})$ = (15°,15°), (30°,30°), (15,0°), (15°,15°), (30°,0°), (30°,15°), (30°,-15°), (30°,-30°) },
- Three values for the length L_s (L_s = 150, 225 and 300 ft.), and
- One value for the deck width w (w = 30 ft.)

Three of the four tub-girder bridges selected in this category have the shortest span length of 150 ft. The selection of short-span cases is based on the fact that the torsional effects due to skew are likely to be larger for the shorter spans. The short-span bridges selected are NTSSS1 and NTSSS2 with parallel skewed supports of 15° and 30°, and NTSSS4 with equal but opposite skew of 16°. NTSSS4 was modified to a skew angle of 16° in order to make the orientation of the supports similar to the curved and radially supported bridge NTSCR1 shown subsequently. NTSSS4 also highlights the equal and opposite skew case discussed in Section 4.3.1.2 and shown in Figure 4.15.

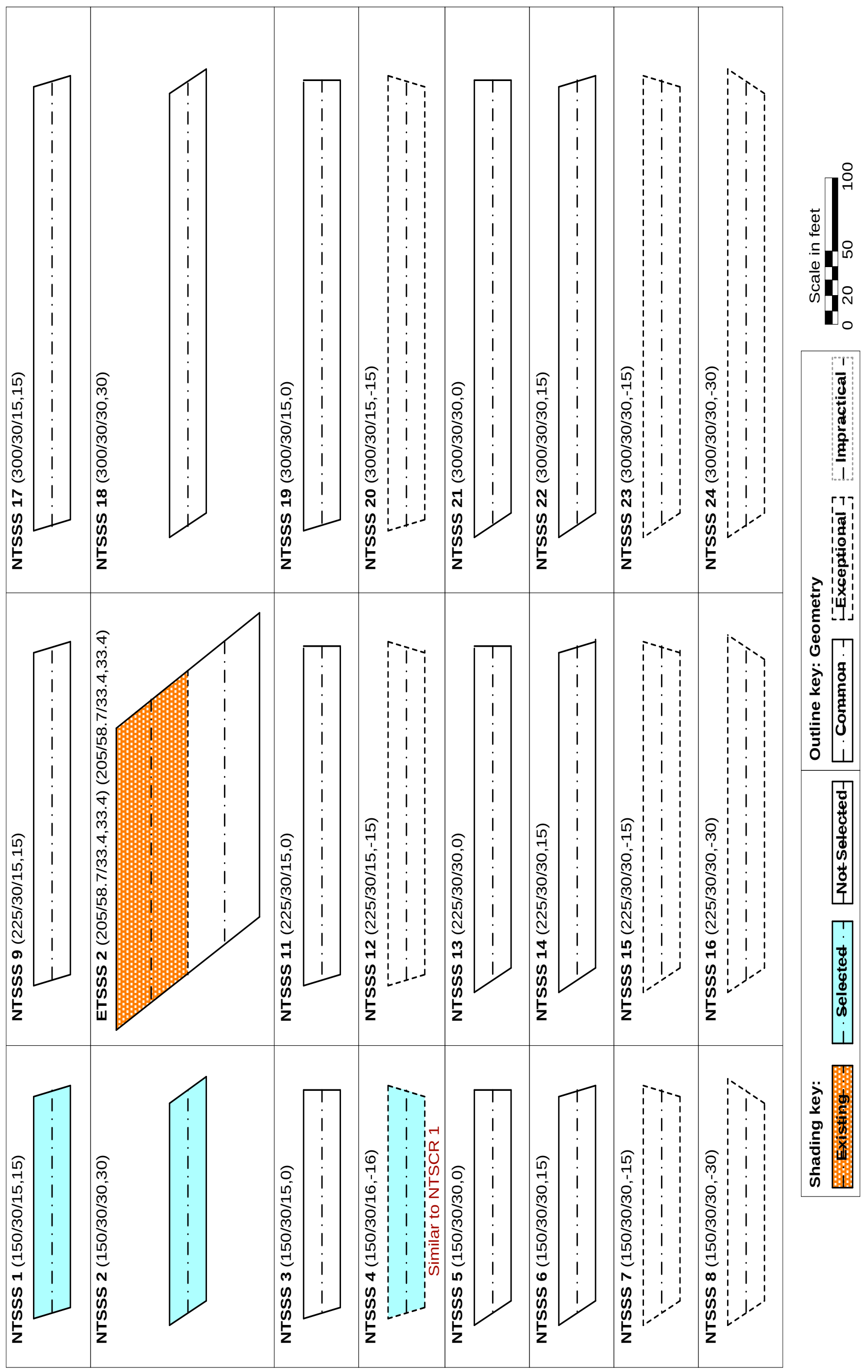

Figure 4.21. Existing and New Tub-girder bridges, Simple-span, Straight with Skewed supports, ETSSS or NTSSS (LENGTH / WIDTH / θ_{Left}, θ_{Right}).

In addition to the above bridges, the NTSSS10 bridge was selected to study the influence of an increase in the span length when the skew support angle is kept constant. The NTSSS10 bridge was replaced by the existing ETSSS2 (Sylvan Bridge). The Sylvan bridge (Figure 4.22) has a span length of 205 ft. and was constructed in two individual longitudinal phases with deck widths of 58.7 ft. and parallel skewed supports of 33.4°.

Figure 4.22. ETSSS 2, Sylvan Bridge over Sunset Highway, Multomah Co., OR (courtesy of Homoz Seradj, Oregon DOT).

4.3.4.3 Continuous-Span Bridges, Straight, with Skewed Supports (ICSS and TCSS)

Figure 4.23 shows four of the six groups of ICSS bridges. The six groups correspond to the combinations of three span lengths and the two deck widths. Two different widths 30 and 80 ft. were considered for L =150 ft. in Figure 4.23, but only 80 ft. wide bridges were considered for L = 250 and 350 ft. This is because the effect of skew was expected to be smaller for the narrower longer-span bridges. Furthermore, for the bridges with L = 250 and 350 ft. and w = 30 ft. are not shown since these combinations and permutations were found to be exceptional due to their large length-to-width ratios.

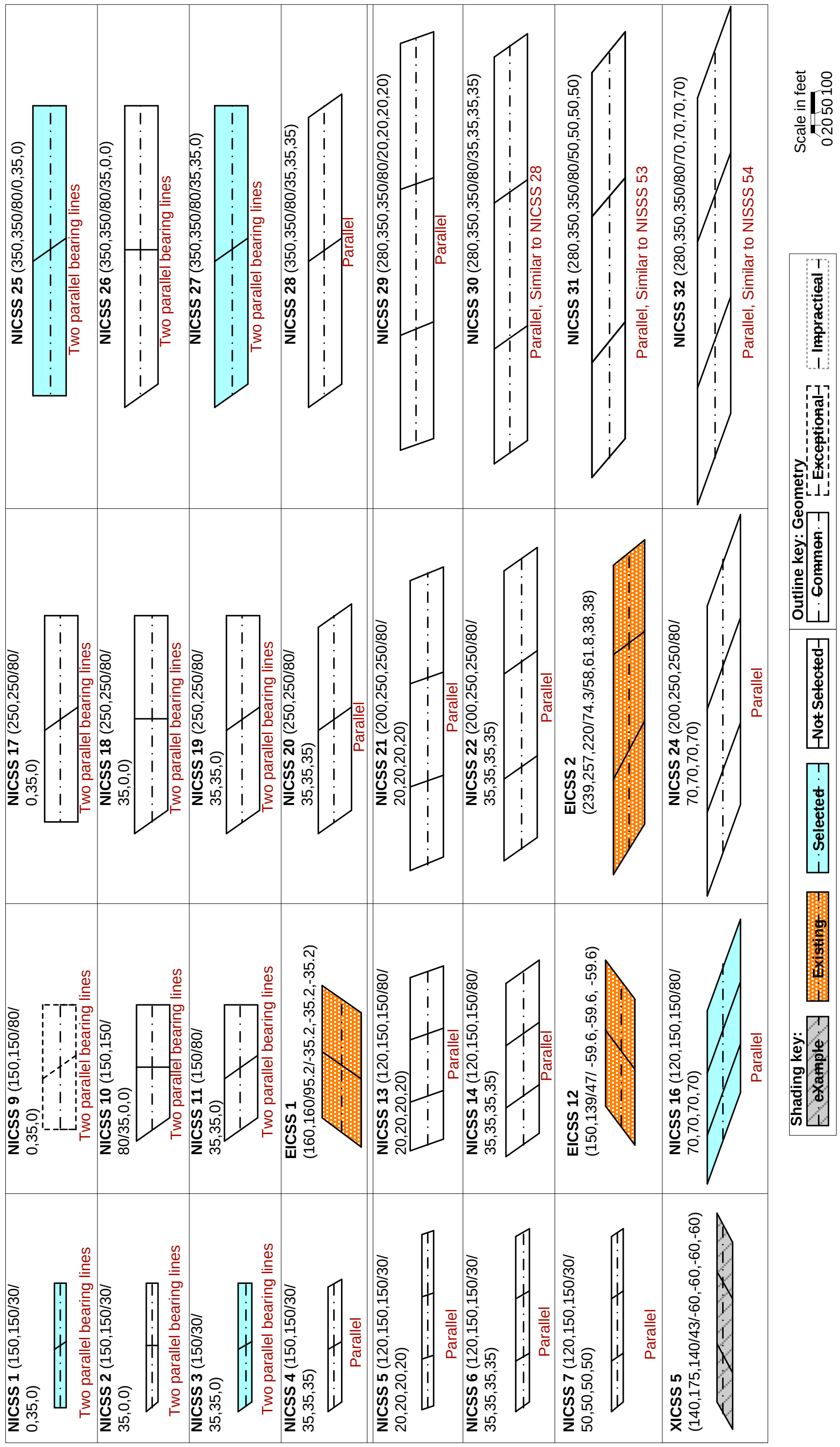

Figure 4.23. Existing, eXample and New I-girder bridges, Continuous-span, Straight with Skewed supports, EICSS, XICSS or NICSS (LENGTH1, LENGTH2, ... / WIDTH / θ_{Left}, …, θ_{Right}). The columns in the matrix for (L = 250 ft., w = 30 ft.) and (L = 350 ft., w = 30 ft.) are not shown.

In Figure 4.23, the top four rows of the matrix include four two-span continuous bridges with unequal skew and one case with parallel skew. Only values of $\theta = 35^{o}$ were considered for these selected cases.

The case with the parallel skew (EICSS1) is a steel overpass on Sunnyside Road Interchange, (I-15B) over I-15, in Bonneville County, ID. This bridge represents a successful implementation of total dead load fit detailing, which aims to ensure that the webs are plumb under the total steel plus concrete dead load. Both field observations and field data are available for this bridge. Figure 4.24 shows the gap at the sole plate at one of the bearings of this bridge under the steel dead load. Although daylight is apparent between the sole plate and the elastomeric bearing pad on one side under the steel dead load condition, the girders rotated as expected during the deck placement such that full contact was established with the elastomeric pads. Figure 4.25 shows the lack of fit between one of the girder connection plates and the bolt holes in a cross-frame during the steel erection on this bridge. This was expected and intentional due in part to the total dead load fit of the cross-frames. That is, the holes in the girder connection plates and in the cross-frame plates had to be aligned. This hole alignment was achieved on the Sunnyside Road job using drift pins without any other mechanical aid.

Trends in the behavior for other skews were targeted by the ISSS cases in Figure 4.18 and the ICCS cases discussed subsequently (see Figure 4.41). The last four rows of Figure 4.23 are three-span continuous designs with parallel skew. Two cases with unequal skew and a narrower deck, NICSS1 and 3, were selected for L = 150 ft. and two comparable cases but with the wider deck, NICSS25 and 27, were selected for L = 350 ft. Parallel skews with the extreme skew angles were considered by selecting bridges XICSS5 and NICSS16, with L = 150 ft. and w = 30 ft. and 80 ft. for the 3-span continuous designs.

The bridge XICSS5 is taken from the NHI Course No.130081A-D (NHI, 2007), which is an LRFD eXample design developed by Grubb et al. (2007) for the National Highway Institute. Since detailed design calculations are shown for this structure, it was selected to serve as an excellent example for the benchmarking.

Figure 4.24. EICSS1, Steel Overpass Sunnyside Road I.C. (I-15B) over I-15, Bonneville Co. ID, gap at sole plate under steel dead load; the girders rotated during the deck placement such that full contact was established with the elastomeric pads (courtesy of Matt Farrar, ITD).

Figure 4.25. EICSS1, Steel Overpass Sunnyside Road I.C. (I-15B) over I-15, Bonneville Co. ID, bolt hole alignment during erection; for this job, drift pins were used to align the holes without mechanical aid (courtesy of Matt Farrar, ITD).

In addition, several cases involving 3-span continuous designs with parallel skews were selected due availability of similar Existing bridges in the literature:

- EICSS2 is located at I-235 EB over E. University Ave., Polk County, IA. This bridge, recommended by Iowa DOT, had difficulty with the installation of cross-frames during the steel erection. According to Iowa DOT, the fabricator detailed and fabricated the cross-frames for the final dead load condition, i.e., total dead load fit. The problem was resolved by requiring the fabricator to supply new cross-frames that were detailed for steel dead load fit. The bridge has an interesting combination of a relatively wide deck, and substantial unequal skew of the bearing lines. Therefore, it represents a potentially useful case where total dead load fit detailing may be problematic.
- EICSS12 is located at US 82 main lane underpass at 19th stress west bound, Lubbock County, TX. This bridge is one of several suggested by TxDOT. This bridge involves a field implementation and evaluation of the use of lean-on cross-frames to alleviate issues of nuisance stiffness in significantly skewed bridges and to eliminate cross-frame diagonals within a large portion of the bridge framing. The design and construction of this bridge are discussed by Helwig et al. (2003). Field data are reported by Romage (2008). This bridge provided an outstanding potential opportunity for validation or verification of the refined analysis methods utilized in the NCHRP research versus available experimental and analytical results.

Figure 4.26 shows the combinations and permutations for the two and three continuous-span TCSS (tub-girder) bridges considering:

- Eight combinations of skew magnitude and pattern for the two-span straight bridges: {(θ_{Left}, θ_{Right}) = (0°, 15°,0°), (0°, 0°, 15°), (0°, 15°, 15°), (15°, 15°, 15°), (0°, 30°, 0°), (0°, 0°, 30°), (0°, 30°, 30°), (30°, 30°, 30°)},
- Two combinations of skew magnitude and pattern for the three-span straight bridges: {(θ_{Left}, θ_{Right}) = (15°, 15°, 15°), (30°, 30°, 30°)},
- Two values for the length L_s (L_s = 150, 250 ft.), L_s = 350 ft. are not shown, and

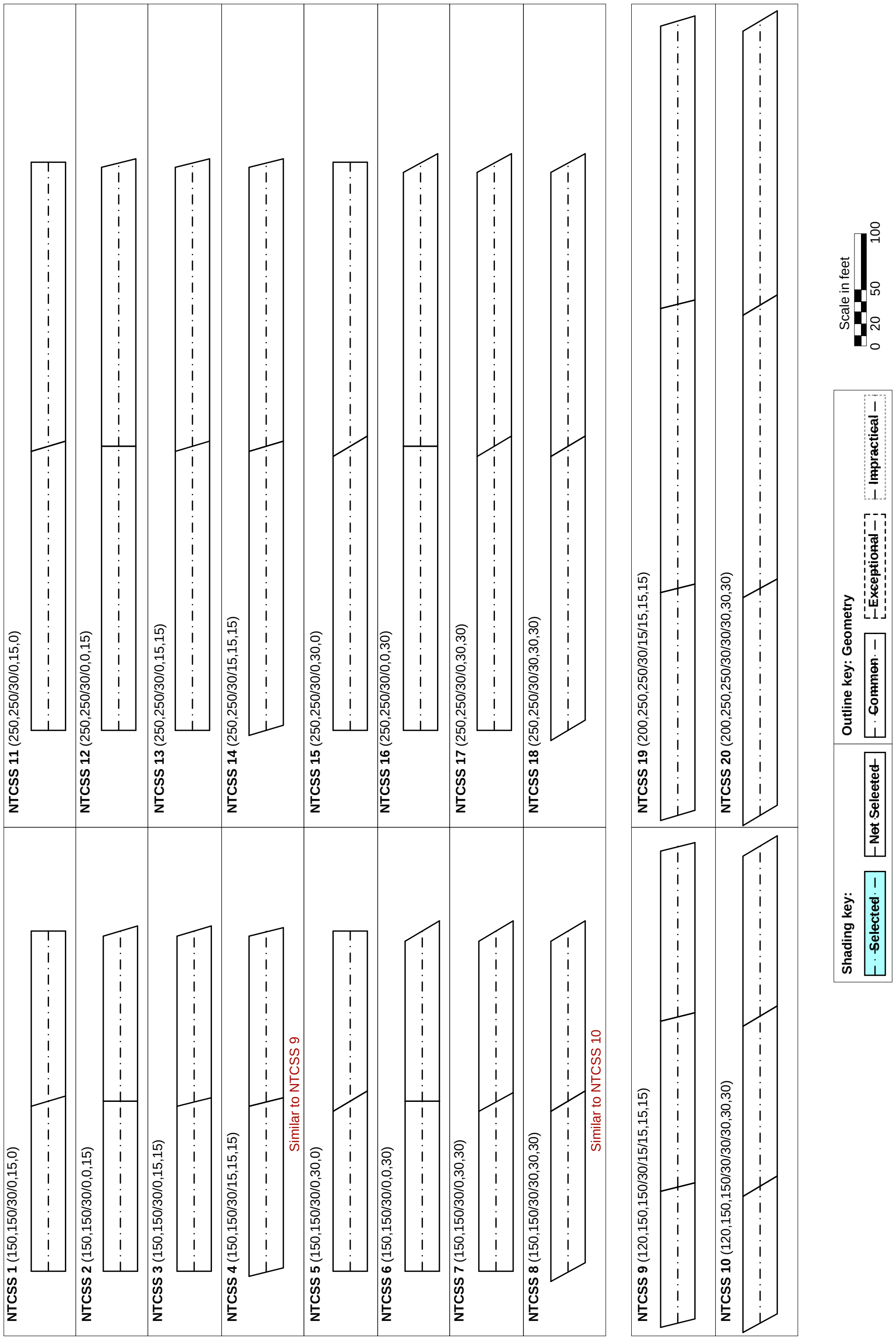

Figure 4.26. New Tub-girder bridges, Continuous-span, Straight with Skewed supports, NTCSS (LENGTH1, LENGTH2, … / WIDTH / θ_{Left}, …, θ_{Right}). The columns in the matrix for (L = 350 ft., w = 30 ft.) are not shown.

- One value for the deck width *w* (*w* = 30 ft.)

None of the continuous-span tub-girder bridges shown in Figure 4.26 were selected. It was decided to focus on the other categories for these bridge types, since the interactions between the spans tend to be less significant in tub-girder bridges, the basic influence of skew could be studied more clearly on simple-span bridges, and curved tub-girder bridges are more common than straight ones for narrow two-tub girder systems. It was anticipated that the torsional behavior of curved and straight bridges would be very similar, due to the relatively small torsional interaction of the spans in continuous-span tub-girder bridges.

4.3.4.4 Simple-Span Bridges, Curved, with Radial Supports (ISCR and TSCR)

Figure 4.27 shows the 12 total combinations including three values for the span length (L_s =150, 225 and 300 ft.), the two values for the deck width (*w* = 30 and 80 ft.), and the two values for the radius of curvature; one corresponding to the largest curvature (smallest *R*) without having uplift at the most critical bearing location(s) under nominal dead plus live loads and other one corresponding to the smaller curvature (larger *R*) for the ISCR bridge designs. Seven of the 12 ISCR bridges in Figure 4.27 are selected. These designs are intended to establish the main trends regarding the structural behavior as a function of horizontal curvature and deck width for the different span lengths.

EISCR1 was inserted into the parametric study, which was a very useful case for initial benchmarking and verification of various analysis methods, including simplified 1D I-girder bridge analysis methods coupled with V-load calculations, as well as virtual test simulations procedures. This is due to the following characteristics of this test bridge:

- There were a large number of channels of instrumentation collected and reduced at various stages of the steel erection, deck placement, and loading of this bridge in its final composite condition. This is one of the largest bridge structures ever tested indoors under carefully controlled conditions.
- The geometry of this structure is relatively basic, and should be one of the cases most amenable to simplified analysis.

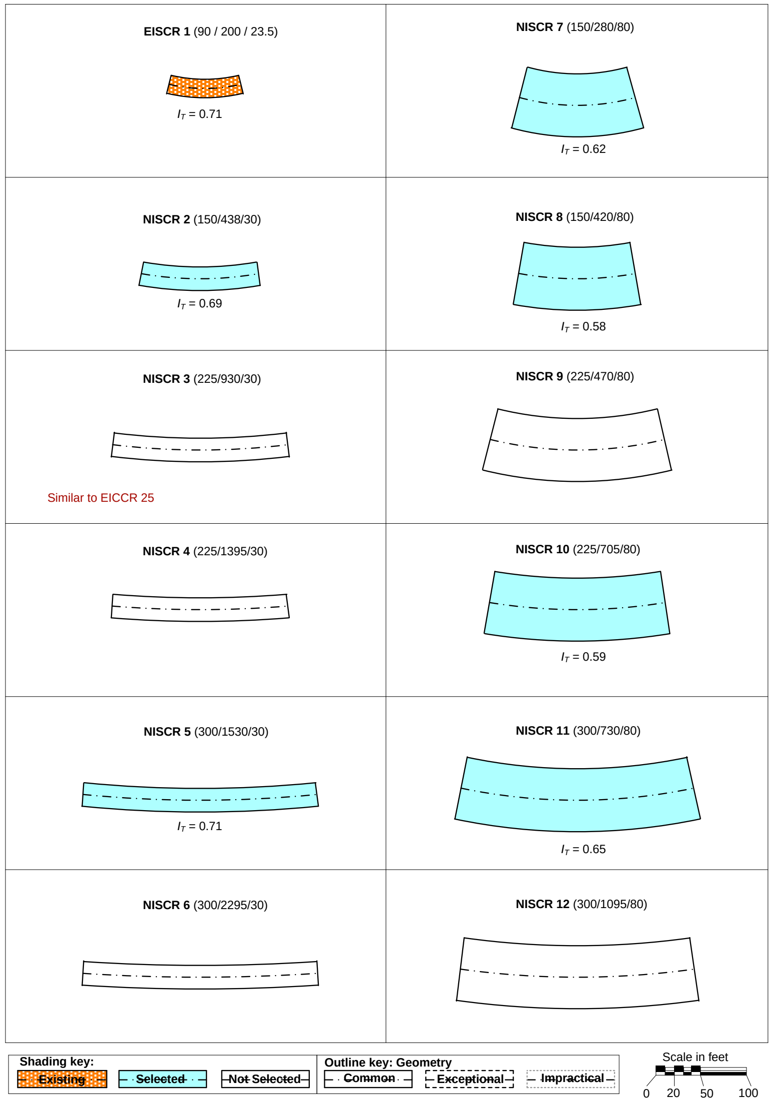

Figure 4.27. Existing and New I-girder bridges, Simple-span, Curved with Radial supports, EISCR or NISCR (LENGTH / RADIUS / WIDTH).

- This test bridge was designed at or slightly above a number of maximum limits in the AASHTO LRFD Specifications. Hence a number of its characteristics are likely to accentuate the effect of certain analysis and/or design approximations.

Jung (2006) and Jung and White (2008) provide a detailed discussion of the characteristics and the behavior of this test bridge. These references also provide substantial prior results from FEA simulation models similar to the types of simulation models that are employed in the NCHRP research. Figure 4.28 shows a view of the FHWA test bridge at an intermediate stage of the steel erection, when the first two of the three girders in this bridge had been placed on their support bearings and connected together by cross-frames.

Figure 4.28. EISCR1, FHWA Test Bridge (Jung, 2006, Jung and White, 2008).

Figure 4.29 shows the 6 combinations for the TSCR (tub-girder) bridges obtained considering:

- Three values for the span length L_s (L_s = 150, 225 and 300 ft.),
- One value for the deck width w (w = 30 ft.), and
- Two values of the curvature radii R for each span length.

NTSCR1 and NTSCR2 (I_T = 0.83 and 0.72) were selected to study for the effects for different curvature at the shorter span length. One bridge, NTSCR5 (I_T = 0.87), was selected to study the effect of larger span length for similar I_T.

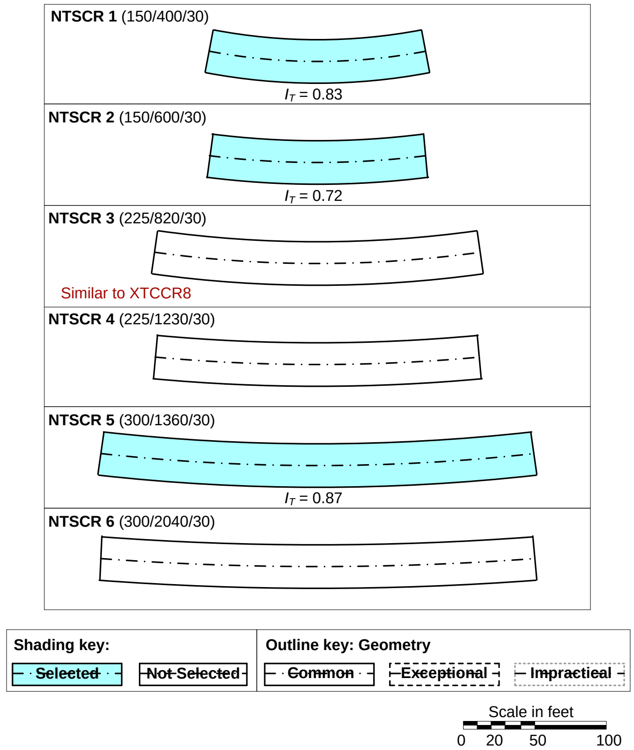

Figure 4.29. New Tub-girder bridges, Simple-span, Curved with Radial supports, NTSCR (LENGTH / RADIUS / WIDTH).

4.3.4.5 Continuous-Span Bridges, Curved, with Radial Supports (ICCR and TCCR)

Figure 4.30 shows 12 total combinations of L_S (= 150, 250 and 350 ft.), w (= 30 and 80 ft.) and the two conceptual values for the radius of curvature discussed previously in Section 4.3.1.1, for the ICCR bridges. The first radius of curvature corresponds to the largest curvature (smallest R) without having uplift at the most critical bearing location(s) under nominal dead plus live loads and the second corresponds to 1.5 times this R value.

In Figure 4.30, all of the cases with the narrower deck are selected, as shown in the first column of this parametric study design matrix, except NICCR5. The selection is mainly driven by the Existing bridge designs. EICCR22a was selected since it has extensive field observations and measurements, reported by Leon et al. (2011). Figure 4.31 shows a photo of EICCR22a during its steel erection.

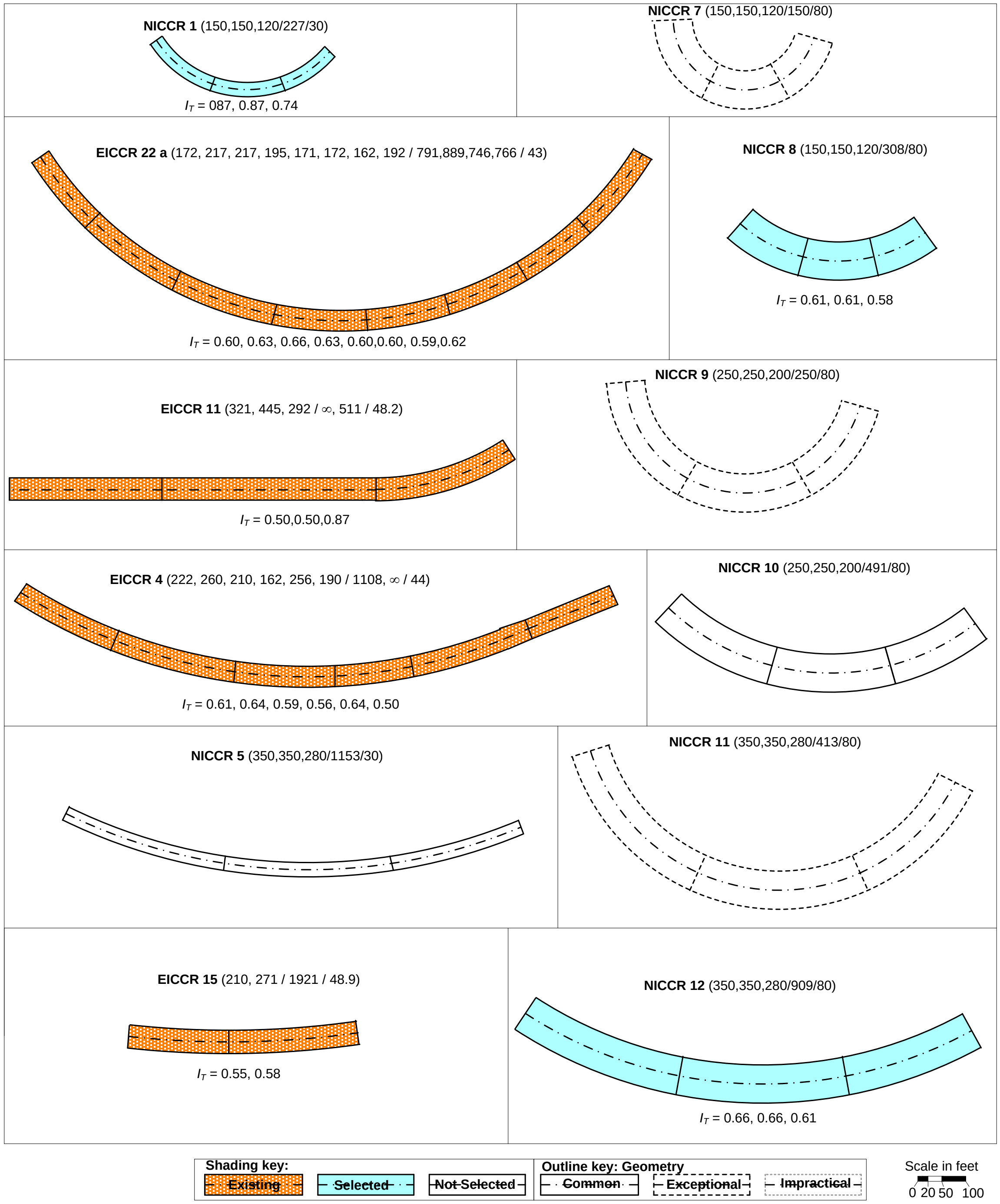

Figure 4.30. Existing, eXample and New I-girder bridges, Continuous-span, Curved with Radial supports, EICCR, XICCR or NICCR (LENGTH1, LENGTH2, ... / RADIUS / WIDTH).

Figure 4.31. EICCR22a, Bridge No. 12 Ramp B over I-40, Robertson Avenue Project, Davidson Co., TN.

EICCR11, which is the Ford City Bridge, in Ford City, PA, was inserted into the analytical study since it represents an important model case where due to combinations of long spans, deep girders with relatively close spacing compared to the girder depths, and relatively tight curvature, substantial erection challenges had to be addressed in the erection engineering of the structure. This bridge has been studied thoroughly in prior work by Chavel and Earls (2006a & b; 2001) as well as by Chang (2006). Hence, it represented another valuable case that can be used to validate the analysis and design methods. Figure 4.32 shows an overall photo of the Ford City bridge during its steel erection. Figure 4.33 emphasizes the overall depth of the girders relative to their horizontal spacing. Figure 4.34 provides several snapshots during the installation of a key drop-in segment on this bridge. The circles in these photos are highlighting a come-along beam that is being used to stabilize the curved girder during lifting. A cable goes to the lifting beam from each end of the come-along beam.

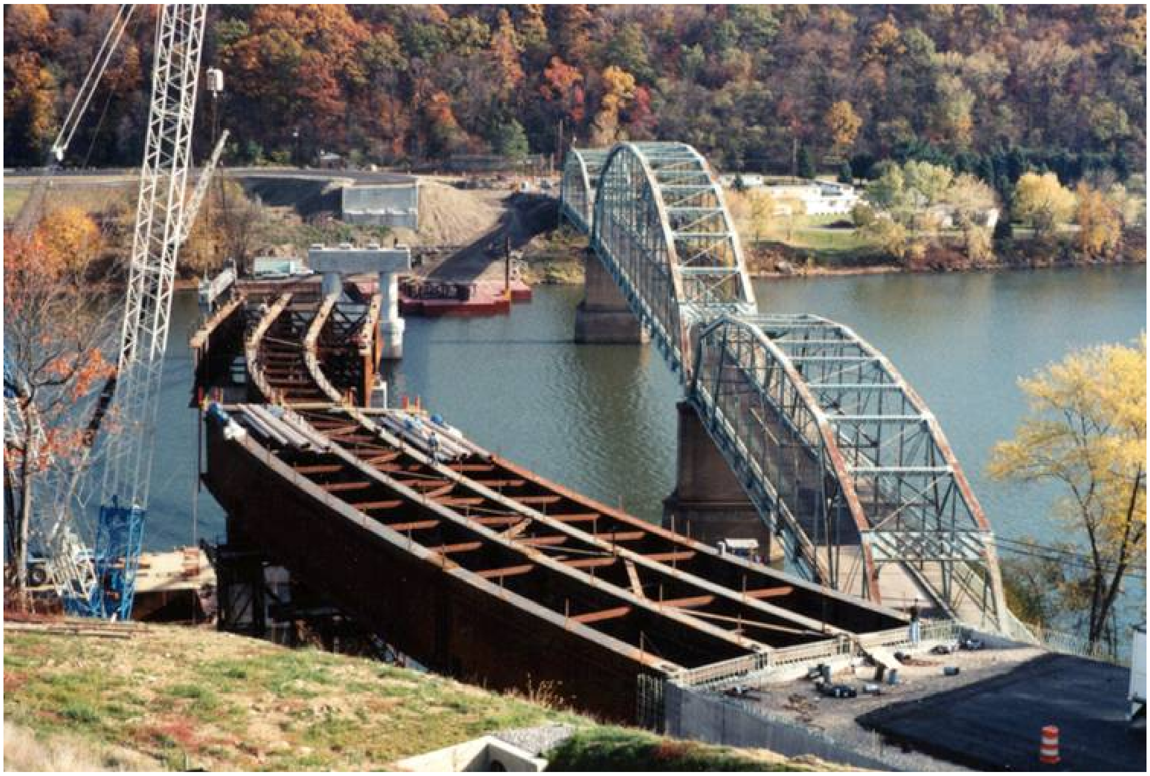

Figure 4.32. EICCR11, Ford City Bridge, Ford City, PA (Chavel, 2008).

Figure 4.33. EICCR11, Ford City Bridge, Ford City, PA, girder depth and spacing (Chavel, 2008).

Figure 4.34. EICCR11, Ford City Bridge, Ford City, PA, installation of drop-in segment (Chavel, 2008).

EICCR4 is one of the units of Ramp GG, John F. Kennedy Memorial Highway, I-95 Express Toll Lanes and I-695 Interchange, Baltimore County, MD. High Steel Structures, Inc. did the fabrication and the steel erection for this bridge. Several members of the NCHRP 12-79 team visited the job site with the High Steel engineers to observe the erection of a drop-in segment on the second span from the right hand end of this bridge in the sketch during August 2007. Figure 4.35 is a photo of the bridge just prior to installation of this drop-in segment.

EICCR15 is located at SR 6220 A11 over SR 6220 NB and SB, Centre County, PA. This bridge was studied experimentally and analytically by Shura (2004) and is discussed by Domalik et al. (2005). Due to its unequal span lengths (ratio of the span lengths of 0.77), this bridge exhibits important torsional interactions between its two spans. The shorter span actually twists in the direction opposite from the torsional deformation of the longer span. That is, the downward deflection of girders toward the outside of the curve in the longer span corresponds to an upward deflection of the girders toward the inside of the curve on the shorter span. As a result, this bridge was selected to serve as an important case for assessment of the sufficiency or limitations of various simplified analysis methods.

Figure 4.35. EICCR4, Ramp GG John F. Kennedy Memorial Highway, I-95 Express Toll Lanes and I-695 Interchange, Baltimore Co., MD (courtesy of R. Cisneros, High Steel Structures, Inc.).

In addition, two of the three cases with wider decks and smaller curvature (larger *R*) were considered in the second column of the matrix. The wider-deck cases with tighter curvature in Figure 4.30 were considered to be exceptional designs. The influence of wide decks with tight curvatures was expected to be captured sufficiently via the combination of the ISCR and ISCS bridges.

Figure 4.36 is based on the combinations for the TCCR (tub-girder) bridges with three continuous-spans considering:

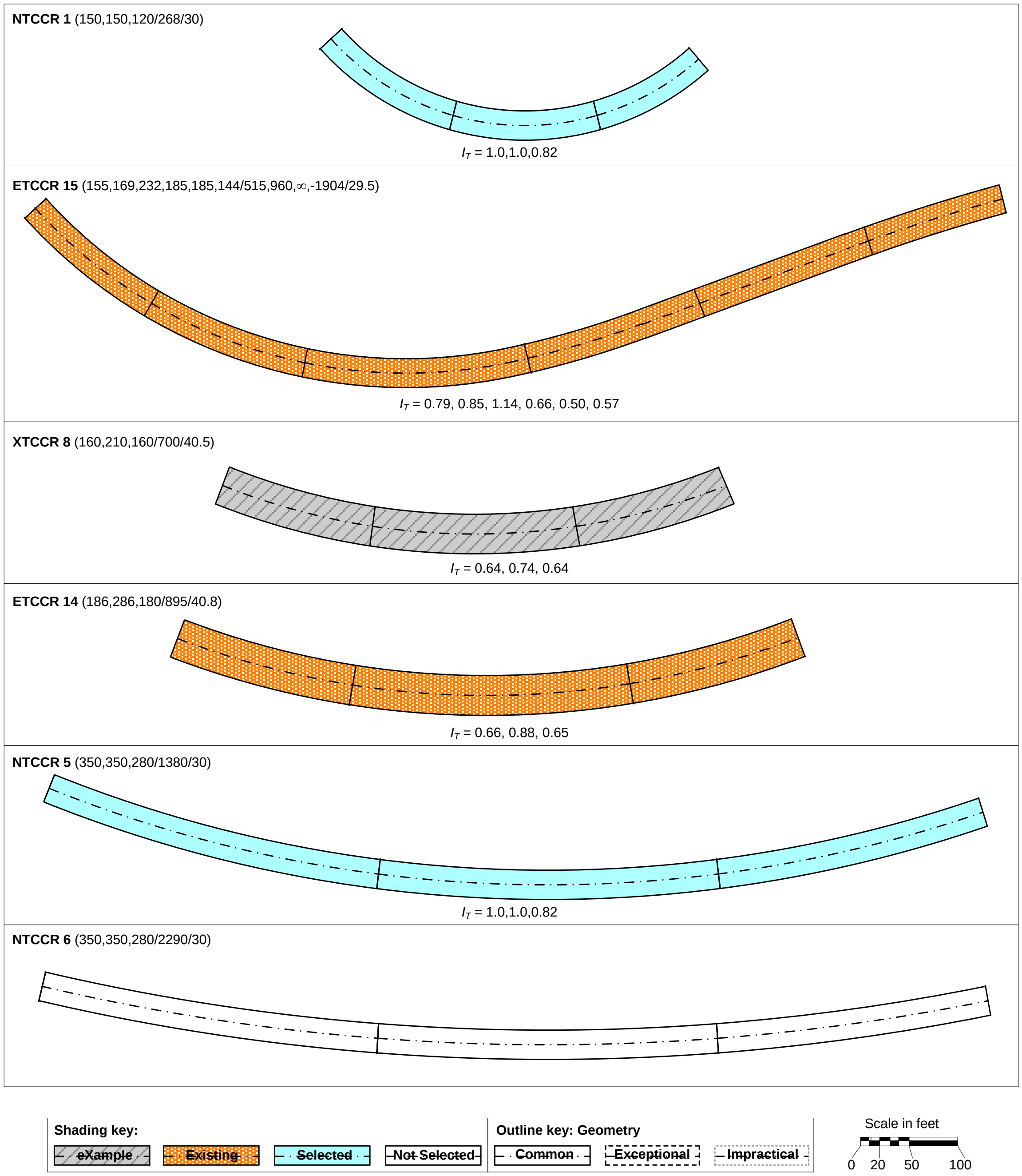

Figure 4.36. Existing, eXample and New Tub-girder bridges, Continuous-span, Curved with Radial supports, ETCCR, XTCCR or NTCCR (LENGTH1, LENGTH2, … / RADIUS / WIDTH).

- Three values for maximum the span length L_s (L_s = 150, 250 and 350 ft.),
- One value for the deck width w (w = 30 ft.), and
- Two conceptual values of the radius of curvature R as discussed in Section 4.3.1.1, the first corresponding to the largest curvature (smallest R) possible

without having uplift at the most critical bearing location(s) under nominal dead plus live loads, and the second corresponding to a radius of curvature of 1.5 times this value.

Five continuous-span tub-girder bridges were selected as this is the most common configuration for tub-girder bridges used as access ramps for highway interchanges. The extreme cases NTCCR1 and NTCCR5 were selected to provide information for sharp curve and large span lengths while the intermediate cases were replaced by existing and example bridges (ETCCR15, XTCCR8 and ETCCR14). ETCCR15 is a six span bridge located in Milwaukee, WI and is part of the Marquette Interchange (see Figure 4.37), XTCCR8 is a design example developed by Kulicki et al. (2005), and ETCCR14 is a three-span bridge instrumented and studied by Fan (1999), located in Houston, TX.

Figure 4.37. ETTCR 15, Unit B-40-1122 of the Marquette Interchange, Milwaukee, WI (courtesy of Tony Shkurti, HNTB Corporation).

4.3.4.6 Simple-Span Bridges, Curved, with Skewed Supports (ISCS and TSCS)

Figure 4.38 displays four of the 12 groups of I-girder bridges considering:

- The twelve combinations of skew magnitude.
- The two values for length, L_s = 150 and 300 ft.
- The two values for the deck width w = 30 and 80 ft.
- The four values of radius of curvature R = 438, 280, 420 and 730 ft. which were selected from ISCR bridges.

Since the effects of skew are generally larger in wider bridges for a given span length, emphasis was placed on bridges with the wider decks in the design of the ISCS studies.

In addition, none of the bridges with 225 ft. span length are considered in Figure 4.38. This is because it was expected that the interactions between the effects of the curvature and skew on I-girder bridges can be captured sufficiently by studying the ISSS, ICSS, ISCR, ICCR, ISCS and ICCS bridges with L_s = 150 ft.

One case with L_s = 300 ft., the case with the wider deck and tighter curvature, was included to investigate the interaction effect on a longer-span design where some type of flange-level lateral bracing system is likely.

In Figure 4.38 one can observe that the bridges in the 2nd and 3rd rows of 1st, 2nd and 3rd columns were selected except NSCS1 and NSCS3 for analytical studies. These bridges were selected to capture the behavior with respect to the variation in the L_s /w and L_s /R ratios. NISCS9 was selected to capture the effect of parallel skewed bearings along with curvature effects.

EISCS3 was inserted into the design matrix. This bridge is SR 8002 Ramp A-1, in King of Prussia, PA, studied extensively by Chavel and Earls (2003) and Chavel (2008) in their prior research (see Figure 4.39). Moreover, the third phase of the EISCS4 was inserted into the study matrix since this phase experienced large differential displacements with respect to the adjacent units due to its large length-to-width ratio.

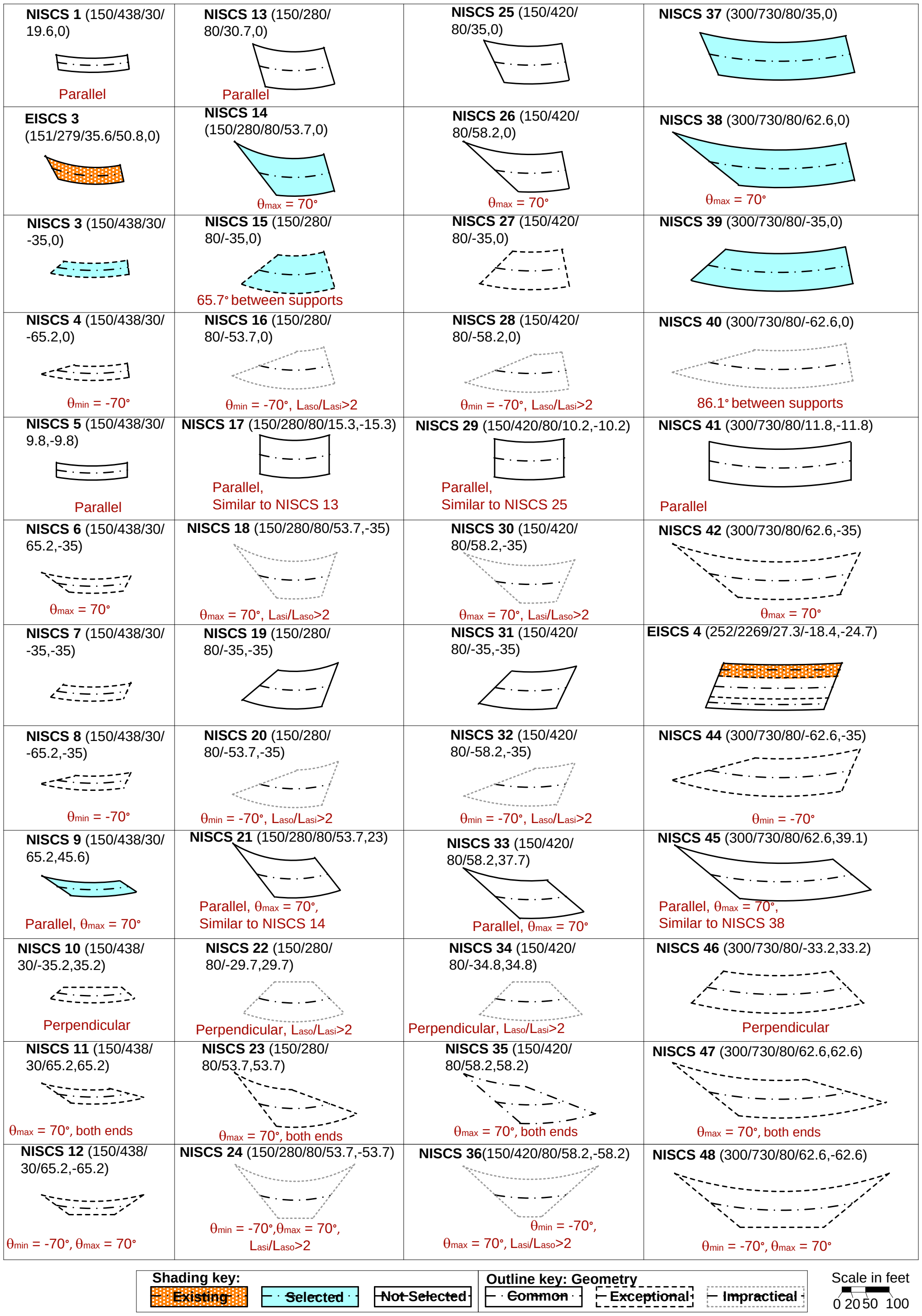

Figure 4.38. Existing and New I-girder bridges, Simple-span, Curved with Skewed supports, EISCS or NISCS (LENGTH / RADIUS / WIDTH / θ_{Left}, θ_{Right}). The columns in the matrix for (L = 150 ft., w =30 ft., R = 292 ft.), (L = 225 ft., w =30 ft., R = 930 and 1395 ft.), (L = 225 ft., w =80 ft., R = 470 and 705 ft.), (L = 300 ft., w =30 ft., R = 1530 and 2295 ft.) and (L = 300 ft., w =80 ft., R = 1095 ft.) are not shown.

Figure 4.39. EISCS3, SR 8002 Ramp A-1, King of Prussia, PA (Chavel and Earls, 2003).

Figure 4.40 displays the possible combinations for the TSCS (tub-girder) bridges considering:

- Twelve combinations of skew magnitude within the ranges of ±30° and two additional configurations for parallel skew previously shown in Figure 4.15,
- Two values for length, L_s =150 and 225 ft., L_s = 300 ft.and their associated radius values are not shown,
- One value for the deck width w =30 ft., and
- Four values of radius of curvature R = 400, 600, 820 and 1230 ft.which are selected from TSCR bridges

The selected cases (NTSCS5 and NTSCS29) have parallel supports since these configurations represent the most likely scenarios for skewed supports combining 150 and 225 ft.spans and skewed supports up to 15.7°. The NTSCS5 bridge is similar to

NTSSS4 shown in Figure 4.21, which has an equal and opposite skew angle at its abutments. The NTSCS29 bridge has skew at only one of its supports.

Figure 4.40. New Tub-girder bridges, Simple-span, Curved with Skewed supports, NTSCS (LENGTH / RADIUS / WIDTH / θ_{Left}, θ_{Right}). The columns in the matrix for (L = 350 ft., w = 30 ft., R = 1390 and 2085 ft.) are not shown.

4.3.4.7 Continuous-Span Bridges, Curved, with Skewed Supports (ICCS and TCCS)

Figure 4.41 shows six of the 12 possible groups of ICCS bridges. Note that the *R* values selected for the ICCR bridges (Figure 4.30) were used also for the subsequent ICCS designs in Figure 4.41. Rows 1 through 3 of the parametric study design matrix shown in this figure correspond to different orientations of the bearing lines relative to the curved geometry, but with the bearing lines parallel (or near parallel in cases where the skew angle is limited by $\theta = + 70^{o}$ at the inside edge of the deck). The bridges in the fourth row are similar to those in row 1, but with zero skew at the bearing line at the right hand end of the bridge. Three of the four combinations of deck width and horizontal curvature for L = 150 ft.are considered in columns 1 through 3 of this matrix. Narrow 250 ft.continuous-spans with the tighter curvature are considered in the fourth column. This case was included because ramp type structures with roughly 250 ft.span lengths are very common. The last two columns of Figure 4.41 show 350 ft.two-span continuous bridges with 80 ft.wide decks and each of the values of horizontal curvature determined previously. The narrower bridges were not considered for these span lengths, since it was expected that the influence of skew will be more minor for these bridges. Lastly, all the 150 ft.span bridges in column 1 of the Figure 4.41 test matrix were selected. In addition, all the 250 and 350 ft.span bridges in columns 4 and 6 were selected except the ones with perfect symmetry about the center pier (NICCS15 and 23) and NICCS22 since this bridge is similar to NICCR12. The case with perfect symmetry about the center pier was believed to be less common for these types of bridge geometry. The two non-exceptional cases with the wider decks were considered in the third column of this parametric study design matrix. NICCS11 was not selected since this bridge is similar to NICCR8 in Figure 4.30.

EICCS 10 was inserted into the design matrix. This is the MN DOT Bridge No. 27998, TH94 between 27th Avenue and Huron Boulevard in Minneapolis, MN. This bridge has been studied extensively, both experimentally and analytically, by Galambos et al. (1996). Also, it has been used by Nowak et al. (2006) as part of the calibration of the AASHTO LRFD Specifications for curved steel bridges. Therefore, this bridge was selected to be of particular value in relating the implications of analysis accuracy in the context of structural reliability calibration and assessment of strengths.

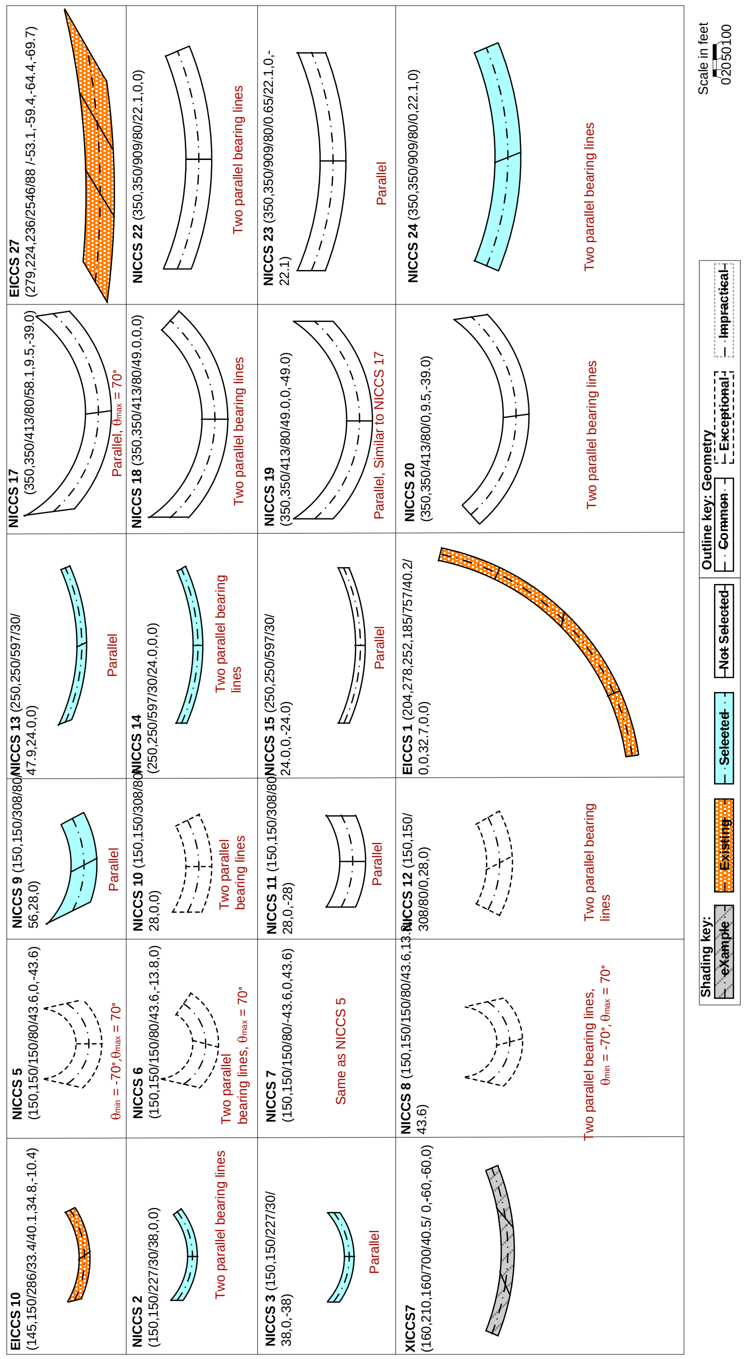

Figure 4.41. Existing and New I-girder bridges, Continuous-span, Curved with Skewed supports, EICCS or NICCS (LENGTH1, LENGTH2, ... / RADIUS / WIDTH / θ_{Left}, …, θ_{Right}). The columns in the matrix for (L = 150 ft., w =30 ft., R = 438 ft.), (L = 250 ft., w =30 ft., R = 1179 ft.), (L = 250 ft., w =80 ft., R = 250 and 491 ft.), (L = 350 ft., w =30 ft., R = 1153 and 2291 ft.) are not shown.

EICCS1 was also inserted into the parametric study matrix. This bridge is the I-459 / US31 Interchange Flyover A in Jefferson County, AL. The construction of this bridge was observed and thoroughly documented by Osborne (2002). This bridge represents a successful implementation of total dead load fit detailing on a significantly curved span with one pier location that is substantially skewed relative to a radial line. Figure 4.42 shows a photo looking along the length of the bridge at the skewed bearing line during construction. Figure 4.43 shows another snapshot of the steel erection.

Figure 4.42. EICCS1, I-459 / US31 Interchange Flyover A, Jefferson Co. AL (Osborne, 2002).

Figure 4.44 shows the two-span continuous TCCS (tub-girder) bridges considering:

- Eight combinations of skew magnitude and pattern when only one support is skewed in the rage of ±30° and two additional configurations when two supports are skewed to accommodate three parallel support lines,
- Two values for the length L_s (L_s = 150 and 250 ft.), L_s = 350 ft.and their associated radius values are not shown,
- Two values of the curvature radii R for each span length, and
- One value for the deck width w (w = 30 ft.)

Figure 4.43. EICCS1, I-459 / US31 Interchange Flyover A, Jefferson Co. AL (Osborne, 2002).

In this category several cases fall into the exceptional cases since a 30° skew for curved bridges distorts the geometry at the support lines causing undesired layouts for a narrow configuration. Two existing bridges with an intermediate skewed support were included in this category (ETCCS5a and ETCCS6) and a third case was selected NTCCS22.

NTCCS22, which has a moderate skew of 20° at one abutment, was selected because this configuration results in two parallel support lines. ETCCS5a, which is located at the SR 9A and SR202 interchange in Duval Co. FL, has an intermediate support that is skewed at 4.8°. These two bridges were targeted to gain insight about the effect of skew at an intermediate support and at the abutment.

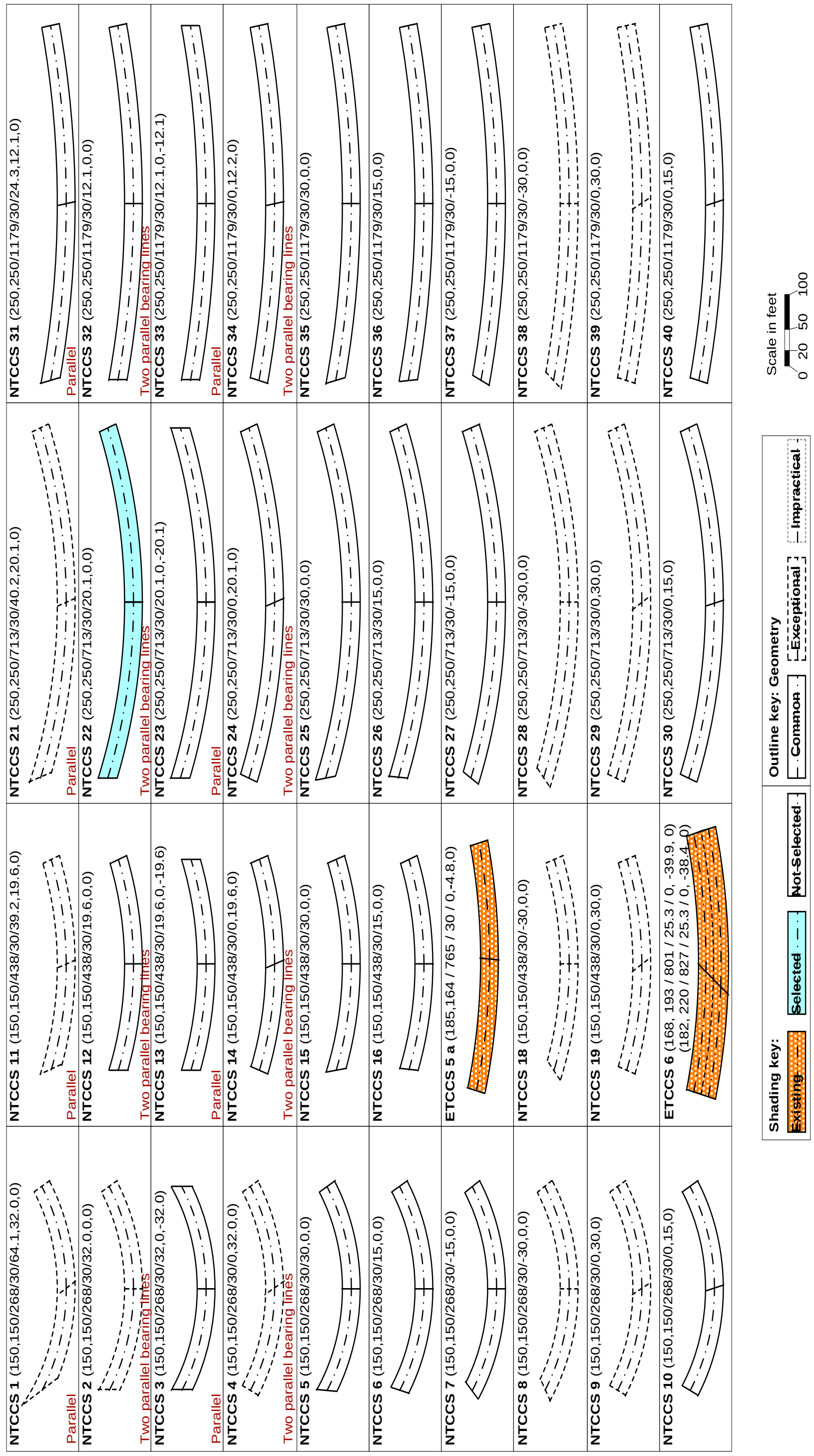

Figure 4.44. Existing and New Tub-girder bridges, Continuous-span, Curved with Skewed supports, ETCCS or NTCCS (LENGTH1, LENGTH2, … / RADIUS / WIDTH / θ_{Left}, …, θ_{Right}). The columns in the matrix for (L = 350 ft., w = 30 ft., R = 1380 and 2291 ft.) are not shown.

ETCCS6 is the Magruder Blvd. bridge over I-64 in Hampton, VA. This bridge was constructed in two phases, with 2 tub-girders each phase, and has a maximum skew angle of 40° at the interior phase. This bridge does not include any external cross-frames or diaphragms between the girders at its skewed interior support, and it does not contain any intermediate external diaphragms between the girders within its spans. Figure 4.45 shows the underside of the completed Magruder Blvd. bridge.

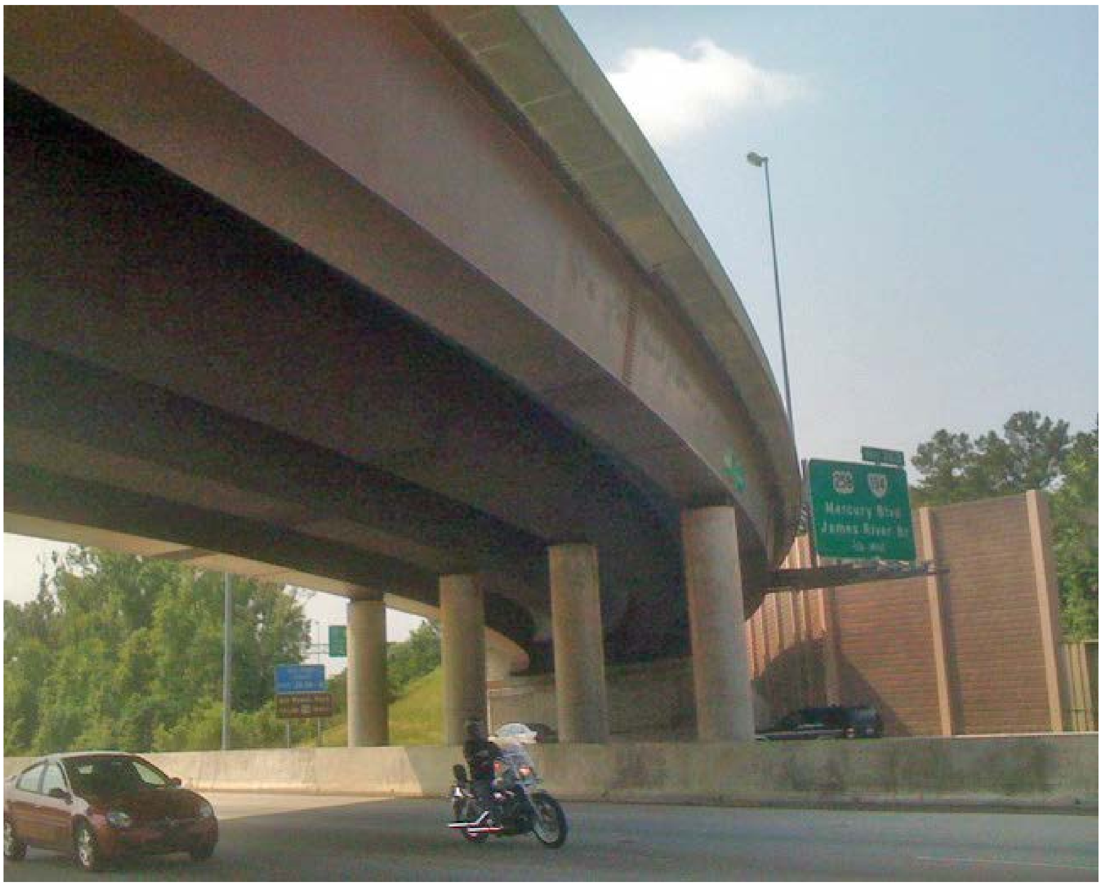

Figure 4.45. ETCCS6, McGruder Blvd. bridge over I-64 in Hampton, VA.

4.3.4.8 Tub-Girder Skew Sensitivity Studies

Skew sensitivity studies were performed for six of the above tub-girder bridges to assess the impact of skew on the simplified torsional moment estimates. No changes to the tub-girder bridge original designs were made but minor modifications were made to accommodate the changes on the framing plan. The bridges and their variations are NTSSS2 (30°, 15° and 0°), NTSSS4 (16°, 10° and 0°), NTSCS5 (10.7° and 0°), NTSCS29 (15.7° and 0°), ETCCS5a (-4.8°, 0°, -10° and 10°) and NTCCS22 (20.1° and 0°). The first angle in the above parentheses corresponds to the original design. The bridge layouts of the sensitivity studies are shown in Figure 4.46.

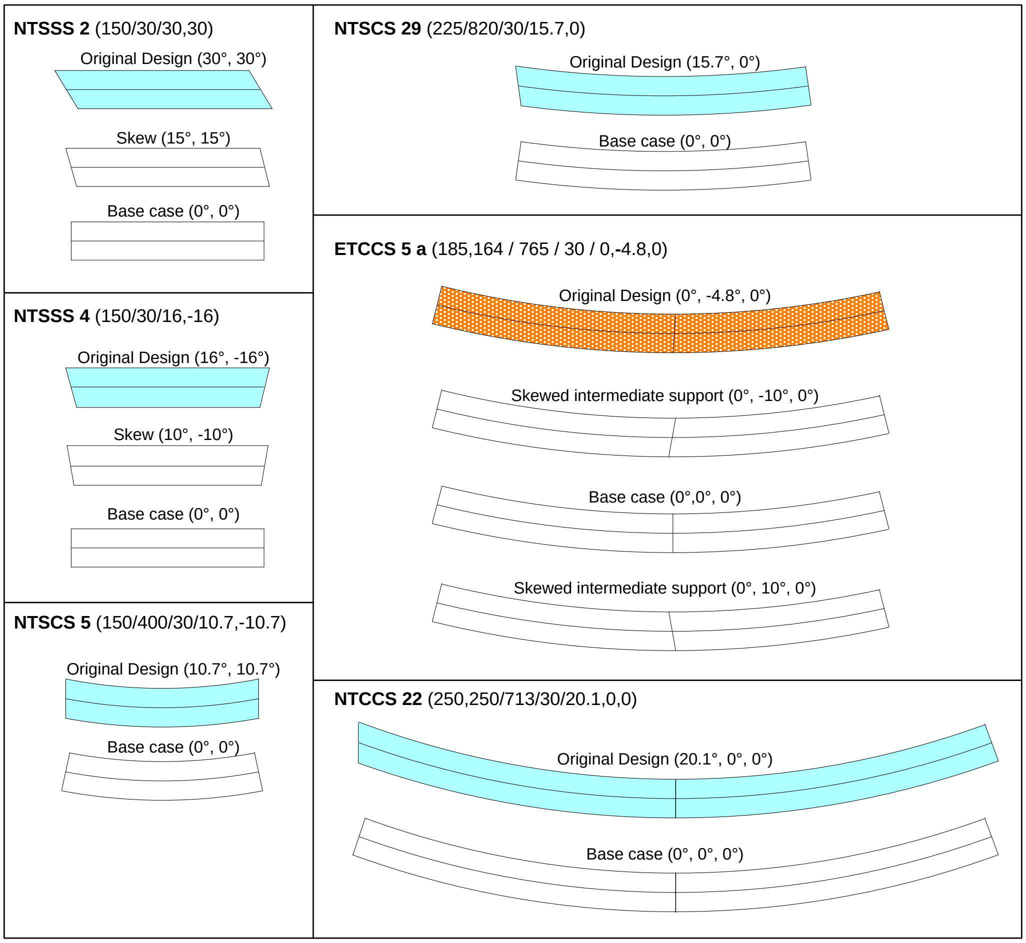

Figure 4.46. Cases considered in the tub-girder bridge sensitivity studies.

4.3.5 Final Summary of the Parametric Study Bridges

Tables 4.2 and 4.3 provide an overall summary of the number of New, Existing and eXample bridges developed in the above parametric study design for each of the major groups of bridges. Eighty-six bridges were selected in total, including 58 I-girder bridges and 28 tub-girder bridges, or 26 existing bridges and 60 parametric study designs.

Table 4.2. Overall summary of New, Existing and eXample I-girder bridges.

Description		Cases
eXample I-girder, Continuous-span, Straight, No skew (Base comparison case)		**1**
ISSS	(EISSS) Existing, I-girder, Simple-span, Straight, Skewed supports	3
	(XISSS) eXample, I-girder, Simple-span, Straight, Skewed supports	0
	(NISSS) New, I-girder, Simple-span, Straight, Skewed supports	12
	Total: ISSS	**15**
ICSS	(EICSS) Existing, I-girder, Continuous-span, Straight, Skewed supports	3
	(XICSS) eXample, I-girder, Continuous-span, Straight, Skewed supports	1
	(NICSS) New, I-girder, Continuous-span, Straight, Skewed supports	5
	Total: ICSS	**9**
ISCR	(EISCR) Existing, I-girder, Simple-span, Curved, Radial supports	1
	(XISCR) eXample, I-girder Simple-span, Curved, Radial supports	0
	(NISCR) New, I-girder Simple-span, Curved, Radial supports	6
	Total: ISCR	**7**
ICCR	(EICCR) Existing, I-girder, Continuous-span, Curved, Radial supports	4
	(XICCR) eXample, I-girder, Continuous-span, Curved Radial supports	0
	(NICCR) New, I-girder, Continuous-span, Curved Radial supports	3
	Total: ICCR	**7**
ISCS	(EISCS) Existing, I-girder, Simple-span, Curved, Skewed supports	2
	(XISCS) eXample, I-girder, Simple-span, Curved, Skewed supports	0
	(NISCS) New, I-girder, Simple-span, Curved, Skewed supports	7
	Total: ISCS	**9**
ICCS	(EICCS) Existing, I-girder, Continuous-span, Curved, Skewed supports	3
	(XICCS) eXample, I-girder, Continuous-span, Curved, Skewed supports	1
	(NICCS) New, I-girder, Continuous-span, Curved, Skewed supports	6
	Total: ICCS	**10**
Total: Existing I-girder bridges		16
Total: eXample I-girder bridges		3
Total: New I-girder bridges		39
Total: I-girder bridges		58

Appendix E of the NCHRP 12-79 final report provides a concise summary of the most important considerations for each of the bridges (one-third to one-half page per bridge), while Appendix K explains the organization of the detailed electronic data for each of the bridges. Appendix I of the final report provides a more detailed summary of the results for each of the bridges.

Table 4.3. Overall summary of New, Existing and eXample tub-girder bridges.

Description		Cases
eXample Tub-girder, Continuous-span, Straight, No skew (Base comparison case)		**1**
TSSS	(ETSSS) Existing, Tub-girder, Simple-span, Straight, Skewed supports	1
	(XTSSS) eXample, Tub-girder, Simple-span, Straight, Skewed supports	0
	(NTSSS) New, Tub-girder, Simple-span, Straight, Skewed supports	3
	Total: TSSS	**4**
TCSS	(ETCSS) Existing, Tub-girder, Continuous-span, Straight, Skewed supports	0
	(XTCSS) eXample, Tub-girder, Continuous-span, Straight, Skewed supports	0
	(NTCSS) New, Tub-girder, Continuous-span, Straight, Skewed supports	0
	Total: TCSS	**0**
TSCR	(ETSCR) Existing, Tub-girder Simple-span, Curved, Radial supports	0
	(XTSCR) eXample, Tub-girder Simple-span, Curved, Radial supports	0
	(NTSCR) New, Tub-girder Simple-span, Curved, Radial supports	3
	Total: TSCR	**3**
TCCR	(ETCCR) Existing, Tub-girder, Continuous-span, Curved, Radial supports	2
	(XTCCR) eXample, Tub-girder, Continuous-span, Curved, Radial supports	1
	(NTCCR) New, Tub-girder, Continuous-span, Curved Radial supports	2
	Total: TCCR	**5**
TSCS	(ETSCS) Existing, Tub-girder, Simple-span, Curved, Skewed supports	0
	(XTSCS) eXample, Tub-girder, Simple-span, Curved, Skewed supports	0
	(NTSCS) New, Tub-girder, Simple-span, Curved, Skewed supports	2
	Total: TSCS	**2**
TCCS	(ETCCS) Existing, Tub-girder, Continuous-span, Curved, Skewed supports	2
	(XTCCS) eXample, Tub-girder, Continuous-span, Curved, Skewed supports	0
	(NTCCS) New, Tub-girder, Continuous-span, Curved, Skewed supports	1
	Total: TCCS	**3**
Total: Existing Tub-girder bridges		5
Total: eXample Tub-girder bridges		2
Total: New Tub-girder bridges		11
Total: Additional skew sensitivity studies		10
Total: Tub-girder bridges		28

5. Assessment of Conventional Simplified Methods of Analysis

NCHRP 12-79 has conducted a wide range of studies on the bridges introduced in Chapter 4 to determine the ability of the approximate 1D and 2D methods of analysis to capture the behavior predicted by refined 3D FEA models. The line-girder (1D) analyses of straight I- and tub-girder bridges, as well as curved tub-girder bridges, were performed using the STLBRIDGE package (Bridgesoft, Inc., 2010). The line-girder analyses of curved I-girder bridges were based in the V-load method using the program VANCK (NSBA, 1996). The line-girder analyses of curved tub-girder bridges were modified using a spreadsheet implementation of the M/R Method (Tung and Fountain, 1970). In addition, the line-girder analysis results for skewed tub-girder bridges were modified using the developments described in Sections 2.1.5 and 2.7.1.2. The simplified 2D-grid analyses were conducted using the LARSA 4D (LARSA, 2010) and MDX (MDX Software, 2011) software systems.

A quantitative assessment of the analysis accuracy was obtained by identifying error measures that compare the simplified approximate solutions to the 3D second-order elastic FEA benchmarks. The approach to quantify the error is as follows. First, an error function is defined as the absolute value of the difference between the FEA representation and the approximate analysis response, as shown in Figure 5.1. The errors are calculated at the locations along the length of the girders where the responses are sampled in the approximate method. Next, the error function is used to calculate the normalized mean error, μ_e. This index provides an *overall* measure of the performance of the approximate models and is calculated as:

$$\mu_e = \frac{1}{N \cdot R_{FEA,max}} \sum_{i=1}^{N} e_i \qquad (5.1)$$

where N is the total number of sampling points along the girder length used in the simplified analysis, $R_{FEA,max}$ is the absolute value of the maximum response obtained from the FEA benchmark, and e_i is the absolute value of the error relative to the 3D FEA benchmark solution at point i. In this equation, the mean error is normalized with respect to the maximum value of the response obtained from the FEA to avoid a comparison of “small numbers to small numbers.” For example, the vertical displacements near the supports in a simple-span bridge are relatively small. The percent error in the response prediction relative to the physical displacement may be large at these locations, but the deflections are small compared to the deflections expected near mid-span. Hence, in Eq. (5.1), the errors are weighted with respect to the maximum value of the response. In addition, by dividing the error by $R_{FEA,max}$, the influence of the load magnitude is removed from the analyses. Given this practice, the mean errors can be compared for different bridges.

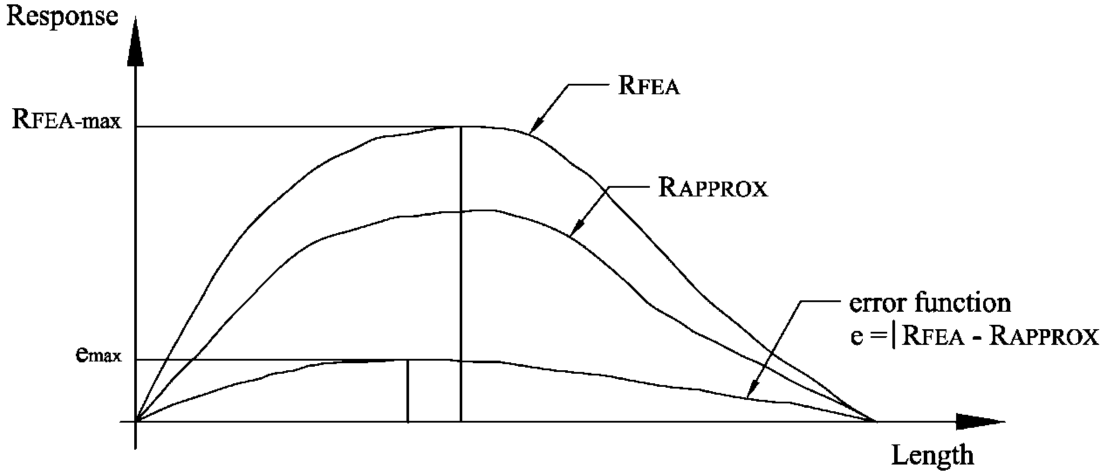

Figure 5.1. Schematic representation of the error function.

5.1 Assessment of I-Girder Bridges

Table 5.1 shows the percent normalized mean errors in the major-axis bending stresses and vertical displacements obtained for the 58 I-girder bridges studied in the NCHRP 12-79 research. These bridges are divided into six different groups based on their geometry. The first group corresponds to the curved radially-supported bridges (labeled as "C") with connectivity indices $I_C > 1$. As discussed in Section 3.1.3, the connectivity index provides an indication of when the inaccurate representation of the girder torsional stiffness in conventional 2D-grid models tends to have a significant impact on the overall error. The second group includes curved and radial bridges with $I_C \leq 1$. The straight and skewed structures (labeled as "S") are subdivided based on the skew index I_S, which differentiates the bridges where skew has a minor influence on the structural behavior from those where the collateral effects from the skew are more important (see Section 3.1.2). The groups correspond to $I_S < 0.30$, $0.30 \leq I_S < 0.65$, and $I_S \geq 0.65$. The sixth group contains the curved and skewed bridges studied in the project (labeled as "C&S"). It is important to note that the skew and curvature indices, I_S and I_C should not be used in combination to estimate the accuracy of the approximate models in a curved and skewed bridge.

No clear trends in the normalized mean errors were identified as a combined function of I_S and I_C with the exception that, as the skew or the horizontal curvature approaches zero, then the error characteristics should approach the values shown for the "C" and the "S" categories respectively.

Table 5.1 compares the results of the first-order (*geometrically linear*) 3D FEA, 2D-grid, and 1D analysis results to the predictions obtained from elastic *second-order* 3D FEA. In the table, f_b is the major-axis bending stress and Δ_z is the vertical displacement. A mean error value is calculated for each response on each girder of the bridges. The values reported in Table 5.1 are the largest mean errors determined by inspecting the values obtained for each girder in a given bridge.

Upon inspection of the results in Table 5.1, the following important trends can be observed:

Second-Order Amplification

The results obtained from the first-order 3D FEA show that the response amplifications due to second-order effects are negligible in most of the bridges. With the exception of bridges NISCR5 and EISCS4, the differences between the linear and nonlinear FEA results are less than 10 %. For bridges NISCR5 and EISCS4, the analyses show that these long-and-narrow structures experience significant global second order amplification. Section 2.9 discusses this behavior in the context of bridge EISCS4. It should be noted that unless noted otherwise, the benchmark second-order stresses in Table 5.1 are evaluated at 1.5 times the nominal dead load, corresponding to the AASHTO LRFD Strength IV load combination. However, the benchmark second-order displacements are evaluated at the nominal (unfactored) dead load level.

It is recommended that the loss of accuracy due to large global second-order amplification should be addressed separately from the other factors affecting accuracy. The estimated global second-order amplification, AF_G (Eq. 2.101), is relatively large for the above two bridges. As noted in Section 2.9, if the AASHTO constructability checks do not pass due to a large AF_G, this should be taken as an indication that a second-order 3D FEA may need to be conducted, or the design should be changed to avoid the large second-order effects. Therefore, these bridges are excluded from the subsequent error syntheses.

Table 5.1. I-girder bridge percent normalized mean errors compared to 3D second-order elastic FEA for major-axis bending stresses (f_b) and vertical displacements (Δ_z).

Group	Bridge Name	I_S	I_C	I_T	I_L	3D-FEA Linear		2D-Grid - P1		2D-Grid - P2		1D	
						f_b μ_e	Δz μ_e	f_b μ_e	Δz μ_e	f_b μ_e	Δz μ_e	f_b μ_e	Δz μ_e
C ($I_C \leq 1$)	EICCR22a	0	0.98	0.66	1.11	0	0	6	3	4	2	10	6
	NICCR12	0	0.69	0.66	1.18	1	1	8	7	8	4	9	8
	EICCR11	0	0.67	0.87	1.17	9	4	11	7	9	3	12	16
	EICCR4	0	0.68	0.64	1.09	1	1	4	3	6	3	7	5
	NISCR5[a]	0	0.58	0.71	1.02	20	9	18	1	15	4	14	19
	EICCR15	0	0.35	0.58	1.05	3	1	5	3	6	2	12	11
C ($I_C > 1$)	EISCR1	0	18.8	0.71	1.09	1	1	8	157	10	147	11	20
	NISCR7	0	6.70	0.62	1.30	1	1	22	90	17	117	15	13
	NISCR2	0	4.89	0.69	1.06	3	2	6	38	5	32	6	15
	NISCR8	0	4.46	0.58	1.19	1	0	11	91	12	97	13	29
	NICCR1	0	4.13	0.87	1.11	0	0	11	96	7	5	8	10
	NICCR8	0	3.04	0.61	1.63	0	0	9	57	9	53	7	5
	NISCR10	0	1.93	0.59	1.11	1	1	12	40	10	37	17	17
	NISCR11	0	1.08	0.65	1.11	5	2	13	44	6	14	13	16

[a] NISCR5 is excluded from the error synthesis since this bridge has large second-order amplification. The stresses and displacements for this bridge are reported at 1.5 and 1.0 of the TDL respectively.

Table 5.1 (continued). I-girder bridge percent normalized mean errors compared to 3D second-order elastic FEA for major-axis bending stresses (f_b) and vertical displacements (Δ_z).

Group	Bridge Name	I_S	I_C	Max. I_T	Max. I_L	3D-FEA Linear		2D-Grid - P1		2D-Grid - P2		1D	
						f_b μ_e	Δz μ_e	f_b μ_e	Δz μ_e	f_b μ_e	Δz μ_e	f_b μ_e	Δz μ_e
S ($I_S \leq 0.30$)	XICSN1	0	0	0.50	1.00	0	0	4	3	3	3	5	6
	NISSS2	0.11	0	0.50	1.00	1	0	5	4	5	2	8	5
	EISSS3[b]	0.24	0	0.50	1.00	4	6	9	9	9	9	10	12
	NISSS6	0.19	0	0.53	1.21	4	2	5	2	7	3	5	2
	NISSS11	0.18	0	0.50	1.00	0	0	4	4	2	1	4	4
	NISSS37	0.18	0	0.54	1.44	2	1	3	2	2	1	10	6
	NISSS53	0.29	0	0.50	1.00	1	1	5	5	5	5	5	6
	NISSS56	0.30	0	0.53	1.34	4	2	5	1	4	1	8	6
	NICSS1	0.11	0	0.52	1.25	1	1	2	3	2	11	4	3
	NICSS3	0.11	0	0.52	1.25	1	0	3	2	3	8	4	3
	NICSS25	0.15	0	0.52	1.16	0	1	2	3	2	4	3	3
	NICSS27	0.15	0	0.52	1.16	1	1	3	3	3	3	4	3

[b] EISSS3 is excluded from the error synthesis since this bridge has large second-order amplification and is unable to support the total dead load (TDL). The stresses and displacements reported in the table for this bridge are at 1.3 and 1.0 of the TDL respectively.

Table 5.1 (continued). I-girder bridge percent normalized mean errors compared to 3D second-order elastic FEA for major-axis bending stresses (f_b) and vertical displacements (Δ_z).

Group	Bridge Name	I_S	I_C	Max. I_T	Max. I_L	3D-FEA Linear		2D-Grid - P1		2D-Grid - P2		1D	
						f_b μ_e	Δz μ_e	f_b μ_e	Δz μ_e	f_b μ_e	Δz μ_e	f_b μ_e	Δz μ_e
S ($0.30 < I_S \leq 0.65$)	NISSS4	0.44	0	0.50	1.00	3	3	9	6	7	6	10	7
	EISSS5	0.54	0	0.50	1.00	2	2	7	6	4	6	9	8
	EISSS6	0.43	0	0.50	1.00	3	0	9	5	7	2	6	6
	NISSS36	0.40	0	0.55	1.49	3	1	9	2	7	2	8	3
	XICSS5[c]	0.53	0	0.50	1.00	1	1	NA	NA	16	12	NA	NA
	EICSS1[c]	0.42	0	0.50	1.00	0	0	NA	NA	11	12	NA	NA
	XICSS5	0.53	0	0.50	1.00	1	1	12	8	6	7	16	12
	EICSS1	0.42	0	0.50	1.00	0	0	4	4	4	6	8	3
	EICSS2	0.50	0	0.55	1.35	1	0	6	6	6	6	9	8
	NISSS13	0.60	0	0.50	1.00	1	1	6	5	5	6	5	5
	NISSS16	0.59	0	0.58	1.83	2	2	9	6	8	6	9	7
	EICSS12	0.58	0	0.50	1.00	1	0	7	5	4	3	7	7
S ($I_S > 0.65$)	NISSS14	1.36	0	0.50	1.00	4	0	27	26	26	27	28	27
	NICSS16	1.69	0	0.50	1.00	1	0	15	12	15	16	15	13
	NISSS54	0.68	0	0.50	1.00	4	2	17	16	16	13	16	13

[c] Considering staged deck placement in the 3D FEA and in Program 2

Table 5.1 (continued). I-girder bridge percent normalized mean errors compared to 3D second-order elastic FEA for major-axis bending stresses (f_b) and vertical displacements (Δ_z)

Group	Bridge Name	I_S	I_C	I_T	I_L	3D-FEA Linear		2D-Grid - P1		2D-Grid - P2		1D	
						f_b μ_e	Δz μ_e	f_b μ_e	Δz μ_e	f_b μ_e	Δz μ_e	f_b μ_e	Δz μ_e
C&S	EISCS3	0.25	2.99	0.68	0.86	1	1	7	25	5	5	19	38
	NISCS3	0.11	3.44	0.71	1.18	4	2	10	2	5	1	29	23
	NISCS9	0.35	3.11	0.63	0.88	2	1	10	36	10	5	24	23
	NISCS14	0.67	4.46	0.55	0.65	0	0	9	76	7	3	10	15
	NISCS15	0.36	4.46	0.67	1.88	1	1	19	74	14	12	11	16
	NISCS37	0.35	1.03	0.35	0.62	1	1	9	42	23	36	37	40
	NISCS38	0.48	0.94	0.59	0.68	1	0	4	39	4	5	15	18
	NISCS39	0.17	1.21	0.68	1.32	7	3	13	53	10	2	10	17
	EISCS4[d]	0.04	0.55	0.64	1.00	53	52	41	48	43	48	43	50
	EICCS10	0.16	2.19	0.73	1.07	0	0	10	25	10	19	14	12
	NICCS2	0.13	3.67	0.87	1.24	0	0	7	36	4	3	9	10
	NICCS3	0.13	3.30	0.81	0.98	1	0	17	62	5	4	11	13
	XICCS7	0.36	1.33	0.65	1.51	0	0	12	21	9	9	15	6
	NICCS9	0.73	3.04	0.58	0.77	0	0	13	73	5	7	8	21
	NICCS13	0.11	1.05	0.85	0.98	2	1	7	21	3	2	10	13
	NICCS14	0.04	1.12	0.88	1.04	2	1	6	21	4	3	11	11
	EICCS1	0.08	0.99	0.80	1.25	1	1	10	20	29	5	30	14
	EICCS27	0.92	0.17	0.47	0.90	1	0	15	10	17	7	18	11
	NICCS24	0.09	0.46	0.68	1.18	1	1	6	19	3	1	7	6

[d] EISCR4 is excluded from the error synthesis since this bridge has large second-order amplification and is unable to support the total dead load (TDL). The stresses and displacements reported in the table for this bridge are at 82 % of the TDL.

It is recommended that the factor AF_G (Eq. 2.101) should be calculated and used in performing the AASHTO constructability checks for two and three-girder units (or intermediate stages of the steel erection), as well as for relatively narrow units or intermediate stages with L_s/w_g ratios greater than about five. In addition, in I-girder bridges involving lean-on bracing systems, the lean-on effects from all the girders being stabilized must be considered. The reader is referred to Helwig et al. (2005) and Hermann et al. (2005) for presentation of simplified procedures for checking girder system stability including lean-on effects.

Although the analysis results considered are based on the final constructed geometry of the bridge for NISCR5, and the final constructed geometry of the bridge unit that experienced excessive displacements for EISCS4, these results are representative of results that can be expected for other intermediate stages of the steel erection where the partially completed structure is composed of only a few girders and/or is relatively narrow compared to the span length.

In addition to global second-order amplification due to stability effects, the potential local second-order amplification of the flange lateral bending should be checked between the cross-frame locations in bridge I-girders. Equation 6.10.1.6-4, from AASHTO LRFD Article 6.10.1.6, serves generally as an accurate to conservative estimate of this local second-order amplification. In particular, large values of the *AF* estimated by this equation on fascia girders may indicate a condition where the flange lateral bending due to overhang eccentric bracket loads and/or horizontal curvature may lead to excessive torsional rotations that can cause local dips in the deck elevations between cross-frames. These rotations can be exacerbated by web distortional deformations in cases where the height of the overhang brackets is significantly less than the girder web depths. Therefore, local web distortional deformations on fascia girders always should be checked.

Lastly, the benchmark 3D-FEA model of the "S ($I_S \leq 0.30$)" bridge EISSS3 is unable to support the factored total dead load (1.5 x TDL) due to large second-order amplification associated with the flexibility of the V-type cross-frames without top chords utilized in this structure. Therefore, EISSS3 is excluded from further consideration in the synthesis of the errors below. V-type cross-frames without top chords often do not have sufficient stiffness to brace the I-girders prior to the deck becoming composite. Their effectiveness may often depend on incidental stiffnesses developed by the formwork or other construction devices serving as top chord elements. These incidental stiffnesses can be highly variable and difficult to gage or to control, and thus the use of V-type cross-frames can result in significant difficulties in the ability to predict the physical constructed geometry in the field. Therefore, as discussed subsequently in Chapter 9, V-type cross-frames without top chords should be used with extreme caution.

2D-Grid Solutions

Several observations can be made regarding the 2D-grid solutions from Table 5.1:

- The 2D-grid solutions from Programs P1 and P2 are very similar for the major-axis bending stresses in all the cases of Table 5.1, with the exception of only three of the “C&S” bridges, NISCS37, NICCS3, and EICCS1. Program P1 gives significantly better f_b results for NISCS37 and EICCS1, whereas P2 gives much better f_b results for NICCS3. There is no clear reason why the solutions differed significantly for just these three bridges.
- For all the “C” bridges and for all the “S” bridges, the vertical displacement solutions are very similar from both 2D-grid programs with the exception of bridges NICCR1 and NISCR11, where program P2 gives much better results. Similar to the above cases, there is no clear reason for the larger error exhibited by P1 for just these two bridges.
- For the “S” bridges with $I_S \leq 0.30$ and $0.30 < I_S < 0.65$, all of the conventional 2D-grid solutions for the major-axis bending stresses and vertical displacements are reasonably good (a more quantitative assessment of the errors as a function of the bridge type is presented in the next section). However, for the “S” bridges with $I_S > 0.65$, the conventional 2D-grid solutions give relatively poor predictions for both the major-axis bending stresses and the displacements. The reason for this behavior is discussed in detail subsequently in Chapter 6. Basically, due to the poor (highly flexible) girder torsion model, the conventional 2D-grid solutions are unable to capture the transverse load paths that develop in skewed bridges with large I_S values.
- For the “C” bridges with $I_C > 1$, both the 2D-grid programs P1 and P2 give poor displacement solutions in the majority of the cases. The only cases of this group where the results are reasonably accurate are the P2 solutions for bridges NICCR1 and NISCR11. A key reason for this behavior is explained below.

- For the “C&S” bridges, the displacement results are reasonably accurate for the 2D-grid program P2, with the exception of bridges NISCS37 and NICCS10 (after excluding EISCS4 due to large AF_G). However, the 2D-grid program P1 exhibits very large displacement errors for the majority of the “C&S” bridges. NISCS3 and EICCS27 are the only bridges that have reasonably accurate displacement predictions from P1. A key reason for this behavior, as well as for the above poor displacement results for the “C” bridges with $I_C > 1$, is explained below.

The key reason for the poor displacement results in the last two of the above observations is the use of multiple elements between the cross-frame locations in modeling the curved girders in these structures. As noted at the beginning of this chapter, the models in program P1 were created using four elements between each of the cross-frames for all of the bridges, and the program P2 models were created with a “high-resolution mesh” for all of the bridges, which typically means that P2 also uses four elements between each cross-frame member. However, P2 was also set up to include the effect of the composite slab via the Plate-Eccentric Beam approach in subsequent solutions. The P2 Plate-Eccentric Beam solution is effectively just a 2D-grid solution prior to the slab being made composite. Unfortunately, program P2 is unable to create a high-resolution mesh in its Plate-Eccentric Beam solution when a bridge has skew, and hence P2 defaults back to a “low-resolution mesh” in these situations. With a low-resolution mesh in P2, only one element is utilized between each of the cross-frame members.

Interestingly, contrary to what one might expect, the use of a single element between the cross-frame locations results in more accurate solutions with the conventional 2D-grid procedures. The reason for this behavior can be explained in basic terms by considering an isolated conventional 2D-grid model of an I-section member, subjected to uniform moment along a circular arc between two cross-frame locations, i.e., equal and opposite end moments (see Figure 5.2). The vector direction of the moments, by the right-hand rule, is indicated by the double arrows in the figure. In the common “high-resolution” representation of this curved member, the arc is modeled with four straight elements, with each of the nodes located along the arc. Major-axis bending moments perpendicular to the chord between the member ends resolve into both a major-axis bending and a torsional component within the individual elements. If one considers the equilibrium at one of the intermediate nodes, major-axis bending in one element is generally resolved into both major-axis bending and torsion in the next element. However, unfortunately, in the conventional methods, the torsional model substantially underestimates the true stiffness of the I-girder, since only the St. Venant term (*GJ*/*L*) is considered. The torsional stiffness coming from the restraint of warping, related to the cross-section rigidity term EC_w, is neglected. As such, the twisting deformations are grossly over-estimated.

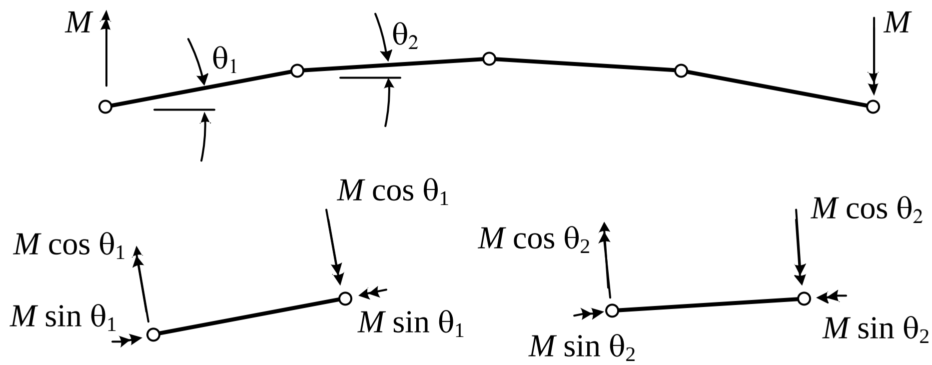

Figure 5.2. Behavior for a chorded representation of a curved I-girder using four straight elements.

Furthermore, because of the curved geometry (represented in a chorded fashion by the four elements in Figure 5.2), the small torsional stiffness reduces the overall stiffness of the approximate model in resisting vertical deflection. The twisting of one element causes not only a torsional rotation in the next element, but because of the change in orientation of the elements in the chorded representation of the arc, it causes major-axis bending rotation and corresponding vertical deflections in the next element. Furthermore, the overall major-axis bending rotational stiffness that this member provides to the rest of the bridge, about an axis perpendicular to its chord and at its ends, is reduced by the above effects. This results in an increase in the vertical deflections at other locations in the bridge.

Interestingly, if a curved I-girder is represented by only one straight element between its cross-frame locations, the cross-frames are able to resist the components of the moments that cause twisting of the girder. As a result, the overall model of the bridge structure responds in a much stiffer fashion. This same behavior is obtained if multiple elements are used between the cross-frames with the overall geometry represented as a straight chord between the cross-frames.

(This helps explain why the vertical deflections in straight skewed I-girders are still represented reasonably well with a high resolution mesh).

Modeling of the girders as straight segments between the cross-frames tends to improve the results in the conventional 2D-grid analysis of curved bridges, since in effect, this approach completely neglects the influence of the horizontal curvature between the cross-frames (with the exception of separate calculations to estimate girder flange lateral bending stresses). Studies conducted with “C&S” bridges to address this peculiarity demonstrate that the responses obtained from the P1 models, when the discretization is reduced to one element between every set of cross-frames, are essentially the same as with the P2 models.

Completely neglecting the horizontal curvature effects between the cross-frames of course cannot generally produce an accurate model either. Therefore, using a coarse grid of elements with only one straight element between each cross-frame is not generally recommended as a proper way to obtain accurate predictions. It should be noted that the “C&S” bridges NISCS37 and EICCS10 have relatively poor displacement predictions in spite of the fact that the P2 solutions were based on a single element between each of the cross-frames. Nevertheless, in many bridges, the girder arcs between the cross-frames are small enough such that a single element between the cross-frames should be sufficient to accurately represent the overall curved geometry of the structure (assuming that a more accurate girder torsional stiffness than the conventional GJ/L is employed, as discussed in Chapter 6). The flange lateral bending stresses between the cross-frames can still be estimated using “component stress” equations such as Eqs. (2.13) through (2.17), or by more accurate means as discussed subsequently in Chapter 6.

Chapter 6 discusses modeling practices that can be implemented to improve the predictions obtained from 2D-grid analyses. The practices discussed in Chapter 6 are based on the principles of structural mechanics, and do not rely on the discretization level used in the model. The large errors associated with the more refined discretization are due to the dramatic under-representation of the girder torsional stiffness in the conventional 2D-grid models, along with the coupling between twist rotations and vertical displacements in curved members.

1D Line-Girder Solutions

The 1D line-girder results in Table 5.1 exhibit the following characteristics:

- The solutions are reasonably good for all the “C” bridges with $I_C < 1$. However, for the “C” bridges with $I_C > 1$, the errors are somewhat larger for several of the bridges, particularly for the displacements. It should be emphasized that the connectivity index, I_C, relates primarily to the influence of the poor girder torsion model on the overall results in conventional 2D-grid solutions. However, some correlation of the errors with I_C is evident also for the line-girder analysis solutions.
- For the “S” bridges, the 1D line-girder solutions are comparable in accuracy to the conventional 2D-grid solutions in all cases. The accuracy is reasonably good using both the 1D and the conventional 2D grid procedures for the $I_S \leq 0.30$ and the $0.30 < I_S \leq 0.65$ bridges. However, both of these types of solutions show relatively large errors for the major-axis bending stresses and the vertical displacements for the bridges with $I_S > 0.65$. Similar to the conventional 2D-grid solutions, 1D line-girder analysis is unable to capture any information about the transverse load paths in the structure. These load paths tend to be a significant characteristic of the overall bridge response in bridges with large I_S values. Of course, engineers would not generally expect to capture the transverse load paths from a 1D line-girder analysis. However, they may expect that these load paths are captured by a 2D-grid solution.
- For the “C&S” bridges, the errors relative to the 3D FEA benchmarks from the 1D-line girder analyses are highly variable. There are no clear trends in the data, other than the fact that the large errors are obviously due to the combination of skew with horizontal curvature. The V-load method does not have any mechanisms for including the influence of skew within its estimates, and therefore, one must expect significant errors with increasing values of skew with this approach. One can observe that the 1D analysis accuracy tends to be better for some of the bridges that have small I_S values. However, this is not generally the case since, in a curved bridge, the orientation of the skew (positive or negative) can have a substantial effect on the resulting bridge geometry.

Staged Deck Placement

For the continuous-span bridges XICSS5 and EICSS1, Table 5.1 shows data both for analyses where staged deck placement was not considered (generated by building the analysis models and simply “turning the gravity loads on”) and for analyses where staged deck placement was considered in the 3D FEA and the conventional 2D-grid solutions. The solutions where the staged deck placement was considered are highlighted by the shaded rows for XICSS5 and EICSS1 in Table 5.1. Program P2 was utilized to conduct the 2D-grid solutions for these bridges. In fact, the Plate Eccentric Beam modeling capabilities of this program were employed to represent the participation of the composite concrete deck. The deck concrete from previous stages was assumed to become fully effective in both the 3D FEA and the Plate Eccentric Beam solutions. Other assumptions are possible regarding the early-age stiffness of the concrete deck; however, the above assumptions are sufficient to evaluate the accuracy of the Plate Eccentric Beam solutions versus the 3D FEA benchmarks. In regions of the bridges where the concrete deck is not fully effective, the Plate Eccentric Beam solution effectively defaults to a conventional 2D-grid solution.

The major-axis bending stress and vertical displacement errors for the above two bridges are reasonable, but are slightly larger for the analyses considering the staged deck placement. The scope and number of these studies is not sufficient to draw broad conclusions regarding the accuracy of the Plate-Eccentric Beam models for general staged deck placement analysis. As noted at the end of Section 2.10, the primary focus of the NCHRP 12-79 research was on the overall accuracy of the 1D line-girder and 2D-grid results independent of the participation of the concrete deck.

5.1.1 Synthesis of Errors in Major-Axis Bending Stresses and Vertical Displacements for I-Girder Bridges

Table 5.2 shows the number of I-girder bridges within specific ranges of the normalized mean errors for the major-axis bending stresses and the vertical displacements from Table 5.1. Both of the 2D-grid programs P1 and P2 are considered, as well as the 1D analysis results. The selected error ranges are assigned letter grades based on the following criteria:

A: $\mu_e \leq 6$ %

B: 6 % < $\mu_e \leq 12$ %

C: 12 % < $\mu_e \leq 20$ %

D: 20 % < $\mu_e \leq 30$ %

F: $\mu_e > 30$ %

This grading scheme is somewhat arbitrary and was set based on the experience of the NCHRP 12-79 project team. The recommended use of this grading scheme is addressed subsequently. Depending on the type of response and the consequences of the error, different ranges of error can be acceptable for different calculations on different jobs. In any case, it is believed that most engineers would agree that analysis results that do not deviate more than 6 % from a highly refined benchmark solution are indeed highly accurate. In addition, analysis results where the errors are larger than 30 % relative to a rigorous benchmark solution might be considered as highly unreliable.

All of the linear 3D FEA results in the non-shaded rows of Table 5.1 fall within the A range for the bridges considered with a two minor exceptions, f_b for EICCR11 and f_b for NISCS39 which have errors or 9 and 7 % respectively. The differences between the 3D FEA linear and second-order analysis results in Table 5.1 are due solely to second-order effects. Bridges EICCR11 and NISCS39 are two of the most extreme geometries considered in the NCHRP 12-79 project. EICCR11 is the Ford City Bridge, which is a continuous-span four girder bridge with a 329 ft.curved span, an adjacent 417 ft.straight span, and a 48.3 ft.total deck width. Therefore, it is not surprising that this bridge would have significant second-order effects. These effects are detectable using Eq. (2.101) (see Section 2.9). NISCS39 is a wide 300 ft.simple-span curved bridge with a skew that increases the length of the girder on the outside of the curve.

Although the potential existence of significant second-order effects in the final erected configuration of this bridge would not be detected by the criteria discussed previously, this bridge nearly nearly achieves an A grade. Given these assessments, the 3D linear FEA results are not considered in Table 5.2. Table 5.2 focuses solely on the accuracy of the 2D-grid and 1D line-girder analysis solutions.

Two rows are highlighted for each of the bridge groups and analysis methods in Table 5.2. The row corresponding to the error range with the largest errors exhibited for a given bridge group and analysis solution is highlighted by a dark shade. In addition, the row corresponding to the most frequently occurring error range (i.e., the mode) is highlighted by a light shade, unless this range is the same as the error range with the largest errors.

The highlighted rows in Table 5.2 are used to generate final simplified scores for each of the bridge groups and analysis methods in Tables 5.3 and 5.4. The letter grades provided in Table 5.3 correspond to the worst-case score in Table 5.2, whereas the grades in Table 5.4 correspond to the most frequently occurring score, i.e., the mode score. Various footnotes are provided in Table 5.3 to identify the reasons for the worst-case scores.

Overall, one can observe the following from Tables 5.3 and 5.4:

- Both of the 2D-grid programs have worst-case grades of B and A as long as $I_C \leq 1$ for the "C" bridges, and as long as $I_S < 0.65$ for the "S" bridges. The mode of the grades in these categories is predominantly an A.
- For the "C" bridges with $I_C > 1$, the worst-case grades for f_b are a D and a C, while the mode of the grades is a B. However, the vertical displacements receive an F even for the mode of the grades, indicating that there are a large number of bridges where the displacement results might be considered unacceptable.
- For the "C" bridges with $I_C \leq 1$, the 1D methods (i.e., line-girder analysis with the V-load method) receive a worst-case score of B for both the major-axis bending stresses and C for the displacements.
- For the "C" bridges with $I_C > 1$, the 1D displacement calculations get a minimum grade of D and a mode of the grades of C. Both the worst-case and mode of the grades for the major-axis bending stresses is a C for this group.

Table 5.2. Number of I-girder bridges within specified error ranges for major-axis bending stress and vertical displacement for each of the types of bridges considered.

Type of Bridge	Number of Bridges	Error Range	Number of Bridges within Error Range					
			Major-Axis Bending Stress			Vertical Displacement		
			2D-P1	2D-P2	1D	2D-P1	2D-P2	1D
C ($I_C \le 1$)	5	A: ≤ 6%	3	3	0	3	5	2
		B: 7-12%	2	2	5	2	0	2
		C: 13-20%	0	0	0	0	0	1
		D: 21-30%	0	0	0	0	0	0
		F: >30%	0	0	0	0	0	0
C ($I_C > 1$)	8	A: ≤ 6%	1	2	1	0	1	1
		B: 7-12%	5	5	3	0	0	1
		C: 13-20%	1	1	4	0	1	5
		D: 21-30%	1	0	0	0	0	1
		F: >30%	0	0	0	8	6	0
S ($I_S < 0.30$)	11	A: ≤ 6%	11	9	8	11	10	11
		B: 7-12%	0	2	3	0	1	0
		C: 13-20%	0	0	0	0	0	0
		D: 21-30%	0	0	0	0	0	0
		F: >30%	0	0	0	0	0	0
S ($0.30 \le I_S < 0.65$)	10	A: ≤ 6%	3	6	2	9	9	4
		B: 7-12%	7	4	7	1	1	6
		C: 13-20%	0	0	1	0	0	0
		D: 21-30%	0	0	0	0	0	0
		F: >30%	0	0	0	0	0	0
S ($I_S \ge 0.65$)	3	A: ≤ 6%	0	0	0	0	0	0
		B: 7-12%	0	0	0	1	0	0
		C: 13-20%	2	2	2	1	2	2
		D: 21-30%	1	1	1	1	1	1
		F: >30%	0	0	0	0	0	0
C&S ($I_C > 0.5$ & $I_S > 0.1$)	18	A: ≤ 6%	3	9	0	1	12	2
		B: 7-12%	11	5	9	1	4	4
		C: 13-20%	4	2	5	2	1	7
		D: 21-30%	0	2	3	5	0	3
		F: >30%	0	0	1	9	1	2

Table 5.3. Worst-case I-girder bridge scores for major-axis bending stress and vertical displacement.

Type of Bridge	Worst Case Scores					
	Major-Axis Bending Stress			Vertical Displacement		
	2D-P1	2D-P2	1D	2D-P1	2D-P2	1D
C ($I_C \leq 1$)	B	B	B	B	A	C[e]
C ($I_C > 1$)	D[a]	C[a]	C	**F**	**F**	D[f]
S ($I_S < 0.30$)	A	B[b]	B	A	B[g]	A
S ($0.30 \leq I_S < 0.65$)	B	B	C[c]	B[h]	B[i]	B
S ($I_S \geq 0.65$)	D	D	D	D	D	D
C&S ($I_C > 0.5$ & $I_S > 0.1$)	C	D	**F[d]**	**F**	**F[j]**	**F**

[a] One bridge, NISCR7, has a mean error of 22 % and 17 % for Programs P1 and P2 repectively. This is believed to be due to the combined poor girder torsion model and inaccurate cross-frame stiffness model along with the large width of this bridge. Program P1 has somewhat larger errors than Program P2 because the curved girders were subdivided into multiple elements along each unbraced length in the Program P1 solution.

[b] One bridge with unequal skew, NISSS6, has a mean error of 7 %.

[c] One bridge with parallel 60^o skew, XICSS5, has a mean error of 16 % due to transverse load path (nuisance stiffness) effects.

[d] One bridge, NISCS37, has a mean error of 37 %. The V-load method removes load from the girder on the inside of the curve in this bridge, but the inside girder is the longest because of the skew. The V-load method is not able to capture the corresponding larger bending within the inside girder.

[e] One bridge, EICCR11, has a mean error of 16 %. This larger error is due to torsional interactions between the spans in this continuous-span bridge, which are not captured accurately by the V-Load Method.

[f] One bridge, NISCR8, has a mean error of 29 %. The V-Load Method does not accurately capture the major-axis bending stresses in the interior girders (e.g., Girders 4 and 5) of this wide 9-girder bridge

[g] One bridge, NICSS3, has a mean error of 8 %, due to over-prediction of the displacements in the first span (having parallel skew) and under-prediction of the displacements in the second span (having unequal skew).

[h] One bridge with parallel 60^o skew, XICSS5, has a mean error of 8 % due to transverse load path (nuisance stiffness) effects.

[i] One bridge with unequal skew, NICSS1, has a mean error of 11 %.

[j] One bridge, NISCS37, has a mean error of 36 %. This is believed to be due to lack of ability of the poor torsional stiffness model in conventional 2D-grid solutions to capture substantial torsional interactions between the girders.

Table 5.4. Mode of I-girder bridge scores for major-axis bending stress and vertical displacement.

Type of Bridge	Mode of Scores					
	Major-Axis Bending Stress			Vertical Displacement		
	2D-P1	2D-P2	1D	2D-P1	2D-P2	1D
C ($I_C \leq 1$)	A	A	B	A	A	B
C ($I_C > 1$)	B	B	C	F	F	C
S ($I_S < 0.30$)	A	A	A	A	A	A
S ($0.30 \leq I_S < 0.65$)	B	A	B	A	A	B
S ($I_S \geq 0.65$)	C	C	C	C	C	C
C&S ($I_C > 0.5$ & $I_S > 0.1$)	B	A	C[a]	F	A	C

[a] Modified from B to C considering the grade for the C ($I_C > 1$) and S ($I_S > 0.65$) bridges

- For the "S" bridges with $I_S \geq 0.65$, both the major-axis bending stresses and the vertical displacements have a worst-case score of D and a mode of the grades of C in all the methods.
- For the "C&S" bridges, the major-axis bending stresses received worst-case grades of C and D with programs P1 and P2 respectively. Furthermore, the 1D analysis major-axis bending stresses scored a worst-case grade of F due to one bridge exhibiting very poor results, while most of the bridges scored in the B range. The displacements generally were very poor for program P1 (due to the discretization of the girder unbraced lengths into multiple elements), whereas they were usually quite good for program P2, due to the defaulting of the element discretization to a low-resolution mesh, although one bridge still fell within the F range with program P2).

It is useful to understand the qualifier indicated on the "C&S" bridges, i.e., "($I_C > 0.5$ & $I_S > 0.1$)" in Tables 5.3 and 5.4. If a bridge has an $I_C < 0.5$ and an $I_S > 0.1$, it can be considered as a straight-skewed bridge for the purposes of assessing the expected analysis accuracy. Furthermore, if a bridge has an $I_C > 0.5$ with an $I_S \leq 0.1$, it can be considered as a curved radially-supported bridge for these purposes.

5.1.2 Generalized I-Girder Bridge Analysis Scores

Table 5.5 provides a synthesis of the analysis scores for the various I-girder bridge responses from traditional 2D-grid and 1D-line girder methods at large. This table addresses the accuracy of the calculations for major-axis bending stresses, vertical displacements, cross-frame forces, flange lateral bending stresses, and girder layovers at the bearings.

Key observations that can be drawn from Table 5.5 are discussed below:

Major-Axis Bending Stresses and Vertical Displacements

For the first two responses in Table 5.5, the major-axis bending stresses and the vertical displacements, the worst-case and mode letter grades are taken as the lower of the scores for programs P1 and P2 in Tables 5.3 and 5.4.

Cross-Frame Forces

The accuracy for the third through fifth responses in Table 5.5 can be estimated based on the grades from the first two responses when considering the "C" bridges. The results for the third response in these bridge types, the cross-frame forces, are roughly one letter grade less in accuracy compared to the major-axis bending stresses when evaluated by the traditional 2D-grid methods. This reduced accuracy is due to the substantial under-representation of the girder torsional stiffnesses and the crude representation of the cross-frame stiffnesses by prismatic beam elements in these methods. However, for curved girder bridges the cross-frame forces are comparable in accuracy to the major-axis bending stresses for the 1D-line girder method (i.e., line girder analysis with the V-load method adjustments).

For the straight-skewed bridges with minor skew, i.e., the "S (I_S < 0.30)" bridges, the gravity load cross-frame forces tend to be relatively small; therefore, the corresponding analysis errors are not of any consequence. However, for straight bridges with larger skew indices, the major flaws of the 2D-grid methods associated with the poor girder torsion model and the poor cross-frame models essentially render the cross-frame force estimates as useless. In addition, the 1D-line girder analysis models do not provide any information about the cross-frame forces due to the skew effects. Therefore, both the traditional 2D-grid and the 1D-line girder analysis methods get an F for these cases.

Table 5.5. Generalized I-girder bridge scores.

Response	Geometry	Worst-Case Scores		Mode of Scores	
		Traditional 2D-Grid	1D-Line Girder	Traditional 2D-Grid	1D-Line Girder
Major-Axis Bending Stresses	C ($I_C \leq 1$)[g]	B	B	A	B
	C ($I_C > 1$)	D	C	B	C
	S ($I_S < 0.30$)[h]	B	B	A	A
	S ($0.30 \leq I_S < 0.65$)	B	C	B	B
	S ($I_S \geq 0.65$)	D	D	C	C
	C&S ($I_C > 0.5$ & $I_S > 0.1$)	D	**F**	B	C
Vertical Displacements	C ($I_C \leq 1$)	B	C	A	B
	C ($I_C > 1$)	**F**	D	**F**	C
	S ($I_S < 0.30$)	B	A	A	A
	S ($0.30 \leq I_S < 0.65$)	B	B	A	B
	S ($I_S \geq 0.65$)	D	D	C	C
	C&S ($I_C > 0.5$ & $I_S > 0.1$)	**F**	**F**	**F**	C
Cross-Frame Forces	C ($I_C \leq 1$)	C	C	B	B
	C ($I_C > 1$)	**F**	D	C	C
	S ($I_S < 0.30$)	NA[a]	NA[a]	NA[a]	NA[a]
	S ($0.30 \leq I_S < 0.65$)	**F**[b]	**F**[c]	**F**[b]	**F**[c]
	S ($I_S \geq 0.65$)	**F**[b]	**F**[c]	**F**[b]	**F**[c]
	C&S ($I_C > 0.5$ & $I_S > 0.1$)	**F**[b]	**F**[c]	**F**[b]	**F**[c]
Flange Lateral Bending Stresses	C ($I_C \leq 1$)	C	C	B	B
	C ($I_C > 1$)	**F**	D	C	C
	S ($I_S < 0.30$)	NA[d]	NA[d]	NA[d]	NA[d]
	S ($0.30 \leq I_S < 0.65$)	**F**[b]	**F**[e]	**F**[b]	**F**[e]
	S ($I_S \geq 0.65$)	**F**[b]	**F**[e]	**F**[b]	**F**[e]
	C&S ($I_C > 0.5$ & $I_S > 0.1$)	**F**[b]	**F**[e]	**F**[b]	**F**[e]
Girder Layover at Bearings	C ($I_C \leq 1$)	NA[f]	NA[f]	NA[f]	NA[f]
	C ($I_C > 1$)	NA[f]	NA[f]	NA[f]	NA[f]
	S ($I_S < 0.30$)	B	A	A	A
	S ($0.30 \leq I_S < 0.65$)	B	B	A	B
	S ($I_S \geq 0.65$)	D	D	C	C
	C&S ($I_C > 0.5$ & $I_S > 0.1$)	**F**	**F**	**F**	C

[a] Magnitudes should be negligible for bridges that are properly designed & detailed. The cross-frame design is likely to be controlled by considerations other than gravity-load forces.

[b] Results are highly inaccurate due to modeling deficiencies addressed in Ch. 6 of the NCHRP 12-79 Task 8 report. The improved 2D-grid method discussed in this Ch. 6 provides an accurate estimate of these forces.

[c] Line-girder analysis provides no estimate of cross-frame forces associated with skew.

[d] The flange lateral bending stresses tend to be small. AASHTO Article C6.10.1 may be used as a conservative estimate of the flange lateral bending stresses due to skew.

[e] Line-girder analysis provides no estimate of girder flange lateral bending stresses associated with skew.

[f] Magnitudes should be negligible for bridges that are properly designed & detailed.

Table 5.5 (continued). Generalized I-girder bridge scores.

---

[g] $I_C = \dfrac{15,000}{R(n_{cf}+1)m}$ is the "connectivity index" (see Section 3.1.3 and Eq. (3.2)), where R is the radius of curvature of the bridge centerline in units of ft., n_{cf} is the number of intermediate cross-frames within the span, and m is a constant equal to 1 for simple-span bridges and 2 for continuous-span bridges.

[h] $I_S = \dfrac{w_g \tan\theta}{L_s}$ is the "skew index" (see Section 3.1.2 and Eq. (3.1)), where w_g is the width of the bridge measured between the centerline of the fascia girders, θ is the skew angle (equal to zero for zero skew), and L_s is the span length.

Flange Lateral Bending Stresses

For the fourth response in Table 5.5, the flange lateral bending stresses, the accuracies from the conventional 2D-grid and the 1D-line girder analysis methods for the "C" bridges, are roughly the same grade as the major-axis bending stresses. This can be understood by recognizing that the flange lateral bending stresses are generally calculated from Eqs. (2.13) through (2.16) in these methods (see Sections 2.1.3.1 and 2.1.3.2). Therefore, the estimate of the maximum flange lateral bending stress from horizontal curvature within the different unbraced lengths, from Eq. (2.15) or (2.16), is proportional to the estimate of the major-axis bending stress. Given that the "proportionality factors" multiplying f_b in Eq. (2.16) provide a reasonable (albeit coarse) estimate of the horizontal curvature effects within each of the unbraced lengths, the accuracy of the flange lateral bending stresses is roughly as good as the accuracy of the major-axis bending stresses in the "C" bridges.

Unfortunately, for the same reasons as described above for the cross-frame forces, the estimates of the flange lateral bending stresses in the "S" and "C&S" bridges are unusable when $I_S \geq 0.30$. The flange lateral bending stress accuracy for the "C&S" bridges with $I_S \leq 0.10$ may be taken roughly as the grade corresponding to its I_C value from the "C" bridges.

Girder Layover at Bearings

As discussed in Section 2.1.4, the girder layovers at skewed bearing lines are closely related to the girder major-axis bending rotations at the bearings, which are in turn closely tied to the vertical displacements within the spans. Therefore, the grades for the 2D-grid and the 1D-line girder estimates of these layovers, the fifth set of responses in Table 5.5, may be taken directly from the scores for the vertical displacements. Of course, the layover at non-skewed bearing lines is essentially zero. Therefore, these estimates are Not Applicable (NA) for the "C" bridges.

5.1.3 Assessment Examples for I-girder bridges

Curved I-Girder Bridge: Figure 5.3 shows the plan view of EICCS1, a basic simple-span bridge with radial supports. It is desired to determine the ability of the approximate analysis methods to capture the behavior of this structure prior to the slab becoming composite, according to the scores shown in Table 5.5.

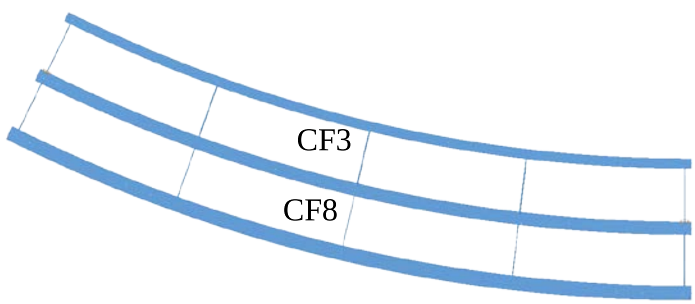

L_{as} = 90 ft./ R = 200 ft./ w = 23.5 ft

Figure 5.3. EICCS1 - Curved and radial simple span I-girder bridge.

This bridge is a relatively simple structure that satisfies the assumptions of the V-load method derivation. For this bridge, the connectivity index is

$I_C = 15{,}000/[(3+1)\cdot 200\cdot 1] = 18.8 > 1.0$

According to Table 5.5, the mode grades for the 1D line-girder and 2D-grid models are:

Response	Analysis Method	
	2D-Grid	1D Line-Girder
f_b	B	C
Vertical deflections	F	C
Cross-frame forces	C	C
f_ℓ	C	C
Girder layovers at bearings	NA	NA

The mode grades may be considered as the more appropriate characterization of the accuracy of this bridge because this bridge is "very regular" in its geometry. The worst-case score is likely the more appropriate one to use when designing a bridge with complicating features such as a poor span balance, or "less regular" geometry characteristics.

Figures 5.4 through 5.6 show the major-axis bending responses on the outside and inside fascia girders of the structure. The vertical displacements in Figure 5.4 are shown at the total noncomposite dead load level (TDL), while f_b in Figures 5.5 and 5.6 is shown at 1.5 times TDL (corresponding to the AASHTO Strengh IV load combination). As shown in Figure 5.4, the vertical displacements are severely over-predicted by the 2D-grid model. The solution obtained from a 1D line-girder model is a better representation of the benchmark. By comparing Figures 5.5 and 5.6, it is observed that the approximate methods properly capture f_b in the outside girder; while in the inside girder, the differences are more noticeable. Since the scores are determined with respect to the girder with the largest errors, which in this case is the inside fascia girder, the score for f_b is B and C for the 2D and 1D methods, respectively.

Figure 5.7 shows the results obtained for the flange lateral bending stresses. In addition, Table 5.6 shows the cross-frame forces calculated from the 2D-grid and the 3D FEA solutions. As in the case of the major-axis bending responses, the scores are a good representation of the predictions obtained with the approximate models. This example shows that the scores are in agreement with the predictions obtained from the approximate analyses.

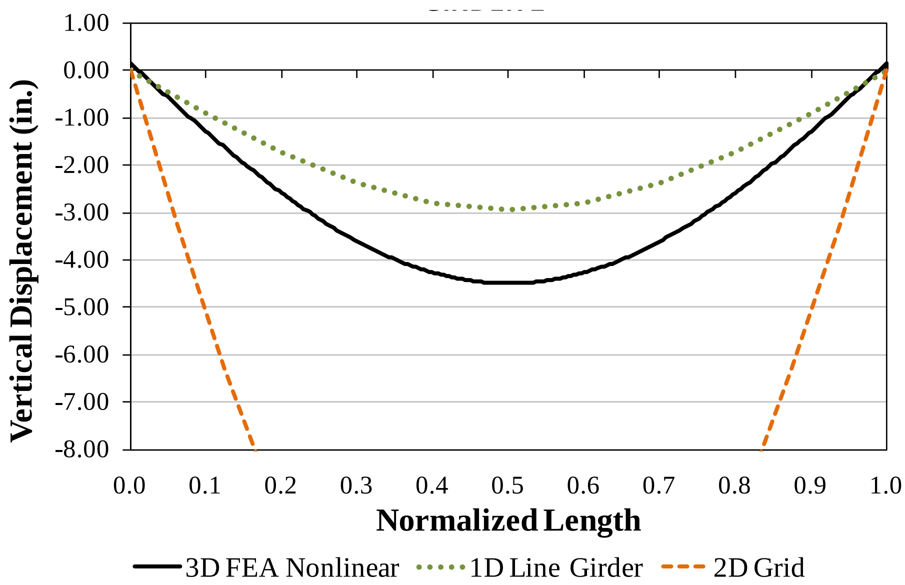

Figure 5.4. Vertical displacements for the fascia girder on the outside of the curve in bridge EISCR1.

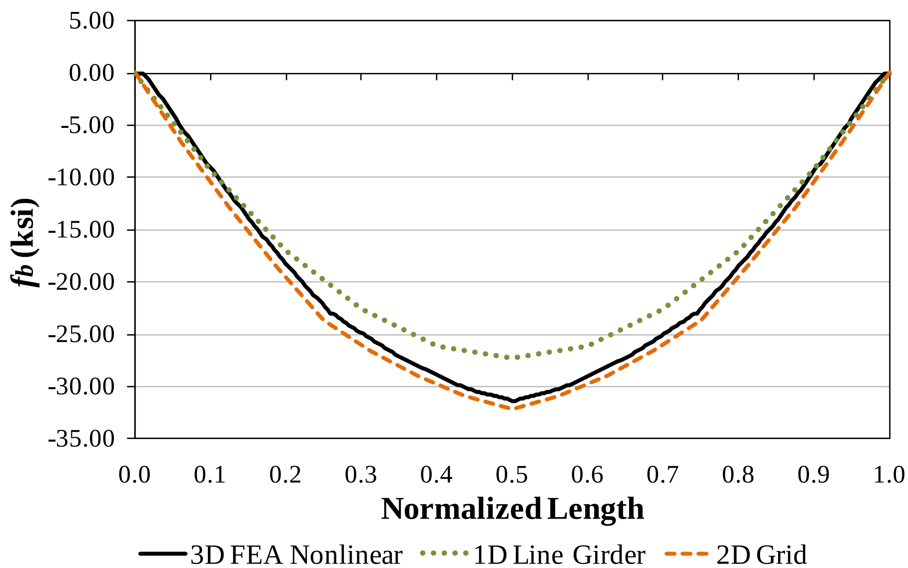

Figure 5.5. Top flange major-axis bending stresses in the fascia girder on the outside of the curve in bridge EISCR1.

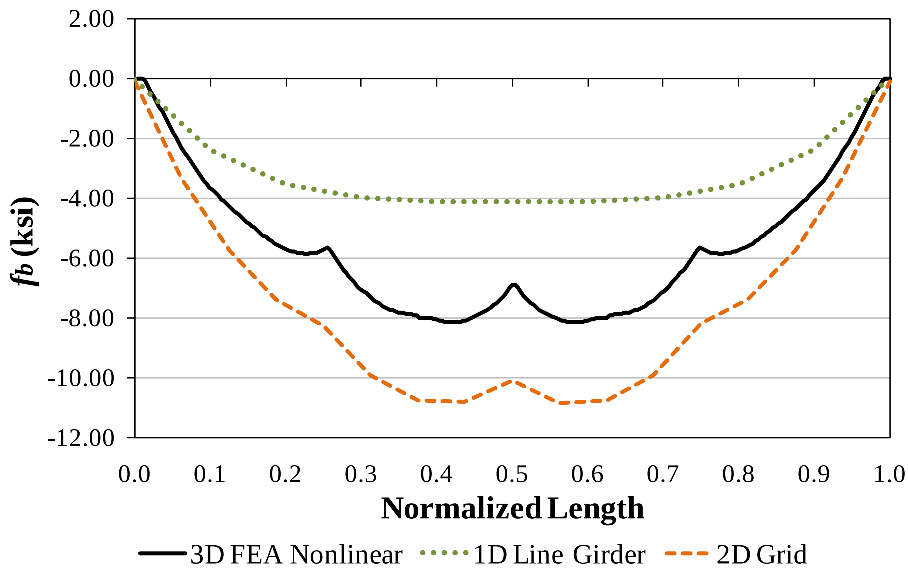

Figure 5.6. Top flange major-axis bending stresses in the fascia girder on the inside of the curve in bridge EISCR1.

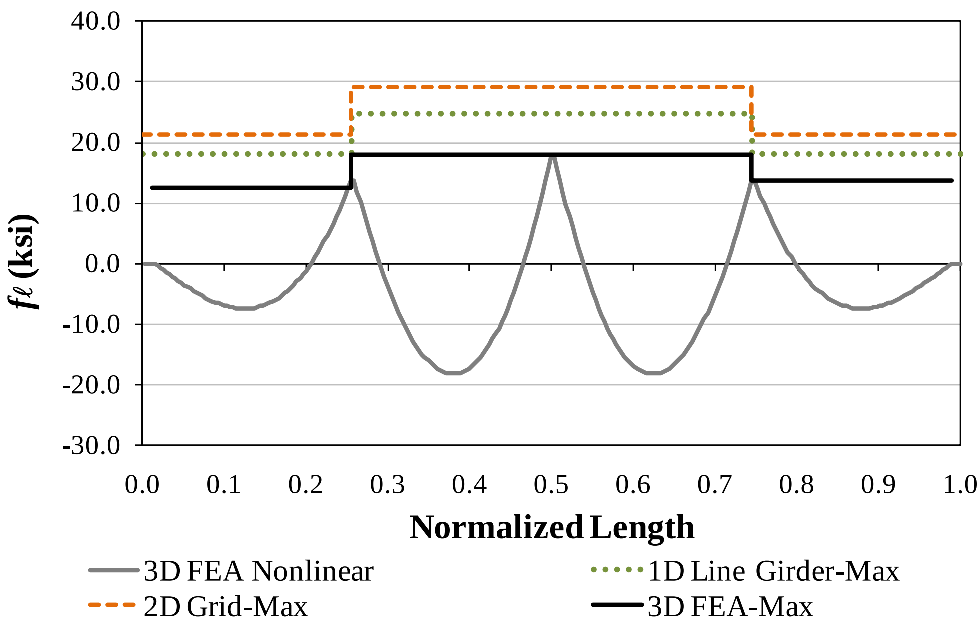

Figure 5.7. Flange lateral bending stresses in the outside fascia girder of bridge EISCR1.

Table 5.6. Cross-frame forces predicted with the 2D-grid and the 3D FEA

Member	CF 3		CF8	
	2D-Grid	3D FEA	2D-Grid	3D FEA
TC	26.6	19.1	24.6	54.5
BC1	-43.1	-46.8	-52.3	-96.6
BC2	-10.1	8.25	3.2	-11.81
D1	23.3	32.7	39.2	49.9
D2	-23.3	-32.3	-39.2	50.2

Skewed I-Girder Bridge: The straight I-girder bridge shown in Figure 5.8, NICSS16, is a severely skewed structure. It is desired to estimate the accuracy of the predictions obtained from a line-girder and a 2D-grid analysis for this bridge, according to the scores shown in Table 5.5.

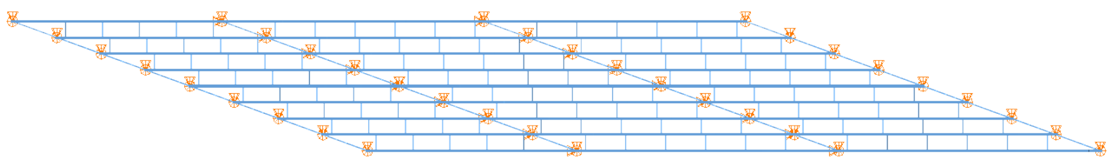

L_1 = 120 ft., L_2 = 150 ft., L_3 = 150 ft./ w = 74 ft./ $\theta_1 = 70^{o}$, $\theta_2 = 70^{o}$, $\theta_3 = 70^{o}$, $\theta_4 = 70^{o}$

Figure 5.8. NICSS 16 - Straight and skewed continuous I-girder bridge.

The skew indices for each span in this structure are 1.69, 1.36, and 1.36, respectively. These indices are above the 0.65 limit. Hence, it is expected that the skew effects have a significant contribution to the system response. The following are the mode scores for a bridge with these characteristics:

Response	Analysis Method	
	2D-Grid	1D Line-Girder
f_b	C	C
Vertical deflections	C	C
Cross-frame forces	F	F
f_ℓ	F	F
Girder layovers at bearings	C	C

As discussed in the previous example, the mode scores may be considered to be the more appropriate ones here, since the bridge is reasonably “regular,” i.e., no severe span imbalance, no significant differences in skew angle of the bearing lines, and no significant variations in the framing of the cross-frames.

Figures 5.9 and 5.10 show the predictions obtained for the girder vertical displacements and stresses in the structure. For simplicity of the discussions, these responses correspond to no-load fit detailing of the cross-frames. As shown in Figure 5.9, both analysis methods overpredict the displacements and stresses in Spans 1 and 3, and slightly underpredict the displacements in Span 2. Similarly, the major-axis bending stresses shown in Figure 5.10, f_b, follow the same trend. In general, it may be considered that the accuracy of the predictions is reasonable.

Conversely, the responses associated with the flow of transverse forces in the system are not captured by the approximate methods. As shown in the stress plot, the local f_ℓ levels are as high as 43 ksi in Span 3. The cross-frame forces associated with the high f_ℓ levels are shown in Figure 5.11. To simplify the observations, they are shown in terms of the cross-frame shear and bending moments rather than in individual chord and diagonal forces. The figure includes the responses obtained from the 3D FEA, a traditional grid analysis, and a grid analysis conducted with the practices recommended in Chapter 6. As shown in the figure, the forces obtained from the traditional grid model are essentially zero. This is due to the limited representation of the cross-frames and the girder torsional stiffness in the traditional method. The plots illustrate that, in this bridge, the physical cross-frame forces are large However, the traditional grid analysis is not able to capture these forces; hence, it is assigned a grade of F.

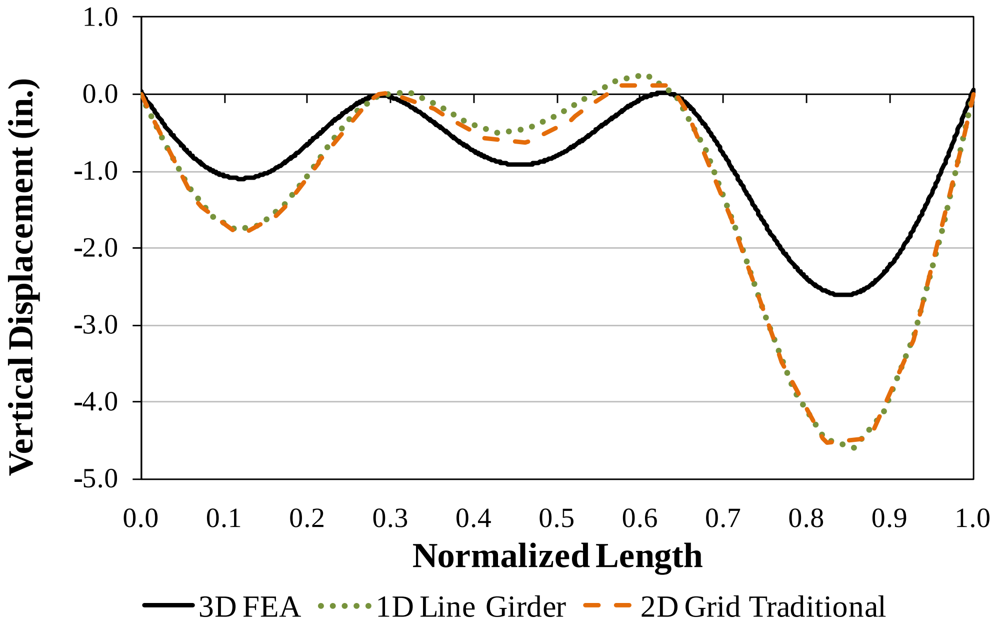

Figure 5.9. Vertical displacement of girder G5 in bridge NICSS16.

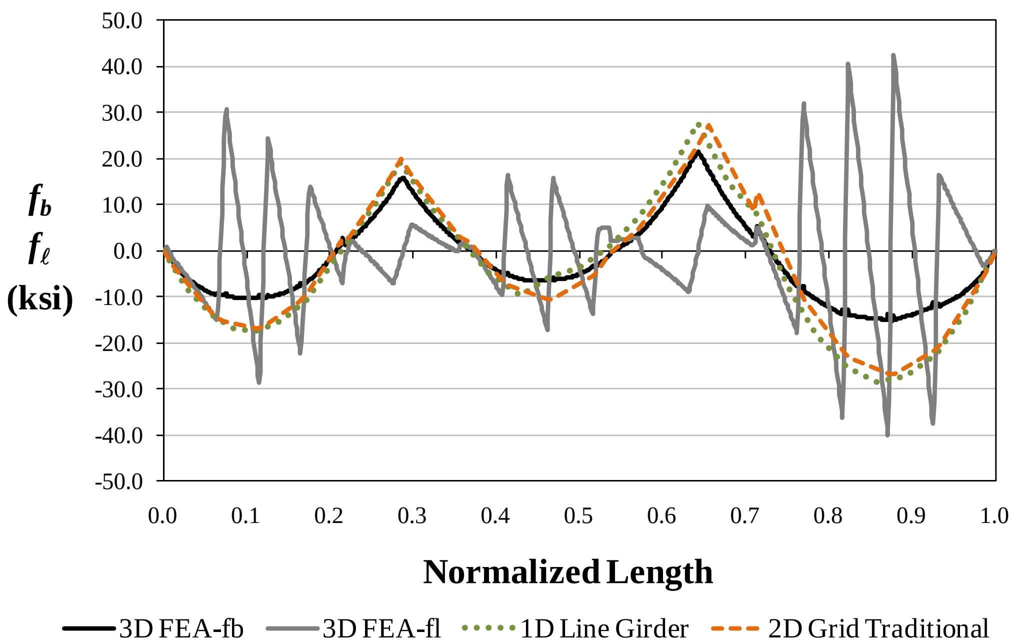

Figure 5.10. Top flange stresses in girder G5 of bridge NICSS16.

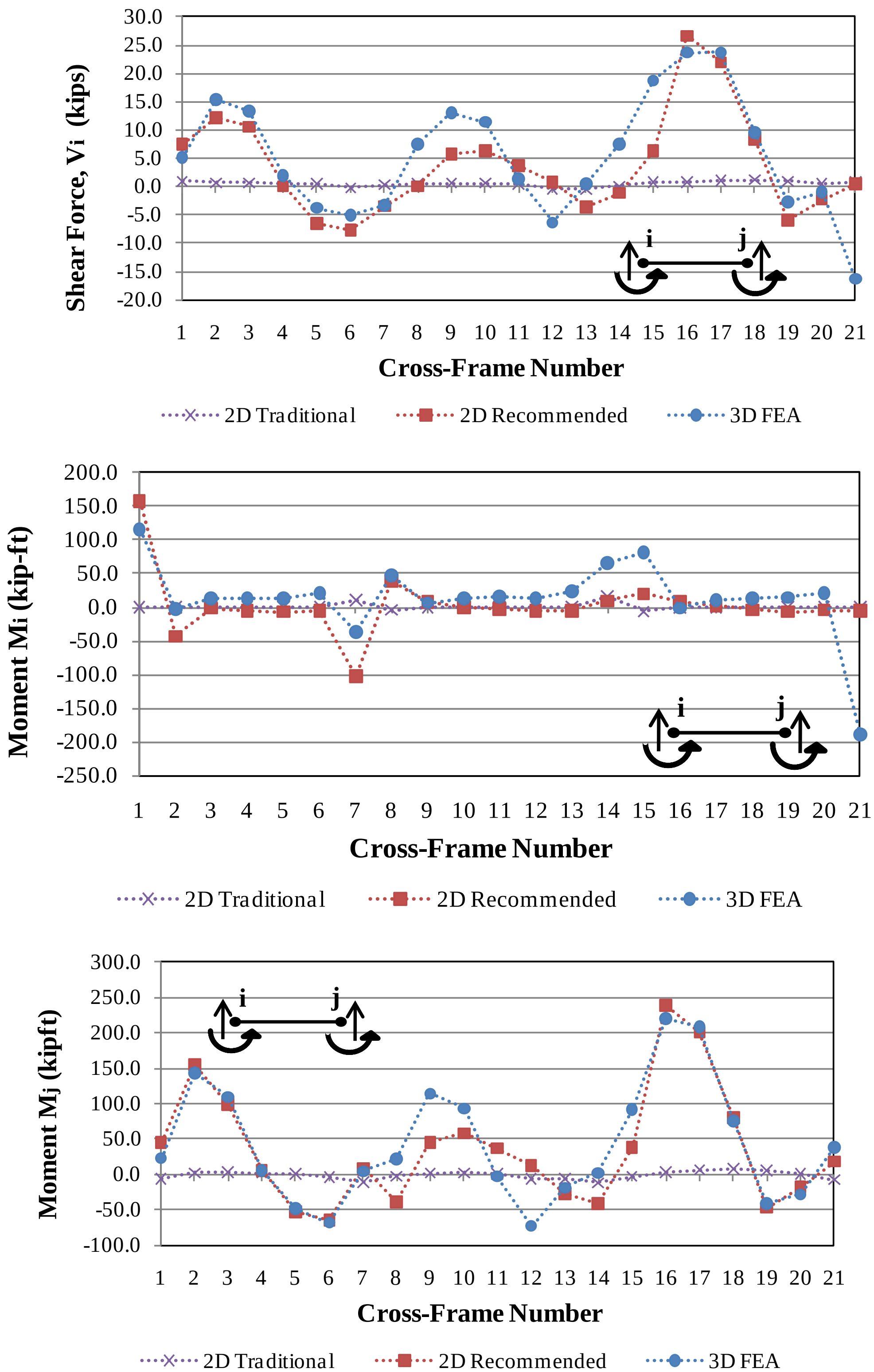

Figure 5.11. Cross-frame forces in Bay 1 (G1-G2) of NICSS16.

5.2 Assessment of Tub-Girder Bridges

Analytical studies also were conducted for the tub-girder bridges introduced in Chapter 4 to determine the ability of the approximate 1D line-girder and 2D-grid methods to capture the behavior predicted by refined 3D FEA models for these bridge types. The software setups used for these studies have already been described at the beginning of Chapter 5. For the simplified 2D-grid solutions the external cross-frames and diaphragms were modeled using the "shear analogy" approach (see Section 6.2.1) with the distance from web-to-web of the tub-girders at the mid-depth of the tubs for the length of the external elements, to determine the moment of inertia of an equivalent Euler-Bernoulli beam element, then using this moment of inertia with the length between the centerline of the tub-girders in the 2D-grid solution. This approach tends to under-estimate the true external diaphragm or cross-frame stiffness, but is a common design practice. A limited number of studies were conducted in which rigid offsets were assumed from the centerline of the tub-girders to the web at the external cross-frame or diaphragm connection. These models indicated that the differences in the girder displacements and internal torsional moments were negligible using either of these modeling approaches.

The tub-girder torsional properties were determined using the Equivalent Plate Method (Kollbrunner and Basler, 1969). The bracing forces were calculated using the component force equations outlined in Section 2.7 in LARSA, in which the results from LARSA were input to a spreadsheet for further calculation. Comparable calculations are handled internally in MDX. The MDX software used one element between each of the panel points of the top flange lateral bracing system for modeling of skewed bridges. Otherwise, a "high-resolution mesh" was used in MDX, i.e., nodes in addition to those at brace locations were placed at twentieth points of the spans, but not closer than span/40 from a brace or support location. The line-girder analyses in STLBRIDGE were conducted with ten elements per span.

The saw-tooth top-flange force effect discussed in Section 2.7 was not included in the calculation of the major-axis bending stresses, in order to focus on the accuracy corresponding to conventional practice (and thus obtain theoretically comparable results between the LARSA-based and MDX-based solutions). The use of the "average" major-axis bending stress, $f_b = M / S_{x.top}$, and the modeling of the external cross-frames and diaphragms neglecting rigid offsets from the centerline of the tub-girders reflect conventional analysis modeling standards of care in professional bridge design practice.

In the following, the normalized mean errors from Eq. (5.1) are presented for the major-axis bending stresses, vertical displacements and girder torsional moments obtained for the 18 tub-girder bridges studied in the NCHRP 12-79 research. However, for the assessment the analysis accuracy for the top flange lateral bracing (TFLB) and internal cross-frame (CF) axial forces, the signed errors for the maximum response are reported. In many designs, it is common to use the same size bracing members along the length of the bridge since this minimizes the detailing efforts and reduces the possibility of construction errors. As such, the top flange lateral bracing and cross-frame components are designed for the maximum axial forces found throughout the length of the bridge. Due to this practice, it is useful to assess the accuracy of the bracing forces by reporting the signed error for the maximum response for each of the different types of components. Furthermore, due to some of the subsequent simplified calculations being substantially conservative, it is useful to reference the signed error to convey that information. The sign on the error is positive for conservative estimates and unconservative for negative estimates. The reporting of these errors is grouped by: (1) the top flange lateral bracing diagonals, (2) the internal cross-frame diagonals, and (3) the combined top flange lateral bracing struts and internal cross-frame top chords.

Table 5.7 compares the program P1 and P2 2D-grid estimates as well as the1D analysis estimates for the major-axis bending stresses and vertical displacements to the predictions obtained from the geometric nonlinear elastic 3D FEA benchmarks. In the table, f_b is the major-axis bending stress, Δ_z is the vertical displacement and T is the torsional moment. A mean error is calculated for each response on each girder of the bridges. The values reported by Table 5.7 are the largest mean errors determined by inspecting the values obtained for each girder in a given bridge. The differences between the linear and geometric nonlinear 3D FEA were negligible and therefore are not shown. The torsional moments results were not obtained from program P2 and therefore the accuracy of the results are not evaluated for this case.

Table 5.7. Tub-girder bridge percent normalized mean errors compared to geometric nonlinear elastic 3D FEA for major-axis bending stresses (f_b), vertical displacements (Δ_z) and torsional moment (T).

Group	Bridge Name	2D-Grid – P1			2D-Grid – P2		1D		
		f_b	Δ_z	T	f_b	Δ_z	f_b	Δ_z	T
		μ_e	μ_e	μ_e	μ_e	μ_e	μ_e	μ_e	μ_e
C	NTSCR1	7	5	5	12	13	10	6	7
	NTSCR2	5	3	6	8	9	8	4	11
	NTSCR5	8	6	8	19	10	12	8	11
	NTCCR1	5	2	6	8	6	7	4	14
	ETCCR15	5	2	20	6	3	7	3	26
	XTCCR8	5	3	23	7	3	8	12	27
	ETCCR14	6	2	12	36	11	17	8	13
	NTCCR5	6	3	3	8	4	6	2	5
S	XTCSN3	3	2	19	5	5	6	6	23
	NTSSS1	4	5	31	11	7	5	1	18
	NTSSS4	4	1	30	6	5	7	3	53
	NTSSS2	8	7	27	19	13	11	5	10
	ETSSS2	5	2	28	10	2	9	7	30
C&S	NTSCS5	7	6	3	21	13	12	7	14
	NTSCS29	7	7	3	15	11	9	4	9
	ETCCS5a	10	6	22	5	5	6	5	29
	ETCCS6	6	2	43	22	3	7	2	33
	NTCCS22	5	4	3	8	8	6	3	11

In Table 5.7 and in the following discussions, the tub-girder bridges are divided into three groups based on their geometry: curved radially-supported bridges (labeled as "C"), straight and skewed structures (labeled as "S") and curved and skewed bridges (labeled as "C&S"). The connectivity index, I_C, does not apply to tub-girder bridges. This index is primarily a measure of the loss of accuracy in I-girder bridges due to the poor modeling of the I-girder torsion properties. For tub-girder bridges, the conventional St. Venant torsion model generally works well as a characterization of the response of the pseudo-closed section tub-girders. Hence, I_C is not used for characterization of tub-girder bridges in Table 5.7. Furthermore, there is only a weak correlation between the accuracy of the simplified analysis calculations and the skew index I_S for tub-girder bridges. Therefore, the skew index is not used to characterize tub-girder bridges in Table 5.7 either. Important differences in the simplified analysis predictions do exist, however, as a function of whether the bridge is curved, "C," straight and skewed, "S," or curved and skewed "C&S."

Similarly, Table 5.8 compares the maximum bracing axial force results from the 2D-grid and 1D analyses to the predictions obtained from the geometric nonlinear elastic 3D FEA benchmarks. In this table, the signed errors for the maximum response are reported for the top flange lateral bracing diagonals (TFLB Diag.), internal cross-frame diagonals (CF Diag.), and the combined top flange lateral bracing struts and internal cross-frame top chords (TFLB & Top CF Strut) for the reasons discussed above.

Table 5.8. Tub-girder bridge percent errors for maximum values of responses compared to geometric nonlinear elastic 3D FEA for the bracing system forces.

Group	Bridge Name	2D-P1			2D-P2			1D		
		TFLB Diag.	CF Diag.	TFLB & Top CF Strut	TFLB Diag.	CF Diag.	TFLB & Top CF Strut	TFLB Diag.	CF Diag.	TFLB & Top CF Strut
C	NTSCR1	8	30	24	55	80	-26	33	19	-1
	NTSCR2	7	27	25	58	74	-7	33	16	5
	NTSCR5	18	36	37	61	91	75	57	17	1
	NTCCR1	12	73	21	54	87	-42	34	90	-2
	XTCCR8	1	200	171	97	265	-18	27	264	54
	ETCCR14	0	241	93	148	51	-80	140	23	48
	NTCCR5	21	71	66	49	99	10	49	60	21
S	NTSSS1	-4	NA[a]	12	165	NA[a]	17	15	NA[a]	6
	NTSSS4	23	NA[a]	13	67	NA[a]	33	-16	NA[a]	6
	NTSSS2	-15	NA[a]	18	119	NA[a]	4	22	NA[a]	15
	ETSSS2	-55	NA[a]	-18	9	NA[a]	-37	15	NA[a]	-16
C&S	NTSCS5	17	24	17	65	75	-30	40	7	-15
	NTSCS29	5	29	35	84	83	-11	14	16	-4
	ETCCS6	12	52	4	46	110	20	51	-24	9
	NTCCS22	8	73	49	97	141	3	25	107	3
Pratt TFLB	ETCCR15	0	NA[b]	-3	-41	NA[b]	-75	56	NA[b]	-19
	XTCSN3	40	NA[a]	49	-74	NA[a]	-84	48	NA[a]	58
	ETCCS5a	0	-12	-3	26	123	-40	1	4	22

[a] The component force equations summarized in Section 2.7 predict negligible forces on the internal CF forces in straight tub-girders.

[b] ETCCR15 uses internal solid plate diaphragms rather than internal CF.

An additional group is shown in Table 5.8 corresponding to the bridges that had a Pratt TFLB system. The simplified analysis methods generally have more difficulty in accurately predicting the bracing forces for these bridges.

5.2.1 Accuracy of the Vertical Displacements, Major-Axis Bending Stresses and Torsional Moments

Upon inspection of the results corresponding to Table 5.7, the following important trends can be observed:

Second-Order Amplification

The results obtained from the first-order 3D FEA show that the response amplifications due to second order effects are negligible for all the tub-girder bridges. Steel tub-girders generally have as much as 100 to more than 1000 times the torsional stiffness of a comparable I-girder section. Therefore, when steel tub girders are fabricated with proper internal cross-frames to restrain their cross-section distortions as well as a proper top flange lateral bracing (TFLB) system, which acts as an effective top flange plate creating a pseudo-closed cross-section with the commensurate large torsional stiffness, second-order amplification is rarely of any significance even during lifting operations and early stages of the steel erection.

2D-Grid Solutions

Based on Table 5.7, several observations can be made regarding the 2D-grid solutions for the major-axis bending stresses, vertical displacements and torsional moments:

- The 2D-grid solutions from program P1 give better estimates than program P2 for the major-axis bending stresses and vertical displacements in all the cases in Table 5.7 with the exception of ETCCS5a. The ETCCS5a bridge uses a Pratt TFLB. The larger errors in the estimates for this bridge are due to the internal behavior associated with the bracing system (e.g., the Pratt TFLB system is not symmetric about the centerline of the tub-girders). Without knowing the details of the internal implementation in program P2, no conclusions can be drawn to confirm that program P2 has better accuracy for bridges using Pratt TFLB systems.
- There is no clear distinction in the results for the major-axis bending stresses and vertical displacements for the different groups “C”, “S” or “C&S”. This means that there is no

clear effect of curvature or skew on the accuracy of the major-axis bending stresses or vertical displacements in the simplified tub-girder bridge analysis solutions.

- Only the torsional moments from program P1 were collected. The errors are the largest for the "S" bridges. However, the groups "C" and "C&S" also have errors that are comparable to those of the "S" group.
- The torsional moment estimates for bridges ETCCR15 and XTCCR8 exhibit the largest errors in the "C" group. ETCCR15 has an irregular TFLB layout using Pratt trusses. The orientation of the TFLB diagonals varies throughout the bridge length. These characteristics (i.e., the non-symmetry relative to the centerline of the tub-girders and the variation in the orientations along the length) are believed to induce a behavior difficult to estimate by simplified 2D and 1D analysis methods. There is no clear reason why the solutions differed for bridge XTCCR8.
- The torsional results are reasonably accurate for three of the "C&S" bridges. The bridge ETCCS5a has large errors. This appears to be due again to the use of a Pratt TFLB system. The bridge ETCCS6 exhibits very large errors in the simplified analysis methods. The reason for this behavior appears to be the lack of external diaphragms at its intermediate pier.
- The torsional moment estimates for the "S" group exhibit errors larger than group "C&S". The "C&S" group bridges have smaller errors even when the independent effects of skew are expected to be comparable to those on the "S" group. However, the effects of curvature are large enough to reduce the relative differences. The reason for the reduced accuracy in the "S" bridges is explained below.

The diaphragm modeling is believed to be an important reason for the lack of accuracy in the internal torsional moments from the 2D-grid analyses. As noted previously, the 2D-grid approach used in the NCHRP 12-79 analytical studies tends to under-estimate the cross-frame or diaphragm stiffnesses. However, it appears that these components behave almost rigidly in many cases due to the small aspect ratio and the stiffening of the diaphragms. Nevertheless, as noted previously, a limited number of studies were conducted in which rigid offsets were assumed from the centerline of the tub-girders to the web at the external cross-frame or diaphragm connection. These models indicated that the differences in the girder displacements and internal torsional moments were negligible using either of these modeling approaches. Therefore, the results collected in the NCHRP 12-79 research are still inconclusive with respect to this consideration.

In addition, the internal bracing response appears to influence the accuracy of the simplified methods in predicting the internal torsional moments. The bridges that are expected to be subjected to constant internal torsional moments exhibited a slightly nonlinear distribution of the internal torques. It appears that the variation of the internal torques from a constant value is related to the TFLB strut lateral forces which follow a similar distribution. The shape also suggests possible correlation with the girder major-axis bending moment or the strut forces induced by major-axis bending. It should be noted that constant total internal torques taken by the full bridge cross-section can be obtained by simple statics in some of these bridges, given the bridge support reactions. The requirement of constant total internal torque on the full bridge cross-section is satisfied. However, the individual girders themselves do not exhibit constant internal torques along their lengths. The reader is referred to Jimenez Chong (2012) for a detailed assessment of the internal torsion estimates from the simplified methods.

Other errors are attributed to the discretization level of the bridge model; however, these errors are considered minor compared to the effects discussed above.

1D Line-Girder Solutions

The 1D line-girder results in Table 5.7 exhibit the following characteristics:

- The vertical displacements and major-axis bending stress solutions are reasonably good for all the bridges and are comparable to the corresponding 2D-grid results.
- For the "S" and "C&S" bridges, the 1D line-girder solutions for the vertical displacements and major-axis bending stresses exhibit better accuracy than the conventional 2D-grid program P1 solutions in the majority of the cases; however, there is no clear reason why the line-girder analysis solutions are better for these cases.
- The torsional moment errors from the line-girder analyses are less than or equal to 14 %. The torsional moment estimates for the ETCCR15, XTCCR8, ETCCS5a and ETCCS6 bridges appear to exhibit larger errors for the same reasons discussed previously regarding the 2D-grid solution accuracy.

- Similar to the 2D-gird solutions above, the torsional moment estimates for the "S" group exhibited errors larger than those from the "C&S" group. The internal bracing behavior is expected to cause these errors as explained previously; however, an additional reason for the reduced accuracy in the "S" bridges is explained below.

Additional errors in the line-girder analyses are attributed to the effects of the external intermediate cross-frames, since the 1D method is unable to capture any information about the transverse load paths in the bridge system through these components. The external intermediate cross-frames transfer forces between girders that modify the major-axis bending moments, torsional moments, and shears in the girders. When skewed external intermediate cross-frames are used, the cross-frames connect at different relative girder lengths resulting in additional transferred force between the girders, since the relative vertical displacements that these cross-frames control are expected to be larger. The effects of external intermediate cross-frames are again more noticeable in straight bridges since the effect in curved bridges is relatively small when compared to the overall combined torques from the curvature and skew.

5.2.2 Accuracy of Bracing Forces

2D Grid Solutions

As with the vertical displacements and major-axis bending stresses, the 2D-grid solutions from program P1 give better estimates than program P2 for the top flange lateral bracing diagonals forces (TFLB Diag.), internal cross-frame diagonal forces (CF Diag.) and the combined top flange lateral bracing strut and internal cross-frame top strut (TFLB & Top CF Strut) for the majority of the cases in Table 5.8. The larger errors in program P2 are attributed to the coarser discretization used for skewed bridges and the internal process for the evaluation of the bracing forces. Since the internal process for program P2 is proprietary, there is no information to confirm the specific differences in the component force calculations between programs P1 and P2. Therefore, only the results from program P1, which explicitly use the component force equations, are discussed below.

The following observations can be drawn from the program P1 results in Table 5.8:

- The TFLB diagonal forces directly depend on the major-axis bending and torsional moments and, consequently, the errors are larger for the "S" group where the torsional responses are estimated less accurately. For the “C” and “C&S” bridges, the accuracy is improved and the estimates are all conservative. The accuracy is affected largely by the accuracy of the torsional moment estimates. The large negative error for bridge ETSSS2 of -55 % is related to the complex internal forces generated by the interior pier supports oriented at a significant skew angle in this bridge without any cross-frames or diaphragms along this bearing line.

- The interior intermediate cross-frame diagonal force estimates show large conservative errors for the “C” and “C&S” groups. These forces are negligible for the “S” group, and therefore, these errors are not addressed. The interior intermediate cross-frame diagonal forces are assumed to depend only on the distortional components of the applied loads (Fan and Helwig, 2002). The largest distortional contribution is the M/Rh distributed lateral load which is characterized by the major-axis bending moments. Since the major-axis bending stresses are captured accurately by the program P2, it is concluded that the conservative estimates in the above forces are caused by the assumption that the internal cross-frames provide the only resistance to cross-section distortion (i.e., zero resistance to cross-section distortion from the girder cross-section itself).
- The combined TFLB & top cross-frame strut force estimates exhibit large conservative errors for the majority of the bridges, with the exception of the bridges that use a Pratt TFLB system. These bracing forces depend on a combination of the major-axis bending moment and torsional moments. The “S” group exhibits smaller errors for these forces. This result is believed to be related to the reduced accuracy of the torsional moment estimates for these bridges.
- Additional localized errors are attributed to the interaction of the external intermediate cross-frames and the internal cross-frames. At the locations that align to the external intermediate cross-frames there is a transverse load path that the component force equations do not consider. This effect causes force increases in the adjacent bracing components.

The bracing force estimates exhibit larger errors than the flange major-axis bending and vertical displacement estimates for the majority of the cases. However, many of these errors are conservative. For bridges using Pratt TFLB layouts, the component force equations exhibit a poorer performance caused by the interaction between these bracing components and the rest of the structural system.

1D Line-Girder Solutions

The 1D line-girder solutions for the bracing component forces in Table 5.8 exhibit larger errors than the corresponding responses provided by the program P1 2D-grid solution. These errors are a consequence of the effects discussed previously in Section 5.2.1. Additional errors are caused by the discretization level used in the 1D line-girder implementation, which results in some of the bracing component forces not being calculated based on their actual positions, but rather based on the closest tenth point.

The following sections synthesize the analysis errors using a grading scheme similar to the one presented in Section 5.1 for I-girder bridges.

5.2.3 Synthesis of Errors in Major-Axis Bending Stresses and Vertical Displacements for Tub-Girder Bridges

Table 5.9 shows the number of tub-girder bridges within specific ranges of the normalized mean errors for the major-axis bending stresses and the vertical displacements based on Table 5.7. Both of the 2D-grid programs P1 and P2 are considered, as well as the 1D analysis results. The specific selected error ranges are assigned letter grades based on the criteria described previously for I-girder bridges.

The highlighted rows in Table 5.9 are used to generate simplified scores for each of the bridge groups and analysis methods in Tables 5.10 and 5.11. The letter grades provided in Table 5.10 correspond to the worst-case scores in Table 5.9, whereas the grades in Table 5.11 correspond to the most frequently occurring score, i.e., the mode score.

Overall, one can observe the following from Tables 5.10 and 5.11:

- For the major-axis bending stresses and vertical displacements, the 2D-grid program P1 and the 1D line-girder analysis get worst-case grades of B and A. The mode of the grades for these analysis solutions is predominantly an A.

- For the major-axis bending stresses and vertical displacements, the 2D-grid program P2 gets worst-case grades of F and C. The mode of the grades in these categories is predominantly a B.
- For the torsional moments, the 2D-grid program P1 and 1D line-girder analysis have worst-case grades of F. However, the mode of the grades in these categories is a B for the 1D analysis of the "C&S" and "C" bridges and an A for the 2D-grid results. The "S" bridges have the lowest mode grades in general, D for the 2D-grid P1 solution and F for the 1D line-girder analysis solution.

Table 5.9. Number of tub-girder bridges within specified error ranges for major-axis bending stress and vertical displacement for each of the types of bridges considered.

Type of Bridge	Number of bridges	Error range	Number of Bridges within Error Range							
			Major-Axis Bending Stress			Vertical Displacement			Girder Torques	
			2D-P1	2D-P2	1D	2D-P1	2D-P2	1D	2D-P1	1D
C	8	A: ≤ 6%	6	1	1	8	4	5	5	1
		B: 7-12%	2	5	6	0	3	3	1	3
		C: 13-20%	0	1	1	0	1	0	1	2
		D: 21-30%	0	0	0	0	0	0	1	2
		F: >30%	0	1	0	0	0	0	0	0
S	5	A: ≤ 6%	4	2	2	4	3	4	0	0
		B: 7-12%	1	2	3	1	1	1	0	1
		C: 13-20%	0	1	0	0	1	0	0	1
		D: 21-30%	0	0	0	0	0	0	3	1
		F: >30%	0	0	0	0	0	0	2	2
C & S	5	A: ≤ 6%	2	1	2	4	2	4	3	0
		B: 7-12%	3	1	3	1	2	1	0	2
		C: 13-20%	0	1	0	0	1	0	0	1
		D: 21-30%	0	2	0	0	0	0	1	1
		F: >30%	0	0	0	0	0	0	1	1

Table 5.10. Tub-girder bridge worst-case scores for major-axis bending stress, vertical displacements, and torques.

Type of Bridge	Worst-Case Scores							
	Major-Axis Bending Stress			Vertical Displacement			Torque	
	2D-P1	2D-P2	1D	2D-P1	2D-P2	1D	2D-P1	1D
S	B	C	B	B	C	B	**F**	**F**
C	B	**F**	C	A	C	B	D	D
C&S	B	**F**[a]	C[b]	B	C	B	**F**	**F**

[a] Modified from D to F based on the score for the C bridges

[b] Modified from B to C based on the score for the C bridges

Table 5.11. Mode of tub-girder bridge scores for major-axis bending stress, vertical displacements, and torques.

Type of Bridge	Mode of Scores							
	Major-Axis Bending Stress			Vertical Displacement			Torque	
	2D-P1	2D-P2	1D	2D-P1	2D-P2	1D	2D-P1	1D
S	A	B	B	A	A	A	D	**F**
C	A	B	B	A	A	A	A	B
C&S	B	D	B	A	B	A	A	B

5.2.4 Synthesis of Errors in Bracing Forces for Tub-Girder Bridges

Table 5.12 categorizes the bracing force errors in a manner similar to Table 5.9. However, in this table, the numbers are collected for both positive (conservative) and for negative (unconservative) errors. Several of the estimated bracing forces fall into F grades. The errors are affected significantly by the low accuracy of the torque estimates. However, the majority of the estimates fall into the conservative categories meaning that the simplified methods still provide usable estimates for these cases.

5.2.5 Generalized Tub-Girder Bridge Analysis Scores

Tables 5.13 and 5.14 give the generalized analysis scores for the various tub-girder bridge responses corresponding to the traditional 2D-grid and 1D-line girder methods at large. Table 5.13 addresses the accuracy of the calculations for major-axis bending stresses, girder torques, vertical displacements, and girder layovers at the bearings, whereas Table 5.14 addresses the accuracy of the calculations for the top flange lateral bracing, internal cross-frames and flange lateral bending stresses.

Tables 5.13 and 5.14 are derived by using just the grades from program P1 as being representative of the true accuracy of 2D-grid methods. Clearly, there was a measurable decrease in the overall accuracy of the 2D-grid solutions for the tub-girder bridges obtained with program P2 compared to program P1. Furthermore, the research team had greater control over the procedures, as well as more detailed information regarding the specifics of the calculations, with program P1.

Table 5.12. Number of tub-girder bridges within specified error ranges for the maximum values of the bracing system forces for each of the types of bridges considered.

Type of Bridge	Number of Bridges	Error Range	Number of Bridges within Error Range								
			TFLB Diag.			TFLB & Top CF Strut			CF Diag.		
			2D-P1	2D-P2	1D	2D-P1	2D-P2	1D	2D-P1	2D-P2	1D
C	7	+F: >30%	0	**7**	**6**	**4**	**1**	**2**	**5**	**7**	**3**
		+D: 21-30%	**1**	0	1	3	0	1	2	0	1
		+C: 13-20%	1	0	0	0	0	0	0	0	3
		+B: 7-12%	**3**	0	0	0	1	0	0	0	0
		+A: ≤ 6%	2	0	0	0	0	2	0	0	0
		-A: ≤ 6%	0	0	0	0	0	**2**	0	0	0
		-B: 7-12%	0	0	0	0	1	0	0	0	0
		-C: 13-20%	0	0	0	0	1	0	0	0	0
		-D: 21-30%	0	0	0	0	1	0	0	0	0
		-F: >30%	0	0	0	0	**2**	0	0	0	0
S	4	+F: >30%	0	**3**	0	0	**1**	0			
		+D: 21-30%	**1**	0	**1**	0	0	0			
		+C: 13-20%	0	0	**2**	**2**	1	**1**			
		+B: 7-12%	0	1	0	1	0	0			
		+A: ≤ 6%	0	0	0	0	1	**2**			
		-A: ≤ 6%	1	0	0	0	0	0			
		-B: 7-12%	0	0	0	0	0	0			
		-C: 13-20%	1	0	**1**	**1**	0	**1**			
		-D: 21-30%	0	0	0	0	0	0			
		-F: >30%	**1**	0	0	0	**1**	0			
C&S	4	+F: >30%	0	**4**	**2**	**2**	0	0	**2**	**4**	**1**
		+D: 21-30%	0	0	1	0	0	0	2	0	0
		+C: 13-20%	**1**	0	1	1	**1**	0	0	0	1
		+B: 7-12%	**2**	0	0	0	0	**1**	0	0	1
		+A: ≤ 6%	1	0	0	1	1	1	0	0	0
		-A: ≤ 6%	0	0	0	0	0	1	0	0	0
		-B: 7-12%	0	0	0	0	1	0	0	0	0
		-C: 13-20%	0	0	0	0	0	1	0	0	0
		-D: 21-30%	0	0	0	0	**1**	0	0	0	**1**
		-F: >30%	0	0	0	0	0	0	0	0	0
Pratt TFLB	3	+F: >30%	**1**	0	**2**	**1**	0	**1**			
		+D: 21-30%	0	**1**	0	0	0	1			
		+C: 13-20%	0	0	0	0	0	0			
		+B: 7-12%	0	0	0	0	0	0			
		+A: ≤ 6%	**2**	0	1	0	0	0			
		-A: ≤ 6%	0	0	0	**2**	0	0			
		-B: 7-12%	0	0	0	0	0	0			
		-C: 13-20%	0	0	0	0	0	**1**			
		-D: 21-30%	0	0	0	0	0	0			
		-F: >30%	0	**2**	0	0	**3**	0			

Table 5.13. Generalized tub-girder bridge scores for girder major-axis bending stresses, torques, and displacements.

Response	Geometry	Worst-Case Scores		Mode of Scores	
		2D-P1	1D-Line Girder	2D-P1	1D-Line Girder
Major-Axis Bending Stresses	S	B	B	A	B
	C	B	C	A	B
	C&S	B	C[b]	B	B
Girder Torques	S	F	F	D	F
	C	D	D	A	B
	C&S	F	F	A	B
Vertical Displacements	S	B	B	A	A
	C	A	B	A	A
	C&S	B	B	A	A
Girder Layover at Bearing Lines	S	B	B	A	A
	C	NA[a]	NA[a]	NA[a]	NA[a]
	C&S	B	B	A	A

[a] Magnitudes should be negligible where properly designed and detailed diapharagms or cross-frames are present.
[b] Modified from B to C based on the score for the C bridges.

In Tables 5.13 and 5.14, there are several cases where the letter grade for the "C&S" bridges was lowered from the result derived from Table 5.12 because a grade for a "C" or an "S" bridge was lower. The table footnotes indicate when these modifications were made. It should be noted that in Table 5.13, the "C&S" mode scores of A and B for the prediction of the internal torques by the 2D-grid and the 1D line-girder solutions are not modified. This is because the torque due curvature is typically much larger than the torque due to skew, and the contribution of the torque due to curvature tends to be estimated more accurately in general.

Key observations that can be drawn from Tables 5.13 and 5.14 are as follows:

Table 5.14. Generalized tub-girder bridge scores for bracing system forces and flange lateral bending stresses.

Response	Sign of Error	Geometry	Worst-Case Scores 2D-P1	Worst-Case Scores 1D-Line Girder	Mode of Scores 2D-P1	Mode of Scores 1D-Line Girder
TFLB Diagonal Force	Positive (Conservative)	S	D	D	D	C
		C	D	F	B	F
		C&S	D[a]	F	B	F
		Pratt TFLB System	C	F	A	F
	Negative (Unconservative)	S	F[b]	C		
		C	--	--		
		C&S	--	--		
		Pratt TFLB System	--	--		
TFLB & Top Internal CF Strut Force	Positive (Conservative)	S	C	C		
		C	F	F		
		C&S	F	F[c]		
		Pratt TFLB System	F	F		
	Negative (Unconservative)	S	C	C		
		C	--	A		
		C&S	--	C		
		Pratt TFLB System	D	D		
Internal CF Diagonal Force	Positive (Conservative)	S	NA[d]	NA[d]		
		C	F	F		
		C&S	F	F		
		Pratt TFLB System	--	F[e]		
	Negative (Unconservative)	S	NA[d]	NA[d]		
		C	--	--		
		C&S	--	D		
		Pratt TFLB System	B	--		
Top Flange Lateral Bending Stress (Warren TFLB Systems)	Positive (Conservative)	S	C	C		
		C	F	F		
		C&S	F	F[c]		
	Negative (Unconservative)	S	C	C		
		C	--	A		
		C&S	--	C		

[a] Modified from a C to a D considerting the grade for the C and the S bridges.

[b] Large unconsevative error obtained for bridge ETSSS2 due to complex framing. If this bridge is considered as an exceptional case, the worst case unconservative error is -15 % for NTSSS2 (grade = C).

[c] Modified from a B to an F considering the grade for the C bridges.

[d] For straight-skewed bridges, the internal intermediate cross-frame diagonal forces tend to be negligible.

[e] Modified from an A to an F considering the grade for the C and C&S bridges.

Major-Axis Bending Stresses, Vertical Displacements and Girder Layovers

In these categories the worst-case letter grades are dominated by B grades (see Table 5.13). The 1D line-girder falls into the C grade for the major-axis bending stresses in C and "C&S" bridges; however, this should be expected as the complexity of three-dimensional response is not completely represented in the line-girder analysis model. The mode grades are dominated by A's, particularly for the vertical displacements. In summary the simplified analysis methods show good agreement in the prediction of major-axis bending stresses, vertical displacement and girder layovers. For tub-girder bridges the lesser accuracy should be expected from the line-girder analysis since the interaction between the girders cannot be modeled.

Girder Internal Torques

The 2D-grid and 1D-line girder models represent the bridge in terms of idealized longitudinal and transverse equivalent beams. However, the torsional behavior is complex since it involves the interaction of numerous components including the support diaphragms, external intermediate cross-frames, top flange lateral bracing systems, etc. Consequently, the lack of modeling accuracy of each of these components adds up and the worst-case estimates fall to an F grade in curved and/or skewed bridges.

The torque behavior is more difficult to predict accurately as the complexity of the bridge increases. Uniform spacing of internal bracing and of TFLB system panel points, reduced interaction between adjacent girders by elimination of intermediate external bracing, and accurate modeling of support diaphragms generally leads to better torque estimates. Bridges with complex deck geometry, non-uniform brace spacing, multiple external intermediate cross-frames between girders, skewed supports, large eccentric vertical loading, etc., should consider the use of 3D FEA to achieve an accurate representation of the torsional response.

Bracing Forces

Several of the estimated bracing forces in Table 5.14 fall to F grades. The errors are largely caused by the low accuracy on the torque estimates. However, the majority of the estimates fall into the conservative categories meaning that the simplified methods still provide usable estimates.

5.2.6 Assessment Example for Tub-girder Bridges

Curved and Skewed Tub Girder: Figure 5.12 illustrates the TFLB layout of the simple-span tub-girder bridge NTSCS5 having parallel skewed supports. It is desired to determine the ability of the approximate methods of analysis to estimate its responses.

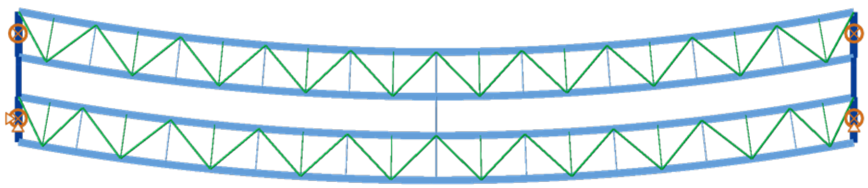

L_{as} = 150 ft./ R = 400 ft./ w = 30 ft./ θ_1 = 10.7°, θ_2 = -10.7°

Figure 5.12. Curved and skewed simple span tub-girder bridge NTSCS5.

The levels of accuracy of the 1D line-girder and 2D-grid models, based on the mode scores in Tables 5.13 and 5.14, are:

Response	Analysis Method	
	2D-grid	1D Line-Girder
f_b	B	B
Girder Torques	A	B
Vertical Deflections	B	B
Girder Layovers	B	B
f_ℓ	F (conservative)	F (conservative)
TFLB & CF forces	F (conservative)	F (conservative)

This structure is reasonably "regular" in its geometry, with uniform spacing of the internal intermediate cross-frames and of the TFLB system panel points along its length with the exception of the panels near the skewed ends, only one external intermediate diaphragm located at the middle of the span, and approximate symmetry about its mid-span. Therefore, the mode scores are considered as more appropriate for estimating the accuracy of the simplified analysis methods rather than the worst-case scores.

Figure 5.13 shows the vertical displacements and Figure 5.14 shows the girder stresses at the total noncomposite dead load level (unfactored). As noted previously, when steel tub girders are fabricated with proper internal cross-frames to restrain their cross-section distortions as well as a proper top flange lateral bracing (TFLB) system, which acts as an effective top flange plate creating a pseudo-closed cross-section with the commensurate large torsional stiffness, second-order amplification is rarely of any significance even during lifting operations and early stages of the steel erection. Therefore, the nominal stresses unfactored dead load stresses may be scaled by the appropriate load factors to conduct any strength checks.

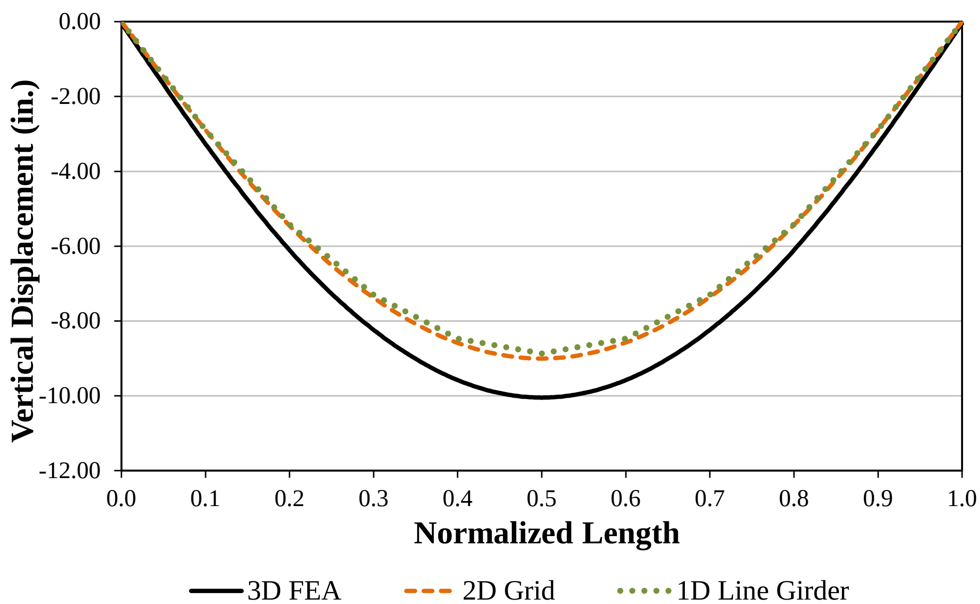

Figure 5.13. Vertical displacements at the centerline of the girder on the outside of the curve in bridge NTSCS5.

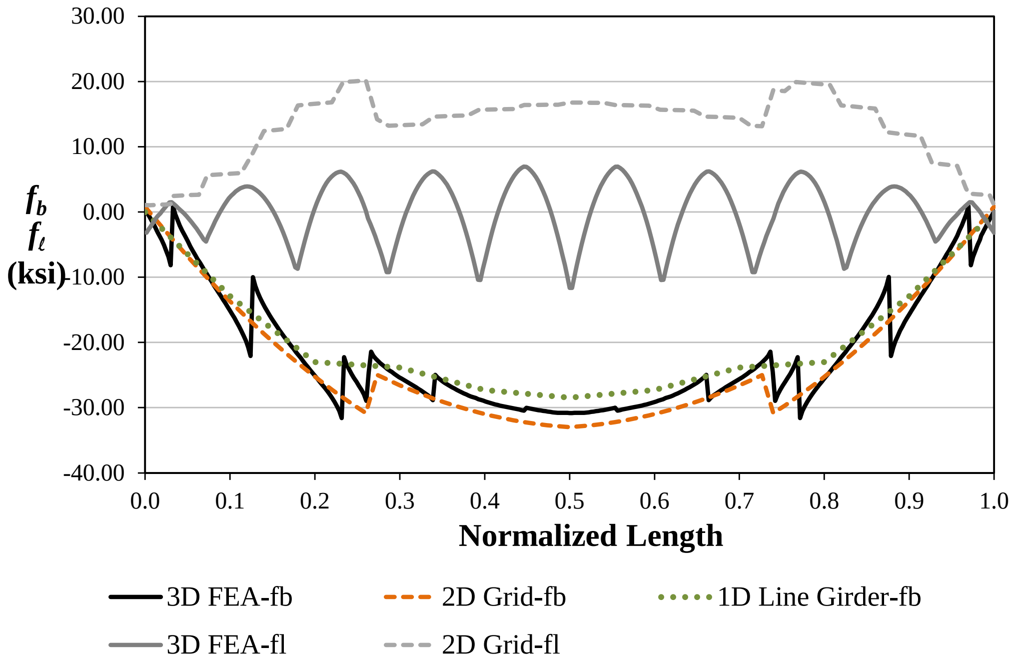

Figure 5.14. Flange major-axis and lateral bending stresses on the outside top flange of the girder on the outside of the curve in bridge NTSCS5.

The top flange lateral bending stresses are estimated conservatively by the 2D-grid calculations. It should be noted that the 2D-grid curve for these stresses is essentially just an estimated envelope curve for the maximum flange lateral bending stresses. The estimated peak flange lateral bending stresses are nearly two times the physical maximum values, and are not located at the same position as the true peak values. Similar predictions (not shown) are obtained using the line-girder analysis calculations. Hence, the grade of F for the top flange lateral bending stresses in Table 5.14 is representative. The vertical deflections are predicted within a normalized mean error of 6 % by both the 2D-grid and the line-girder analysis in this problem.

Figure 5.15 shows the internal torques predicted in the girder on the outside of the curve in NTSCS5. It can be observed that the internal torques are predicted very accurately in this problem, both from the 2D-grid and the 1D line-girder solutions. Because of the equal and opposite skews at the end bearing lines and the symmetry about the mid-span, the internal torque due to skew is small in this problem. The curvature effects dominate the total torque. This performance justifies the mode scores of A and B for prediction of the torques by the simplified analysis solutions. The internal torques are calculated directly from the structural analysis in the 2D-grid solution. The M/R method does not provide any estimate of the girder internal torques due to skew. However, as discussed in Section 2.1.5, the tub-girder internal torques can be estimated reasonably well for simple, "regular" geometries by considering the major-axis bending responses from the M/R method along with the assumption that the bearing line diaphragms are effectively rigid, to calculate the girder relative end twists in each span. The relative end twists can then be multiplied by the St. Venant torsional stiffness (*GJ*/*L*) to obtain an estimate of the internal torques.

Figure 5.16 shows the axial forces for the TFLB system along the length of the exterior girder in NTSCS5. To facilitate the visualization of the results the forces are grouped as positive and negative values, and consecutive results (in every other panel of the TFLB system) are joined by a line.

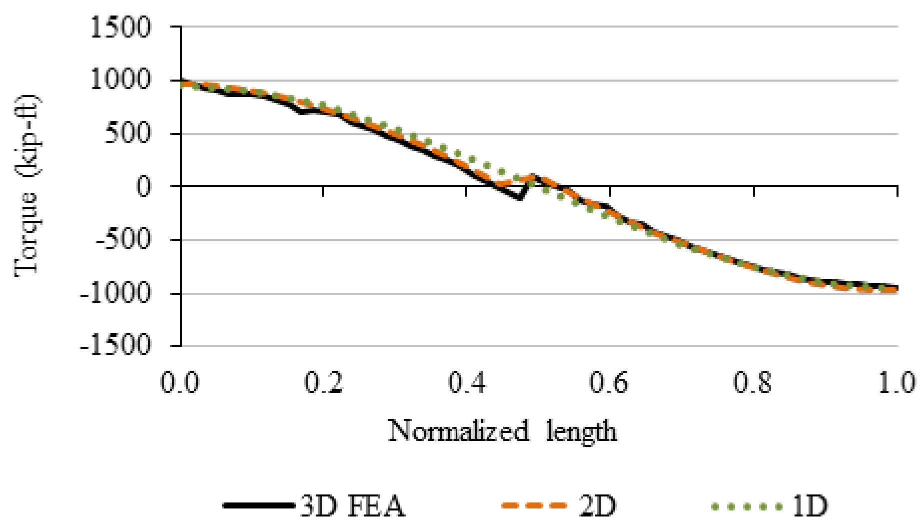

Figure 5.15. Internal torques for the girder on the outside of the horizontal curve in bridge NTSCS5.

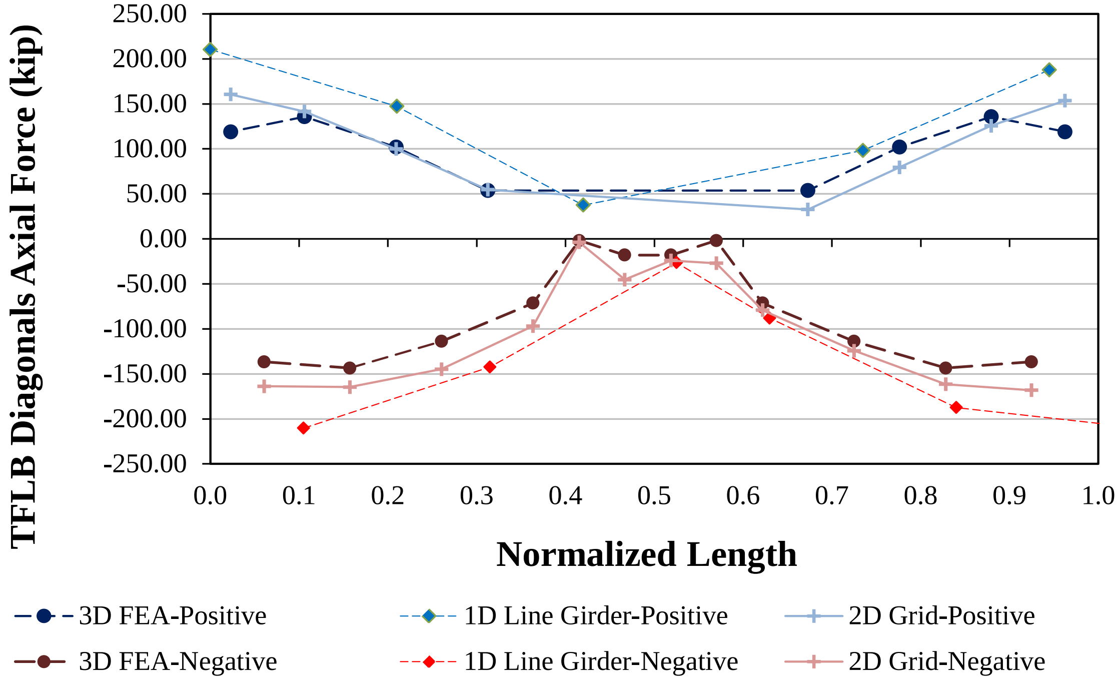

Figure 5.16. Axial forces in the TFLB system diagonals of the girder on the outside of the curve in the NTSCS5 bridge.

One can observe that the overall trends in the predictions from both types of simplified analysis methods are reasonably good, but that the line-girder analysis results generally are significantly conservative relative to the 3D FEA benchmarks. This plot shows that the mode scores of B for the 2D-grid methods are justified, and indicates that scores better than the mode score (F in this case) are certainly attainable with the line-girder analysis solutions.

Figure 5.17 shows the predictions from the 2D-grid and 1D line-girder analyses for the NTSCS5 bridge. Both the 2D-grid and the line-girder analysis predictions appear to be reasonably good in predicting the overall trends in this case, which may seem to be at odds with the grade of F for these responses in Table 5.14. However, upon a closer inspection from Table 5.8, one can observe that the errors in the prediction of the maximum forces are + 24 % and +7 % here, whereas these errors are significantly larger for the other "C&S" bridges.

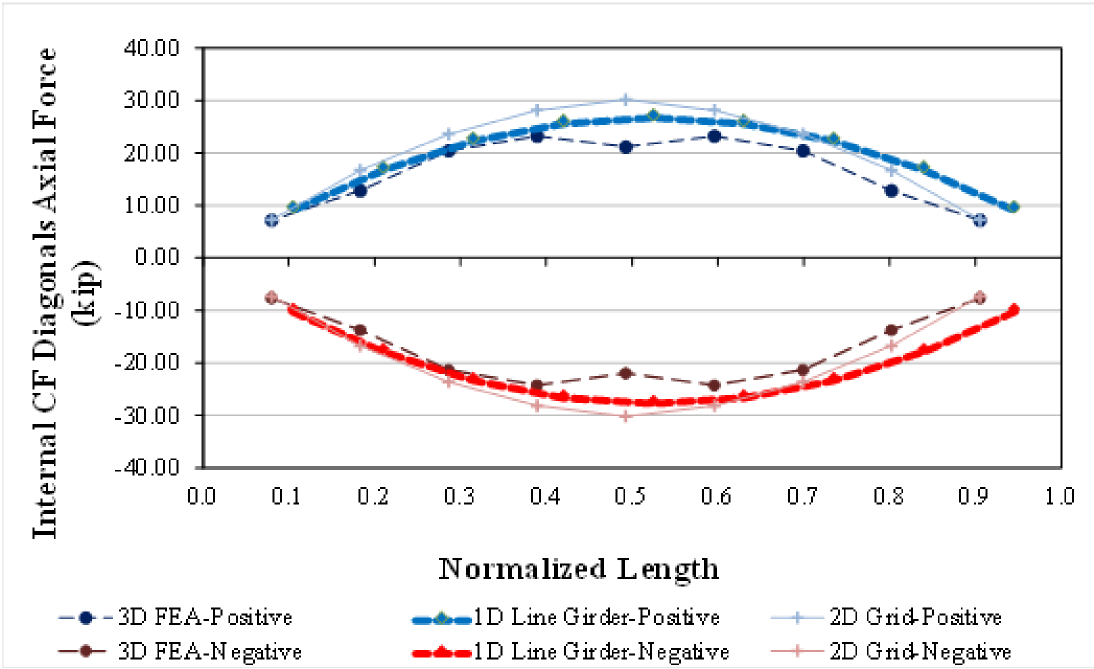

Figure 5.17. Axial forces in the intermediate internal cross-frame diagonals of the girder on the outside of the horizontal curve in the NTSCS5 bridge.

Figure 5.18 compares the line-girder and 2D-grid analysis results for the axial forces in the top chord of the intermediate internal cross-frames in the exterior girder of the NTSCS5 bridge. There are two forces, one on each side of the diagonals, at each position along the bridge length. The force values at these positions are joined together by a vertical line, and the values at the adjacent intermediate internal cross-frames are also connected together by a line to highlight the differences between the two forces. One can observe that the trends in the maximum force in these components are estimated reasonable well for this bridge. The maximum force is over-predicted by 17 % in the 2D-grid solution, whereas this force is predicted quite accurately by the 1D line-girder analysis solution.

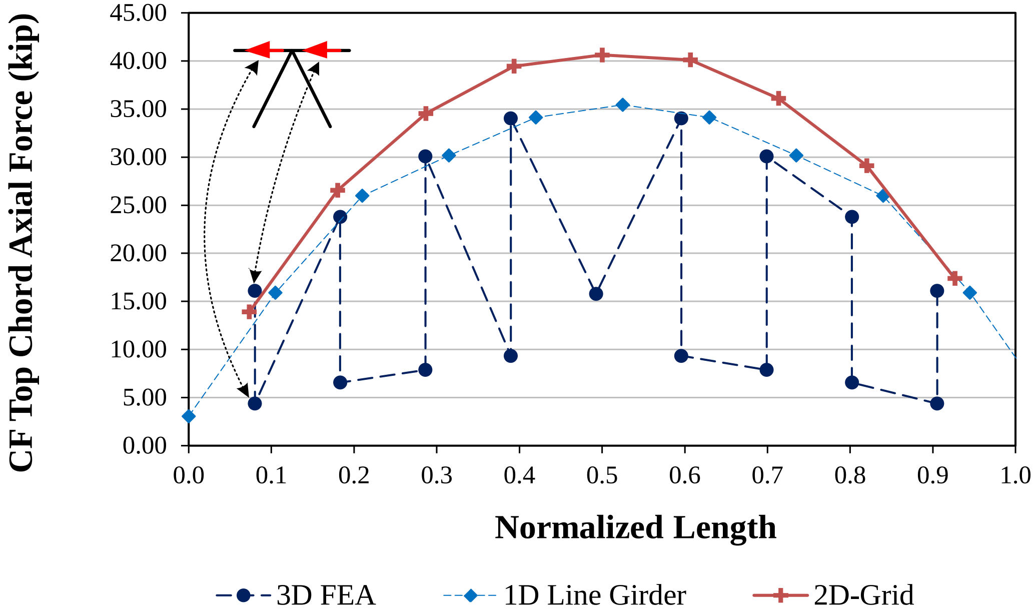

Figure 5.18. Axial forces in the top chord of the intermediate internal cross-frames in the exterior girder of the NTSCS5 bridge.

Lastly, Figure 5.19 shows the results for the 2D-grid analysis predictions of the axial forces in the TFLB struts of the exterior girder for the example bridge. These are the transverse components in the TFLB system at the locations where there is no intermediate internal cross-frame. It can be observed that these forces are predicted quite conservatively by the corresponding component force equations in this case. This is consistent with the conservative F grade shown for this response for the "C&S" bridges in Table 5.14.

The reader is referred to Jimenez Chong (2012) for a more comprehensive summary of example results, similar to the above, from the other tub-girder bridges studied in the NCHRP 12-79 research.

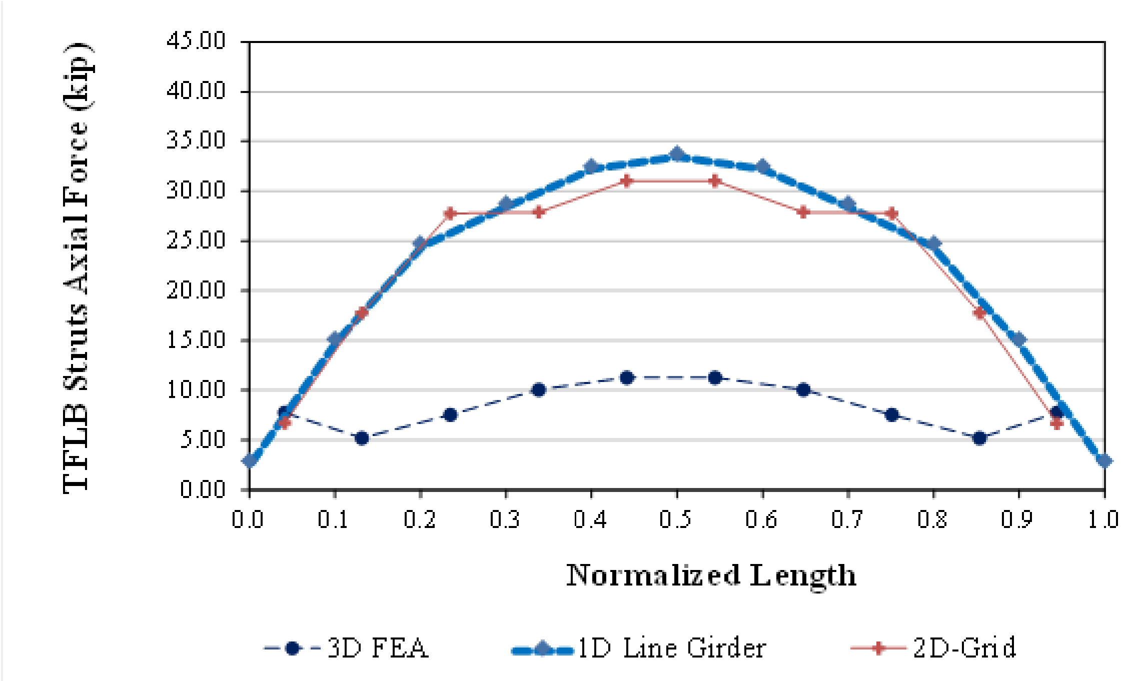

Figure 5.19. TFLB strut axial forces in the exterior girder of the NTSCS5 bridge.

6. Recommended I-Girder Bridge 2D-Grid Analysis Improvements

Chapter 2 provides a broad description of 2D-grid analysis procedures. In the present chapter, the 2D-grid analysis techniques are studied in more detail. Conventional methods used in practice to construct a grid model for the analysis and design of steel I-girder bridges are discussed first to highlight the severe limitations of these approaches. Next, improved modeling techniques are introduced that can be implemented with relative ease in 2D-grid analysis software for a better representation of the structural behavior of I-girder bridges.

6.1 I-Girder Torsional Stiffness for 2D-Grid Analysis

In a thin-walled open-section member, there are two components of torsion resistance, namely the St. Venant or pure torsion resistance and the flange warping or non-uniform torsion resistance. Horizontal curvature, support skew, and overhang eccentric loads subject steel I-girders to torsion. Hence, properly capturing the torsional properties in a curved and/or skewed steel I-girder bridge is essential to obtain an accurate prediction of the structure's performance during construction. Unfortunately, the conventional approaches commonly used to construct 2D-grid models do not have the ability to properly represent the torsion properties of I-section girders. Generally, they only implement the St. Venant torsion component, which results in a substantial misrepresentation of some of the structural responses of interest during the structure's construction.

Consider a beam in cantilever subjected to the external torque, M_z, shown in Figure 6.1a. Due to the applied torque, the free end of the beam rotates an angle ϕ, and the flanges displace laterally, where $u_f = \phi \cdot h/2$, assuming small rotations, and where h is the distance between flange centroids. In this member, the total internal torque is equal to

$$M_z(z) = M_s(z) + M_w(z) \tag{6.1}$$

where the first component, M_s, corresponds to the Saint Venant torsion and the second component, M_w, is the warping torsion. The first component is defined as

$$M_s(z) = GJ\frac{d\phi}{dz} \tag{6.2}$$

where G is the steel shear modulus of elasticity and J is the torsion constant of the girder cross-section. To obtain the warping contribution to the internal torque, one can consider analyzing the flanges as if they are subjected to lateral bending. The warping torque along the longitudinal axis of the beam, z, can be decomposed and represented by a force couple such that $M_w(z) = V_\ell(z) \cdot h$. The forces $V_\ell(z)$, which have an opposite sign in each flange, cause lateral bending of the flanges.

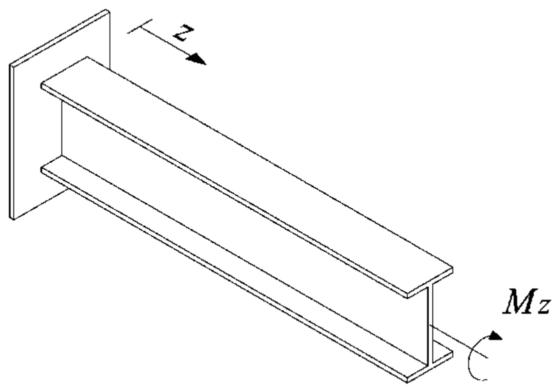

(a) Cantilever beam subject to torque M_z

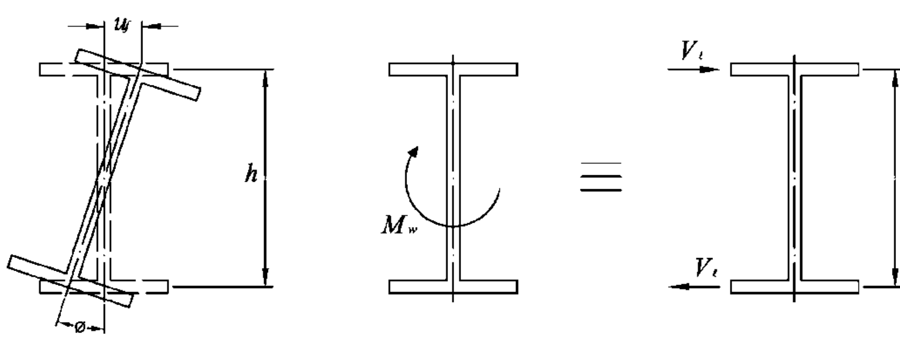

(b) Decomposition of the warping moment, M_w, in an equivalent force couple

Figure 6.1. Warping torsion in a cantilever beam.

The governing differential equation for bending in one of the flanges may be used to determine the flange lateral bending moment, M_ℓ(z), and the shear force V_ℓ(z),

$$EI_f \frac{d^2u_f(z)}{dz^2} = EI_f \frac{h}{2}\frac{d^2\phi(z)}{dz^2} = -M_\ell(z) \tag{6.3}$$

$$V_\ell = \frac{dM_\ell(z)}{dz} = -EI_f \frac{h}{2}\frac{d^3\phi(z)}{dz^3} \tag{6.4}$$

where E is the modulus of elasticity of the steel, and I_f is the flange moment of inertia about the strong axis. Hence, the warping torsion component is

$$M_w = V_\ell h = -EC_w \frac{d^3\phi(z)}{dz^3} \tag{6.5}$$

In the above equation, C_w is the warping constant, which is defined as

$$C_w = I_f \frac{h^2}{2} \tag{6.6}$$

The warping constant defined in Eq. (6.6) is valid for doubly-symmetric sections. The formulae to compute C_w in singly symmetric sections are available in the literature (Ziemian, 2010). The governing differential equation for a straight I-section girder subject to torsion is found by substituting Eqs. (6.2) and (6.5) into Eq. (6.1), giving

$$M_z(z) = GJ\frac{d\phi}{dz} - EC_w \frac{d^3\phi(z)}{dz^3} \tag{6.7}$$

As shown in Eq. (6.7), the twist angle and the applied torsion moment in an I-section beam are related through a third order linear differential equation. This equation is not suitable for implementation using an element with six dofs per node. Hence, an alternate solution is to ignore the term related to flange warping, and assume that the response is dominated by St. Venant torsion. With this simplification, the governing differential equation is reduced to

$$M_z(z) = GJ\frac{d\phi}{dz} \tag{6.8}$$

If the applied torque is constant, Eq. (6.8) can be integrated over the beam length (or bracing points) to obtain a linear relationship between $M_{z,}$ and ϕ, so that

$$M_z = \frac{GJ}{L}\phi \tag{6.9}$$

The term GJ/L is the torsional stiffness of the beam ignoring the warping contribution. It is important to note that the elements used in software packages for modeling of the girders commonly assume only this contribution to the torsional stiffness.

In box or closed-section members, pure torsion dominates the response, and thus the warping effects are minor. However, in an I-girder the torsional resistance is dominated by flange warping. In general, in members with thin-walled open sections, the effects of warping must be included to properly capture the torsional response. Curved and skewed steel I-girder bridges are inherently subjected to torsion. Therefore, the accuracy of the results obtained from the 2D-grid analysis of a curved and/or skewed bridge can be influenced by the assumptions considered when representing the girder torsional stiffness.

6.1.1 Modeling of Warping Contributions via Thin-Walled Open-Section (TWOS) 3D-Frame Analysis

A better representation of the I-girder torsion properties is implemented in some computer programs via an additional warping dof that is provided at each node of the beam or frame element, as shown in Figure 2.21 (dofs u_7 and u_{14}). Various researchers have developed elements formulated with 14 dofs that include warping deformations. As discussed in Section 2.6, these types of elements may be referred to as Thin-Walled Open-Section (TWOS) 3D-Frame elements. These elements generally provide an accurate representation of the physical behavior of non-composite I-girders subjected to torsion (Yang and McGuire, 1984; Chang, 2006). However, these types of elements must be applied cautiously for I-girders in their composite condition (Chang, 2006). This is because these elements do not account for distortional deformation of an I-girder web into an S shape. When the deck hardens, it provides substantial restraint to both the lateral displacement and the twist of the top flange. However, the bottom flange is still able to move due to the web out-of-plane flexibility. Hence, the bottom flange lateral displacements and the bottom flange lateral bending stresses, f_ℓ, may not be properly captured by a TWOS 3D-frame analysis. A 3D FEA as defined in Section 2.8.1 is able to capture these web distortion effects, by virtue of the modeling of the webs by shell finite elements.

6.1.2 Modeling of Warping Contributions in 2D-Grid Analysis via an Equivalent Torsion Constant

Another technique that can be implemented to better capture the torsional properties of an I-girder in a 2D-grid model is the use of an equivalent torsion constant, J_{eq}, as proposed by Ahmed and Weisgerber (1996). The determination of the equivalent torsion constant is further explained in the following.

The general solution of the governing differential equation for a constant torque between the beam supports (or bracing points) is

$$\phi(z) = \frac{M_z z}{GJ} + A_1 \sinh(pz) + A_2 \cosh(pz) + A_3 \tag{6.10}$$

in which

$$p^2 = \frac{GJ}{EC_w} \tag{6.11}$$

In Eq. (6.10), the constants A_1, A_2, and A_3, depend upon the end boundary conditions. For a beam with the flanges fixed against warping at its ends, these boundary conditions are $\phi(0) = \phi(L) = 0$ and $\phi'(0) = \phi'(L) = 0$. Applying these boundary conditions to Eq. (6.10) gives the following results:

$\phi(0) = 0$: $\quad A_2 + A_3 = 0$

$\phi'(0) = 0$: $\quad A_1 p + \dfrac{M_z}{GJ} = 0$

$\phi'(L) = 0$: $\quad A_1 p \cosh(pL) + A_2 p \sinh(pL) + \dfrac{M_z}{GJ} = 0$

and

$$A_1 = -\frac{M_z}{GJp}$$

$$A_2 = \frac{M_z}{GJ}\frac{\cosh(pL)-1}{p\sinh(pL)}$$

$$A_3 = -\frac{M_z}{GJ}\frac{\cosh(pL)-1}{p\sinh(pL)}$$

Substituting the constants A_1, A_2, and A_3 in Eq. (6.10), the twist angle in a beam with warping fixed flanges and subjected to a constant torque is equal to

$$\phi(z) = \frac{M_z z}{GJ} - \frac{M_z}{GJ}\sinh(pz) + \frac{M_z}{GJ}\frac{\cosh(pL)-1}{p\sinh(pL)}\cosh(pz) - \frac{M_z}{GJ}\frac{\cosh(pL)-1}{p\sinh(pL)} \qquad (6.12)$$

From the above equation, the relative twist between the beam ends is

$$\phi = \frac{M_z}{GJ}\left[L - \frac{\sinh(pL)}{p} + \frac{\cosh(pL)-1}{p\sinh(pL)}\cdot\cosh(pL) - \frac{\cosh(pL)-1}{p\sinh(pL)}\right] \qquad (6.13)$$

or

$$\phi = M_z\frac{L}{GJ_{eq}} \qquad (6.14)$$

where J_{eq} is the equivalent torsion constant for the case where flange warping is fully fixed at the beam ends, defined as

$$\begin{aligned} J_{eq(fx-fx)} &= J\left[1 - \frac{\sinh(pL)}{pL} + \frac{\cosh(pL)-1}{pL\sinh(pL)}\cdot\cosh(pL) - \frac{\cosh(pL)-1}{pL\sinh(pL)}\right]^{-1} \\ &= J\left[1 - \frac{\sinh(pL)}{pL} + \frac{\left[\cosh(pL)-1\right]^2}{pL\sinh(pL)}\right]^{-1} \end{aligned} \qquad (6.15)$$

With the equivalent torsion constant, $J_{eq(fx\text{-}fx)}$, it is possible to simulate the torsional stiffness of an I-girder with warping-fixed ends. This equivalent torsion constant may be substituted into the grid model to capture more properly the girder properties.

The above derivation can be used to model the torsional rigidity of the interior girder segments, which are the segments defined between two intermediate cross-frames. At the girder ends, the flanges typically are free to warp. For the end segments, defined between the end and the first intermediate cross-frame, the equivalent torsion stiffness may be determined assuming that the warping boundary conditions are fixed-free at the segment ends. In this case, the boundary conditions necessary to determine the constants A_1, A_2, and A_3 are $\phi(0) = \phi(L) = 0$ and $\phi''(0) = \phi'(L) = 0$. Applying these boundary conditions to Eq. (6.10) gives the following results:

$\phi(0) = 0$: $$A_2 + A_3 = 0$$

$\phi''(0) = 0$: $$A_2 p^2 = 0$$

$\phi'(L) = 0$: $$A_1 p \cosh(pL) + \frac{M_z}{GJ} = 0$$

and

$$A_1 = -\frac{M_z}{GJ}\frac{1}{p\cosh(pL)}$$

$$A_2 = A_3 = 0$$

Substituting these constants in Eq. (6.10), the rotation angle in a beam with free-fixed warping conditions subject to a constant torque is equal to

$$\phi(z) = \frac{M_z z}{GJ} - \frac{M_z}{GJ}\frac{\sinh(pz)}{p\cosh(pz)} \tag{6.16}$$

and

$$\phi = \frac{M_z L}{GJ}\left(1 - \frac{\sinh(pL)}{pL\cosh(pL)}\right) \tag{6.17}$$

Therefore, for an exterior girder segment, the equivalent torsion constant is equal to

$$J_{eq(fr-fx)} = J\left(1 - \frac{\sinh(pL)}{pL\cosh(pL)}\right)^{-1} \tag{6.18}$$

This implementation of the equivalent torsion constant provides a simple method to approximate the overall torsional stiffness of I-girders. For the analysis of an I-girder bridge, J_{eq} is calculated taking L as the distance between cross-frames. Then the torsion constant J is defined in the program using the calculated value of J_{eq}. With this technique, the typical 12-dof frame element available in commercial programs can be used to construct traditional 2D-grid models that are a closer representation of the physical structure than models constructed using conventional practices, where the flange warping contributions are neglected.

Even though the use of the equivalent torsion constant represents a potential improvement for 2D-grid modeling techniques, there is a limitation that has to be considered. In reality, warping is not fully fixed at the girder bracing points (i.e., the relative flange lateral bending rotations are not zero at the cross-frame positions). In a particular flange segment, which is defined by the distance between bracing points, warping restraint is provided by the adjacent segments. In reality, at the segment ends, the flange warping resembles a partially restrained condition. Unfortunately, it is not practical to provide further guidelines on how to determine the equivalent torsion coefficient other than assuming fixed-fixed warping for interior girder segments and free-fixed for the end segments. In general, it is not feasible to capture the girder torsional stiffness exactly unless the actual flange warping displacements at the nodes of the analysis model are known. However, the response predictions obtained from analyses of bridges with challenging geometries and complex bracing systems with equivalent torsion constants calculated based on fixed-fixed and pinned-fixed warping conditions are significantly more accurate than the responses obtained from analyses that ignore the warping contributions (Sanchez, 2011).

Another factor to consider is the calculation of the equivalent torsion constant for different girder segments in the structure. The distance between cross-frames varies depending on how the engineer configures the bracing system in the bridge. As shown in Figure 6.2, cross-frames may be provided at one or both sides of the girder, and the distance between them is not necessarily the same. In the figure, Segments 2 and 3 have different unbraced lengths. Therefore a different equivalent torsion constant must be determined for each segment. In a skewed bridge, different unbraced lengths are common near the skewed supports. Therefore, it is necessary to compute a J_{eq} for each of the different unbraced lengths.

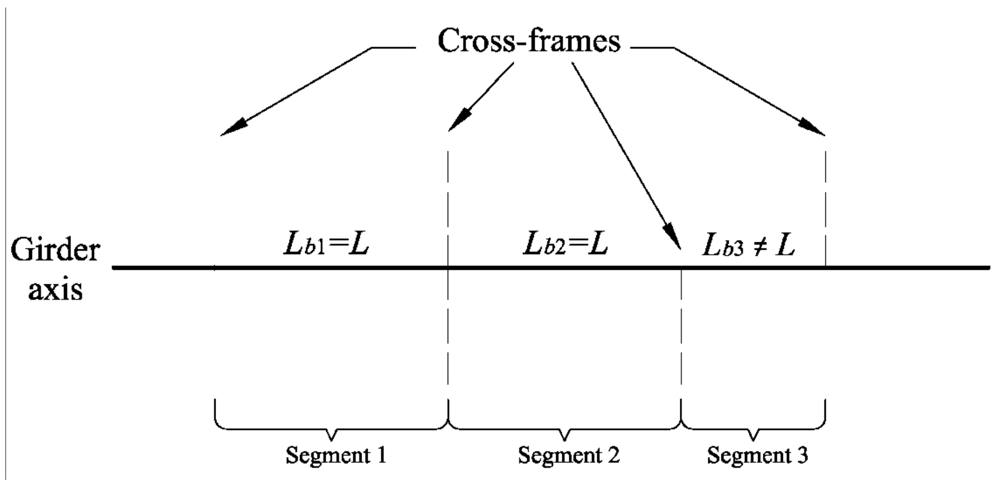

Figure 6.2. Definition of unbraced length for computation of the effective torsion constant, J_{eq}.

6.2 Cross-Frame Element Stiffnesses

In this section, the modeling techniques used to represent the cross-frames in 2D-grid analyses are studied. First, the conventional practices are presented and analyzed, emphasizing their accuracy and their limitations to represent the physical behavior of the cross-frames in the bridge. Next, two-node elements that capture the physical behavior of the X-type, V-type and inverted V-type cross-frames are developed and implemented in LARSA 4D (LARSA, 2010), a software system commonly used for design of steel bridges.

6.2.1 Conventional Cross-Frame Modeling Techniques used in 2D Grid Models

In conventional 2D-grid analysis, the cross-frames are modeled using the same type of element used to model the girders. The frame element based on the Euler-Bernoulli beam theory is used commonly to represent what in reality is a group of elements with the configuration of a truss. Figure 6.3 shows the 2D-grid model and 3D FEA representation of Bridge XICSS7. As shown in the figure, the chords and diagonals that constitute the cross-frame are modeled as a single line element. The section properties of the line element used to represent the cross-frames are determined using ad hoc procedures, such as discussed in Coletti and Yadlosky (2007) and NHI-AASHTO (2010).

One procedure that is used to determine the moment of inertia, I_{eq}, of the equivalent beam element focuses on a particular flexural stiffness of the cross-frame, and is hence referred to as the “flexural analogy” method. As depicted in Figure 6.4, a model of the cross-frame is constructed with boundary conditions that resemble a propped cantilever beam. A force couple is applied at the left-hand end of the cross-frame, resulting in the horizontal displacements Δ_t and Δ_b. Then the rotation angle, θ¸ is calculated as $\theta = (\Delta_t + \Delta_b)/d$. In the equivalent beam element, the moment $M = P \cdot d$ is applied the left-hand end. It is required that the rotation in this node be equal to the rotation θ obtained from the analysis of the cross-frame. If shear deformations are ignored, the rotation angle in the equivalent beam is defined as $\theta = (M \cdot L)/(4EI_{eq})$. Hence, the moment of inertia of the equivalent beam is:

$$I_{eq} = \frac{ML}{4E\theta} \tag{6.19}$$

The equivalent moment of inertia found from this expression is used in the definition of the elements that represent the cross-frames in the 2D model of the bridge.

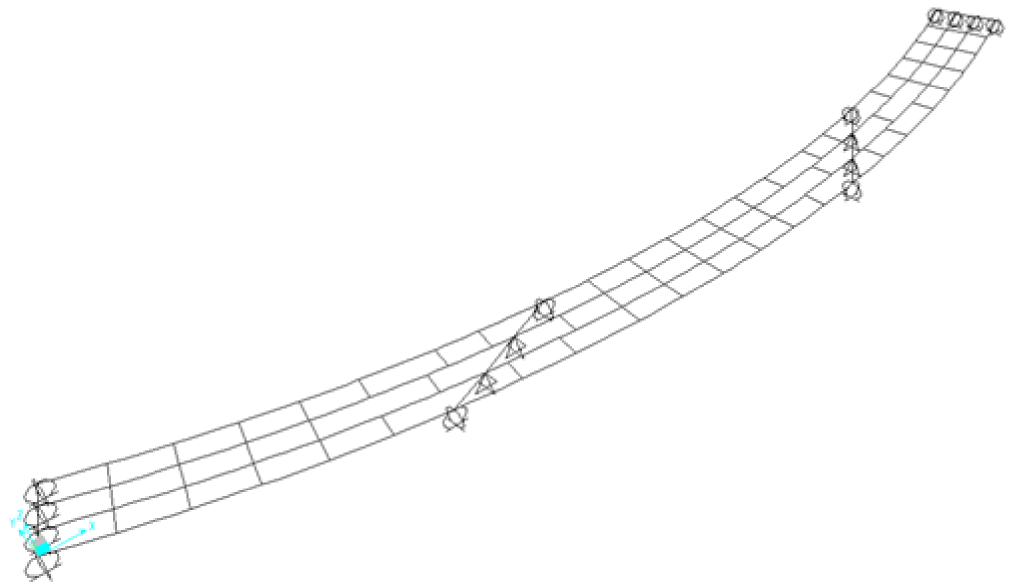

a) 2D Grid model

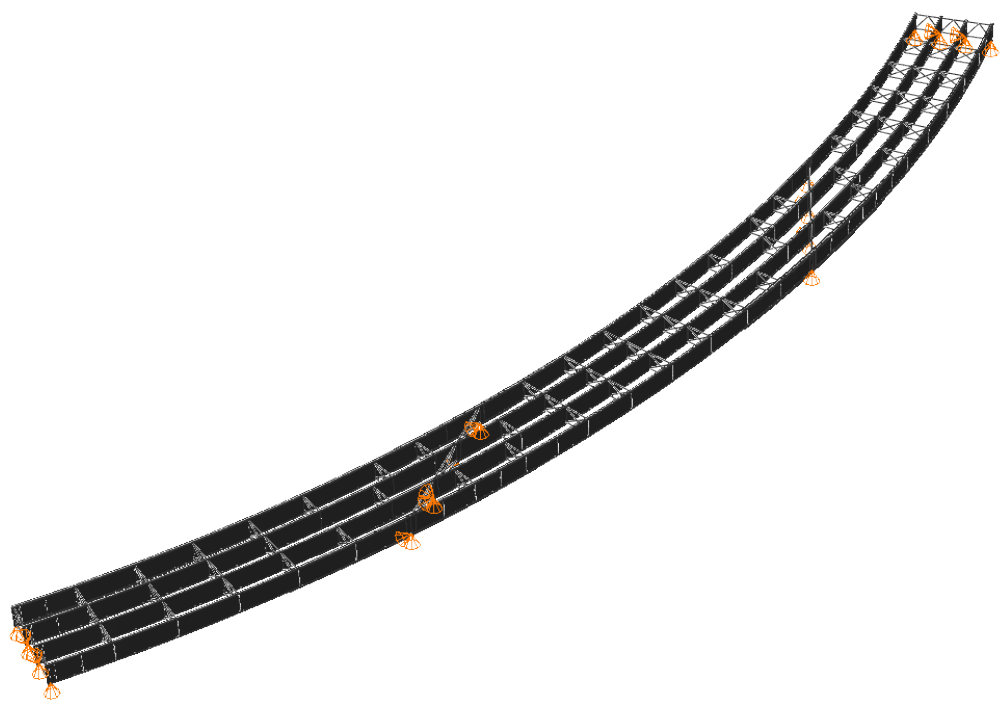

b) 3D FEA model

Figure 6.3. 2D grid and 3D FEA models of XICSS7.

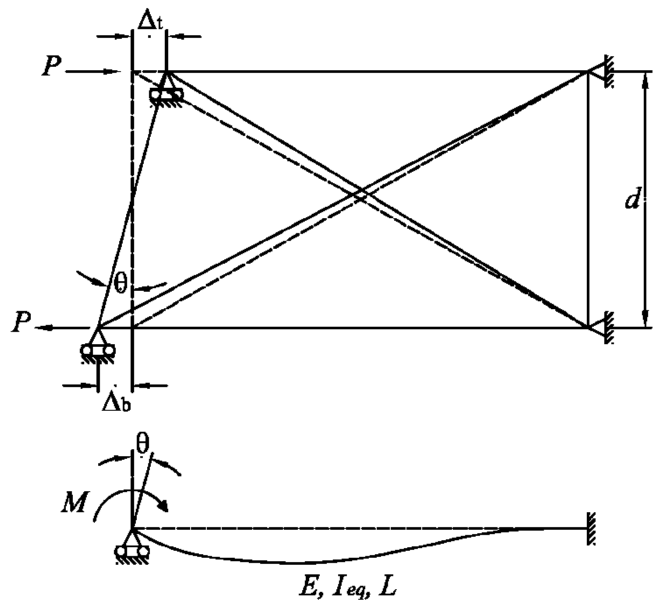

Figure 6.4. Flexural analogy model used in conventional practice to find the moment of inertia of the equivalent beam (adapted from Coletti and Yadlosky (2007)).

Another approximate procedure used to determine the moment of inertia of the equivalent beam elements is the "shear analogy" method. As depicted in Figure 6.5, in this method, the cross-frame is modeled with boundary conditions that allow only the vertical displacement of one of the ends. The force P is applied at the end that is free to move and the vertical deflection is captured. In the equivalent beam, the deflection due to this load is equal to $\Delta = (PL^3)/(12EI_{eq})$. Therefore, the moment of inertia used in the 2D-grid models to represent the cross-frames based on this method is:

$$I_{eq} = \frac{PL^3}{12E\Delta} \tag{6.20}$$

These procedures are highly approximate. It is clear that for a cross-frame, two substantially different equivalent moments of inertia can be obtained, depending on which model is used. Both the flexural analogy and shear analogy methods only capture a part of the structural behavior of the cross-frames and are not necessary a realistic representation of these bridge components.

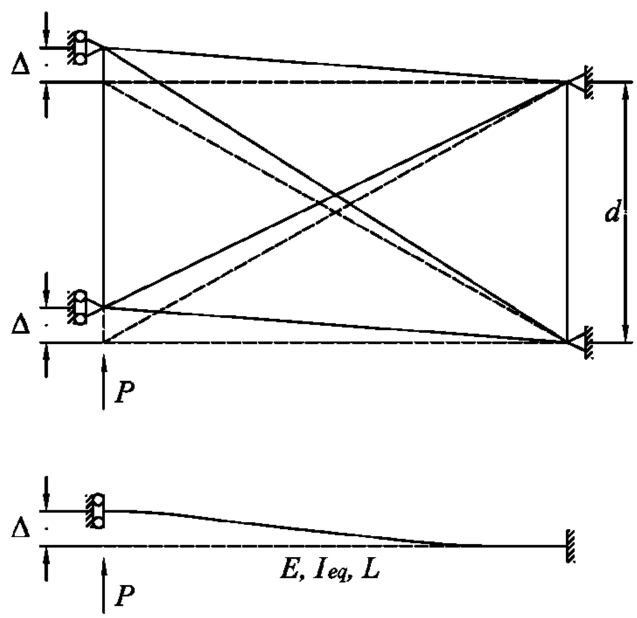

Figure 6.5. Shear analogy model used in conventional practice to find the moment of inertia of the equivalent beam (adapted from Coletti and Yadlosky (2007)).

In many cases, the responses predicted by 2D models constructed using the above procedures are close to the benchmark solutions obtained from 3D FEA analyses. As shown in (Sanchez, 2011), even for bridges with complex geometries, the approximate representation of the cross-frames often does not result in significant differences with respect to the 3D FEA predictions. In particular, the major-axis bending responses of the girders obtained from 2D-grid models constructed with these standard practices are often a close representation of the benchmark solutions. The reason for this incongruence is that in many cases, the cross-frame in-plane rigidity is much larger than the girder torsional rigidity of the I-girders.

The response affected the most by modeling the cross-frames with these ad hoc procedures is the internal forces in the cross-frame elements. In addition, the cross-frame forces generally have a significant influence on the flange lateral bending responses in I-girder bridges. To properly capture the flow of the transverse forces that results from horizontal curvature and support skew and the associated lateral bending response of the girders, it is necessary to perform the analysis with a more realistic model of the cross-frames. If the cross-frame forces are not computed accurately, it is not possible to obtain an accurate prediction of the f_ℓ stresses, either.

The practices used to model the cross-frames along with the poor representation of the torsion stiffness of the I-girders are the most significant limitations of the traditional methods used to conduct 2D-grid analysis. In the next section, simple two-node elements that are a more realistic representation of the cross-frame contributions to the system behavior are developed.

6.2.2 Improved Representation of the Cross-Frames in 2D-Grid Models

In the conventional methods commonly used to model the cross-frames, the structural properties of these components are not properly captured. It is evident that to overcome the limitations of the equivalent beam elements used to model the cross-frames, it is required to capture more efficiently their contributions to the system response. This can be done by applying the direct stiffness method to a model of the physical cross-frame and recovering the coefficients that constitute its stiffness matrix. For this purpose, consider the X-type cross-frame depicted in Figure 6.6a and its line element representation. For simplicity only the in-plane representation (3-dof per node) in shown in the figure. If the connection plates are assumed to be rigid, and the rotational continuity is neglected at the element connections in the plane of the cross-frame, it is possible to apply unit displacements to each of these dofs to recover the stiffness coefficients as shown in Figure 6.6b. Since in the cross-frame plane the chords and the diagonals are simply connected, the coefficients depend exclusively on the axial stiffness of the cross-frame elements. Note that for the formulation of the stiffness matrix, it is necessary to consider that the top chord, bottom chord, and the diagonals can have different cross-sections, i.e., different areas, A_t, A_b, A_{d1}, and A_{d2}, respectively. It is important to formulate the two-node element considering these characteristics, so it can handle cases such as cross-frames without top-chords (i.e., A_t = 0), or with only one diagonal (i.e., A_{d1} or A_{d2} = 0). The generality of an element formulated considering different element cross-sections is also beneficial when modeling bearing line cross-frames. The top-chord of these cross-frames generally has a larger section than the rest of the elements since it supports the deck joint.

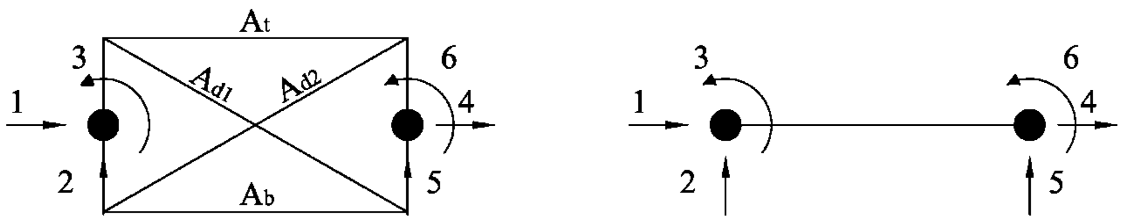

Physical Cross-Frame **Two-Node Element Representation**

a) Reduction of the physical cross-frame to a two-node element

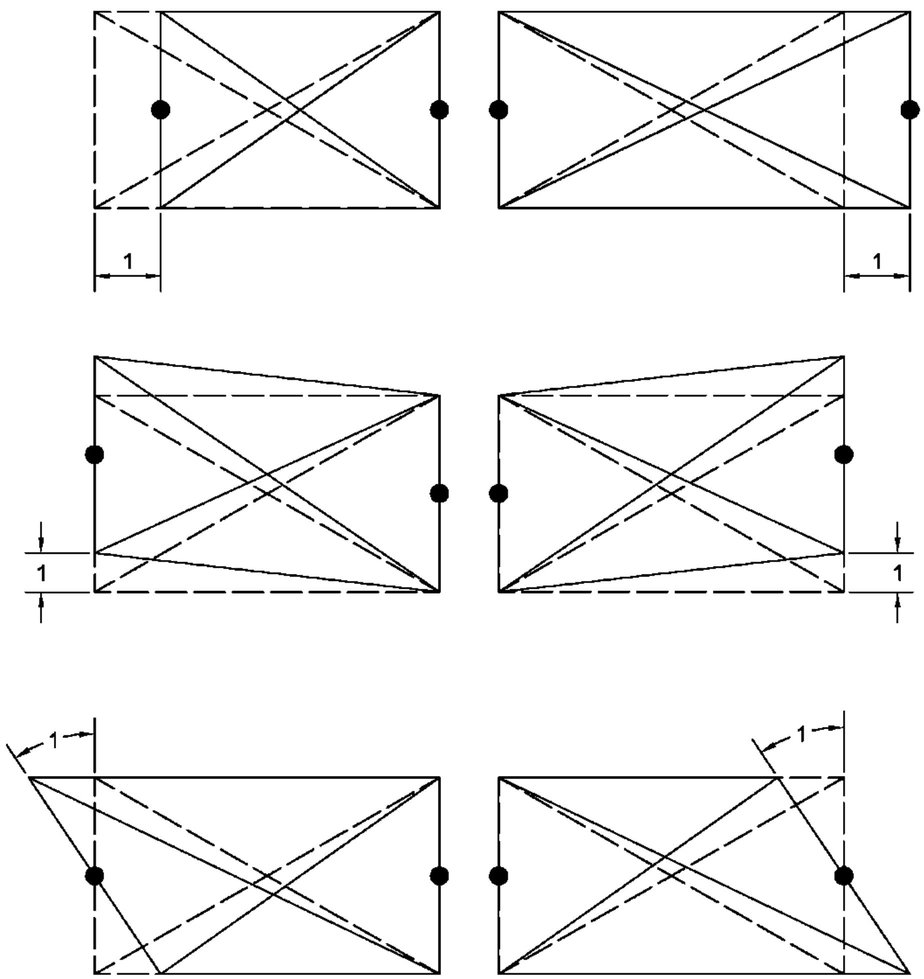

b) Unit displacements for the determination of the stiffness matrix coefficients

Figure 6.6. Determination of the stiffness matrix to represent the X-type cross-frame with a two-node beam element.

The coefficients of the first column of the stiffness matrix are determined by applying a unit displacement at dof 1. The forces in the cross-frame elements due to the applied displacement are shown in Figure 6.7. The coefficients are recovered from this free-body diagram, as shown in the same figure. Applying the same methodology to the other eleven dofs, it is possible to form the 12-by-12 stiffness matrix to represent the three-dimensional two-node element. The details of this formulation are provided in (Sanchez, 2011). Figure 6.8 shows the six-by-six stiffness matrix of the X-type cross-frame, which captures its in-plane behavior.

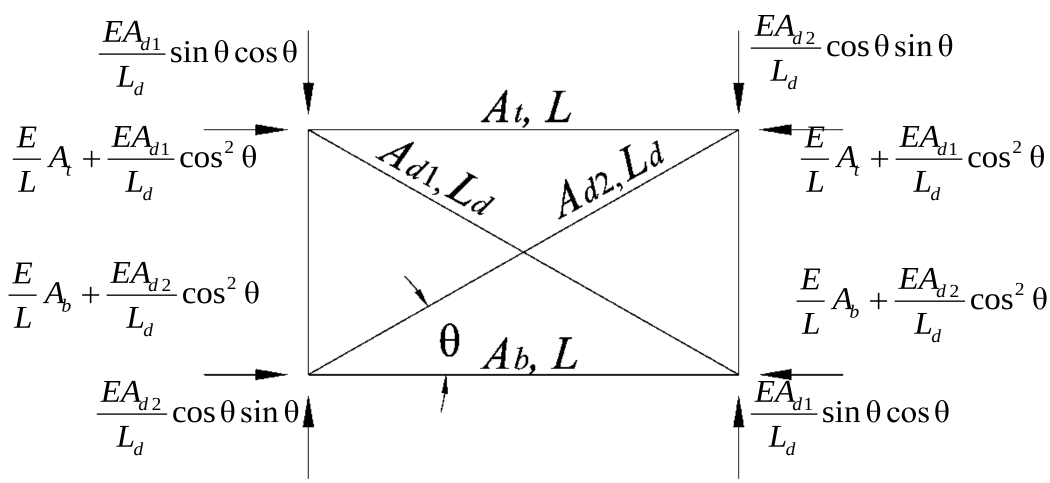

$$k_{11}: \quad \frac{E}{L}(A_b + A_t) + \frac{EL^2}{L_d{}^3}(A_{d1} + A_{d2})$$

$$k_{12}: \quad \frac{ELh}{L_d{}^3}(A_{d2} - A_{d1})$$

$$k_{13}: \quad \frac{Eh}{2L}(A_b - A_t) + \frac{EhL^2}{2L_d{}^3}(A_{d2} - A_{d1})$$

$$k_{14}: \quad -\frac{1}{L}(A_b + A_t) - \frac{L^2}{L_d{}^3}(A_{d1} + A_{d2})$$

$$k_{15}: \quad \frac{Lh}{L_d{}^3}(A_{d1} - A_{d2})$$

$$k_{16}: \quad \frac{h}{2L}(A_t - A_b) + \frac{hL^2}{2L_d{}^3}(A_{d2} - A_{d1})$$

Figure 6.7. Stiffness coefficients associated with dof 1 – X-type cross-frame.

This two-node element is an accurate representation of the contributions of an X-type cross-frame to the system behavior. In comparison to the equivalent beam elements introduced previously, this element captures all the sources of deformation in the cross-frames; in addition, it considers the coupling between the different dofs. Given that its formulation handles cross-frames with different sections for the chords or the diagonals, it can handle cross-frames without top-chords or with a single diagonal. Due to its simplicity, it has the ability to capture the physical cross-frame behavior via a line element.

This element can be implemented in any computer software to conduct 2D-grid analyses of I-girder bridges and overcome the limitations of the conventional models. This cross-frame model has been implemented and tested in the LARSA 4D software package (LARSA, 2010). This software package is selected for the study because of its versatility to handle custom element definitions. The program architecture facilitates the implementation the elements, so they can be used readily in the analyses of steel girder bridges. The tests conducted to determine the ability of the developed cross-frame models and their results are reported in (Sanchez, 2011).

Figure 6.9 shows the stiffness matrix of the two-node element based on Euler-Bernoulli beam theory. By comparing the matrix of this Euler-Bernoulli beam element and the matrix of the X-type cross-frame, it is evident that the equivalent beam cannot capture the physical behavior of these structural components. The chord and diagonal areas and the height and width of the cross-frame are the six variables needed to compute the cross-frame stiffness matrix. The matrix of the Euler-Bernoulli beam, however, only has two properties, A_{eq} and I_{eq}, that can be manipulated to represent the cross-frame. In conventional practice, when the cross-frames are modeled with beam elements based on the shear analogy method, the equivalent moment of inertia is, in effect, calculated from the equation for the term $k_{22.}$ Similarly, when the flexural analogy method is used to determine the beam properties, I_{eq} is calculated from the equation for k_{33}. Hence, instead of constructing a model of the cross-frame to determine the equivalent moment of inertia from Eqs. (6.19) or (6.20), the same approximate I_{eq} can be directly computed from the equations obtained from the terms k_{22} or k_{33}, respectively

$$k=E\begin{bmatrix}
\frac{1}{L}(A_b+A_t)+\frac{L^2}{L_d^3}(A_{d1}+A_{d2}) & \frac{Lh}{L_d^3}(A_{d2}-A_{d1}) & \frac{h}{2L}(A_b-A_t)+\frac{hL^2}{2L_d^3}(A_{d2}-A_{d1}) & -\frac{1}{L}(A_b+A_t)-\frac{L^2}{L_d^3}(A_{d1}+A_{d2}) & \frac{Lh}{L_d^3}(A_{d1}-A_{d2}) & \frac{h}{2L}(A_t-A_b)+\frac{hL^2}{2L_d^3}(A_{d2}-A_{d1}) \\
\frac{Lh}{L_d^3}(A_{d2}-A_{d1}) & \frac{h^2}{L_d^3}(A_{d1}+A_{d2}) & \frac{h^2L}{2L_d^3}(A_{d1}+A_{d2}) & \frac{Lh}{L_d^3}(A_{d1}-A_{d2}) & -\frac{h^2}{L_d^3}(A_{d1}+A_{d2}) & \frac{h^2L}{2L_d^3}(A_{d1}+A_{d2}) \\
\frac{h}{2L}(A_b-A_t)+\frac{hL^2}{2L_d^3}(A_{d2}-A_{d1}) & \frac{h^2L}{2L_d^3}(A_{d1}+A_{d2}) & \frac{h^2}{4L}(A_b+A_t)+\frac{h^2L^2}{4L_d^3}(A_{d1}+A_{d2}) & \frac{h}{2L}(A_t-A_b)+\frac{hL^2}{2L_d^3}(A_{d1}-A_{d2}) & -\frac{h^2L}{2L_d^3}(A_{d1}+A_{d2}) & -\frac{h^2}{4L}(A_b+A_t)+\frac{h^2L^2}{4L_d^3}(A_{d1}+A_{d2}) \\
-\frac{1}{L}(A_b+A_t)-\frac{L^2}{L_d^3}(A_{d1}+A_{d2}) & \frac{Lh}{L_d^3}(A_{d1}-A_{d2}) & \frac{h}{2L}(A_t-A_b)+\frac{hL^2}{2L_d^3}(A_{d1}-A_{d2}) & \frac{1}{L}(A_b+A_t)+\frac{L^2}{L_d^3}(A_{d1}+A_{d2}) & \frac{Lh}{L_d^3}(A_{d2}-A_{d1}) & \frac{h}{2L}(A_b-A_t)+\frac{hL^2}{2L_d^3}(A_{d1}-A_{d2}) \\
\frac{Lh}{L_d^3}(A_{d1}-A_{d2}) & -\frac{h^2}{L_d^3}(A_{d1}+A_{d2}) & -\frac{h^2L}{2L_d^3}(A_{d1}+A_{d2}) & \frac{Lh}{L_d^3}(A_{d2}-A_{d1}) & \frac{h^2}{L_d^3}(A_{d1}+A_{d2}) & -\frac{h^2L}{2L_d^3}(A_{d1}+A_{d2}) \\
\frac{h}{2L}(A_t-A_b)+\frac{hL^2}{2L_d^3}(A_{d2}-A_{d1}) & \frac{h^2L}{2L_d^3}(A_{d1}+A_{d2}) & -\frac{h^2}{4L}(A_b+A_t)+\frac{h^2L^2}{4L_d^3}(A_{d1}+A_{d2}) & \frac{h}{2L}(A_b-A_t)+\frac{hL^2}{2L_d^3}(A_{d1}-A_{d2}) & -\frac{h^2L}{2L_d^3}(A_{d1}+A_{d2}) & \frac{h^2}{4L}(A_b+A_t)+\frac{h^2L^2}{4L_d^3}(A_{d1}+A_{d2})
\end{bmatrix}$$

Figure 6.8. Two-node element stiffness matrix, two-dimensional representation of the X-type cross-frame.

$$k = E\begin{bmatrix}
\frac{A_{eq}}{L} & 0 & 0 & -\frac{A_{eq}}{L} & 0 & 0 \\
0 & \frac{12I_{eq}}{L^3} & \frac{6I_{eq}}{L^2} & 0 & -\frac{12I_{eq}}{L^3} & \frac{6I_{eq}}{L^2} \\
0 & \frac{6I_{eq}}{L^2} & \frac{4I_{eq}}{L} & 0 & -\frac{6I_{eq}}{L^2} & \frac{2I_{eq}}{L} \\
-\frac{A_{eq}}{L} & 0 & 0 & \frac{A_{eq}}{L} & 0 & 0 \\
0 & -\frac{12I_{eq}}{L^3} & -\frac{6I_{eq}}{L^2} & 0 & \frac{12I_{eq}}{L^3} & -\frac{6I_{eq}}{L^2} \\
0 & \frac{6I_{eq}}{L^2} & \frac{2I_{eq}}{L} & 0 & -\frac{6I_{eq}}{L^2} & \frac{4I_{eq}}{L}
\end{bmatrix}$$

k_{11}: $A_{eq}=(A_b+A_t)+\left(L^3/L_d^3\right)(A_{d1}+A_{d2})$

k_{12}: $0=\left(Lh/L_d^3\right)(A_{d2}-A_{d1})$

k_{13}: $0=(h/2L)(A_b-A_t)+\left(hL^2/2L_d^3\right)(A_{d2}-A_{d1})$

k_{16}: $0=(h/2L)(A_t-A_b)+\left(hL^2/2L_d^3\right)(A_{d2}-A_{d1})$

k_{22}: $I_{eq}=\left(h^2L^3/12L_d^3\right)(A_{d1}+A_{d2})$

k_{23}: $I_{eq}=\left(h^2L^3/12L_d^3\right)(A_{d1}+A_{d2})$

k_{33}: $I_{eq}=\left(h^2/16\right)(A_b+A_t)+\left(h^2L^3/16L_d^3\right)(A_{d1}+A_{d2})$

k_{36}: $I_{eq}=\left(-h^2/8\right)(A_b+A_t)+\left(h^2L^3/8L_d^3\right)(A_{d1}+A_{d2})$

Figure 6.9. Comparison of the stiffness matrices of the X-type cross-frame and the Euler-Bernoulli beam.

Another type of element that is sometimes used to represent the cross-frames is based on Timoshenko beam theory. This element incorporates the contributions of the shear deformations to the beam response. Figure 6.10 shows the stiffness matrix of the line element formulated with this theory. In this element an additional variable, the shear area, A_v, can be manipulated in combination with the full cross-section area A_{eq} and the moment of inertia I_{eq} to represent the cross-frames with equivalent beams. Section 3.2.3 of the NCHRP 12-79 Final Report shows that the use of the Timoshenko beam element can provide substantial improvement in the modeling accuracy for a V-type cross-frame, and points out that other cases such as X-frames with or without a top chord can be modeled with good accuracy. However, this model is not sufficient to fully capture the cross-frame behavior. As mentioned before, it is necessary to define six variables to fully represent the cross-frame stiffness. Since there are only three section properties that can be modified in the equivalent Timoshenko beam (A_{eq}, A_v, and I_{eq}), this type of element is insufficient to fully model a general X-type cross-frame. However, for an X-type cross-frame that has the same top and bottom chord areas, as well as equal diagonal areas (not necessarily the same as those for the top and bottom chord), the Timoshenko beam element is capable of exactly matching the stiffness of the cross-frame.

$$k = E\begin{bmatrix} \frac{A_{eq}}{L} & 0 & 0 & -\frac{A_{eq}}{L} & 0 & 0 \\ 0 & \frac{12A_vGI_{eq}}{L\left(A_vGL^2+12EI_{eq}\right)} & \frac{6A_vGI_{eq}}{A_vGL^2+12EI_{eq}} & 0 & -\frac{12A_vGI_{eq}}{L\left(A_vGL^2+12EI_{eq}\right)} & \frac{6A_vGI_{eq}}{A_vGL^2+12EI_{eq}} \\ 0 & \frac{6A_vGI_{eq}}{A_vGL^2+12EI_{eq}} & \frac{4I_{eq}\left(A_vGL^2+3EI_{eq}\right)}{L\left(A_vGL^2+12EI_{eq}\right)} & 0 & -\frac{6A_vGI_{eq}}{A_vGL^2+12EI_{eq}} & \frac{2I_{eq}\left(A_vGL^2-6EI_{eq}\right)}{L\left(A_vGL^2+12EI_{eq}\right)} \\ -\frac{A_{eq}}{L} & 0 & 0 & \frac{A_{eq}}{L} & 0 & 0 \\ 0 & -\frac{12A_vGI_{eq}}{L\left(A_vGL^2+12EI_{eq}\right)} & -\frac{6A_vGI_{eq}}{A_vGL^2+12EI_{eq}} & 0 & \frac{12A_vGI_{eq}}{L\left(A_vGL^2+12EI_{eq}\right)} & -\frac{6A_vGI_{eq}}{A_vGL^2+12EI_{eq}} \\ 0 & \frac{6A_vGI_{eq}}{A_vGL^2+12EI_{eq}} & \frac{2I_{eq}\left(A_vGL^2-6EI_{eq}\right)}{L\left(A_vGL^2+12EI_{eq}\right)} & 0 & -\frac{6A_vGI_{eq}}{A_vGL^2+12EI_{eq}} & \frac{4I_{eq}\left(A_vGL^2+3EI_{eq}\right)}{L\left(A_vGL^2+12EI_{eq}\right)} \end{bmatrix}$$

Figure 6.10. Stiffness matrix of a beam element including shear deformations (Timoshenko beam).

The above discussion shows that neither the Euler-Bernoulli beam nor the Timoshenko beam have the characteristics required for an exact representation of general X-type cross-frames. The two approximate methods used in conventional practice (i.e., the flexural analogy method and the shear analogy method) yield different cross-frame properties that capture only one part of the cross-frame behavior. Therefore, the equivalent beam concept generally is not an accurate representation of the structural behavior of these components. This section illustrates the development of the two-node element for the X-type cross-frame. Sanchez (2011) also discusses the development of the V-type and inverted V-type cross-frames, which are other configurations commonly used for girder bridges. For these types of cross-frames, the Timoshenko beam element is not able to capture the exact physical stiffness properties. The most significant errors in the approximation are for V-type cross-frames without a top chord, where the cross-frame flexural stiffness is critically dependent upon the characteristics of the bottom chord and the connection plates in the vicinity of the joint at the cross-frame mid-length.

The two-node equivalent beam elements developed by (Sanchez, 2011) can be implemented in any computer program used to conduct 2D-grid analyses. In the NCHRP 12-79 research, these elements were implemented in the LARSA 4D program since this software facilitates the inclusion of user-defined elements. However, the cross-frame two-node elements can be implemented in other programs that have user-defined elements, or by software developers, with minor effort.

6.3 Cross-Frame Forces

In 2D-grid models, the primary analysis output is the joint displacements. These displacements are multiplied by the corresponding element stiffness coefficients to calculate the joint forces. To obtain the forces in the chords and diagonals of the cross-frames, the joint forces commonly are decomposed as shown in Figure 6.11. The V_i and V_j shears are essentially the same; the difference between them is equal to the weight of the cross-frame. This effect is negligible, so the largest of these forces is typically selected and equally divided between the top and bottom nodes of the cross-frame (assuming an X-type cross-frame). In most of the other cross-frame types, a single diagonal frames into the girders at each end of the cross-frame, and therefore, the shear force is applied to the cross-frame node corresponding to this diagonal. In the case of a V-type cross-frame with no top chord, the flexural stiffness of the cross-frame is highly dependent upon the flexural properties provided by the combination of the bottom chord and any connection plates across the joint at the cross-frame mid-length. In this case, the distribution of the shear between the diagonal and the bottom chord is statically indeterminate, but it is reasonable to assume that any shear is taken predominantly by the diagonal.

In most situations in girder bridges, the axial forces, P_i and P_j, are negligible. In the case that they are not, they are also equally divided between the top and bottom nodes. This is necessary to satisfy equilibrium, assuming that the reference axis of the equivalent beam element is located at the mid-depth of the cross-frame.

The left and right moments, M_i and M_j, are decomposed into force couples with magnitude equal to M/h and applied to the cross-frame nodes. Once this is accomplished, the forces in the chords and the diagonals can be obtained by statics.

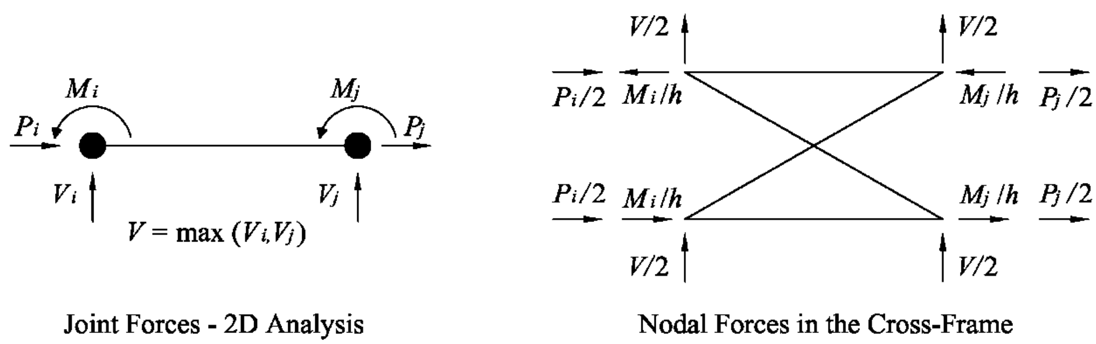

Figure 6.11. Conventional practices for determination of cross-frame member forces from 2D-grid analysis results.

It is important to note that, in general, when the cross-frame geometry is symmetric about the equivalent beam reference axis, as in the case of an X-type cross-frame with equal diagonals and equal top and bottom chords, the axial and bending responses of the cross-frame are fully uncoupled. For the Timoshenko beam element (Figure 6.10), this behavior is captured by the zero terms in the stiffness matrix, and for this specific cross-frame case, the corresponding terms in Figure 6.8 are also zero. However, if the cross-frame is not symmetric about the equivalent beam reference axis, its exact stiffness properties involve coupling between the cross-frame bending and axial degrees of freedom. For instance, for a V-type cross-frame without a top chord, the flexural deformations tend to occur approximately about the bottom chord around the mid-length of the cross-frame. This deformation causes and axial displacement at the nodal positions of the equivalent beam element (assuming that the equivalent beam element is located at the mid-depth of the cross-frame). These axial displacements in turn correspond to weak-axis flexure of the I-girders.

The above coupling is fully captured in any explicit modeling of the cross-frames in a 3D FEA, and it is fully captured in the equivalent beam element stiffness matrices developed by Sanchez (2011). Furthermore, this coupling can be included in any 2D-Frame model of a girder bridge. However, it is common to neglect all the specific depth information such as the actual position of the cross-frames relative to the mid-depth of the girders, the location of the girder shear centers and cross-section centroids relative to the girder mid-depths, and the elevation of the bearings in 2D-Frame models. Therefore, there are other potential sources of significant approximations associated with the cross-frame axial stiffnesses in 2D-Frame models.

If the "exact" cross-frame equivalent beam models are used, they should be used in a 2D-Frame approach. Furthermore, it is acceptable to model all of the components in a common plane, to formulate the singly-symmetric girder stiffnesses using the equations detailed in Section 6.1.2 along with the appropriate girder cross-section warping constant (neglecting the effect of the shift in the shear center relative to the cross-section centroid), and neglecting other height effects such as the depth of the bearings. All of the improved 2D-grid solutions presented from the NCHRP 12-79 research are conducted in this way. Alternately, the Timoshenko beam element (Figure 6.10) provides a significantly improved approximation for all types of cross-frames. This element neglects the coupling between the axial and flexural degrees of freedom, consistent with the assumptions commonly employed for 2D-grid analysis.

In the recommended exact two-node equivalent beam elements, the forces in the chords and diagonals of the cross-frames are calculated considering the fundamental force-displacement relationships from the element stiffness matrices. The forces are computed by recovering the joint displacements to determine the element deformations. The deformations are then multiplied by the corresponding stiffness coefficients to obtain the element forces. Applying this criterion, the forces in the chords and the diagonals of an X-type cross-frame are:

$$F_{TC} = \frac{E \cdot A_t}{L}\left[\left(u_4 - u_1\right) + \frac{h}{2}\left(u_3 - u_6\right)\right] \tag{6.21}$$

$$F_{BC} = \frac{E \cdot A_b}{L}\left[\left(u_4 - u_1\right) + \frac{h}{2}\left(u_6 - u_3\right)\right] \tag{6.22}$$

$$F_{D1} = \frac{E \cdot A_{d1}}{2{L_d}^2}\left[2L\left(u_4 - u_1\right) + 2h\left(u_2 - u_5\right) + Lh\left(u_3 + u_6\right)\right] \tag{6.23}$$

$$F_{D2} = -\frac{E \cdot A_{d2}}{2{L_d}^2}\left[2L\left(u_1 - u_4\right) + 2h\left(u_2 - u_5\right) + Lh\left(u_3 + u_6\right)\right] \tag{6.24}$$

where u_i is the displacement at dof i. Figure 6.6 shows the dof numbering associated with the displacements and the orientation of Diagonals 1 and 2. Similar equations for the computation of the forces in V-type and inverted V-type cross-frames are provided in (Sanchez, 2011).

6.4 Calculation of I-Girder Flange Lateral Bending Stresses Given Cross-Frame Forces

In a steel I-girder bridge, the flange lateral bending stresses, f_ℓ, that result from the horizontal curvature and the skew effects must be considered in the design of the structure. As required by the AASHTO Bridge Specifications (AASHTO, 2010), these stresses are combined with the major-axis bending stresses to conduct the strength checks in the noncomposite and composite structure. However, at present, there is limited guidance on how to determine the f_ℓ stresses associated with skew.

In a skewed bridge, the cross-frames induce forces in the I-girders, subjecting their flanges to lateral bending stresses, f_ℓ. Currently, the only methods to compute these cross-frame forces are via refined 3D frame models that explicitly include the warping stiffness contributions, or via a rigorous 3D FEA. However, with some exceptions, these analysis methods are used predominantly for research purposes or for bridges with particularly complex geometry, since significant effort may be required to construct the model and post-process the results (many of the emerging software systems provide substantial reductions in these efforts).

To obtain the flange lateral bending stresses, f_ℓ, it is necessary to have an accurate prediction of the cross-frame forces. In the approximate 1D line-girder analysis methods, the forces in the cross-frames due to the skew are not captured; therefore, it is not feasible to determine these f_ℓ stresses with a 1D analysis. Similarly, as shown in the second case study of Section 5.1.3, due to the poor representation of the cross-frame in-plane properties and the poor representation of the torsional characteristics of the I-girders, the 2D-grid models developed with conventional techniques often substantially underpredict the physical cross-frame forces. For these reasons, and in the absence of an alternative predictor, the AASHTO Bridge Specifications (AASHTO, 2010), Article C6.10.1 provides the coarse estimates for the flange lateral bending stresses discussed previously in Chapter 2. Unfortunately, no estimates are provided within the AASHTO Specifications for the corresponding cross-frame forces.

In this section, a method to estimate the f_ℓ stresses in straight and skewed bridges is introduced. Bridge NISSS16 is used to illustrate the calculations. Figure 6.12a shows the plan view of the bridge. It is intended to capture the flange lateral bending stresses in the top flange of girder G6. Figure 6.12b shows the free-body diagram of the second cross-frame in Bay 6, B6-CF2. The cross-frame forces (i.e., F_{TC}, F_{D1}, F_{D2}, and F_{BC}) are transferred to the girders in the form of nodal forces (*A*, *B*, *C*, and *D*). The horizontal and vertical components of the vertical loads are determined by applying the equilibrium equations at nodes A to D, such that:

$$
\begin{aligned}
A_x &= -F_{BC} - F_{D2}\cos(\theta) \\
A_y &= -F_{D2}\sin(\theta) \\
B_x &= -F_{TC} - F_{D1}\cos(\theta) \\
B_y &= F_{D1}\sin(\theta) \\
C_x &= F_{TC} + F_{D2}\cos(\theta) \\
C_y &= F_{D2}\sin(\theta) \\
D_x &= F_{BC} + F_{D1}\cos(\theta) \\
D_y &= -F_{D1}\sin(\theta)
\end{aligned}
\tag{6.25}
$$

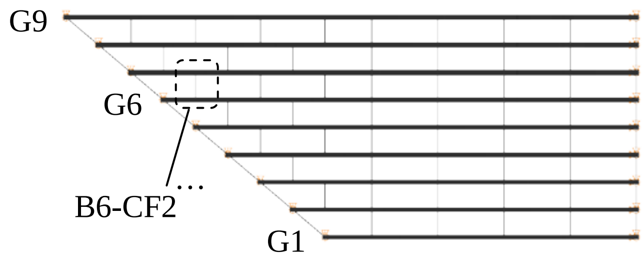

(a) Plan view of Bridge NISSS16

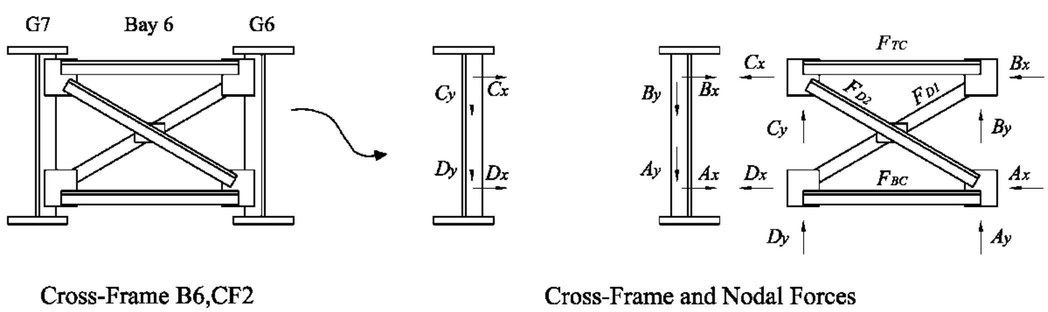

(b) Forces transferred from cross-frame B6-CF2 to girders G6 and G7

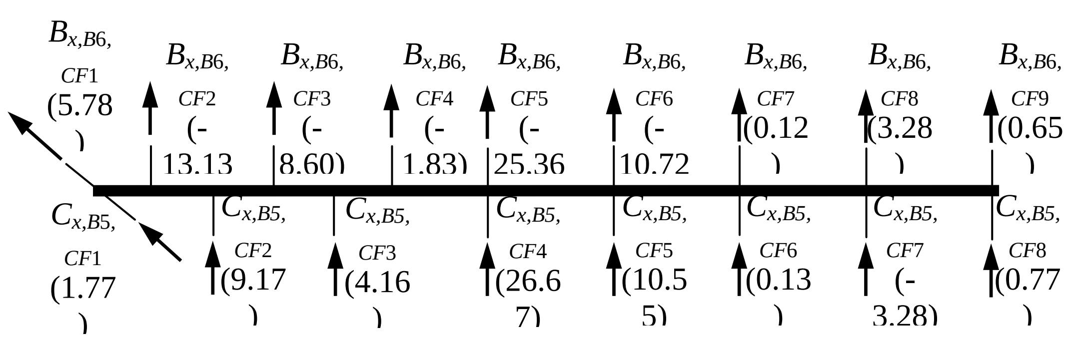

(c) Top flange of girder G6 subject to the horizontal components of the nodal forces

Figure 6.12. Determination of cross-frame forces as the first step in the calculation of flange lateral bending, top flange of girder G6, NISSS16, at TDL level.

where θ is the angle between the chords and the diagonals. Next, the lateral forces A_x and B_x are converted to statically-equivalent lateral forces at the level of the girder flanges, based on a girder cross-section free-body diagram. For simplicity of notation, these converted flange-level forces are referenced using the same symbols in the following.

Given the various flange level forces applied from the cross-frames, the girder flanges are isolated from the rest of the structure and subjected to the horizontal components of the nodal forces, as illustrated in Figure 6.12c. Notice that the C_x force components of the cross-frames in Bay 5 are applied on one side of the flange, while the B_x components of the Bay 6 cross-frames are applied on the other side. The magnitudes of the forces acting on the flange under consideration are included in the figure. They are computed with Eqs. (6.21) to (6.24), by using the cross-frame force estimates obtained from the improved 2D-grid analysis of this bridge. The 2D-grid model is constructed following the recommendations discussed in Sections 6.1 and 6.2.

The above nodal lateral forces are the source of the lateral bending in the flange of girder G6; however, only the forces acting in the region where the cross-frames are staggered cause large flange lateral bending stresses in bridge NISSS16. As shown in Figure 6.12c, the forces in the region where the cross-frames are contiguous can be larger than those where they are staggered, but these lateral forces tend to cancel each other out. For example, in the intermediate contiguous cross-frame line that is closest to the skewed support, the forces are 26.67 kips and -25.36 kips, and the resultant is 1.31 kips. Hence, although the nodal forces are larger than at other locations, the force resultant causes a minor effect on the flange lateral bending. The cross-frames, and the connections between the cross-frames and the girders, however, must be designed considering these forces.

Another important aspect to consider regarding this approximate procedure is that the nodal lateral forces are not completely balanced in Figure 6.12c. This is because the girder torsional stiffnesses, upon which the calculation of the cross-frame forces is based, include a contribution both from the girder warping torsion as well as the girder St. Venant torsion. As such, a portion of the above forces is transferred (by the interaction of the flange with the girder web) into the internal St. Venant torsion in the girders. More specifically, corresponding small but undetermined distributed lateral forces are transferred to the flange from the web in Figure 6.12c.

In the case of the flange under consideration, the unbalance calculated by adding all the lateral forces acting on the flange (including the lateral components of the forces from the skewed bearing line cross-frames) is -2.58 kips. If the distributed lateral load transferred from the web is added to the above nodal lateral forces, the flange would be in equilibrium.

Solutions to this problem include:

(1) Use the girder torsional rotations and displacements along with the detailed open-section thin-walled beam stiffness model associated with J_{eq} to directly determine the flange lateral bending stresses. This results in an imbalance in the flange lateral bending moments on each side of the intermediate cross-frames (since J_{eq} is based the assumption of warping fixity at the cross-frame locations). This moment imbalance could be re-distributed along the girder flange to determine accurate flange lateral bending moments. A procedure analogous to elastic moment distribution could be utilized for this calculation. Although this approach is a viable one, it is relatively complex. Therefore, it was not pursued in the NCHRP 12-79 research.

(2) Focus on an approximate local calculation in the vicinity of each cross-frame, utilizing the forces delivered to the flanges from the cross-frames as shown in Figure 6.12c. Because of its relative simplicity this approach was selected in the NCHRP 12-79 research.

It should be noted that the girder flange lateral bending stresses are calculated directly and explicitly from the element displacements and stiffnesses in the TWOS 2D-grid and TWOS 3D-frame solutions. Therefore, these methods provide the best combination of accuracy and simplicity for the grid or frame element calculation of the flange lateral bending stresses. However, the disadvantage of this approach is the additional complexity of the element formulation, and the requirement that an additional warping degree of freedom has to be included in the global structural analysis.

Figure 6.13 illustrates the simplified approach adopted in the NCHRP 12-79 research for calculating the I-girder flange lateral bending moments given the statically-equivalent lateral loads transferred at the flange level from the cross-frames. The calculation focuses on a given cross-frame location and the unbraced lengths, *a* and *b*, on each side of this location. For simplicity of the discussion, only the force delivered from the cross-frame under consideration is shown in the figure, and the cross-frame is assumed to be non-adjacent to a simply-supported end of the girder. In general, the lateral forces from horizontal curvature effects and/or from eccentric bracket loads on fascia girders also would be included. Two flange lateral bending moment diagrams are calculated as shown in the figure, one based on simply-supported end conditions and one based on fixed end conditions at the opposite ends of the unbraced lengths. For unbraced lengths adjacent to simply-supported girder ends, similar moment diagrams are calculated, but the boundary conditions are always pinned at the simply-supported end. The cross-frame under consideration is located at the position of the load *P* in the sketches. In many situations, the moments at the position of the load are the controlling ones in the procedure specified below.

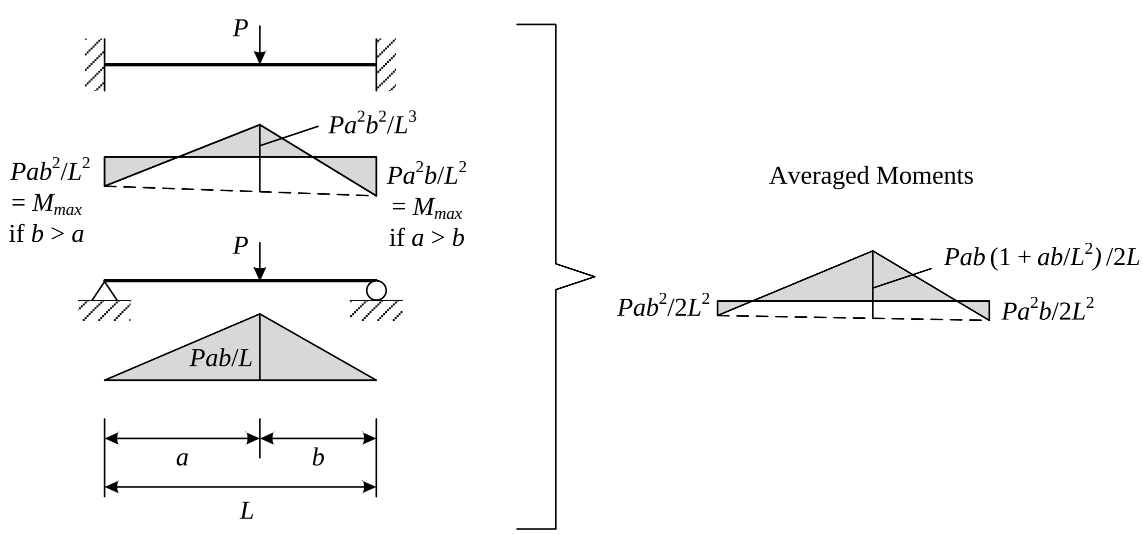

Figure 6.13. Lateral bending moment, M_ℓ, in a flange segment under simply-supported and fixed-end conditions.

Given the moment diagrams for the above cases, the NCHRP 12-79 research determined that an accurate to conservative solution for the flange lateral bending moments and stresses is obtained generally by:

(1) Averaging the above moment diagrams, and

(2) Taking the largest averaged internal moment in each of the unbraced lengths as the flange lateral bending moment for that length.

This solution is repeated cross-frame location by cross-frame location along the length of the girders and the largest moment from the two solutions obtained for each unbraced length is taken as the estimate of the flange lateral bending moment in that unbraced length. (For the unbraced lengths at girder simply-supported ends, only one solution is performed.)

The above procedure recognizes that the true flange lateral bending moment is bounded by the “pinned” and “fixed” moment diagrams (neglecting the small St. Venant torsional contributions from the interaction with the web) and ensures that the flange lateral bending moments required for static equilibrium are never underestimated. Also, the average of the pinned and fixed moment diagrams is analogous to the use of the approximation $qL_b^2/10$ rather than $qL_b^2/12$ when estimating the flange lateral bending moments due to horizontal curvature, where q is the equivalent flange radial load. In

Figure 6.14 shows the plots of the response predictions obtained using the above approach and the results obtained from the 3D FEA for the top flange of Girders G3 and G6. The plots include the responses for fully fixed and simply supported end conditions. Additionally, a trace that represents the average between these two responses is also included. As shown in these plots, the estimates obtained with the proposed approach and using the results derived from the improved 2D-grid model are a reasonable representation of the benchmark. As expected, the responses predicted by the FEA lay between the predictions determined assuming fully fixed and pinned ends, and are accurately estimated by taking the average of the last two predictions.

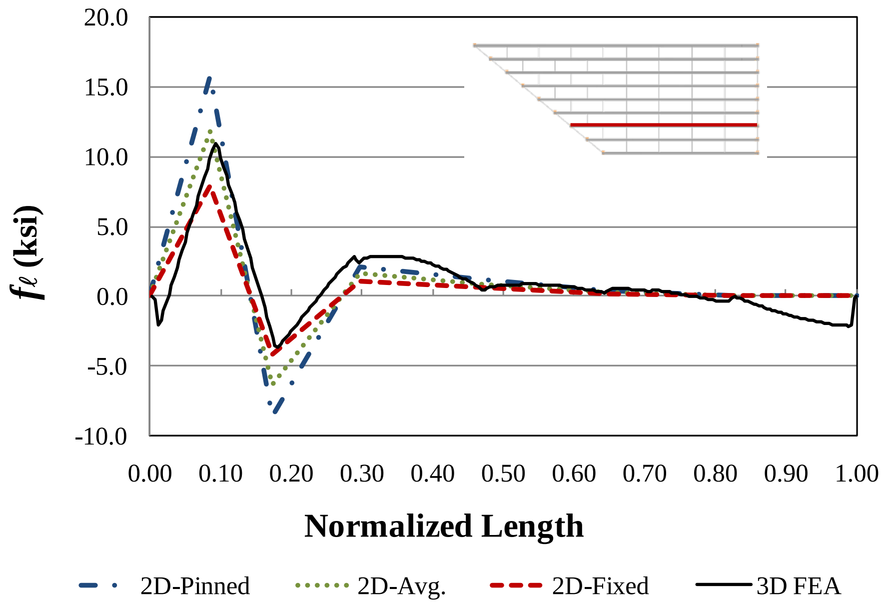

Girder G3

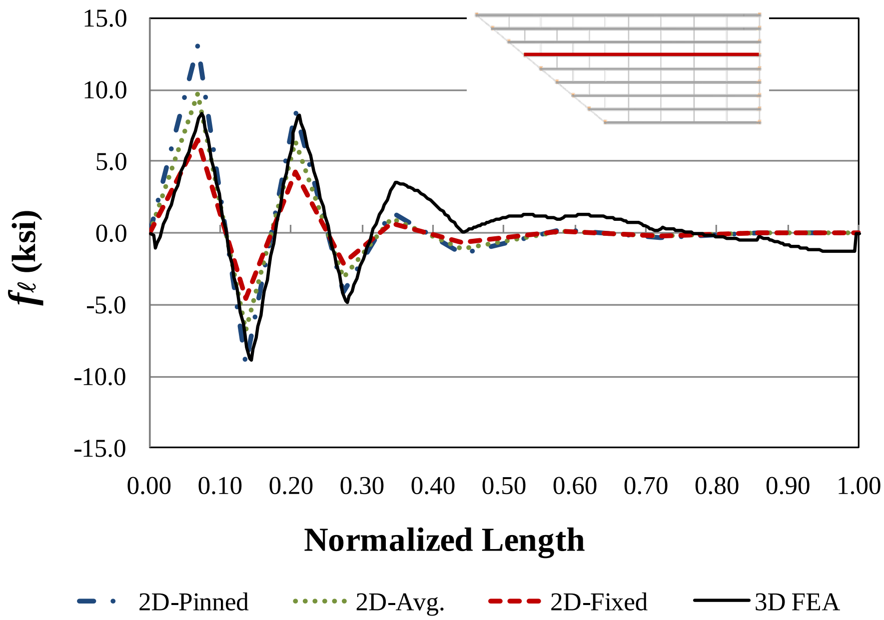

Girder G6

Figure 6.14. Flange lateral bending stresses in Bridge NISSS16 at TDL level.

It should be emphasized that to predict the flange lateral bending stresses using the proposed method, it is necessary to first have an accurate prediction of the cross-frame forces. Hence, the results of a 2D-grid analysis conducted with conventional practices cannot be used for this purpose. The cross-frame forces should be obtained from an analysis where the recommendations of Sections 6.1 and 6.2 are implemented in the model.

6.5 . Summary of Proposed Improvements for the Analysis of I-Girder Bridges using 2D-Grid Analysis

The previous sections highlight the characteristics of the 2D-grid models and the limitations of the conventional techniques to properly represent the behavior of an I-girder bridge during construction. Essentially, there are two modeling practices that can considerably affect the accuracy of the analyses. The first practice is related to the representation of the torsional properties of the I-girders. In computer programs commonly used for 2D-grid modeling, the torsional resistance of the I-girders is formulated considering only the pure or St. Venant torsion contributions. The other factor that can affect the response predictions of a 2D-grid analysis is the model used to represent the cross-frames. In most of cases, the cross-frames are modeled using an equivalent beam element, which is based on the Euler-Bernoulli beam theory.

The improved modeling techniques discussed in this chapter can be implemented with minor effort in design offices. The equivalent torsion constant as a means to simulate the warping contributions to the girder torsional stiffness is a concept that requires a simple manipulation of the cross-section properties in the model definition. This modification, however, can improve the predictions obtained from a grid model of bridges where the torsional responses have a major role in the structural response, as is the case of curved and/or skewed bridges.

Similar to the girder torsional properties, a better representation of the cross-frames can be accomplished by formulating two-node elements that consider all the stiffness contributions to the system response. The elements developed in the NCHRP 12-79 research were included and tested in the LARSA 4D program since the architecture of this software allows the inclusion of user defined finite elements. However, the element potentially could be implemented in the library of any commercial software used for bridge engineering.

Finally, it is worth emphasizing on the relevance of an accurate model of cross-frames and girder torsional stiffness. In many structures, wide fluctuations in cross-frame stiffness do not have a significant effect in the structural responses. Similarly, in some cases, the poor torsion model of the girders does not represent a considerable source of error. The studies conducted in this research show that in straight and skewed bridges with skew indices below 0.30, torsion induced by skew is minor and the participation of the cross-frames may be negligible. Hence, bridges of these characteristics are insensitive to the cross-frame and girder torsional stiffness model. In fact, a line girder analysis may be sufficient in these cases. However, when the index goes above this limit, due to the torsion that the girders experience as a result of the transverse load path, the system becomes more sensitive to the torsion model and changes in the cross-frame stiffness. In bridges with $I_S \geq 0.30$, it is important how the torsional girder stiffnesses and the cross-frame in-plane stiffnesses are represented in the program since they can have a substantial influence on the system responses.

In curved and skewed bridges it is not clear how the horizontal curvature and the support skew interact to determine when the structure is sensitive to the cross-frame and girder torsional stiffness models. For these bridges, the NCHRP 12-79 research shows that it is difficult to determine limits on when a traditional 2D-grid analysis provides acceptable results. For these structures it is suggested to implement the approaches discussed in this chapter to obtain accurate predictions.

7. Consideration of Locked-In Forces in I-Girder Bridges due to Cross-Frame Detailing

7.1 Cross-Frame Detailing Methods

Curved and skewed I-girder bridges exhibit significant torsional displacements of the individual girders and of the overall bridge cross-section. As a result, the girder webs can be plumb only in one configuration. If the structure is built such that the webs are plumb in the ideal no-load position, they generally cannot be plumb under the action of the structure's steel or total dead load. The deflected geometry resulting from these torsional displacements can impact the fit up of the members (i.e. come-along and jacking forces), the erection requirements (crane position and capacities, number of temporary supports and tie downs), and the bearing cost and type. Furthermore, significant layover (i.e., relative lateral deflection of the flanges associated with twisting) can be visually objectionable. This is particularly the case at piers and abutments.

If the torsional deflections are large enough, then the cross-frames often are detailed with a lack-of-fit that induces opposing torsional displacements to offset the dead load torsional rotations. As explained in the AASHTO LRFD Specifications Article C6.7.2 (2010), different types of cross-frame detailing are used to achieve approximately plumb webs in the theoretically no-load, steel dead load, or total dead load conditions. These methods are summarized below.

No-Load Fit (NLF): For NLF detailing, the cross-frames are fabricated to fit the girders in their cambered, plumb, no-load geometry without inducing any locked-in forces (i.e., there is no lack-of-fit). Figure 7.1 illustrates the behavior associated with NLF detailing at a representative intermediate cross-frame in the no-load geometry and under the action of the dead loads. (Geometric factors such as cross-slope, super-elevation and profile grade line are not shown in this figure and in the subsequent figures for clarity.) The cross-frame is assumed to be normal to the girders for purposes of the following discussion. The girders deflect from their plumb no-load geometry into an out-of-plumb position under the action of the dead loads. In Figure 7.1, this twisting of the girders is driven primarily by the larger vertical deflection of the girder on the right compared to the one on the left. Since the cross-frame deformation is relatively small within its plane, the cross-frame induces a twist into the girders due to the differential vertical displacements.

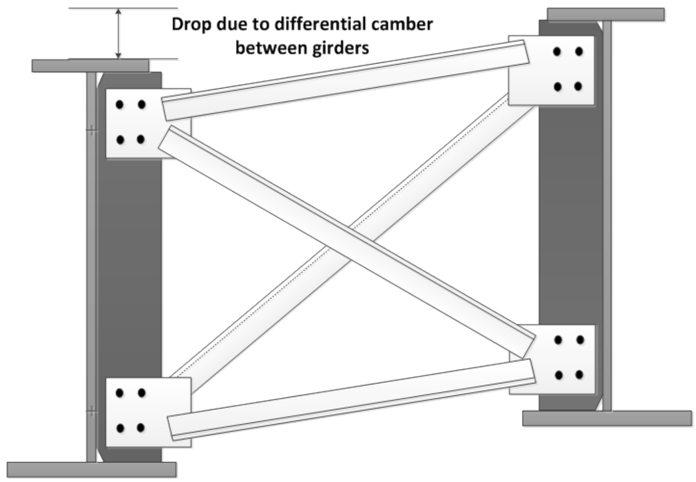

(a) No-load geometry

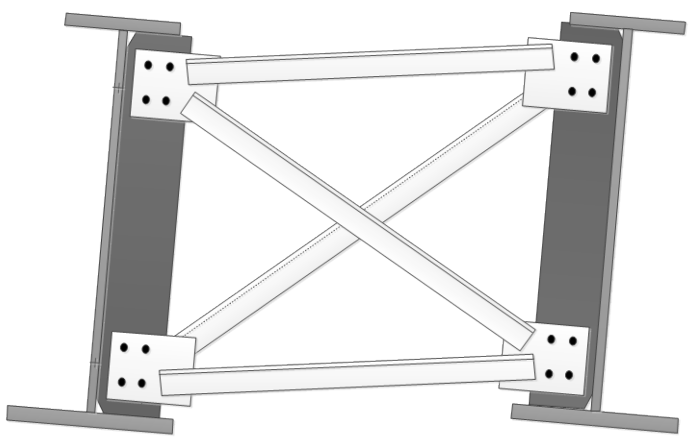

(b) Under the action of dead loads

Figure 7.1. Illustration of the behavior associated with No-Load Fit (NLF) detailing at intermediate cross-frames (geometric factors such as cross-slope, super-elevation and profile grade line are not shown for clarity).

In addition, as explained in Section 2.1.4, the cross-frames at skewed bearing lines tend to rotate about their own skewed axis and warp (twist) out of their plane. However, the cross-frame in-plane stiffnesses are again relatively large compared to the girder lateral and torsional stiffnesses. Therefore, the girders must lay over at any skewed bearing line to maintain compatibility with the cross-frames under the dead load rotations at the bearing line. This is illustrated by Figure 7.2, which is repeated from Figure 2.7 for ease of reference.

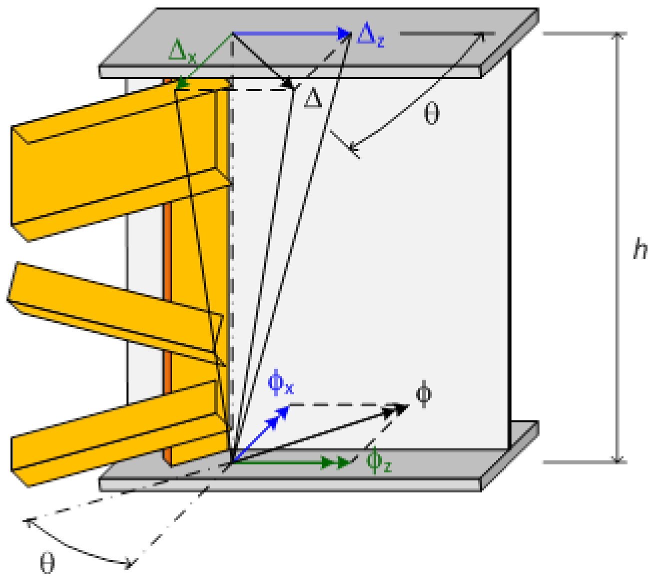

Figure 7.2. Girder top flange deflections and girder rotations at a fixed bearing location on a skewed bearing line.

The above two sources of girder layover work both jointly and independently. That is, if the bearing line cross-frames were theoretically taken out, the layovers at the bearing lines caused by the intermediate cross-frames would be somewhat different (but generally in the same direction). Similarly, if the bearing line cross-frames were left in and the intermediate cross-frames taken out, the girder layovers would be different at the intermediate cross-frame locations, although the direction of the layover tends to be the same.

Total Dead Load Fit (TDLF): For TDLF detailing, the cross-frames are fabricated to fit to the girders in their ideal final plumb position under total dead load (that is plumb webs but with the total dead load vertical deflections subtracted from the initial girder camber). Figure 7.3 illustrates the behavior associated with TDLF detailing at an intermediate cross-frame (assumed normal to the girders) before it is connected to girders in the no-load geometry, after it is connected to girders in the theoretical no-load position (if the cross-frames could be connected to the girders without any dead load on the structure), and under the total dead load. The intermediate cross-frame does not fit-up with the girder connection points in the no-load geometry since it is fabricated for the final plumb geometry. Also, as noted above, the cross-frame is relatively stiff in its own plane. Therefore, the girders, which are relatively flexible, must be twisted in a direction opposite to their dead load torsional rotations to make the connections to the cross-frame. However, under the action of the total dead loads, the girder webs rotate back to an approximately plumb position. The lack-of-fit between the girders and the cross-frame, due to the differential vertical camber, induces additional locked-in internal stresses and corresponding deformations in the structure when the girders and cross-frames are forced together to make their connections.

All of the illustrations of the deflections, rotations and deformations in Figure 7.3 correspond to a generic location within the span. To achieve a web plumb condition under the total dead load at a skewed bearing line, the opposite of the layover under the total dead load is applied at this location initially (i.e., due to the initial lack-of-fit). Based on the assumption that the in-plane cross-frame deformations are relatively small, this is achieved by fabricating the end cross-frames to fit the final geometry of the girders, but attaching the cross-frames to the girders in their initial cambered geometry. It is commonly assumed that the girder end connection plates, which are also the bearing stiffeners, are vertical in the reference geometry shown in Figure 7.2. Due to the total dead load camber, the girder end connection plates are rotated by the negative of the total dead load major-axis bending rotations shown in Figure 7.2 ($-\phi_x$) to achieve the initial cambered geometry. Correspondingly, if the cross-frames at the bearing line are to be connected to the girders in the theoretical no-load geometry, the girder top flange must be laid over by the negative of the dead load layover shown in Figure 7.2 ($-\Delta_x$). In this work, the girders are assumed to be fabricated with plumb webs in their initial no-load geometry. Therefore, the girder top flange in Figure 7.2 must be forced over by $-\Delta_x$ to make the connection to the bearing line cross-frame in the ideal no-load condition.

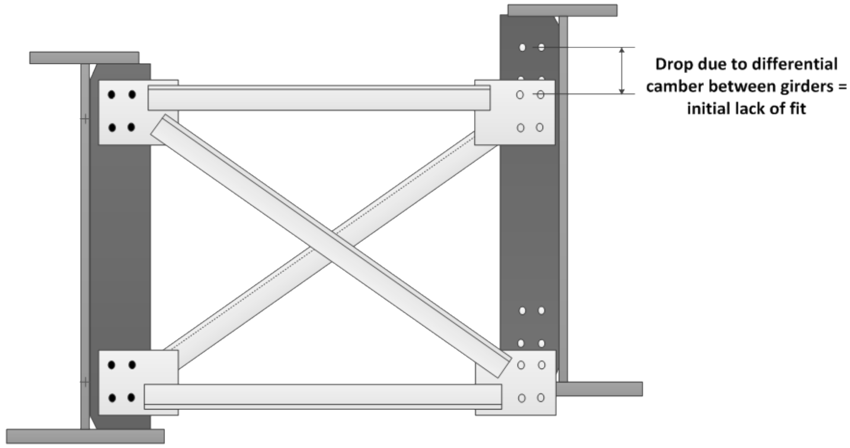

(a) No-load geometry before connecting the cross-frames

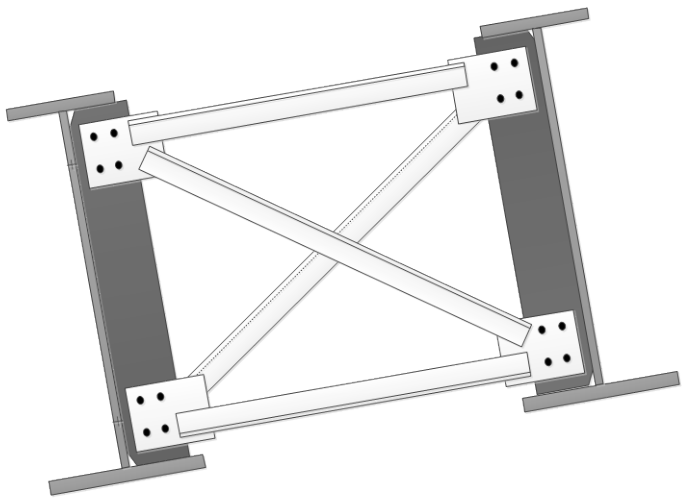

(b) No-load geometry after connecting the cross-frames

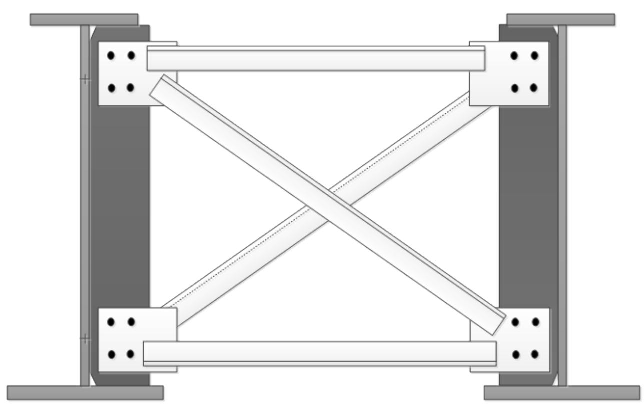

(c) Under the total dead load

Figure 7.3. Illustration of the behavior associated with Total Dead Load Fit (TDLF) detailing at intermediate cross-frames (geometric factors such as cross-slope, super-elevation and profile grade line are not shown for clarity).

When the total dead load has been applied to the structure, the girders "unwind" under the application of the load such that they come back to an approximately plumb position in the final constructed configuration. The girders deflect into the approximately plumb position shown in Figure 7.3(c) at the intermediate cross-frame locations, the girders rotate approximately back to the plumb reference geometry at the skewed bearing lines, and the end connection plates (i.e., the bearing stiffeners) rotate approximately back to the vertical position at the bearings.

Steel Dead Load Fit (SDLF): For SDLF detailing, the cross-frames are fabricated to fit the girders in their idealized final plumb position under the steel dead load (that is plumb webs but with the steel dead load vertical deflections subtracted from the initial girder camber). SDLF detailing is similar to TDLF detailing in that locked-in stresses and deformations are developed due to a lack-of-fit. However, the lack-of-fit between the cross-frames and girders in the no-load geometry for SDLF is often smaller than that due to TDLF. When SDLF is used, the webs rotate back to an approximately plumb position under the action of the *steel* dead loads.

7.2 Procedures for Determining Locked-In Forces

As demonstrated in the subsequent sections of this chapter, the locked-in forces in the bridge system associated with SDLF and TDLF detailing are generally of comparable magnitude to the corresponding steel or total dead load forces. For example, in a straight-skewed I-girder bridge constructed with TDLF detailing of the cross-frames, the locked-in cross-frame forces and girder flange lateral bending stresses are nearly equal and opposite to the corresponding total dead load values. As such, the final cross-frame forces and girder flange lateral bending stresses (equal to the sum of the locked-in and total dead load values) tend to be relatively small. Engineers typically expect this once it is understood that the girders are essentially "reverse twisted" by the initial lack-of-fit associated with the TDLF detailing, but then they "unwind" back to their plumb geometry under the total dead loads. Since the girders unwind back to an approximately plumb position under the total dead load, it is anticipated that the corresponding flange lateral bending stresses and the cross-frame forces are small.

When an engineer conducts an accurate 2D-grid analysis using the improvements discussed in Chapter 6, or an accurate 3D FEA using methods such as those outlined in Section 2.8.1, one might expect that the corresponding internal cross-frame forces and girder flange lateral bending stresses are calculated accurately. Unfortunately, if the cross-frames are detailed for anything other than NLF, the calculated internal distribution and magnitude of the cross-frame forces and girder flange lateral bending stresses will be substantially different from the values in the physical bridge. Without the calculation of the locked-in forces due to the initial lack-of-fit between the cross-frames and the girders, an accurate 2D-grid or 3D FE analysis captures only the *applied* dead load effects.

Technically, the inclusion of the lack-of-fit effects from SDLF or TDLF detailing in analysis is relatively straightforward. Analysis solutions for the locked-in forces associated with DLF detailing are fundamentally no different than typical lack-of-fit problems students first solve in undergraduate Strength of Materials; however, the lack-of-fit due to DLF detailing is generally a 3D geometry problem. One way of capturing the influence of cross-frame detailing is to construct a full model of any intermediate erection stage of the bridge with the girders in their initial no-load cambered and plumb positions, with the cross-frames connected to the girders, and with initial strains introduced into the cross-frames corresponding to the initial lack-of-fit caused by the cross-frame detailing. An analysis of this specific stage is then performed by simply including the cross-frame member initial strains in the analysis and "turning gravity on."

The initial strains corresponding to the lack-of-fit are introduced to each cross-frame member. These strains are calculated by using the cross-frame member length in the final dead load position, which is the fabrication length of the cross-frame members, (Configuration A) and length between the work points of the girders in the initially-plumb cambered geometry (Configuration B). Figure 7.4 shows an example intermediate cross-frame. The differential cambers between the girders often generate large initial axial strains in the cross-frame members. However, this is not a problem physically, since the initial strains are just an analytical device to determine the locked-in forces. The actual strains in the structure are generally much smaller.

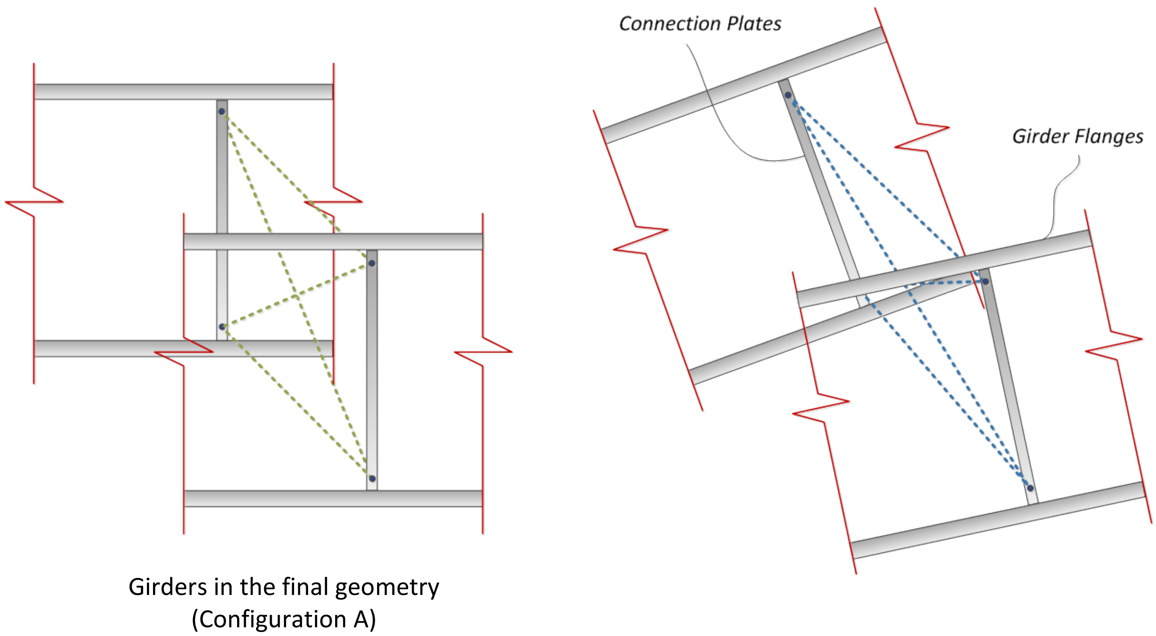

Figure 7.4. Configurations used for calculation of initial lack-of-fit strains in cross-frame members.

The initial strains should be calculated based on the element formulation. If the element formulation is based on engineering strain, then the initial strains may be expressed as

$$\varepsilon_{\text{initial strain}} = \frac{L_{\text{Configuration.B}} - L_{\text{Configuration.A}}}{L_{\text{Configuration.A}}} \tag{7.1}$$

On the other hand, if the element formulation is based on the log strain for example, then the initial strains should be calculated as the log strains (Ozgur, 2011). It should be noted that the length changes of the intermediate cross-frame members are mainly due to the differential vertical cambers between the girders (the steel dead load cambers for SDLF or the total dead load cambers for TDLF), assuming that the cross-frames are normal to the girders, whereas at skewed bearing-line cross-frames, they are mainly due to the component of the girder major-axis bending rotations, due to the girder cambers, causing in-plane distortion of the cross-frames. At skewed intermediate cross-frames, there is a contribution both from the differential vertical cambers and the component of the girder major-axis bending rotations (due to the camber) causing in-plane distorton of the cross-frames.

In 2D-grid analysis models, the cross-frames typically are modeled with single equivalent beam elements. It is possible to include the initial lack-of-fit effects in the analysis using the equivalent beam elements presented in Chapter 6 and in Sanchez (2011), as well as using conventional beam elements. For this purpose, the initial nodal forces associated with the lack-of-fit between the girders and cross-frames are calculated by taking the product of the cross-frame equivalent beam element stiffness matrices with the following equivalent beam element lack-of-fit displacements:

- For intermediate cross-frames that are normal to the girders, the differential total dead load camber (for TDLF) or the differential steel dead load camber (for SDLF) (see Figure 7.5).
- For cross-frames on skewed bearing lines, the cross-frame end rotations caused by the girder total dead load camber rotations (for TDLF) or the steel dead load camber rotations (for SDLF) (see Figures 7.6 and 7.7).
- For skewed intermediate cross-frames, a combination of the above two effects.

It should be noted that the twisting of the cross-frames has a negligible effect on initial lack-of-fit forces; therefore, the twisting of the cross-frames can be neglected when calculating the initial lack-of-fit forces.

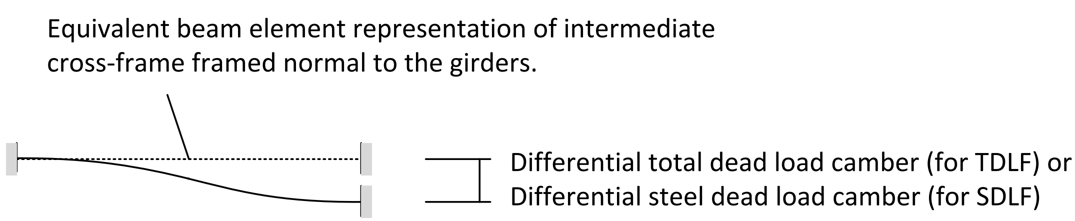

Figure 7.5. Imposed differential vertical camber to calculate initial lack-of-fit forces in the plane of an intermediate cross-frame framed normal to the girders.

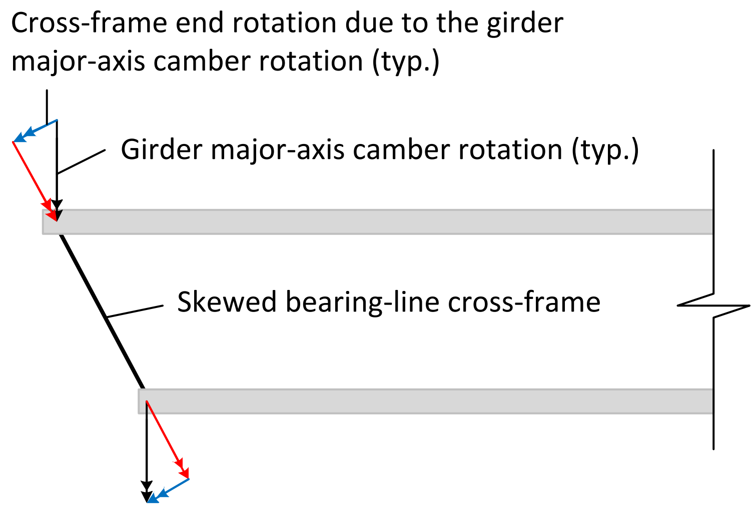

Figure 7.6. Illustration of the cross-frame initial lack-of-fit bending rotations caused by the girder camber rotations for a skewed bearing-line cross-frame.

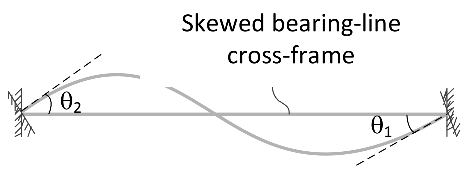

Figure 7.7. View of imposed initial lack-of-fit rotations on bearing-line cross-frame, used to calculate the initial lack-of-fit forces in the plane of a bearing-line cross-frame.

7.3 Impact of Locked-in Forces

Although AASHTO Article C6.7.2 (2010) states that engineers may need to consider the potential for any problematic locked-in stresses for horizontally curved I-girder bridges, engineers practically never include the inherent lack of fit in their structural analysis in current practice. However, the locked-in forces can significantly influence the girder layovers, the cross-frame forces, and the girder major-axis bending and/or flange lateral bending stresses in certain cases. It is important to understand when these forces due to lack-of-fit can be neglected and when they need to be considered in design, and how they can be calculated when they need to be accounted for.

7.3.1 Girder Layovers

As noted previously, bridge I-girders in curved and/or skewed bridges generally can be plumb only in one load condition. The cross-frames are relatively stiff within their planes compared to the torsional stiffness of the I-girders. Therefore, a common assumption is that the girders can be twisted and forced to fit the cross-frames under any lack-of-fit. However, twisting of the girders can be difficult in cases where the twist is coupled significantly with major-axis bending rotations and vertical deflections. This is often the case for curved girders for example. The ultimate goal with any DLF (Dead Load Fit, i.e., TDLF or SDLF) detailing is to obtain plumb webs at the targeted load level by using the rigidity of the cross-frames to impose girder torsional rotations opposite to the dead load torsional rotations. Within the span, the direction of the torsional rotations is mainly driven by the differential vertical camber (assuming that the cross-frames are normal to the girders). At the bearing lines, it is driven mainly by the rotational compatibility with the bearing line cross-frames and the direction of the girder end rotations due to the camber. The differential vertical camber between the girders and the rotational compatibility at the bearing lines associated with the girder camber rotations are the primary sources of the lack-of-fit for SDLF and TDLF detailing.

Figures 7.8 and 7.9 show a representative set of total dead load girder camber profiles and the corresponding differential camber between the girders for a straight I-girder bridge with parallel skew and curved I-girder bridge with radial supports respectively. In these figures, the sign of the differential camber is positive when the girder with the larger number has the larger camber. For instance, the differential camber between girders G2 and G1 at the bottom left corner of the bridge in Figure 7.8(b) is +3.4, meaning that the camber is 3.4 inches higher in girder G2 at the first intermediate cross-frame from the bearing line. Conversely, the differential camber between girders G8 and G9 at the upper right corner of the bridge is -3.4 inches, indicating that the camber in G8 is 3.4 inches higher than in G9 at the first intermediate cross-frame. The differential camber between the girders can be either positive or negative depending on the difference between the girder camber profiles at the cross-frame locations, as illustrated in Figure 7.10.

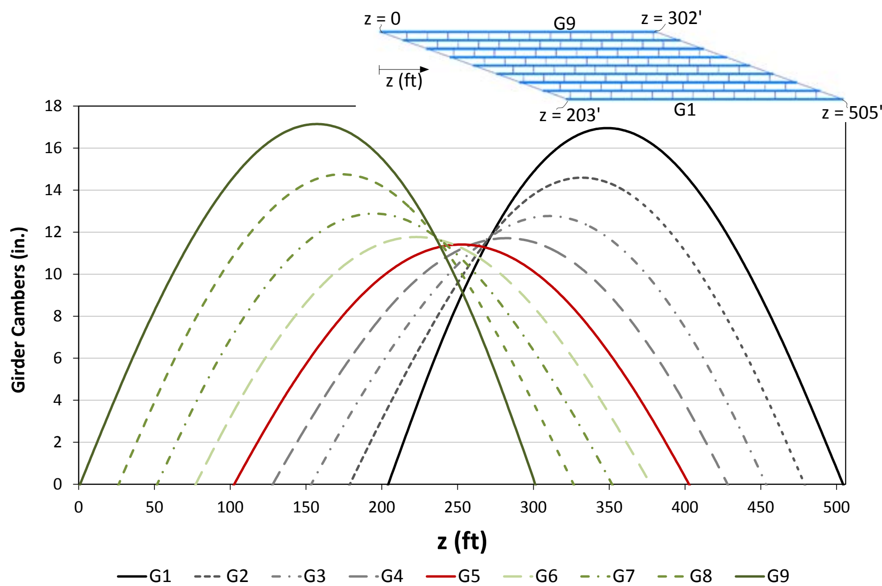

(a) Girder cambers under total dead load

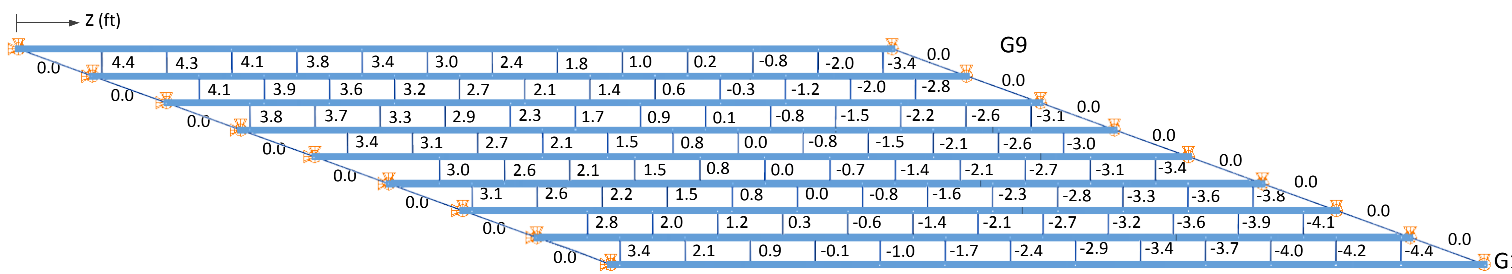

(b) Differential camber between the girders

Figure 7.8. NISSS54, Girder cambers and the differential camber between the girders obtained from FEA vertical deflections.

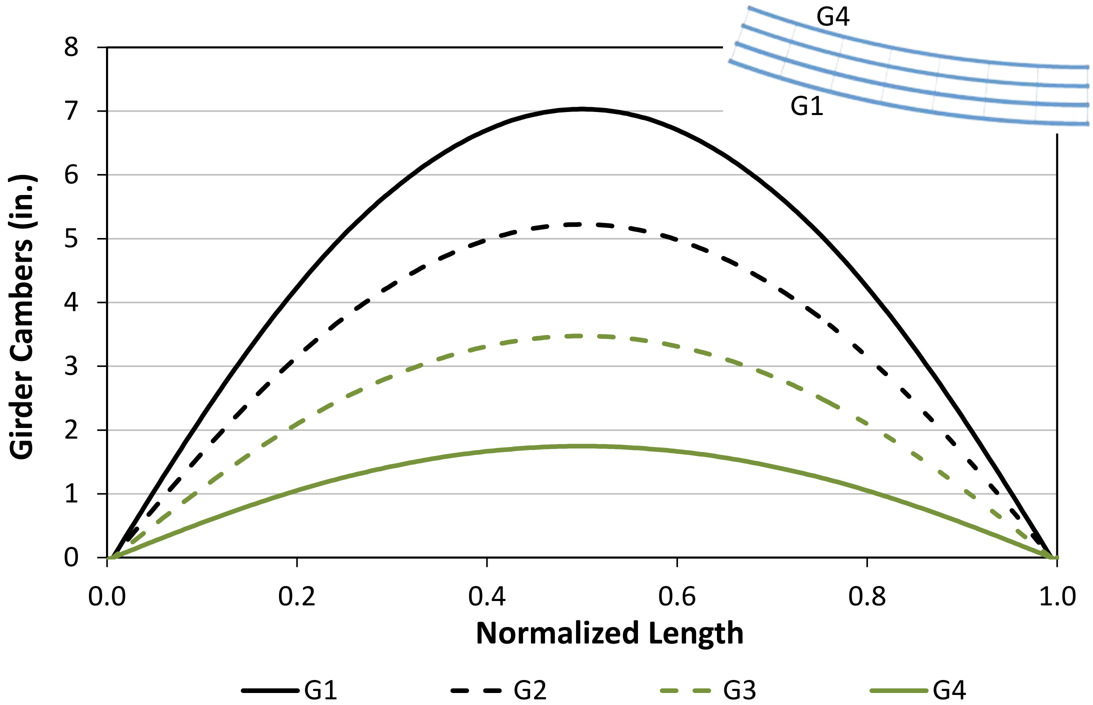

(a) Girder cambers under total dead load

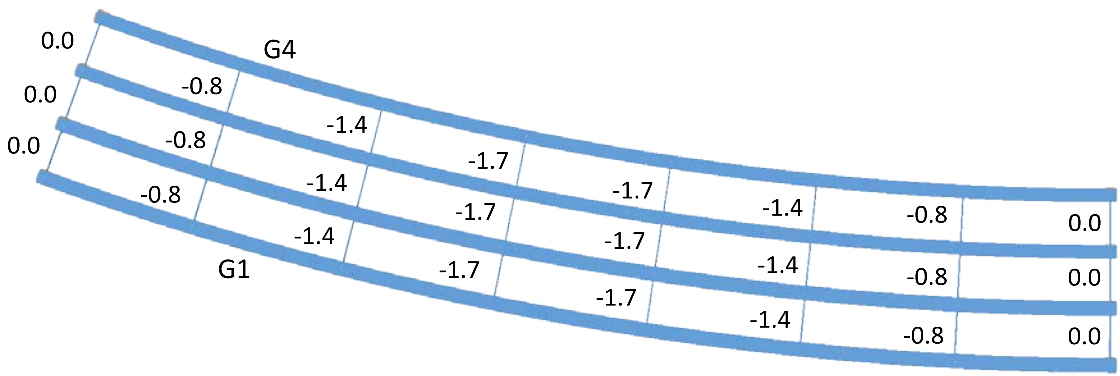

(b) Differential camber between the girders

Figure 7.9. NISCR2, Girder cambers and the differential camber between the girders obtained from FEA vertical deflections.

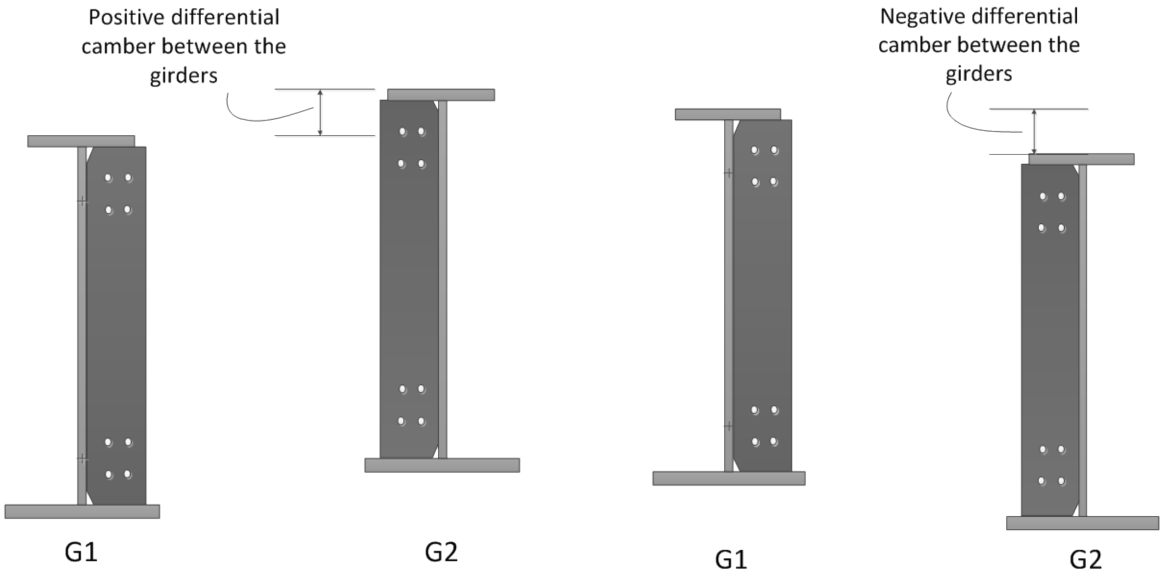

(a) Positive differential camber between the girders

(b) Negative differential camber between the girders

Figure 7.10. Representative sketch of positive and negative differential camber between the girders (geometric factors such as cross-slope, super-elevation and profile grade line are not shown for clarity).

For DLF (Dead Load Fit, i.e., TDLF or SDLF) detailing of the intermediate cross-frames, the girders need to be twisted to connect the cross-frames between them. The movements at the intermediate cross-frames are illustrated in Figure 7.11 for locations with positive and negative differential camber between the girders in the no-load geometry. In the case of straight bridges with parallel skew orientations, both positive and negative differential camber are obtained between the girders since the parallel skew orientation of the bearing lines offsets the camber profiles of the girders as shown in Figure 7.8(a). For instance, the camber profiles for the fascia girders G1 and G9 are the same; however, the left-hand bearing location for G1 is located at a z coordinate of 203 ft., i.e., G1 starts at 203 ft. into the span of G9. The opposite sign of the differential cambers at each end of the bridge results in a twisting of the girders, due to the lack of fit of the cross-frames, that is in opposite directions at the two ends. These lack-of-fit twist rotations are in turn opposite in sign relative to the twist rotations of the girders under dead load.

For curved-radially supported bridges, the differential camber between the girders is always negative, moving from the girders that are farther from the center of curvature toward the center of curvature, due to larger deflection of the “outside” girders compared to the “inside” girders. This enforces a twist opposite to the layovers caused by the dead loads

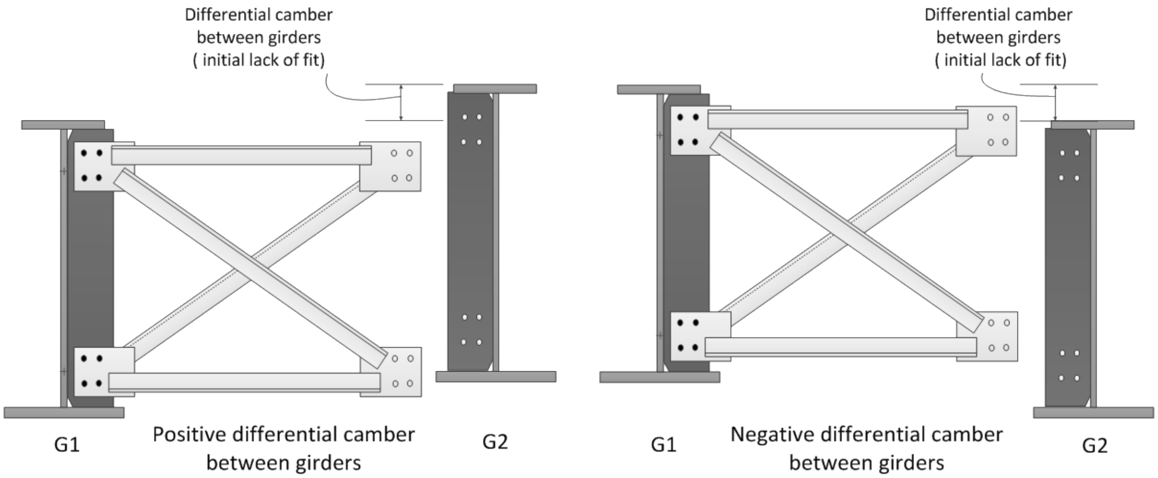

(a) Initially plumb no-load geometry of girders

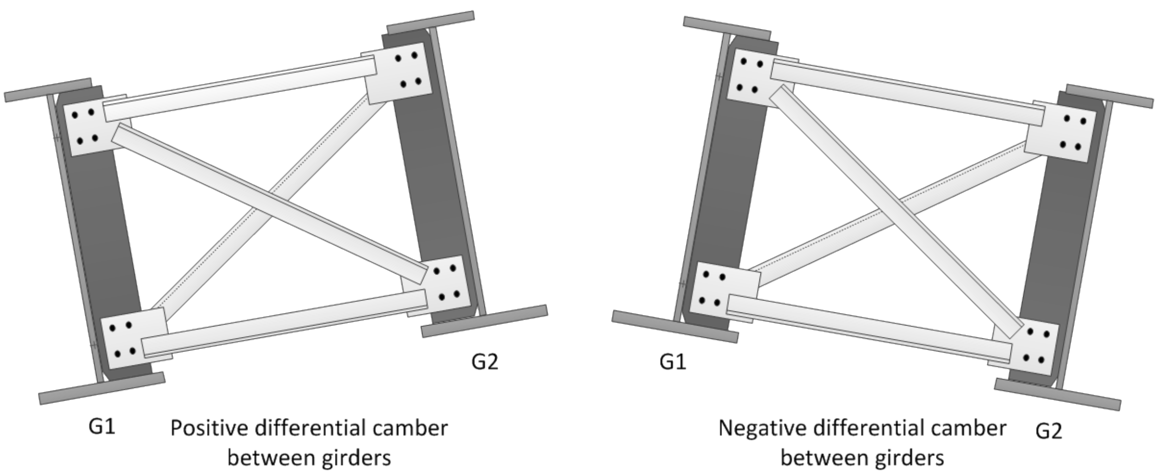

(b) Cross-frames connected in ideal initial no-load geometry

Figure 7.11. Induced girder twist at intermediate cross-frame locations for positive and negative differential camber between girders in ideal no-load geometry (geometric factors such as cross-slope, super-elevation and profile grade line are not shown for clarity).

The compensating girder layovers generated by DLF detailing are never exactly equal and opposite to the dead load layovers. (The term “DLF detailing” is used here and in the following discussions to indicated either SDLF or TDLF detailing.) This is mainly because:

- The stress state due to the torsional effects of the dead load cannot possibly be matched exactly by the cross-frame forces induced by the DLF detailing. The difference between the girder stress state induced by the locked-in forces and the girder stress state associated with the dead load torsion causes additional deformations within the structure.
- The girder camber profiles may have been obtained from an analysis that does not fully capture the true interactions between the girders associated with the three-dimensional response of the bridge. Furthermore, the SDLF and TDLF detailing practice of working just with the differential vertical cambers generally neglects other torsional interactions between the girders and the rest of the structure that occur via the cross-frames.

As a result, slight deviations from the plumb configuration are observed generally at the targeted load conditions. However, (Ozgur, 2011) shows that the layover of the girders at the targeted load conditions tends to be less than a tolerance of ± D /96, where D is the web depth, regardless of the bridge type and geometry.

Figures 7.12 and 7.13 illustrate the deflected shape of the representative straight-skewed bridge from Figure 7.8 (NISSS54) under the steel and total dead loads respectively. Each of these figures shows the magnified deflections associated with each of the three main types of cross-frame detailing. Similarly, Figures 7.14 and 7.15 illustrate the magnitudes of the girder layovers of this straight-skewed bridge under the steel and total dead load respectively for each of the types of cross-frame detailing. The girder layovers are plotted along the length of bridge starting from the left acute corner. The NISSS54 bridge has a large skew index (I_S = 0.68), indicating that the influence of skew is large on the response of the structure and on the accuracy of the simplified methods of analysis. The torsional rotations at the bearings due to the total dead load are more than 0.04 radians in this structure.

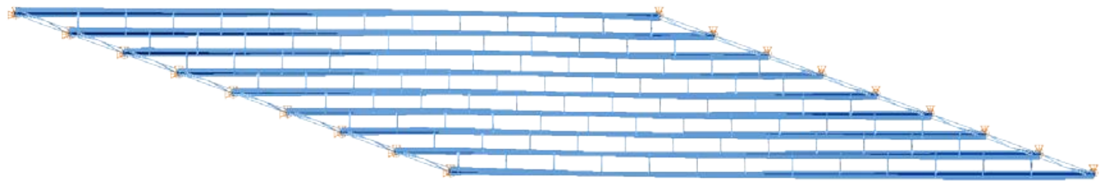

(a) NLF

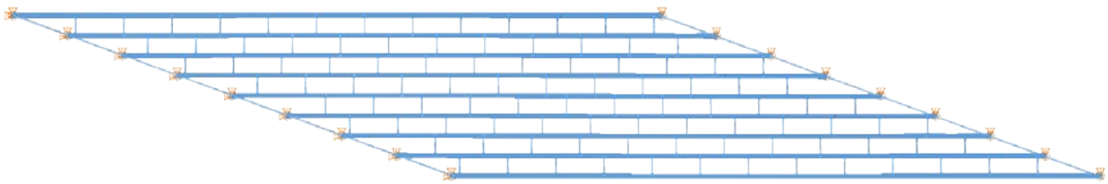

(b) SDLF

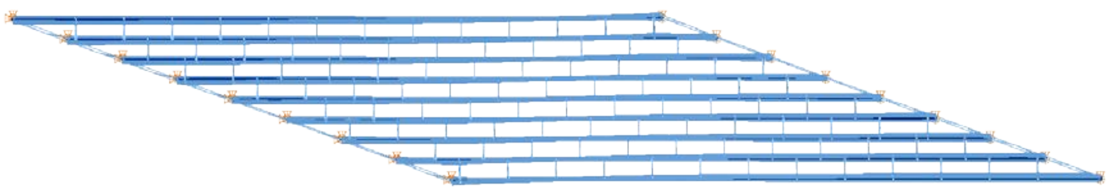

(c) TDLF

Figure 7.12. NISSS54, Deflected shape under steel dead load for different types of detailing methods (magnified by 10x).

Approximately plumb girders are obtained under the steel dead load if the bridge is constructed with SDLF detailing as shown in Figures 7.12(b) and 7.14(b). For TDLF detailing, the cross-frames are detailed such that they approximately compensate for the total dead load deflections. Therefore, layovers in the opposite direction from those due to the total dead load are obtained under the *steel dead load* when TDLF detailing is used, as shown in Figures 7.12(c) and 7.14(c). However, approximately plumb girders are obtained for the bridge where the cross-frames are detailed for TDLF, once the total dead load is placed on the bridge, as illustrated in Figures 7.13(c) and 7.15(c).

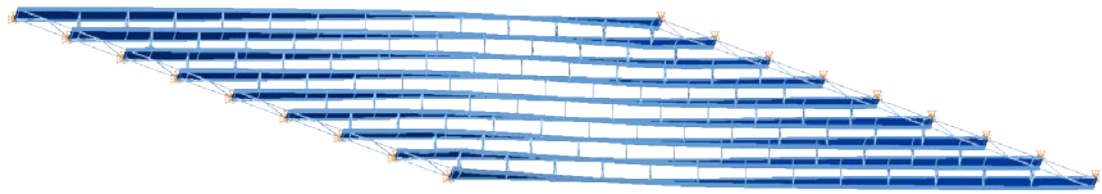

(a) NLF

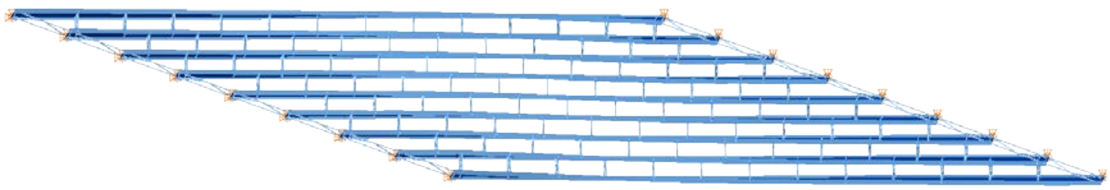

(b) SDLF

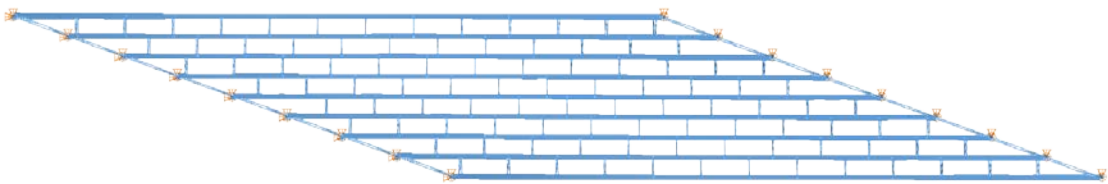

(c) TDLF

Figure 7.13. NISSS54, Deflected shape under total dead load for different types of detailing methods (magnified by 10x).

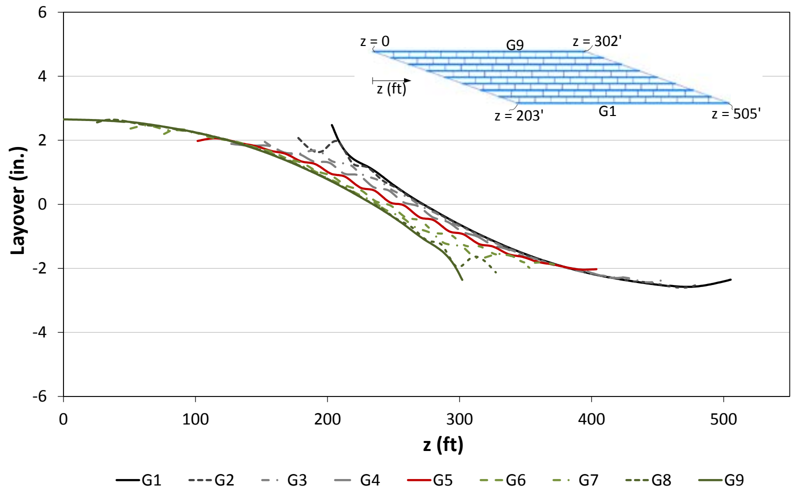

(a) NLF

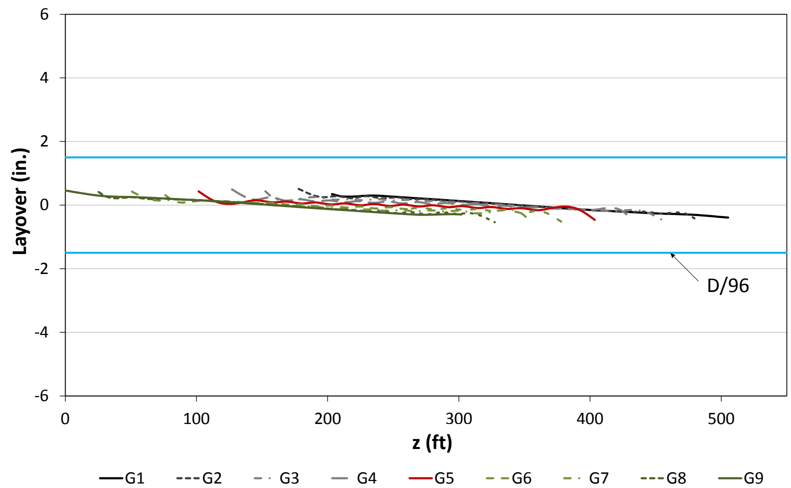

(b) SDLF

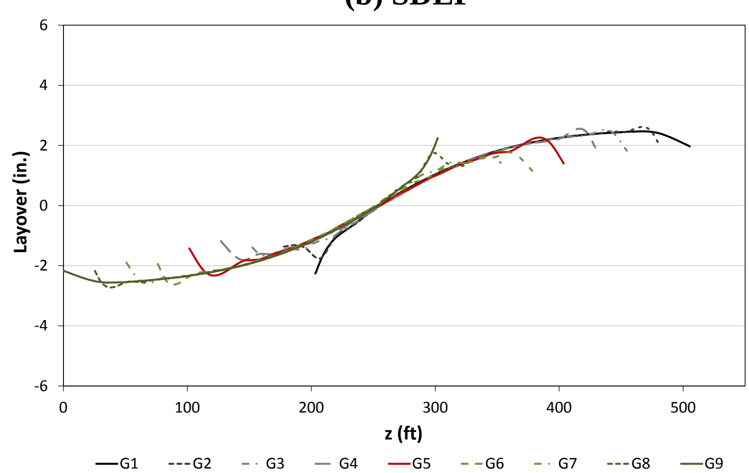

(c) TDLF

Figure 7.14. NISSS54, steel dead load girder layovers associated with different types of detailing methods.

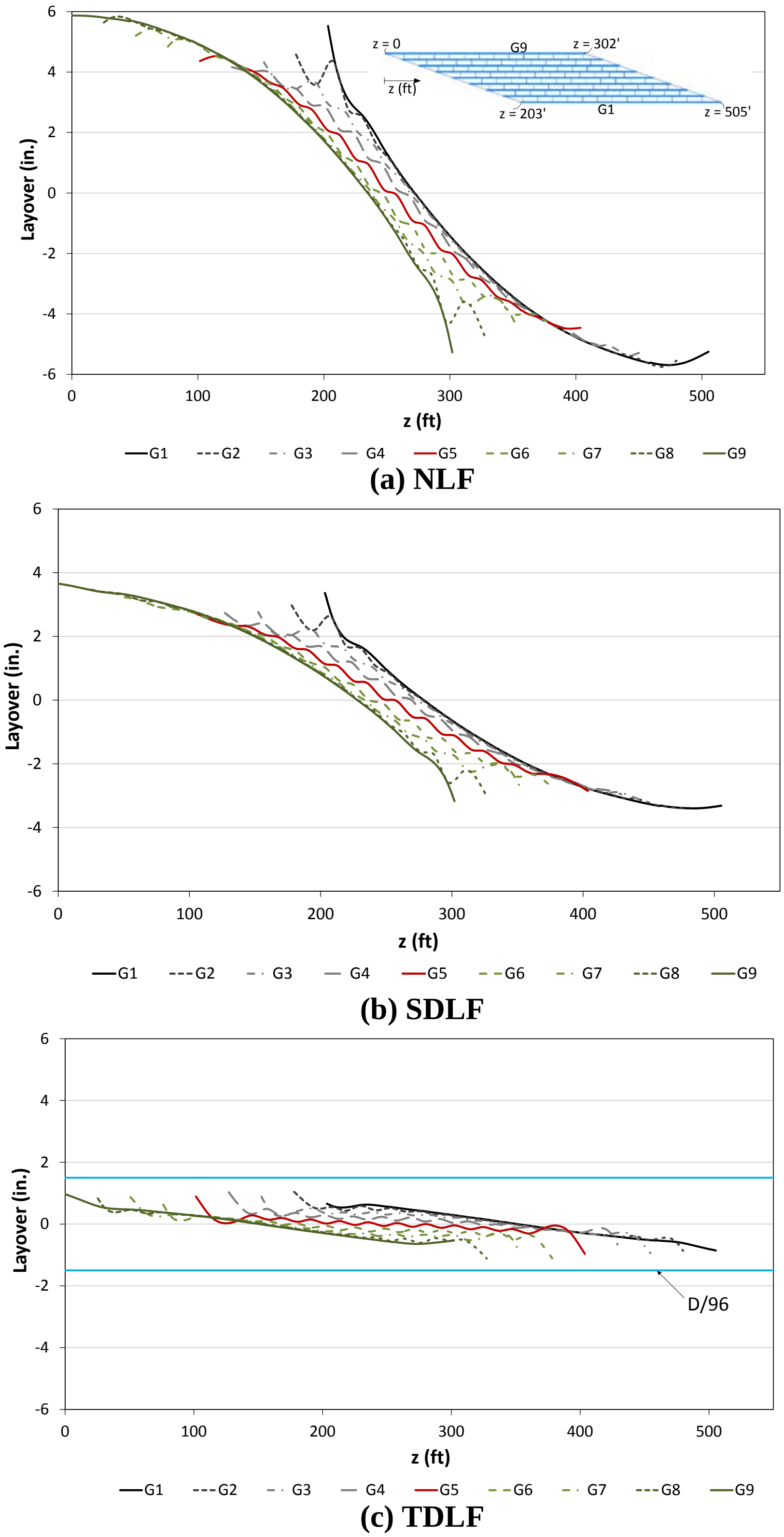

Figure 7.15. NISSS54, total dead load girder layovers associated with different types of detailing methods.

7.3.2 Cross-Frame Forces

<u>Straight-Skewed I-girder Bridges</u>

In straight-parallel skewed bridges constructed with NLF detailing, relatively large forces tend to be developed in the cross-frames along the shorter (and stiffer) diagonal direction between the corners of the structure. Figure 7.16 illustrates this transverse load path in the NISSS54 bridge by indicating the magnitude of the largest component force in each of the intermediate cross-frames, normalized by the largest cross-frame component force. The cross-frames with ratios larger than 0.5, located between the obtuse corners of the bridge, are highlighted by a different shade.

For straight bridges constructed with TDLF detailing, the locked-in cross-frame forces are approximately equal and opposite to the total dead load forces in the regions having the largest transverse stiffness, i.e., in the highlighted region of Figure 7.16. However, the locked-in forces in the cross-frames tend to be substantially different than the dead load forces outside of this region.

Large locked-in forces can be developed outside the stiff transverse load paths depending on the relative lateral stiffness of the adjacent girders and the differential camber. These "problem" cross-frame locations are typically at intermediate cross-frames that are at framed too close to the skewed bearing lines.

It should be emphasized that the dead load cross-frame forces from a NLF analysis are not the opposite of the locked-in forces from a lack-of-fit analysis or vice-versa. These two sets of forces can be close to being equal and opposite in the regions of the bridge having the largest transverse stiffness (highlighted in Figure 7.16), but in other regions, they can be substantially different. This is because stresses and deformations induced by DLF detailing are not exactly the same as the stresses and deformations induced by the dead loads.

In the bridge shown in Figure 7.16, the cross-frames in the vicinity of the short direction between the obtuse corners of the plan tend to have their total dead load forces mostly relieved by the effects of the TDLF detailing, while the cross-frames in the vicinity of the acute corners tend to have their total dead load forces increased relative to the NLF case. Figures 7.17 and 7.18 show the distribution of the largest total dead load cross-frame component axial forces in each of the cross-frames throughout the NISSS54 bridge associated with NLF and TDLF detailing cases respectively. The most highly loaded cross-frame members are highlighted in the darker color, while the more lightly loaded cross-frame members are shaded light grey. One can observe that the cross-frame forces along the stiff diagonal direction are significantly reduced by the TDLF detailing, but they are not zero. In addition, the forces in several of the cross-frame diagonals near the acute corners are significantly increased.

In straight-skewed bridges constructed with TDLF detailing, cross-frames located along the stiff transverse load paths may see their largest forces during the steel erection since the locked-in cross-frame forces are not yet relieved by the dead load forces from the deck weight. Conversely, straight bridges constructed with SDLF detailing tend to see the lowest cross-frame forces under the steel dead load.

Curved-Radially Supported I-girder Bridges

The behavior of curved bridges with respect to cross-frame detailing is significantly different than straight bridges. In curved-radially supported bridges, locked-in cross-frame forces due to SDLF or TDLF detailing tend to add with the dead load forces in the cross-frame members, although it should be noted that SDLF detailing generally results in smaller locked-in forces compared to TDLF detailing. Figures 7.19 and 7.20 illustrate the maximum amplitude of the total dead load component axial forces in each of the cross-frames for the curved-radially supported bridge considered in Section 7.3.1 (NISCR2). Figure 7.19 shows the results for NLF detailing, whereas Figure 7.20 shows the results for TDLF detailing. The maximum locked-in cross-frame forces occur in the cross-frames close to the mid-span. This is because the lack-of-fit between the girders and cross-frames is largest at these locations.

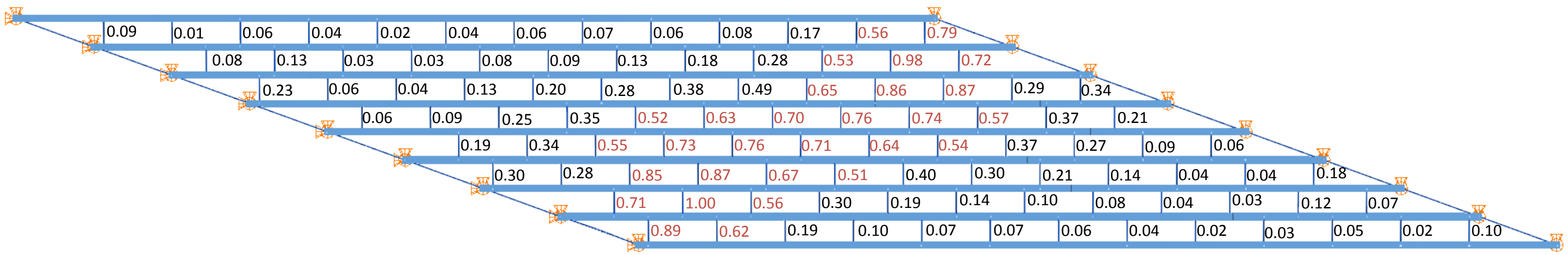

Figure 7.16. NISSS54, Normalized maximum amplitude of the component axial forces in each of the cross-frames under total dead load (NLF detailing).

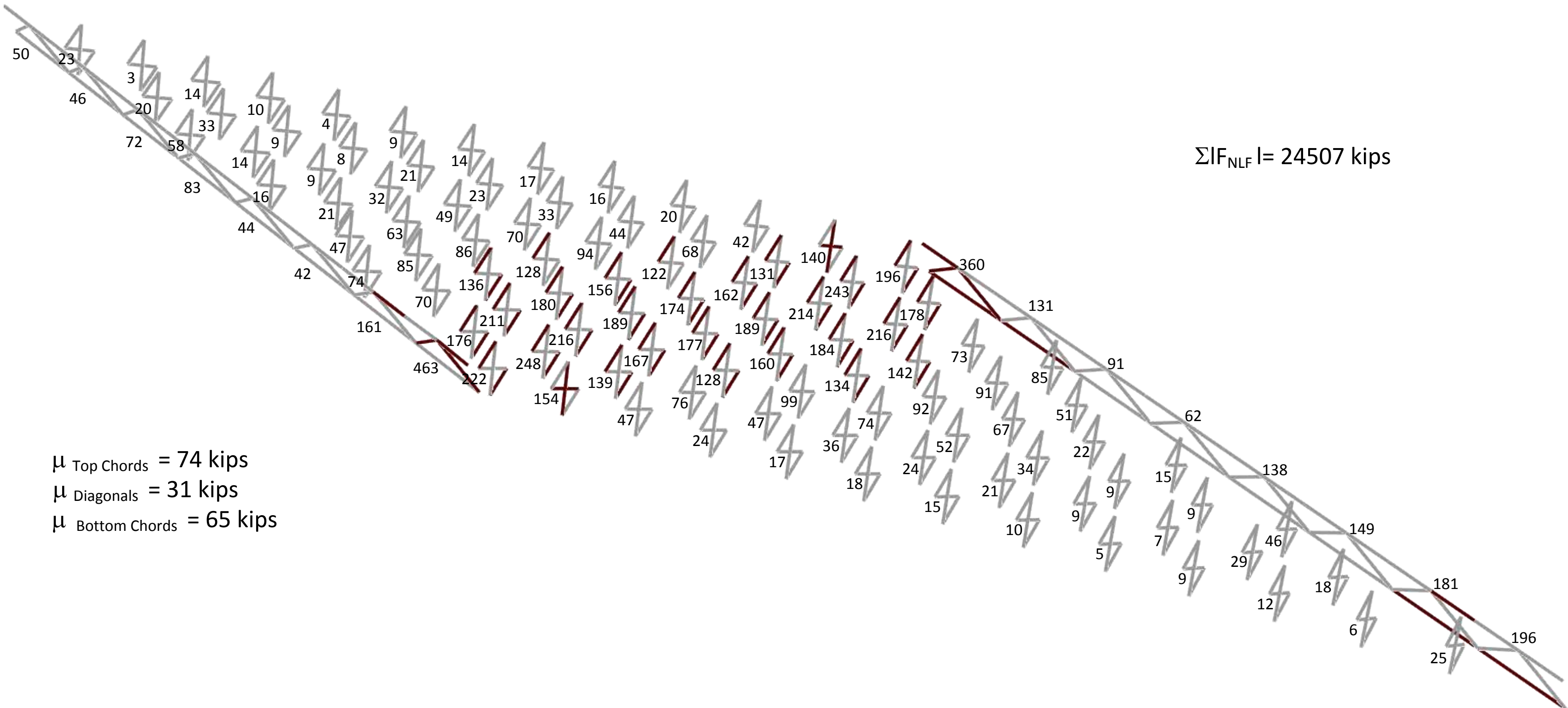

Figure 7.17. NISSS54, maximum amplitude of the component axial forces in each of the cross-frames under total dead load (NLF detailing).

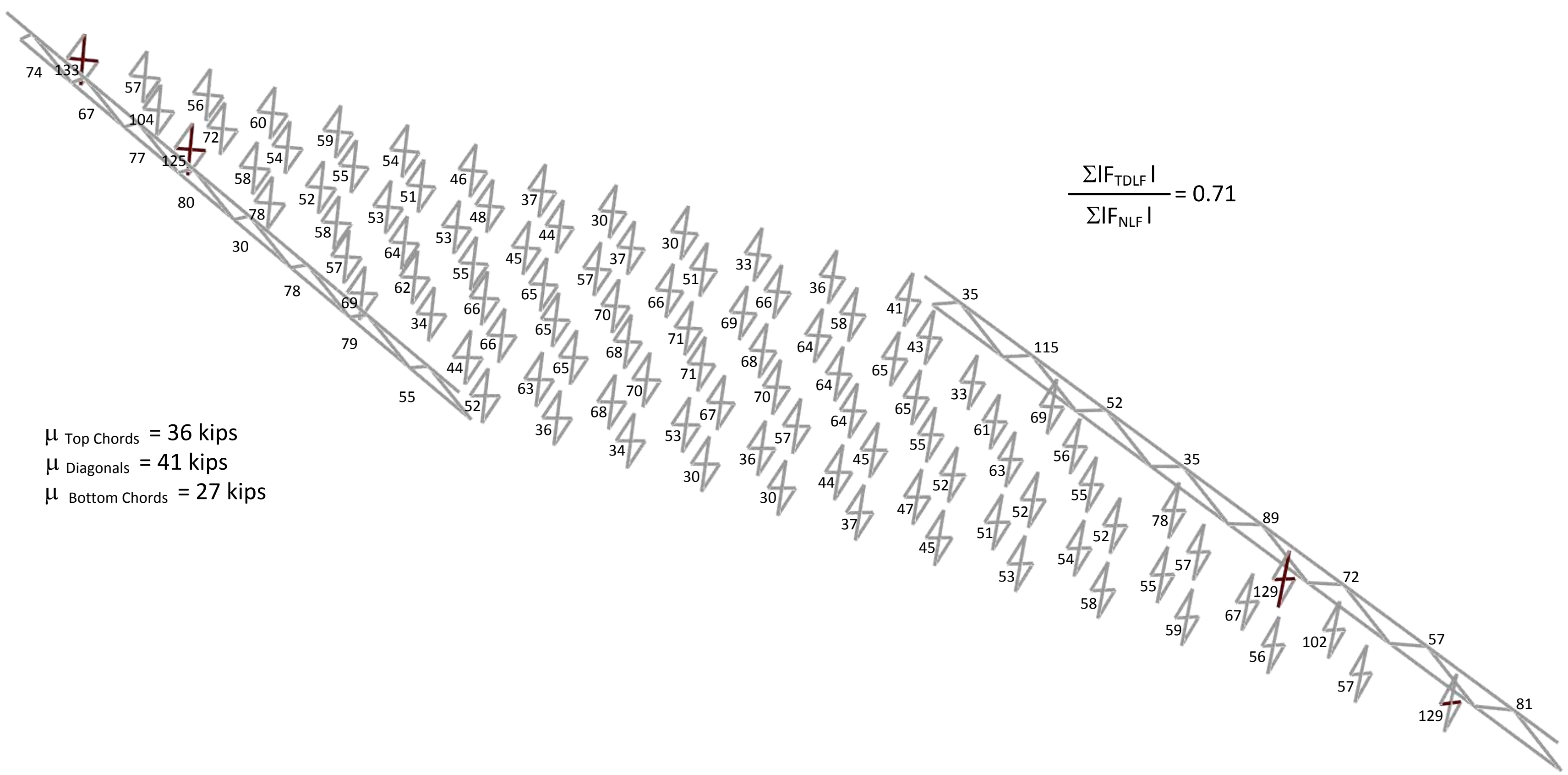

Figure 7.18. NISSS54, maximum amplitude of the component axial forces in each of the cross-frames under total dead load plus the TDLF detailing effects.

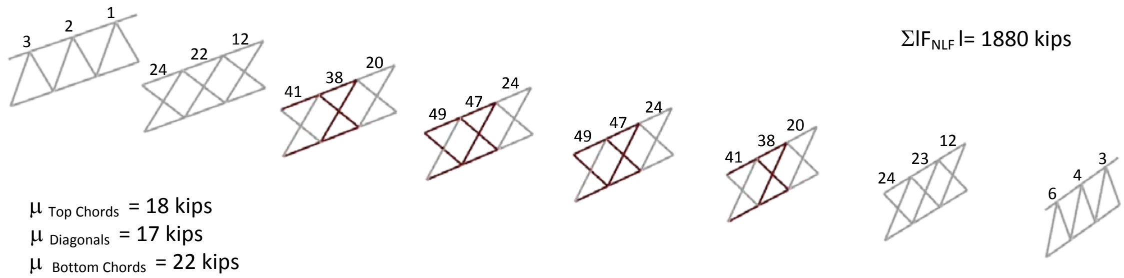

Figure 7.19. NISCR2, maximum amplitude of the component axial forces in each of the cross-frames under total dead load (NLF detailing).

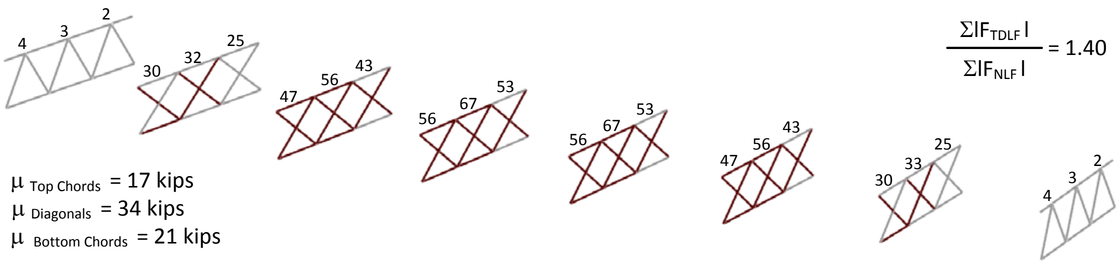

Figure 7.20. NISCR2, maximum amplitude of the component axial forces in each of the cross-frames under total dead load plus the TDLF detailing effects.

7.3.3 Vertical Displacements

In current practice, the girder camber diagrams are practically always determined without considering locked-in force effects. However, locked-in forces due to SDLF or TDLF detailing potentially can have a significant influence on the vertical deflections. Hence, the physical bridge may exhibit different vertical deflections than assumed in setting the cambers. This can lead to deviations from the predicted final deck profile and final girder elevations.

Straight-Skewed I-girder Bridges

For straight and skewed bridges, the locked-in forces from SDLF or TLDF detailing tend to have a small effect on the vertical displacements. This is because there is little to no coupling between the individual girder vertical displacements and the individual girder twisting for straight I-girders. Figure 7.21 shows total dead load vertical deflections for the straight-skewed NISSS54 bridge considering each of the types of cross-frame detailing. It can be observed that there is essentially no difference in the vertical deflections of the two fascia girders due to the type of cross-frame detailing in this bridge. Both of these girders exhibit approximately 17 inches of vertical deflection at their mid-span under the total dead load regardless of the method of cross-frame detailing. The middle girder (Girder 5) has slightly more than 12 inches of vertical deflection under the total dead load if TDLF detailing is used, whereas it has slightly more than 11 inches of vertical deflection if NLF detailing is used. These small differences in the vertical deflections are due to the restraint from the stiff transverse load path discussed in Section 7.3.2. That is, part of the total dead load tributary to girder G5 is distributed transversely to the bearing lines by the staggered cross-frames framing between the obtuse corners of the bridge. The development of the forces along this path causes significant flange lateral bending in girder G5.

The total dead load vertical deflections generally are compensated for by the total vertical camber in the girders. In current practice, the above differences in the NLF and TDLF vertical deflections due to the initial lack-of-fit between the girders and cross-frames are practically never accounted for. One can conclude that the 1 inch difference in the vertical deflection of Girder 5 is relatively minor. It can be accommodated in the girder haunch depths when setting the forms for the concrete deck (if the contractor anticipates the above behavior).

Curved-Radially Supported I-girder Bridges

Conversely, for curved-radially supported bridges, the locked-in forces due to SDLF or TDLF detailing generally have a significant effect on the vertical displacements of the girders. This is due to the significant coupling between the major-axis bending and torsion in curved I-girders. Figure 7.22 shows a representative example from the bridge NISCR5. The outside girder displacement is reduced by approximately 6 inches due to the TDLF detailing effects, while the inside girder vertical deflection is reduced by approximately 4 inches. It should be noted that this bridge is a relatively extreme case also involving significant global second-order amplification due to the long span and narrow width of the structure.

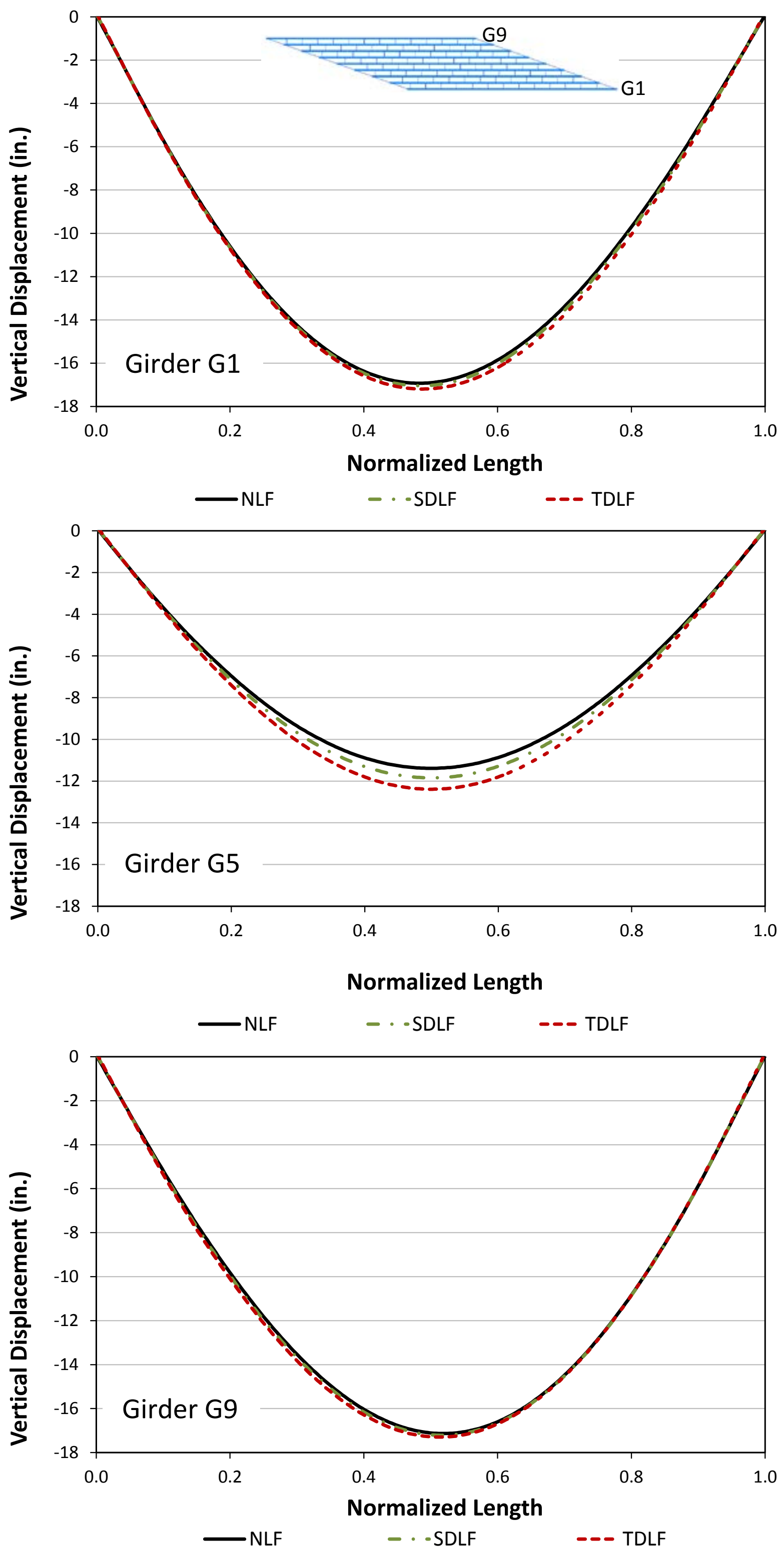

Figure 7.21. NISSS54, Vertical deflections under total dead load associated with different detailing methods.

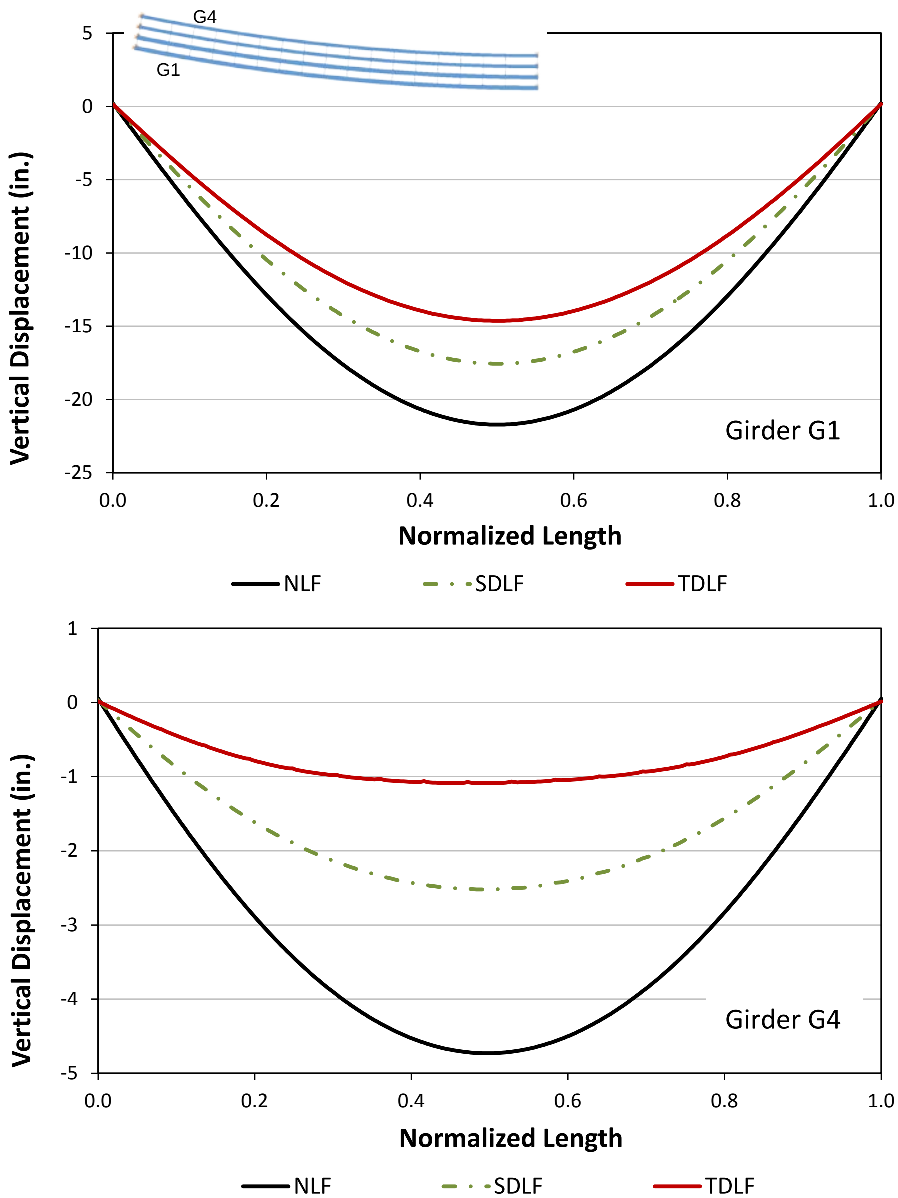

Figure 7.22. NISCR5, Vertical deflections under total dead load associated with different detailing methods.

7.3.4 Major-Axis Bending Stresses, f_b

The NCHRP 12-79 research studies show that the changes in the girder major-axis bending stress predictions are minor due to either SDLF or TDLF detailing for both straight-skewed and curved-radially supported bridges. For straight I-girder bridges, this can be understood by observing the general lack of coupling between torsion and major-axis bending in straight I-girders. For curved I-girder bridges, this can be understood by considering a basic simply-supported curved I-girder with torsionally simply-supported end conditions subjected to transverse loads as shown in Figure 7.23. The girder torsional deformations near the end supports have a substantial impact on the mid-span vertical displacements. However, the girder internal major-axis bending moments and the corresponding major-axis bending stresses at the mid-span are not affected significantly by the horizontal curvature.

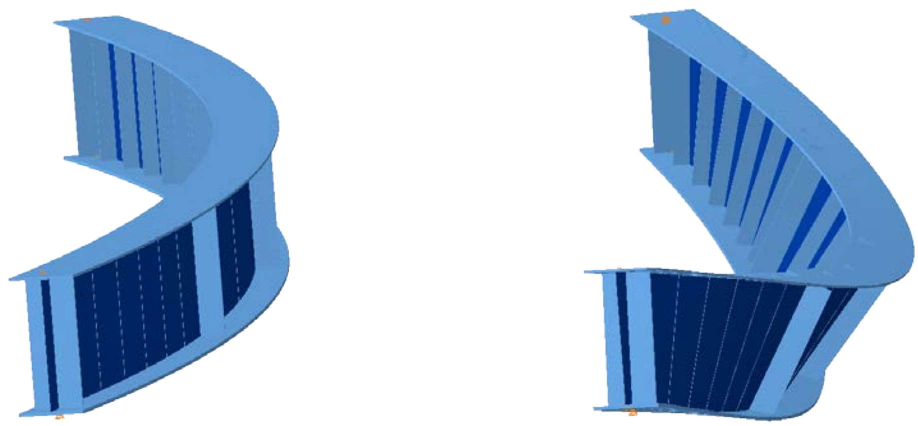

(a) Undeformed shape **(b) Magnified Deflected shape**

Figure 7.23. Illustrative curved girder deformations under dead loads.

7.3.5 Girder Flange Lateral Bending Stresses, f_ℓ

<u>*Straight-Skewed I-girder Bridges*</u>

The girder flange lateral bending stresses under the total dead load are reduced significantly in straight-skewed bridges due to DLF detailing. If SDLF detailing is used, the smallest flange lateral bending stresses tend to occur under the steel dead load. Conversely, if TDLF detailing is used, the smallest flange lateral bending stresses tend to occur under the total dead load. In these cases the girders largely unwind into their approximately plumb positions under the corresponding dead load effects.

Engineers sometimes conclude that since the girders were plumb in their no-load condition, and since they are also plumb in the targeted dead load condition, the girder flange lateral bending stresses are zero, the cross-frame forces are zero, and the girders respond essentially in the manner assumed in a line girder analysis when the bridge is in the targeted dead load condition. However, it is important to note that the girder flange lateral bending stresses generally do not completely vanish due to the differences between the locked-in stresses from the DLF detailing and the stresses related to the torsion of the girders under the targeted dead load. There are several reasons for this behavior:

- In particular, local peaks in girder flange lateral bending stresses, as well as cross-frame forces, can be observed due to "nuisance stiffness effects" at locations such as intermediate cross-frames that are located too close to skewed bearing lines. The stresses in the girders due to locked-in force effects do not tend to match the torsional stresses due to the three-dimensional loading effects in these regions.
- Furthermore, when staggered cross-frames are utilized such as in the NISSS54 bridge, there is substantial flange lateral bending in the interior girders due to the transverse load transfer effects. The interior girder flanges are loaded "back-and-forth" in opposing directions by the cross-frames. The corresponding flange lateral bending in these girders is generally reduced, but it is not completely nullified by the locked-in force effects.
- Lastly, in the fascia girders, significant flange lateral bending can occur in some cases due to eccentric overhang bracket loads. These bending effects are of course not nullified by the locked-in forces from DLF detailing. The NCHRP 12-79 research shows that flange lateral bending stresses in the fascia girders often are predominantly due to eccentric overhang bracket loads and are not significantly affected by any of the detailing methods.

In cases with contiguous intermediate cross-frame lines, the total flange lateral bending stresses associated with DLF detailing are found to be close to zero except in the fascia girders and at cross-frame locations with nuisance stiffness effects (Ozgur, 2011).

Figure 7.24 shows selected girder major- and minor-axis flange bending stresses under total dead load for the different types of detailing methods in the NISSS54 bridge. In this structure, the major-axis bending stresses in the fascia girders are essentially unaffected by the type of cross-frame detailing. The maximum total dead load flexural stress in the top flange of these girders is 30 ksi. The total dead load major-axis bending stresses in the middle girder (Girder 5) are slightly increased for the TDLF detailing case, consistent with the larger vertical displacements in Girder 5 for TDLF detailing. However, the differences in the stresses for the major-axis bending of Girder 5 are relatively minor. The maximum f_b in Girder 5 is approximately 20 ksi under the total dead load for the TDLF detailing case.

The flange lateral bending stresses are relatively small in the fascia girders for all the methods of detailing in the NISSS54 bridge, and are predominantly due to eccentric overhang bracket loads with the exception of the locations near the obtuse corners of the bridge. At the obtuse corners, relatively large lateral forces are introduced into the fascia girders from the chords of the first two intermediate cross-frames near the bearing lines. This causes a "spike" in the flange lateral bending stresses near the ends of the fascia girders. This spike in f_ℓ is largest for the NLF detailing case. It is reduced by the locked-in stresses introduced into the girders in the cases of SDLF and TDLF detailing.

The total dead load lateral bending stresses are significant in Girder 5 regardless of the method of cross-frame detailing. They are largest for the NLF detailing case, reaching peak values of nearly 22 ksi near the mid-span. These flange lateral bending stresses are reduced by the lack-of-fit effects introduced into the girders by SDLF or TDLF detailing. The resulting maximum total dead load f_ℓ values are approximately 15 ksi for SDLF detailing and 8 ksi for TDLF detailing. These significant flange lateral bending stresses in Girder 5 are due to the use of the staggered cross-frames in this bridge and the "back-and-forth" load transfer effects mentioned previously. Staggered cross-frames generally are expected to reduce the magnitude of the cross-frame forces that need to be resisted due to the skew effects, but they introduce "back-and-forth" lateral loads on the girder flanges in the middle regions of the bridge. These forces are highest near the mid-span of the middle girders because these locations are in the middle of the stiff transverse load path first discussed in Section 7.3.2.

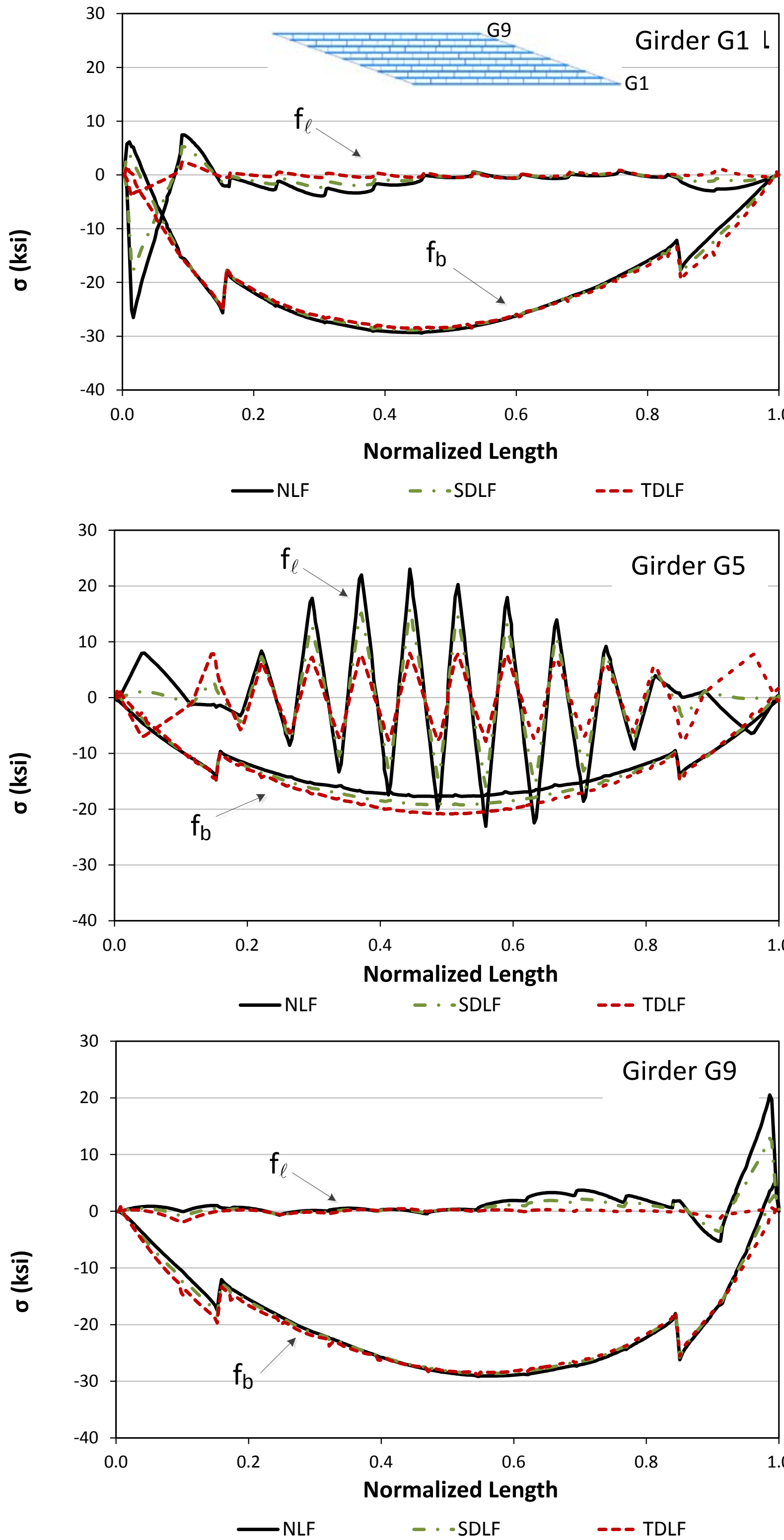

Figure 7.24. NISSS54, top flange stresses under total dead load for different detailing methods.

There is no “spike” in the flange lateral bending stresses in Girder 5 near its ends. This is because the forces coming into the girder from the intermediate cross-frames near the support are not as large in Girder 5 as in the exterior fascia girders. The predominant lateral bending action on Girder 5 is near the middle of the span. Unfortunately, this is also where the major-axis bending stresses are the highest.

Curved-Radially Supported I-Girder Bridges

For curved-radially supported bridges, the “local” flange lateral bending effects between the cross-frames due to the horizontal curvature, i.e., the effects associated with Eq. (2.16), are not influenced by the DLF detailing. However, DLF detailing of curved bridges induces an overall global lateral bending in the girder flanges in the direction:

- opposite to the overall lateral bending of the girders due to the torsional rotation of the bridge cross-section,
- opposite to the bending within the girder unbraced lengths between the cross-frames, and
- in the same direction as the “negative” flange lateral bending stresses due to the continuity of the curved flanges across the cross-frame locations.

That is, the locked-in forces due to DLF detailing tend to reduce the overall “global” girder flange lateral bending stresses in curved bridges. Figure 7.25 illustrates this effect in the NISCR2 bridge. In many curved bridge structures, this overall flange lateral bending effect is relatively minor. However, in some cases, such as narrow curved bridge units, this effect can be substantial. These effects are relatively minor in the NISCR2 bridge, although the percentage change in the flange lateral bending stresses on the inside girder is somewhat large.

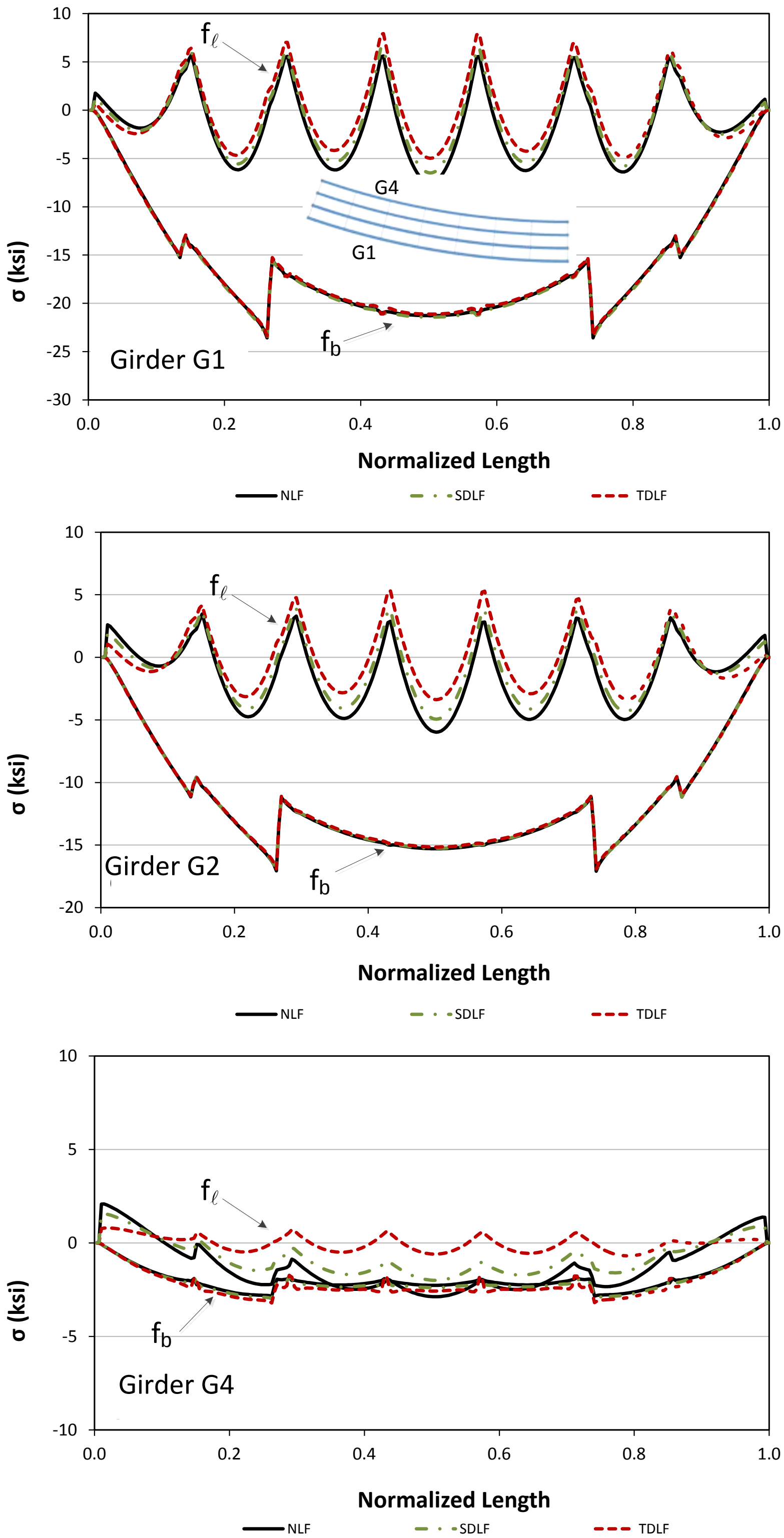

Figure 7.25. NISCR2, Top flange stresses under total dead load for different detailing methods.

7.4 Impact of Locked-in Force Effects on Strength

Locked-in force effects tend to be additive with the dead load responses for the cross-frame forces and the maximum (“negative”) girder flange lateral bending stresses in curved and radially-supported bridges. The AASHTO LRFD Specifications provide explicit provisions for checking of strength during construction. Ozgur (2011) observes that additional locked-in force effects due to DLF detailing do not affect the bridge system strength significantly assuming that the cross-frames are sized adequately and that the critical components are the girders. In fact, Ozgur (2011) demonstrates that locked-in force effects can increase the strength of the curved bridges that are susceptible to overall second-order effects or significant overall (global) flange lateral bending. One example of this bridge type is provided in Section 2.9. Unfortunately, DLF detailing of horizontally curved bridges tends to increase the cross-frame member forces.

Example load-deflection curves from two bridges studied by the NCHRP 12-79 project, NISCR2 and NISCR5, are shown in Figures 7.26 and 7.27 respectively. The applied load fraction (ALF) is the multiple of the nominal total dead load applied to the bridge.

NISCR2 is a shorter bridge (150 ft.span) with a 30 ft.deck width that shows relatively little influence of the type of detailing on the overall bridge capacity. However, NISCR5 is a more extreme 300 ft.simple-span bridge with a 30 ft.deck width and no flange-level lateral bracing system. This bridge experiences significant second-order effects under the total dead load. It is only able to develop 1.34 times the total dead load before reaching its capacity for the case with NLF detailing. However, with TDLF detailing, the overall torsional rotations are reduced, thus reducing the second-order amplification and resulting in a load capacity of 1.54 times the nominal total dead load.

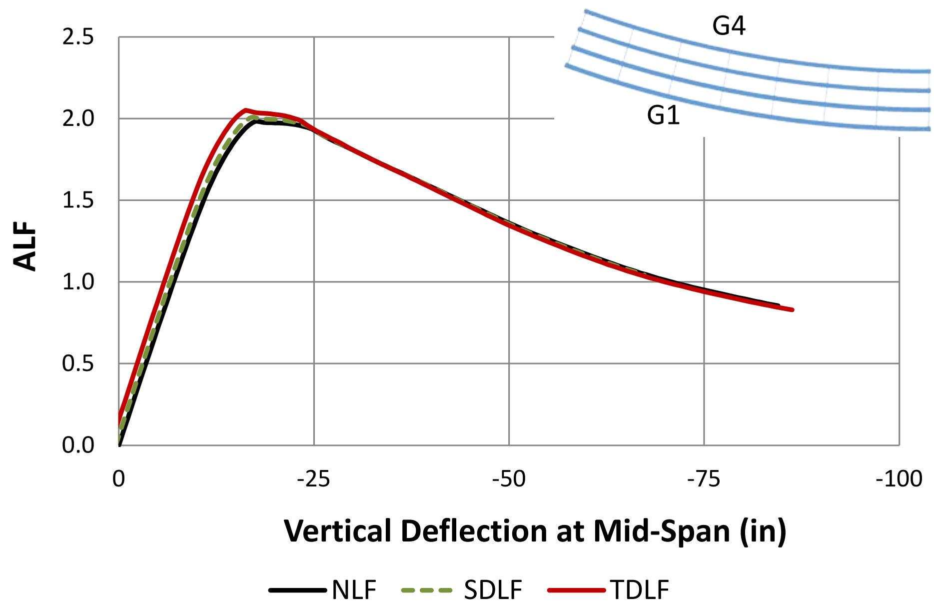

Figure 7.26. NISCR2, vertical displacements at the mid-span of Girder G1 versus the fraction of the total dead load for different detailing methods.

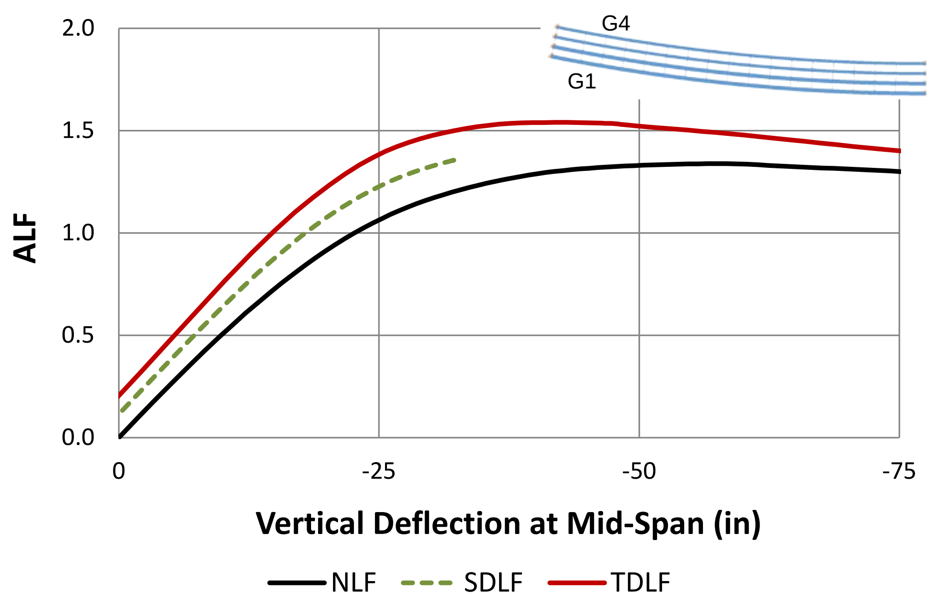

Figure 7.27. NISCR5, vertical displacements at the mid-span of Girder G1 versus the fraction of the total dead load for different detailing methods.

7.5 Special Cases

7.5.1 Special Cases where a Line Girder Analysis Predicts Accurate Results for Straight-Skewed Bridges

Engineers widely use line-girder analysis solutions to design straight skewed I-girder bridges. The corresponding analysis predictions impact the responses associated with the detailing of the cross-frames since the camber profiles are set based on these predictions. Figure 7.28 shows two sets of total dead load girder camber profiles for the bridge NISSS54, one based on line-girder analysis and one based on 3D-FEA. The 3D-FEA solution is conducted assuming NLF detailing, which neglects the small influence of the SDLF or TDLF cross-frame detailing on the corresponding vertical displacements. It is obvious that the line-girder analysis solutions are not capable of capturing any interactions of the individual girders with the NISSS54 bridge system.

In the line-girder analyses, the girders are modeled individually disregarding any interactions with the other framing. The dead loads applied to the individual girders are based on their tributary areas, and the interactions between the cross-frames and girders are neglected. Therefore, the line-girder analyses do not predict any torsion of the girders. Of course, if the cross-frames are detailed for SDLF or TDLF, and if this detailing works as intended, then the girders ideally will not be subjected to any torsion under the steel dead load or the total dead load respectively. Hence, it may be possible that a line-girder analysis will be sufficient to capture the physical vertical displacements and major-axis bending stresses with good accuracy for straight skewed bridges, constructed with DLF detailing, under the load level at which the girder webs are theoretically plumb.

Ozgur (2011) shows that if Total Dead Load Fit (TDLF) detailing is used on straight skewed I-girder bridges (i.e., the cross-frames are detailed for plumb webs in the final dead load condition), and if the girder cambers are set based on the results from 1D line-girder analyses, the locked-in stresses due to the cross-frame detailing come very close to canceling the stresses due to the torsion of the girders under the total dead load condition. As such, the physical girder layovers are approximately zero under the total dead load, and the basic 1D line girder analysis flexural model is sufficient to capture the physical vertical displacement and major-axis bending stresses with good accuracy. This result is essentially independent of the magnitude and pattern of the support skews. Furthermore, Ozgur (2011) illustrates that the cross-frame forces along the stiff diagonal direction, as well as the corresponding flange lateral bending stresses, are significantly reduced if the bridge is constructed with TDLF detailing based on the cambers from line girder analysis. However, they are not zero. Unfortunately, the line girder analysis does not provide any predictions for these non-zero flange lateral bending stresses and the cross-frame forces.

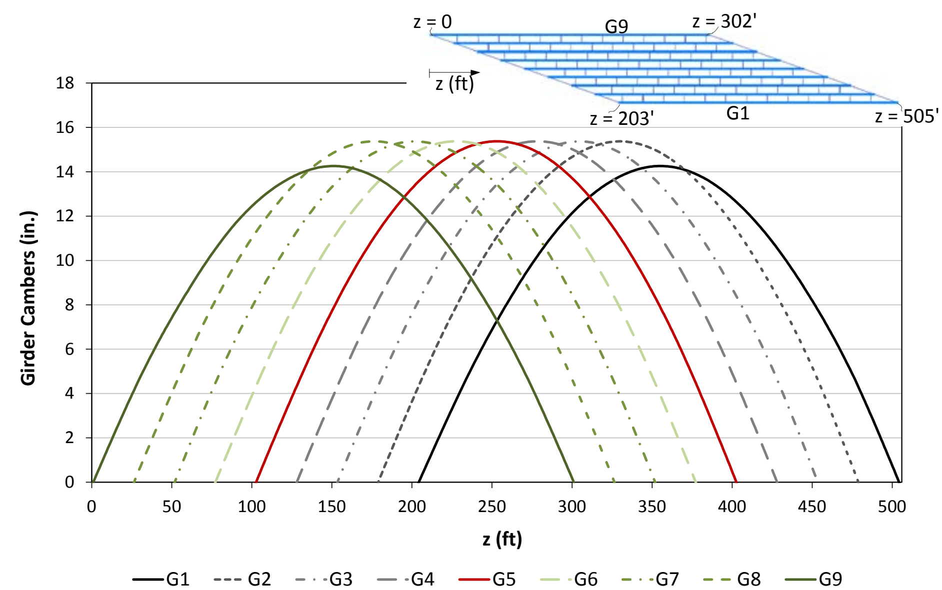

(a) Line girder analysis

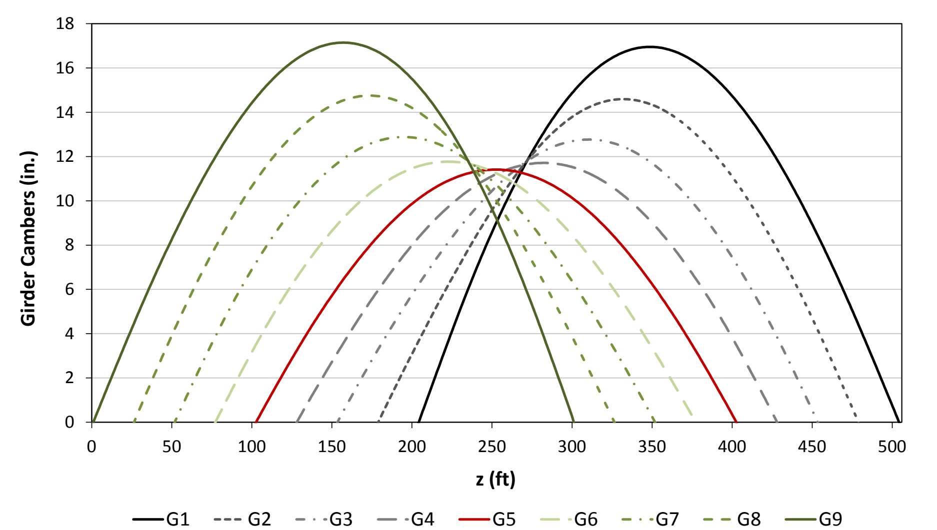

(b) 3D FEA

Figure 7.28. NISSS54, Girder camber profiles, obtained from different analysis solutions.

Figure 7.29 shows the final total dead load vertical displacements and girder major-axis bending and flange lateral bending stresses for NLF and TDLF detailing based on the line-girder analysis cambers in the NISSS54 bridge. Also, this figure illustrates the stress predictions from the line-girder analysis solutions. Interestingly, the 3D-FEA solutions demonstrate the fact that the physical vertical displacements and major-axis bending stresses in straight-skewed I-girder bridges tend to match well with the line girder analysis solutions when TDLF detailing is used along with the line-girder analysis cambers. Also, the flange lateral bending stresses are significantly reduced relative to the responses for NLF detailing.

Unfortunately, the line-girder analysis predictions generally do not produce accurate results for cases other than the dead load condition that the cross-frames are detailed for. For instance, for the above case with TDLF detailing, line-girder analysis generally does not give an accurate prediction of the steel dead load responses.

Similarly, Ozgur (2011) shows that if Steel Dead Load Fit (SDLF) detailing is used on straight-skewed I-girder bridges (i.e., if the cross-frames are detailed to fit to plumb webs in the completed steel dead load condition), and if the girder cambers are set based on the results from 1D line girder analyses, a basic 1D line girder analysis is sufficient to obtain accurate predictions of the girder major-axis bending stresses and displacements under steel dead load. The girder flange lateral bending stresses and the cross-frame forces are essentially zero in the steel dead load condition in this case.

The correctness of this solution can be understood by considering a hypothetical case of a straight-skewed I-girder bridge erection in which all the girders are set on the bearings and the top chord of the cross-frames is connected between all the girders, but otherwise the cross-frames are not engaged. In this situation, the girders remain plumb and deflect vertically under the steel dead load exactly as predicted by the line girder analysis. If the cross-frames are detailed such that they fit-up perfectly with the connection workpoints on the girders in this geometry, then obviously the bottom chord connections can be made between the cross-frames and the girders without applying any force, the cross-frames will have zero force under the steel dead load, and the girder flange lateral bending stresses will be zero.

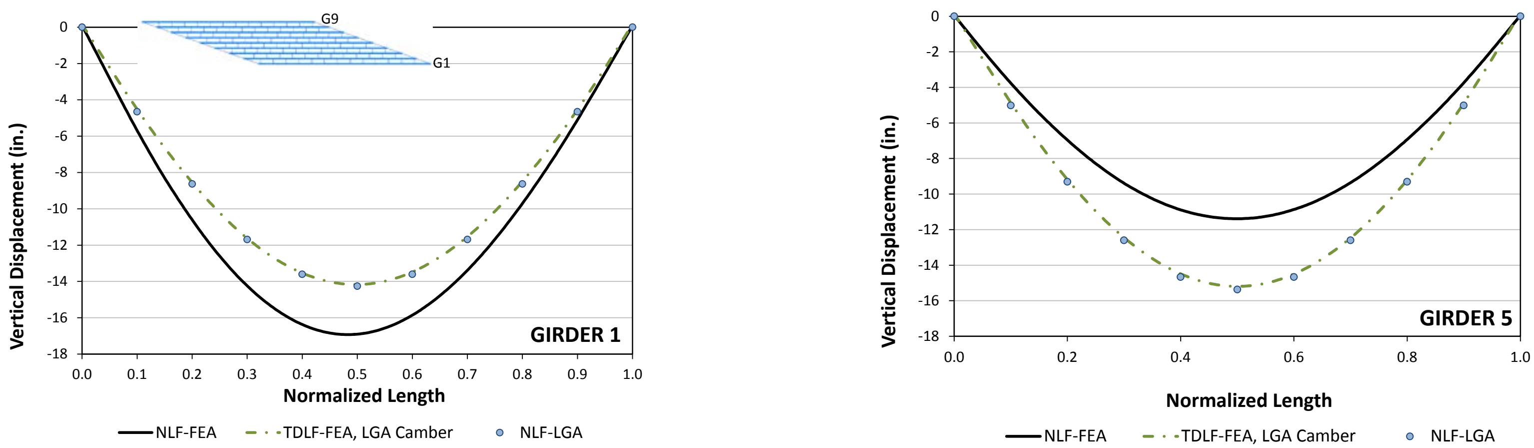

(a) Vertical Displacements

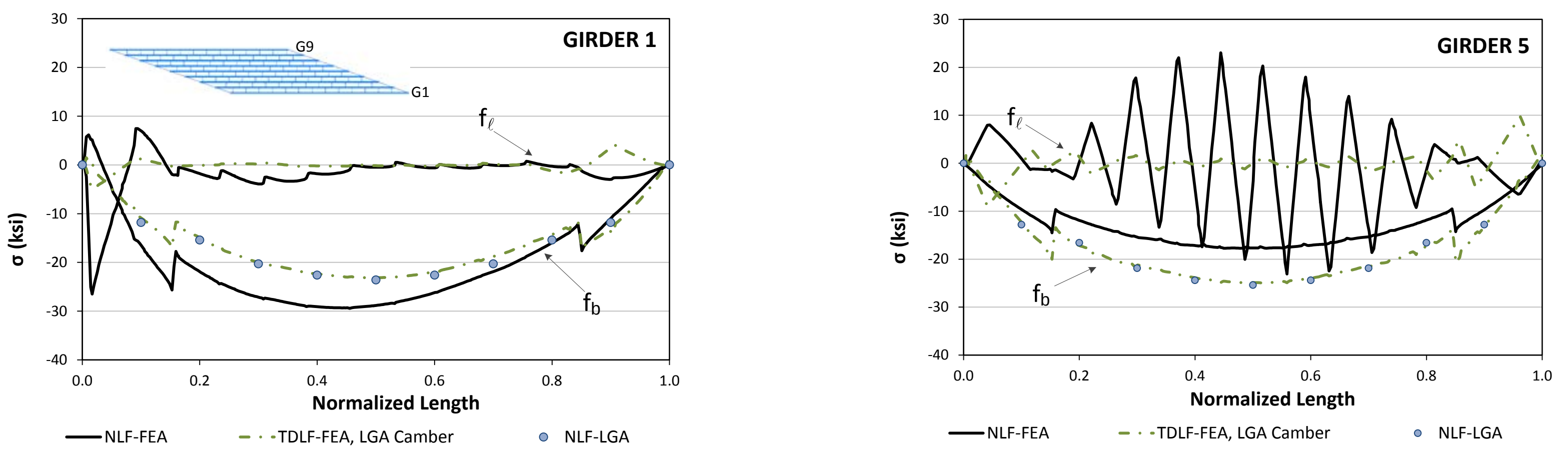

(b) Top Flange Stresses

Figure 7.29. NISSS54, total dead load vertical deflections and top flange stresses associated with NLF and TDLF detailing where the cambers are set based on line girder analysis results.

This solution is achieved via an accurate 2D-grid analysis (satisfying the recommendations of Chapter 6), or via the above 3D FEA, by including the effect of the corresponding lack-of-fit between the girders and the cross-frames in the initial no-load geometry. This lack-of-fit induces cross-frame forces and girder flange lateral bending stresses that in this ideal case are equal and opposite to the cross-frame forces and girder flange lateral bending stresses in the three-dimensional structural system under the steel dead load. Interestingly, if the cambers are obtained as the negative of the vertical displacements associated with this three-dimensional response (Figure 7.28b), the locked-in forces will tend to offset the dead-load forces in the cross-frames under the steel dead load such that the sum of these two effects will be relatively small. However, the resulting cross-frame forces are not zero, and the corresponding flange lateral bending stresses are not zero. The cambers determined from the line girder analysis (Figure 7.28a) are the ones that produce locked-in forces, due to the corresponding initial lack-of-fit, that perfectly offset the steel dead load cross-frame forces.

7.5.2 Special Cases where Line Girder Analysis with the V-load Approximation Predicts Accurate Results for Curved Radially-Supported Bridges

Line-girder analysis, using the V-load approximation to account for horizontal curvature effects, is used widely for the analysis and design of curved bridges with radial supports. In the V-Load analysis, curved girders are modeled as straight girders by using the girder length along the arc. In addition to dead loads, which are based on the tributary area of the girders, vertical loads are applied along each span at the connection points of the cross-frames with girders. The V-load approximations tend to provide good estimates of the girder stresses and cross-frame forces for simple-span curved radially-supported bridges. However, variations in flange lateral bending stress predictions can be observed due to the overall lateral bending of the flanges. Moreover, the vertical displacement predictions can be off due to the coupling between vertical displacements and torsional rotations of the girders.

Figure 7.30 shows total dead load girder camber profiles of the NISCR2 bridge, constructed with NLF detailing based on V-load approximations and 3D-FEA. It can be observed from this figure that that the V-load approximations underpredict the vertical displacements of this bridge.

Ozgur (2011) shows that if Total Dead Load Fit (TDLF) detailing is used on simply-supported curved I-girder bridges with radial supports (i.e., the bridges are detailed to have plumb webs in their final dead load condition), and if the girder cambers are set based on the results from the 1D line-girder analyses with the V-load approximation, the locked-in stresses due to the cross-frame detailing reduce the overall (global) flange lateral bending effects. As such, the physical girders are approximately plumb under total dead load and the flange lateral bending stresses are solely due to overhang bracket loadings and horizontal curvature effects. That is, the “global” lateral bending of the flanges due to the overall torsional rotation of the bridge cross-section (which results in out-of-plumbness of the girder webs along the span) is taken out by the corresponding locked-in forces. As a result, the basic 1D line-girder analysis flexural model provides a good representation of the physical vertical displacement and major and minor axis bending stresses. However, the V-load solutions still do not produce accurate results for the cross-frame forces, which tend to be increased significantly due to TDLF detailing. It should be noted that torsional rotation of the bridge cross-section under general dead load is unavoidable though. Therefore, the V-load analysis does not necessarily produce accurate results for other dead load conditions in which the webs are not essentially plumb at the cross-frame locations. In addition, for continuous-span bridges, other factors enter which can lead to errors in the simplified method. For instance, the V-load method does not capture the tendency for the vertical reactions at intermediate supports on the inside of the horizontal curve in a continuous-span bridge to be somewhat larger due to the transverse load paths provided by the cross-frames.

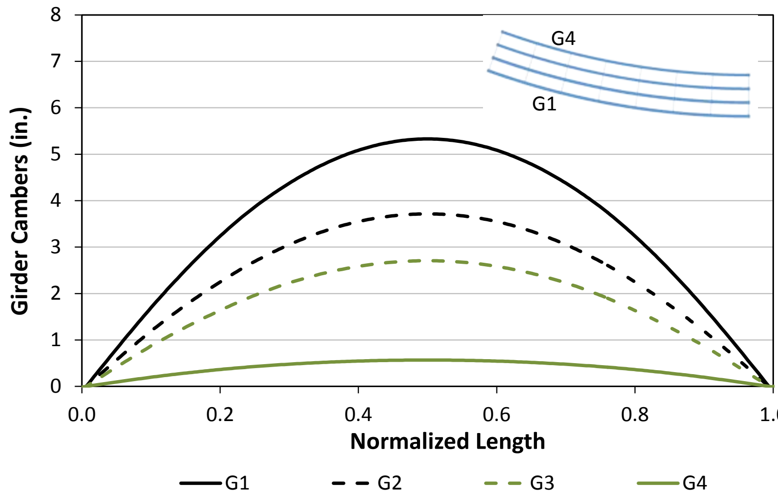

(a) Camber based on line girder analysis

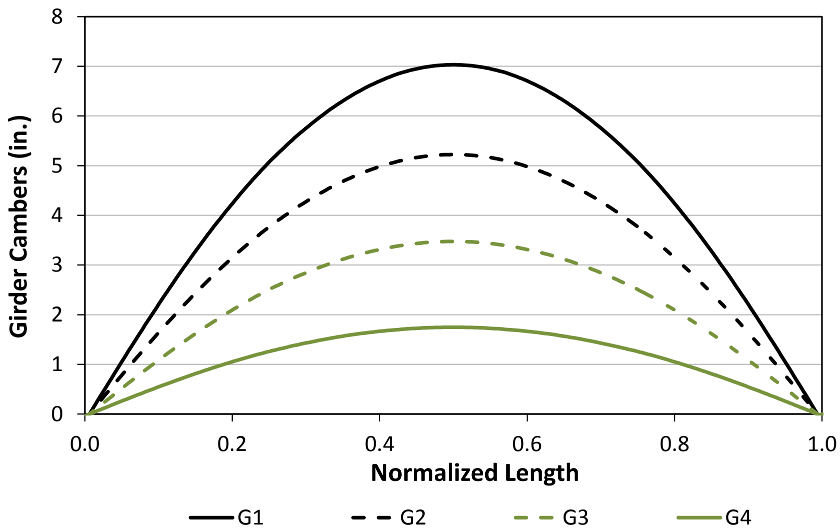

(b) Camber based on FEA deflections

Figure 7.30. NISCR2, Total dead load cambers obtained from line girder and finite element analysis solutions.

Figure 7.31 illustrates the total dead load vertical displacements and girder major-axis bending and flange lateral bending stresses for NLF and TDLF detailing based on the cambers from line girder analysis (with V-load adjustments included) in the NISCR2 bridge. Also, Figure 7.31 shows the V-load analysis predictions. The physical vertical displacements, girder major-axis and flange lateral bending stresses associated with TDLF detailing are captured accurately by the V-load analysis predictions if the girder cambers are set based on the V-load analysis solutions.

Similarly, if Steel Dead Load Fit (SDLF) detailing is used on curved I-girder bridges with radial supports (i.e., the bridges are detailed to have plumb webs in the completed steel dead load condition) and, if the girder cambers are set based on the results from 1D line-girder analyses, a basic 1D line-girder analysis (with the V-load method adjustments) is sufficient to obtain accurate predictions of the girder stresses and displacements in the steel dead load condition. Unfortunately, in this case, the V-load analysis generally does not produce accurate results with respect to the physical girder vertical displacements, major and minor axis bending stresses for other than the steel dead load condition.

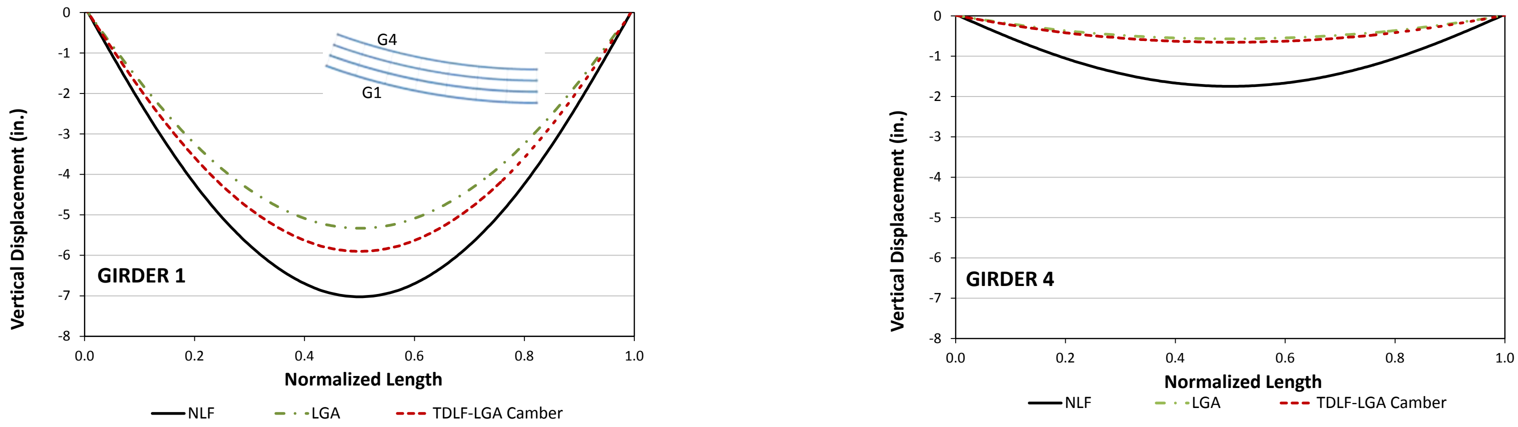

(a) Vertical Displacements

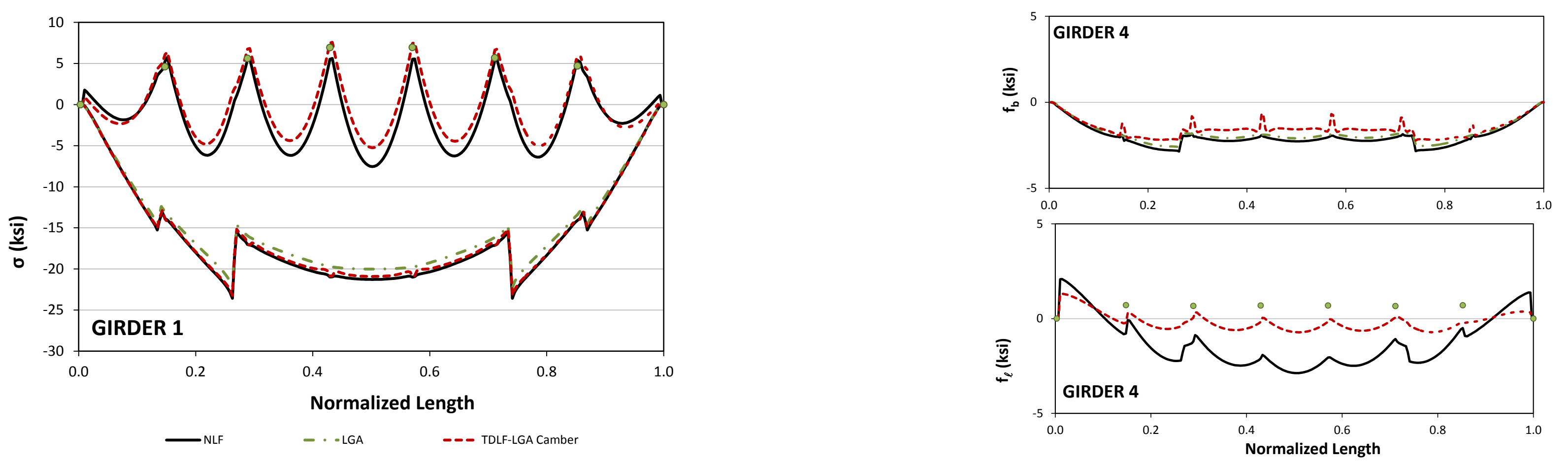

(b) Top Flange Stresses

Figure 7.31. NISSS54, total dead load vertical deflections and top flange stresses associated with NLF and TDLF detailing where the cambers are set based on line girder analysis results.

7.5.3 Estimating Maximum Dead-Load Fit Cross-Frame Forces and Girder Flange Lateral Bending Stresses Using an Analysis Based on NLF Detailing

In current practice (2012), cross-frame members of straight-skewed bridges are commonly sized without considering the locked-in forces from SLDF or TDLF detailing of the cross-frames. However, the physical member-by-member cross-frame forces corresponding to the sum of the dead load effects plus the locked-in forces from the DLF detailing can differ substantially from those obtained from an accurate 2D-grid or 3D FE analysis assuming NLF detailing.

In the previous sections, it is shown that SDLF or TDLF detailing of straight-skewed bridges tends to develop locked-in cross-frame forces due to the initial lack-of-fit that are approximately equal and opposite to the dead load stresses in the region having the largest transverse stiffness, i.e., the shortest diagonal direction across the bridge plan. However, the locked-in forces in the cross-frames can be substantially different from the dead load stresses outside this region. Ozgur (2011) shows that the locked-in cross-frame forces can be relatively large for cross-frames at the vicinity of the skewed bearing lines outside the short diagonal direction across the bridge plan.

For skewed I-girder bridges, (Ozgur. 2011) provides a minimum ratio of adjacent unbraced lengths at the first intermediate cross-frame offset from a bearing line such that large relative lateral stiffness from the adjacent bearing line and large magnitudes of the differential camber between the girders (and corresponding substantial initial lack-of-fit vertical displacements) can be alleviated. This ratio is discussed in detail in Chapter 8. If the minimum ratio of the adjacent unbraced lengths at the first intermediate cross-frame offset from a bearing line is larger than approximately 0.4, large spikes in the locked-in cross-frame forces in this cross-frame tend to be eliminated. Furthermore, it is noted that the maximum cross-frame forces obtained from a 3D FEA assuming NLF detailing are an accurate to conservative estimate of the maximum cross-frame forces for the physical bridge using either SDLF or TDLF detailing. Therefore, separate single-size intermediate and bearing-line cross-frames can be designed conservatively and used throughout the bridge based on the maximum member forces obtained from an accurate 2D-grid or 3D

FE analysis neglecting lack-of-fit effects (top chord members designed for the maximum tension and the maximum compression determined in the top chord at the cross-frames throughout the bridge, bottom chord members designed similarly, and diagonal members designed similarly). One cross-frame type can be designed for all the intermediate cross-frames, and another for the bearing-line cross-frames. In addition, the girder flange lateral bending stresses tend to be predicted conservatively from an accurate 2D-grid or 3D FE analysis neglecting lack-of-fit effects given the above caveat.

For curved I-girder bridges, the DLF detailing effects tend to add with the dead load forces in the cross-frames; therefore, the influence of DLF detailing on the cross-frame forces, as well as on the girder flange lateral bending stresses at the cross-frames, generally needs to be included in curved bridges. Fortunately, NLF is often a good option for curved radially-supported bridges.

For curved and skewed bridges constructed with SDLF or TDLF detailing, the above effects can go both ways depending on the location within the structure and the relative magnitudes and directions of the curvature and skew.

Unfortunately, for bridges with larger skew indices, the conservatism of designing single-size cross-frames in the above fashion can be prohibitive. Since the distribution of the internal cross-frame forces based on NLF detailing (see Figure 7.17) can be very different from that obtained based on SDLF or TDLF detailing (see Figure 7.18), the only alternative if the cross-frames are detailed for SDLF or TDLF is to account for the corresponding locked-in force effects in the analysis. In addition, note that generally, the total forces in the steel dead load condition (i.e., the steel dead load forces plus the locked-in forces) need to be considered. For cases with TDLF detailing, the locked-in force effects may be significantly larger than the steel dead load effects.

8. Design and Construction Considerations for Ease of Analysis Via Improved Behavior

8.1 Limiting the Values of the Bridge Response Indices

The skew effect, torsion, and girder length indices discussed in Chapter 3 can be used to predict potential difficulties in the early stages of the design of steel girder bridges. Whenever it is practical, the bridge geometry should be laid out so the indices are as close to the values of a straight bridge with normal supports, i.e., $I_S = 0$, $I_T = 0.5$, and $I_L = 1.0$.

Coletti et al. (2010) discuss procedures to reduce the severity of the skew effects in straight bridges. In all cases, the efforts are aimed at simplifying the structure's geometry, which in terms of the proposed indices, is equivalent to reducing the value of the skew index. As discussed in Section 3.1.2, the possible complications associated to the skew in both the analysis and the construction of the structure are lessened when I_S is less than 0.30.

Similarly, the torsion index, I_T, is a tool that can be used to detect undesired girder uplift as early as in the preliminary design of a curved and/or skewed bridge (see Section 3.1.4). As discussed in Ozgur (2011), a suggested limit of the torsion index to avoid uplift under nominal (unfactored) dead plus live load in simple-span I-girder bridges is 0.65. If I_T is above this limit in a given structure, the engineer should anticipate that significant uplift issues may need to be addressed. Similarly, for simple-span tub-girder bridges with single bearings on each tub, $I_T = 0.87$ was identified as a limit beyond which bearing uplift problems are likely. Continuous-span bridges can tolerate larger I_T values due to the continuity with the adjacent spans.

8.2 I-Girder Bridge Design Considerations

8.2.1 Minimum Ratio of Adjacent Unbraced Lengths at First Cross-Frame Offset from a Bearing Line

Ozgur (2011) provides recommendations on how far from the bearing line the first intermediate cross-frame should be connected, so that the forces in the cross-frame components are at acceptable levels. Figure 8.1 shows the variation in the relative lateral stiffness of the offset length and the adjacent unbraced length, χ_{Offset}, versus the ratio of these two lengths,

$$\alpha = \frac{\text{Offset length}}{\text{Adjacent unbraced length}}$$

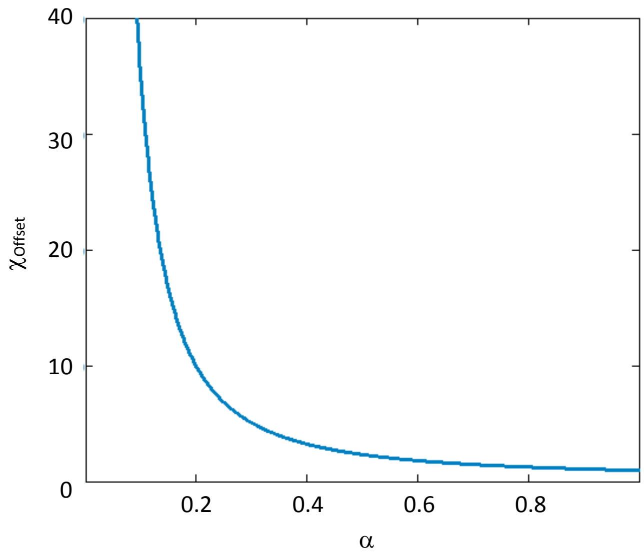

Figure 8.1. Relative lateral stiffness of offset length and the adjacent unbraced length versus the ratio of the two lengths.

at the first intermediate cross-frame from a bearing line. Figure 8.2 shows an example of these two lengths. Ozgur (2011) suggests that the minimum value of α, should be at least 0.4 since the relative lateral stiffness increases significantly for smaller ratios. Conventionally, engineers use at least 1.5 times the depth of the web as the offset for the first intermediate cross-frame. This limit should also be observed. However, for the bridges with severe skew and long spans, the first intermediate cross-frame should be offset by a greater length than this conventional distance (i.e., $a \geq 0.4b$).

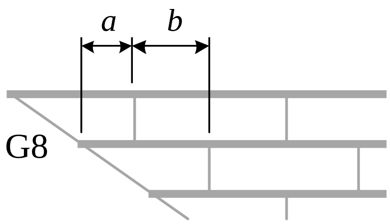

a = offset distance for G8
b = adjacent unbraced length for G8

Figure 8.2. Illustration of offset distance and adjacent unbraced length.

8.2.2 Framing of Cross-Frames to Mitigate Skew Effects

The magnitude of the collateral skew effects depends highly on the configuration of the bracing system. If the cross-frames are laid out so they do not “interfere” with the rotations that the girders experience at the bearing lines, the flange lateral bending stresses, and the cross-frame forces are relatively small. Based on this concept, Sanchez (2011) recommends a scheme that can be implemented in the design of straight I-girder bridges to mitigate the undesirable effects of skew. The approach is to place the cross-frames following an orientation similar to the skew. This practice relaxes the large forces in the cross-frames and the associated girder flange lateral bending stresses that may result due to skew effects. The basic principle is to connect the girders at the points where the layovers are similar, so the twists induced by the cross-frames are reduced (Sanchez (2011) shows that most of the contributions to cross-frame forces and flange lateral bending come from enforcing layover compatibility). In cases where the skew of the bearing lines is unequal, the cross-frames can be placed in a “fanned” configuration. With this layout of the bracing system, the effects of the skew decrease as compared to a configuration where the cross-frames are connected perpendicular to the girder longitudinal axis. Figure 8.3 shows an example of this mitigation scheme. The structure depicted in the figure is Bridge NISSS16. The cross-frame layout shown in Figure 8.3a is the layout that was considered for the studies of Task 6.

Table 8.1 shows the results of the analyses conducted using both configurations. If the cross-frames are fanned out from the point where the projection of the bearing line intersect (Figure 8.3b), the cross-frame forces decrease significantly as compared to the responses obtained with the original configuration. In addition, this reduction of the cross-frame forces also results in a decrease in the flange lateral bending stresses. The only potential negative of this approach is that the cross-frames have different lengths for each cross-frame line. Section 9.4 discusses several options for the connection of these cross-frames to the girders. Further illustrations of the potential improvements of the structural behavior of skewed I-girder bridges are presented in Sanchez (2011).

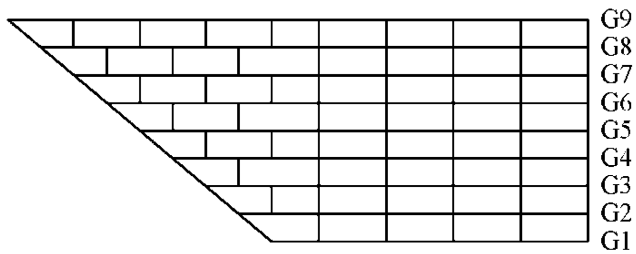

(a) Framing plan of NISSS16 with the cross-frames oriented perpendicular to the longitudinal axis of the girders (Layout 1)

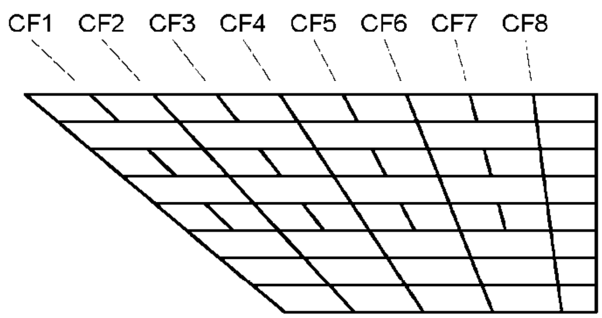

(b) Fanned cross-frame configuration with girders grouped in pairs to diminish the skew effects (Layout 2)

Figure 8.3. Different cross-frame configurations implemented in bridge NISSS16.

Table 8.1. Maximum forces in the cross-frames, predicted for two different cross-frame layouts, bridge NISSS16, TDL level.

Element	Cross-Frame Layout	Number of Interior Cross-Frames	Maximum Compression Force (kips)	Maximum Tension Force (kips)
Top Chord	(1)	48	9.3	62.6
	(2)	44	1.4	46.4
Diagonals	(1)	48	33.9	34.2
	(2)	44	15.4	15.2
Bottom Chord	(1)	48	58.0	8.6
	(2)	44	42.4	0.9

8.2.3 Selection of Cross-Frame Detailing Methods

Given the results discussed in Chapter 7, it should be apparent that different methods of cross-frame detailing work well for different I-girder bridge geometries. Furthermore, in many cases, steel I-girder bridges can be built successfully using a wide range of methods. Generally, the appropriate selection of a cross-frame detailing method depends in large part on the priority that one assigns to various objectives and tradeoffs. The NCHRP 12-79 project main report discusses these objectives and tradeoffs in detail, and provides a number of general recommendations. A few of these considerations are discussed in brief below.

Alleviating layover of the girders at bearing lines

As mentioned in Chapter 2, girder layovers under dead load are unavoidable at skewed bearing lines when NLF detailing is used. The torsional rotation capacity of the bearings can be insufficient if the layovers are excessive. Therefore, for bridges that have a sharp skew of their bearing lines, particularly the bearings at a simply-supported end of a bridge, alleviating the excessive layover of the girders at these positions is a primary objective of SDLF or TLDF detailing of the cross-frames.

The most commonly used bearing types are plain elastomeric bearings and steel reinforced elastomeric bearings. Typical maximum rotational capacities of the above bearing types are 0.01 radians for elastomeric bearings and 0.04 radians for steel reinforced elastomeric bearings (NHI, 2011). Figures 8.4 and 8.5, from (Ozgur, 2011), show the admissible bearing rotation limits as a function of the skew angle and major-axis bending rotation at the bearing. Figure 8.4 is developed for plain elastomeric bearings while Figure 8.5 is developed for steel reinforced elastomeric bearings. Percentages of the maximum rotational capacity of the bearing are provided to accommodate the fact that part of the rotation is taken up by live loads.

In these figures, if the intersection point of the skew angle and ϕ_x for a bridge falls below the targeted bearing rotation curve, the bridge can be detailed for NLF detailing without exceeding the targeted maximum dead load rotation. Otherwise, SDLF or TDLF detailing should be considered to reduce the layovers, or other solutions such as the use of beveled sole plates or more expensive bearings that can accommodate the larger rotations should be evaluated. It should be noted that beveled sole plates are already common in many bridges to accommodate grade changes along the length of the bridge.

Facilitating Fit-Up During the Steel Erection

In addition to the above, the engineer must be aware of the fact that the type of the detailing also can impact the erection requirements. There are various attributes that result in coupling between the twist rotations and other rotations and between the twist rotations and other displacements in curved and skewed I-girder bridges. These include:

- Skewed end cross-frames create a coupling between the girder torsional and major-axis bending rotations (see Figure 2.7 or Figure 7.2)
- Intermediate cross-frames perpendicular to the members enforce the same layovers between the adjacent girders at the cross-frame locations.
- Major-axis bending rotations and vertical displacements are coupled with torsional rotations in curved girders.

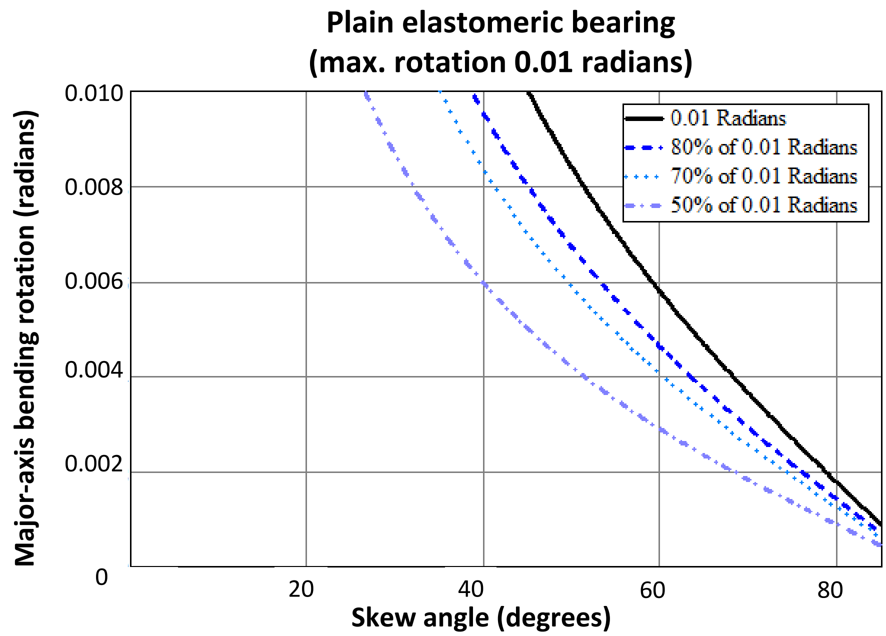

Figure 8.4. Torsional rotation levels for plain elastomeric bearings for given major-axis bending rotation and skew angle of the bearing.

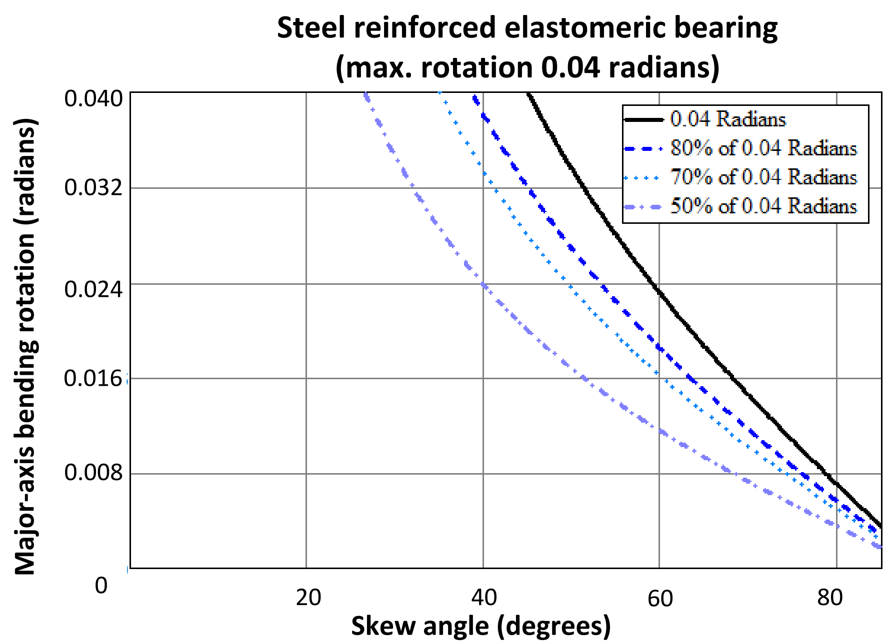

Figure 8.5. Torsional rotation levels for steel reinforced elastomeric bearings for given major-axis bending rotation and skew angle of the bearing.

For bridges constructed with NLF detailing, any variation from the no-load geometry due to dead load deflections requires fit-up forces to assemble the cross-frames in bridges constructed with NLF. In addition, for bridges constructed with TDLF detailing, fit-up forces are required at any stage due to lack-of-fit between the cross-frames and girders (since the total dead load is not yet in place on the girders at the time of the steel erection). In either case, large fit-up forces can be required if the girders need to be displaced vertically since the girders generally have large stiffness against major-axis bending deformations. These cases are more likely to occur at the locations with large differential vertical displacements between the girders, close spacing between cross-frames, and deformations for each of the above "coupled interactions" that unfortunately can be somewhat different from one another. One key location where these factors are combined is at intermediate cross-frames that are framed close to skewed bearing lines). SDLF detailing often reduces the incompatibilities between the cross-frames and the girders close to sharply-skewed bearing lines.

It should be noted that the forces required to assemble the structure during the erection can depend significantly on the erection procedures. The selected erection procedure can have a considerable effect on the dead load deflections during erection. For instance using temporary supports for bridges constructed with NLF detailing or using the dead load deflections during the erection for bridges constructed with DLF detailing can reduce any potential large differential vertical displacements. Therefore, fit-up forces can be reduced based on the selected erection scheme. All these attributes need to be considered when selecting a particular detailing method.

General Considerations

For straight-skewed bridges, SDLF or TDLF detailing are effective ways to control the plumbness of the girders, but the minimum ratio of the offset length to the adjacent unbraced length at the first cross-frame from a bearing line should be taken to be at least 0.4 to avoid large locked-in cross-frame forces. TDLF detailing is typically a good option (or the cross-frames can be detailed for an intermediate condition between TDLF and SDLF) for cases where SDLF detailing does not limit the bearing rotations to less than the admissible bearing rotation capacity. It should be noted that in straight-skewed bridges the fit-up forces tend to be minimal for SDLF detailing and reduced significantly for TDLF detailing if the steel dead load deflections are used during the erection of the steel.

For curved-radially supported bridges, NLF detailing is generally an effective approach since the locked in stresses due to SDLF and TDLF detailing are additive with the dead load stresses. The fact that the cross-frame forces tend to be smallest with NLF detailing of these types of bridges (in any dead load condition) is also an indicator that the fit-up of the steel during the steel erection is easier with NLF detailing. The effect of the resulting girder layovers on the strength tends to be small (less than approximately 3 %). For cases with three or more girders, the true system capacities tend to be larger than those implied by the AASHTO LRFD strength calculations regardless of the method of cross-frame detailing (assuming that the system capacity is governed by the strength of the girders, i.e., the cross-frames have adequate strength). This is because the girders generally are able to provide some redistribution of forces to other locations in the bridge after the first girder limit state is reached.

For I-girder bridges with combined curvature and skew, NLF detailing is effective for the cases where the bearing rotation limits are not exceeded (see Figures 8.4 and 8.5) as long as fit-up problems near highly-skewed bearing lines are not exacerbated. Otherwise, SDLF detailing is often a better option for curved and skewed I-girder bridges. In the case of SDLF detailing of curved and skewed bridges, the engineer should consider the locked-in vertical displacements and locked-in force effects in the design. This is because the locked-in force effects are largely additive with the dead load effects with respect to the cross-frame forces and the girder maximum (“negative”) flange lateral bending stresses.

8.3 Tub-Girder Bridge Design Considerations

8.3.1 Avoid Flange Connections of Diaphragms where Practicable

As discussed previously in Section 2.1.5, the external support diaphragms play an essential role in the torsional behavior of the system in tub-girder bridges. Also it has been discussed that the behavior of the diaphragms is based mainly on their in-plane stiffness while their out-of-plane response is relatively small compared to the system stiffness.

Previous studies (Helwig et al., 2007) have shown that the flanges of the diaphragms often do not need to be connected to the tub-girders. The recommended practice is that the top flange of the diaphragms should not be connected to the top of the girder as long as the behavior of the diaphragm is dominated by shear. This occurs when the diaphragm length to depth is less than about 5, a limit that is frequently met by tub-girder bridge diaphragms. The 3D FEA studies performed for this research agree with the findings by (Helwig et al., 2007). These recommendations are applicable to full depth diaphragms only.

8.3.2 Avoid Skewed Intermediate Support Diaphragms

Intermediate support diaphragms connect the tub-girders to distribute the reaction forces between consecutive girders and restrain the girder cross-section rotations. However, for continuous span bridges with skewed pier supports, avoiding the external support diaphragms can be a good design decision. The ETCCS6 (Magruder Blvd Bridge) shown in Figures 4.44 and 4.45 uses this approach. The plan layout for this bridge is illustrated in Figure 8.6 where the bearing supports are denoted as crossed circles. In this figure, it can be observed that the girders are not connected at the skewed intermediate pier. The omission of the external support diaphragms avoids complex details at the skewed bearing line, and avoids additional torsional-flexural interactions from the skew that would have introduced large forces into the bridge. The girders have sufficient torsional stiffness such that the external support diaphragms may not be necessary in situations like this. In cases such as this bridge, where there are significant span differences between the girders due to the skew, external intermediate cross-frames or diaphragms perpendicular to the girders within the spans may be useful to control relative displacements between the girders leading to uneven deck thickness.

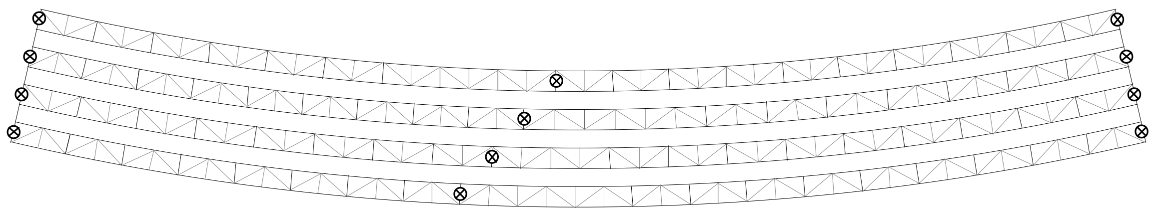

Figure 8.6. Plan view of the ETCCS6 bridge (McGruder Boulevard Bridge) showing intermediate bearing line without external diaphragms.

8.4 Construction Considerations

Forces required to assemble the structure during erection can depend significantly on the erection procedures (e.g., selection of temporary shoring towers, selection of holding cranes, etc.) and the sequence of erection, as well as the type of cross-frame detailing, although the final steel dead load geometry is unique. However, in many cases, the erection procedures may be driven by the site constraints.

Generally, it is more efficient to erect the girders from the outside of the curve to the inside of the curve for curved systems. Erecting girders from outside to inside is preferred since the top flanges of curved girders tend to lay-over in the direction away from the center of curvature under their dead load. Erecting subsequent girders from the outside (girders further away from the center of curvature) to the inside (girders closer to the center of curvature), the self-weight of the components being assembled into the partially erected structure helps to rotate the previously erected girders back into the desired geometry. If the girders are erected from inside to outside, large forces may be required in certain cases to lift the outside girder of the partially erected structure to achieve fit-up with a new outside girder.

I-girder bridges generally experience 3D deflections during erection, due to torsion, which can reduce or increase the displacement incompatibilities between connection points of the structural components. Also, for the given erection stage, displacement incompatibilities between connections can be different for different types of cross-frame detailing.

For NLF detailing, the cross-frames are detailed such that they connect to the girders in no-load geometry. However, differential displacements between girders can develop due to dead loads during erection. For I-girder bridges constructed with NLF detailing, temporary supports (falsework) can be used to control the differential vertical deflections between adjacent girders by limiting the dead load deflections and stabilizing the bridge during erection. This is particularly important for I-girder bridges with large span lengths. Relatively large differential vertical deflections due to dead loads can cause fit-up problems.

For I-girder bridges with large span-to-width ratios, the girder deflections and stresses tend to be amplified due to global second-order (stability) effects, as discussed in Section 2.9. Excessive girder layovers and large differential vertical displacements due to second-order amplification can lead to fit-up problems or can cause a failure during erection. However, these problems can be eliminated by the use of temporary supports. Moreover, significant reduction in the girder stresses and cross-frame forces are observed for long and narrow I-girder bridge units.

Large differential vertical displacements can be observed between different parallel bridge units. Figure 8.7 shows a representative bridge NISCS37 where large differential vertical displacements are observed for a particular erection stage, as shown in Figure 8.8. Large fit-up forces can be required to connect the different bridge units. However, temporary supports can reduce the differential vertical displacements between adjacent girders by limiting the dead load deflections. As a result, fit-up forces required to connect the cross-frames can be significantly reduced, particularly for bridges constructed with NLF detailing. Ozgur (2011) shows that that providing temporary supports across the width of the bridge between the units significantly reduces the large differential vertical deflections, as illustrated in Figure 8.9 for the bridge NISCS37.

Steel Dead Load Fit (SDLF) detailing of I-girder bridges tends to minimize the fit-up forces (and stresses) during the steel erection in straight bridges, unless the bridge is essentially supported in its no-load condition during the erection. This is because the steel dead load deflections (and deformations) in the various partially erected units often are close to the final steel dead load deflections (and deformations). However, in curved radially-supported bridges, the fit-up forces generally tend to be increased by using SDLF or TDLF detailing (since the cross-frame forces generally tend to be increased by the corresponding locked-in forces in these types of bridges).

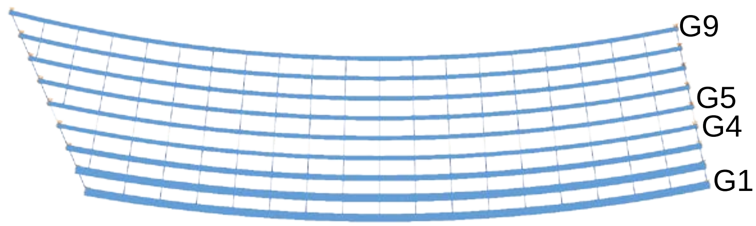

(i) NISCS37, Possible example of an erection stage.

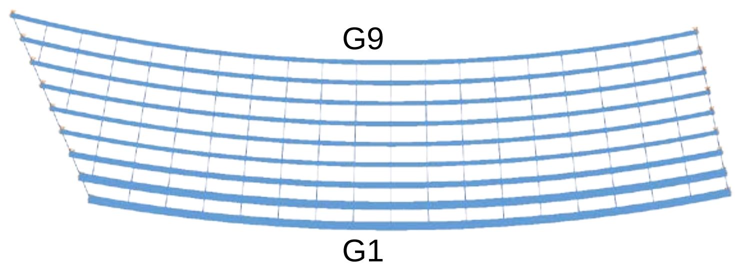

(ii) NISCS37, Completed steel structure.

Figure 8.7. NISCS37, illustration of long narrow units during construction.

If one provides sufficient temporary supports, holding cranes, etc. such that the partially erected structure is essentially in a no-load condition, then No-Load Fit (NLF) detailing minimizes the fit-up forces.

Total Dead Load Fit (TDLF) detailing generally leads to larger fit-up forces since the steel structure has not yet experienced the concrete dead load, but the cross-frames are detailed to fit up with the girders once the total dead load cambers are taken out of the girders.

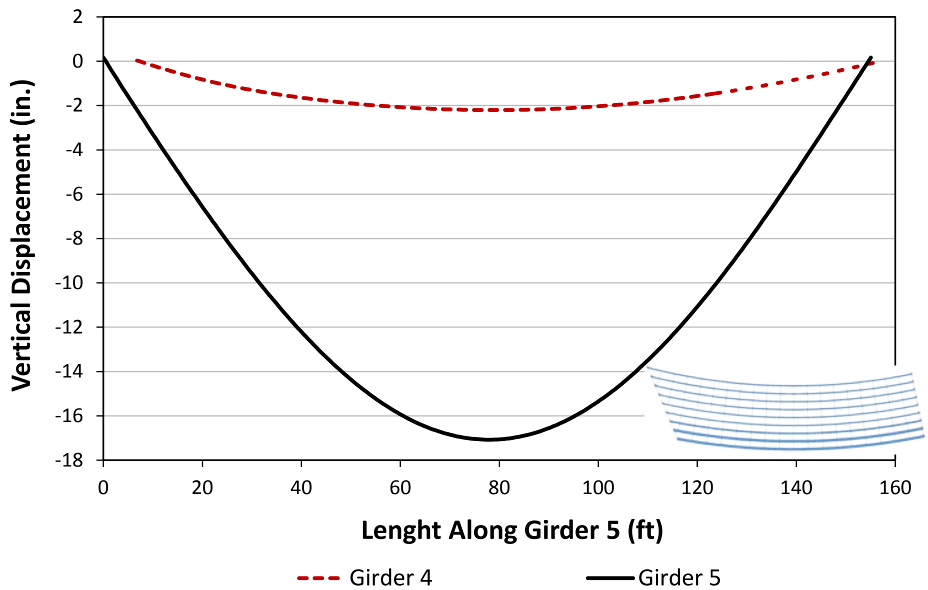

Figure 8.8. NISCS37, Vertical displacements for G4 and G5.

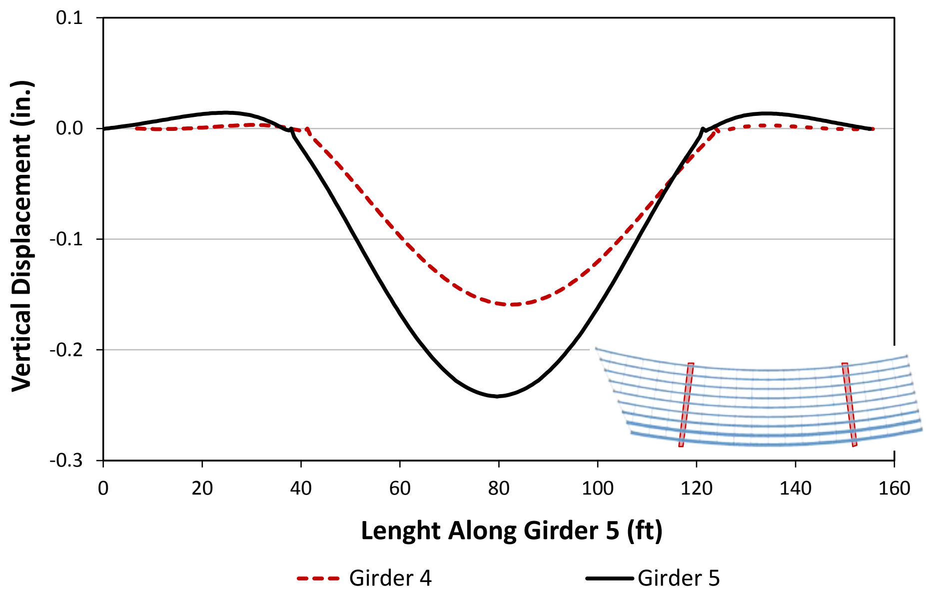

Figure 8.9. NISCS37, illustration of temporary supports between bridge units to minimize differential vertical displacements.

9. Problematic Physical Characteristics and Details

9.1 Oversize or Slotted Holes, Partially-Connected Cross-Frames

In curved and/or skewed bridges, the intermediate cross-frames stabilize the girders at all construction stages. In addition, the cross-frames participate in the control of the deformed geometry of the bridge, facilitating the deck placement. In some cases, erectors prefer not to install a selected number of cross-frames for deck placement operations, especially cross-frames that are close to the supports in skewed bridges. Instead, these cross-frames are erected in an element-by-element basis once the concrete has hardened. This practice, however, may be a detriment to the system performance. Potential amplifications due to second-order effects and other stability related problems are some of the consequences of not erecting all the cross-frames in the bridge. Therefore, prior to the deck placement, it is recommended to erect all the components of the steel structure. Moreover, the fasteners that connect cross-frames and girders must be tightened according to the design requirements.

Another technique that is sometimes used to overcome the difficulties of erecting cross-frames near skewed supports is the use of oversized or slotted holes. With larger holes in the gusset and connection plates, it is possible to maneuver and install the cross-frames with relative ease. However, there are cases where the fasteners do not bear on the surfaces of the gusset and connection plates, reducing the efficiency of the connection. In these cases, the stability bracing efficiency of the cross-frames and their ability to participate in the control of the bridge deformed geometry can be influenced significantly. Hence, it is not recommended to use this technique as a solution to the problem of installing cross-frames located near skew ends. Instead, the cross-frames can be detailed according to the guidelines discussed in Chapter 7. An appropriate detailing method can be used to facilitate the steel erection and in general, to enhance the structural performance of the bridge.

In summary, it is important to note that the cross-frames are the primary means of establishing the vertical alignment and bracing of the girders during the construction of I-girder bridges. Leaving out a cross-frame, or providing oversize or slotted holes and leaving the connections loose amounts to removal of a brace and release of some control of the geometry.

9.2 Narrow Bridge Units

Under certain circumstances, I-girder bridges can be susceptible to large response amplifications due to global second-order effects. Contrary to local stability related problems that involve individual unbraced lengths (see Section 9.3), structures with relatively large spans-to-width ratios are sensitive to global nonlinear behavior. As discussed in Section 2.9, these structures may experience excessive displacements that can compromise the bridge constructability and in some cases, its structural integrity. Some examples of structures with these characteristics are: widening projects of existing bridges, pedestrian bridges with twin girders, phased construction, and erection stages where only a few girders of the bridge are in place.

When the bridge strength is a concern, the equations proposed by Yura et al. (2008) can be applied to estimate the system buckling load of I-girder bridges. These equations give a simple approximation of the theoretical load level at which a perfectly straight system will bifurcate into its buckled configuration. However, the physical bridge may experience excessive amplification of its lateral-torsional displacements associated with horizontal curvature, skew, unbalanced construction loads, and dissimilar girders long before reaching the theoretical buckling load level.

The amplification factor, AF_G, can be used to anticipate possible large second-order amplifications of girder stresses and displacements on a long-and-narrow bridge unit. To improve the structural performance, it is desirable to limit the value of AF_G to less than approximately 1.25 under the total dead load. If this index is above this limit, there is a potential for the structure to experience undesired deflections that may affect the construction process; specifically, the concrete deck placement. It is important to point out that bridges with $AF_G \geq 1.25$ do not necessarily need to be redesigned to avoid global second-order amplification. The construction process can be modified to reduce this index. For example, the use of temporary shoring towers at mid-span represents a significant reduction of AF_G. However, it is best for this level of second-order amplification to be avoided by appropriate consideration at the design stage whenever possible.

If a bridge has a sufficient number of girders, so that its width is comparable to its span length, global second order amplifications may be negligible. A decision based on engineering judgment is required to assess when a bridge structure is vulnerable to global second-order amplification. The factor AF_G is the means to quantify this behavior.

9.3 V-Type Cross-Frames without Top Chords

Cross-frames stabilize the I-girders prior deck hardening. In some cases, V-type cross-frames without top chords may not be able to perform this function. The flexural stiffness of this type of cross-frame is substantially smaller than in any other configuration; therefore, its ability to provide stability bracing needs to be scrutinized during design. Studies conducted in an existing structure that used this cross-frame configuration, illustrate the importance of including the top chord. Figure 9.1 shows the plan view of a bridge located in SR1003 (Chicken Road) bridge over US 74, Robeson Co., NC. This bridge was instrumented to monitor its behavior during construction. The field measurements and corresponding original analytical studies are documented in Morera and Sumner (2009).

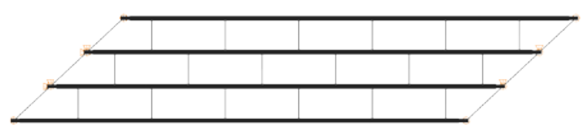

L = 133 ft./ w= 30.1 ft./ $\theta_1 = 46.2^0$, $\theta_2 = 46.2^0$

Figure 9.1. EISCS3 bridge layout.

To investigate the influence of the missing top chord on the structural behavior of this bridge, two cross-frame models are considered in the NCHRP 12-79 research. In the first analysis, the bridge is modeled to represent the as-built condition, without intermediate cross-frame top chords. In the second analysis, the top chords are included. Figure 9.2 shows a 3D view of both models.

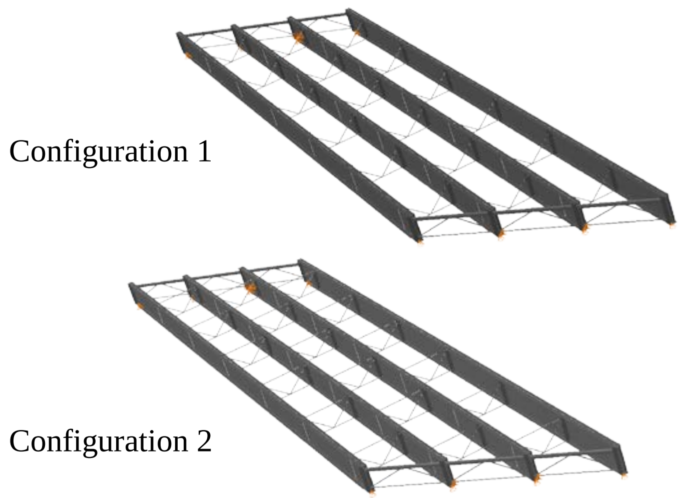

Figure 9.2. Intermediate cross-frame configurations implemented in the analyses.

As observed in the stress and layover plots for the fascia girder, G1, in Figure 9.3, the flange lateral bending response is affected substantially by the presence of the top chord. The results from the analysis conducted with the first configuration show that large lateral displacements may occur in this girder due to the lack of bracing of the top flange. Similarly, the levels of flange lateral bending stress are very high in the segment between 0.4 and 0.7 of the girder length. These two responses indicate that if the incidental contributions from components such as stay-in-place forms, ties between the girders provided by the contractor, and other devices provided to facilitate the concrete placement are not considered, the bridge exhibits substantial second order amplifications, at the TDL level. Sanchez (2011) shows that when the steel structure is properly braced, the influence of the SIP forms on the system responses during the concrete placement is negligible.

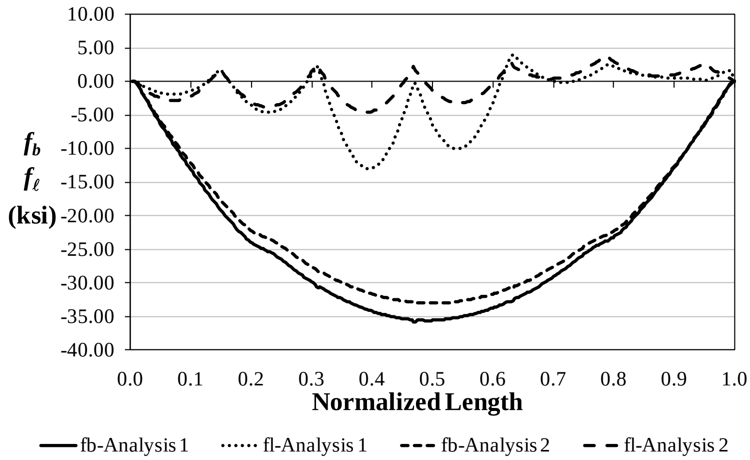

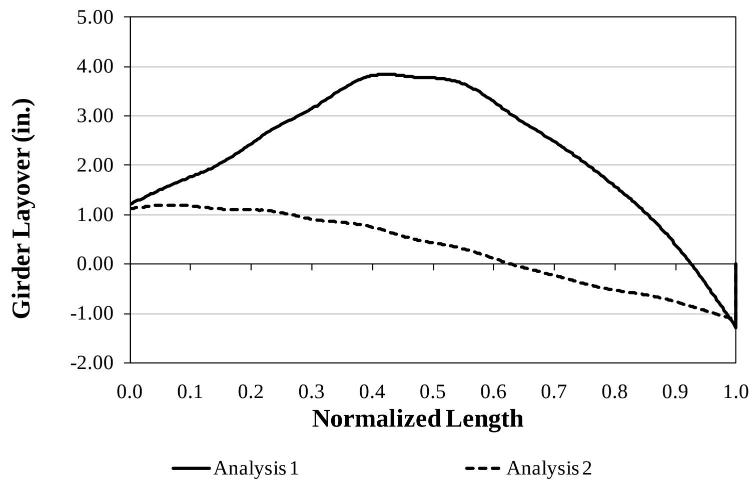

Figure 9.3. Comparison of stresses and relative lateral displacements for EISCS3 with and without a top chord in the cross-frames (Analysis 1 does not have a top chord whereas Analysis 2 has a top chord).

9.4 Connections at Skewed Cross-Frame Locations

Bracing systems have a fundamental role on the behavior of curved and skewed I-girder bridges during construction. In steel bridges, cross-frames are provided to integrate the structure, transforming the individual girders into a structural system that can support larger loads than when the girders work separately. For this purpose, cross-frames must have enough strength and stiffness so they can properly brace the I-girders when the structure is subjected to the noncomposite loads (Ziemian, 2010).

In skewed bridges, the bearing line cross-frames are commonly oriented parallel to the skew. When the cross-frames are skewed at angles less than or equal to 20^{o}, the connection plates are welded to the girder web, as shown in Figure 9.4(a). At larger angles it is difficult to perform the weld between the connection plate and the web. When the skew is larger than 20^{o}, a bent-plate detail is used commonly to connect the cross-frames to the girders, as depicted in Figure 9.4(b). The bent-plate detail facilitates the fabrication and erection of skewed cross-frames; however, it also can introduce excessive flexibility in the cross-frames and affect its stability bracing capacity.

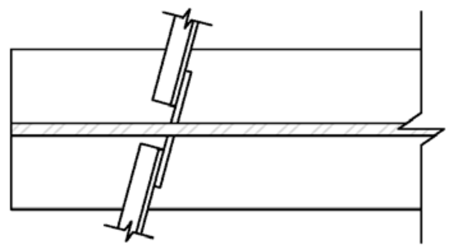

(a) Connection at skew angles equal to or less than 20^{o}

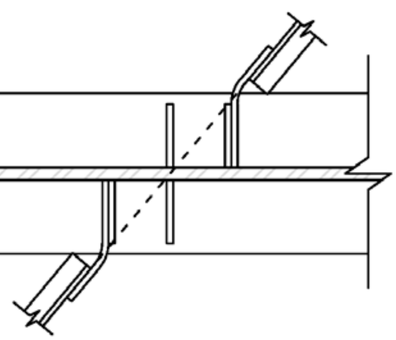

(b) Bent-plate connection detail for skew angles larger than 20^{o}

Figure 9.4. Typical connection details used for skewed cross-frames.

To overcome this limitation, Quadrato et al. (2010) propose the use of a half-pipe stiffener (see Figure 9.5(a)). This detail substantially improves the I-girder bridge structural performance. The advantage of this detail is that due to its circular contour, it is possible to connect the cross-frames at angles larger than 20^{o}, without affecting their bracing capacity. In addition to the half-pipe stiffener, Sanchez (2011) proposes a detail that can be implemented to stiffen the bent-plates. As shown in Figure 9.5(b), the bent-plate can be reinforced to reduce its flexibility by providing stiffeners near the top and bottom flange. Also, a stiffener at the web mid-depth could be provided to increase the rigidity of the bent plate.

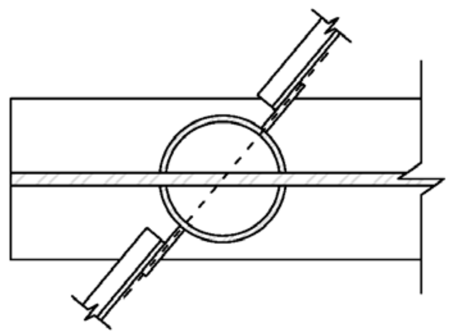

(a) Half-pipe stiffener (adapted from Quadrato et al. (2010))

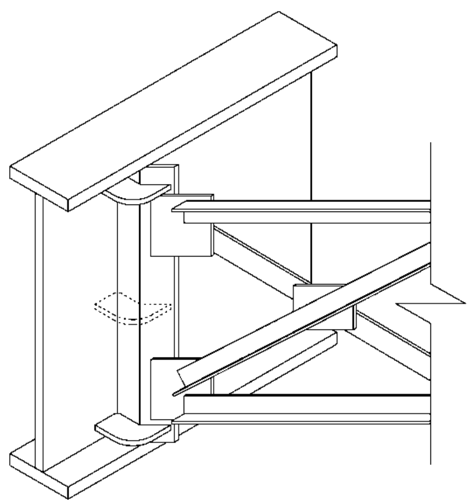

(b) Stiffened bent-plate

Figure 9.5. Improved connection details used for skewed cross-frames.

The improved details shown in Figure 9.5 may be used in combination with the recommendations provided in Section 8.2.2 to mitigate the undesired effects of skew. As discussed in that section, “fanned” configurations can be used in the design of straight I-girder bridges, to layout the intermediate cross-frames and reduce the cross-frame forces and the flange lateral bending stresses.

9.5 Long-Span I-Girder Bridges without Top Flange Lateral Bracing Systems

In many bridges, the second-order effects are expected to be quite small. However, second-order amplification due to global flange lateral bending can be large for individual curved I-girders or for a small number of girders with close spacing relative to the span length. Additionally, second-order amplification and global flange lateral bending effects can be more critical for longer spans without flange level lateral bracing since the stresses are more dominated by dead loads in longer spans. For long-span I-girder bridges without flange level lateral bracing, the overall bridge system can exhibit second-order global lateral deflections without significant twisting of the girders.

Figure 9.6 shows the undeflected and deflected geometry (magnified by 20x) of the bridge NISCR11 under total dead load from the NCHRP project studies. The bridge is 80ft wide and has a 300 ft.span length. However, it does not have a flange-level lateral bracing system. Figure 9.7 shows the magnitudes of the total dead load deflections of girder G1 from first- and second-order analyses. Also, Figure 9.8 shows the girder layovers under total dead load. Although the bridge NISCR11 has nine girders, overall flange lateral bending of the flanges is observed due to lack of flange-level lateral bracing system (see Figures 9.9 and 9.10). Figure 9.11 demonstrates the top flange stresses for the outside girder under total dead load. It should be noted from Figure 9.11 that the girder flange lateral bending stresses are amplified due to the global flange lateral bending effects. This example illustrates that as the span length become relatively large, I-girder bridges without a flange-level lateral bracing system can exhibit significant overall (global) second-order effects during the deck placement, even when the bridge cross-section has a relatively large number of girders.

It is suggested from the NCHRP 12-79 studies that I-girder bridges with spans longer than 200 ft.should be checked for global stability under potential critical stages of construction unless a flange level lateral bracing system is employed. Flange level lateral bracing systems are useful to control the geometry since they cause portions of the structure to act as pseudo-box girders such that large response amplifications due to global second-order effects can be eliminated.

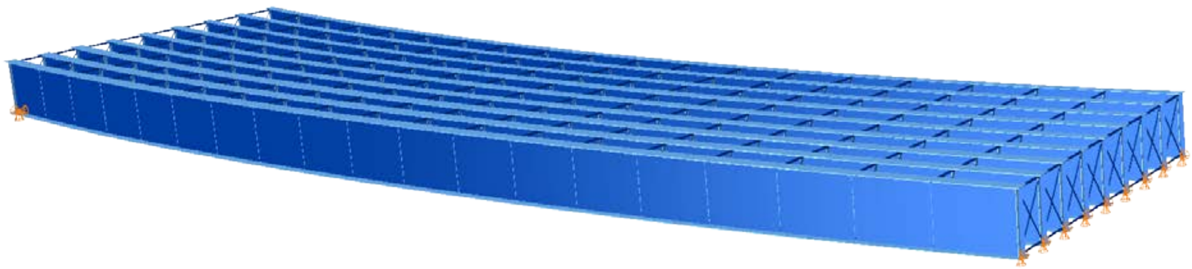

(a) Undeflected Geometry

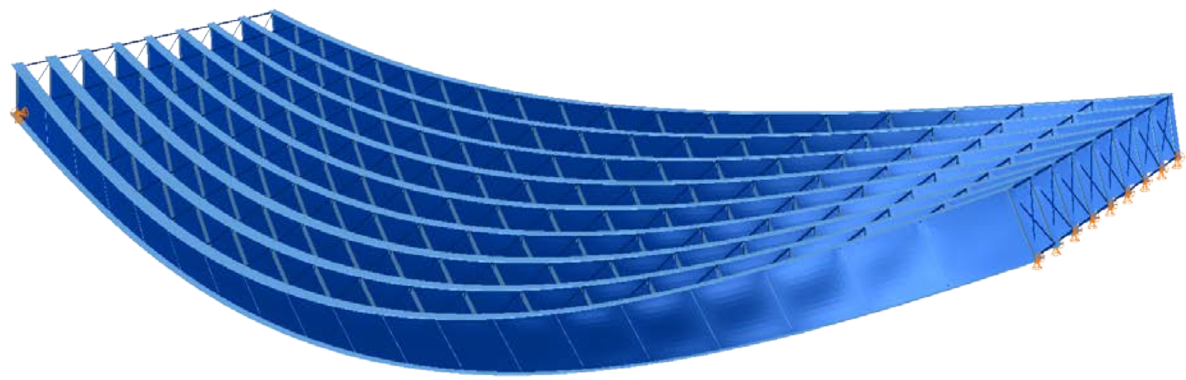

(b) Deflected Geometry

Figure 9.6. NISCR11, undeflected and deflected geometry under total dead load (Magnified by 20x).

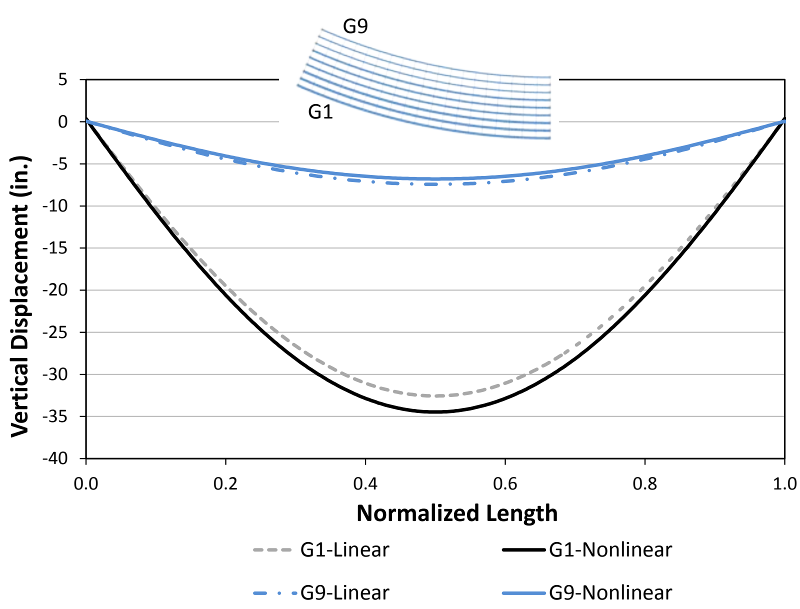

Figure 9.7. NISCR11, total dead load vertical displacements from first- and second-order analyses.

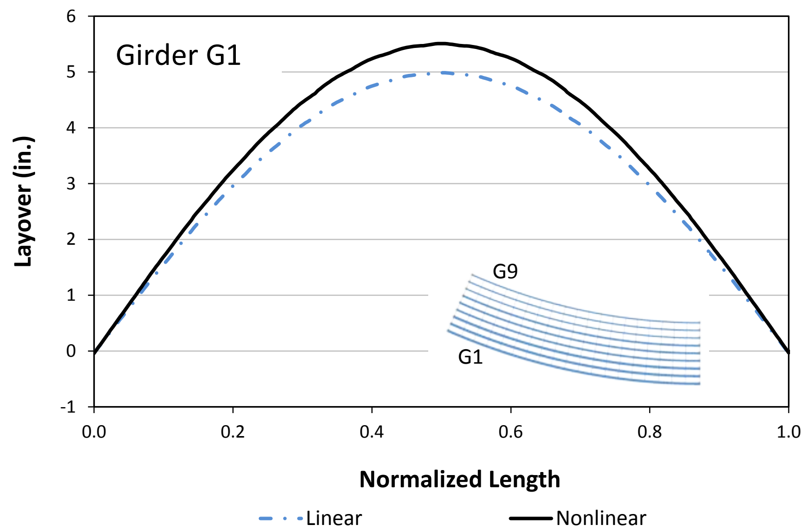

Figure 9.8. NISCR11, Total dead load layovers in Girder G1 from first- and second-order analyses.

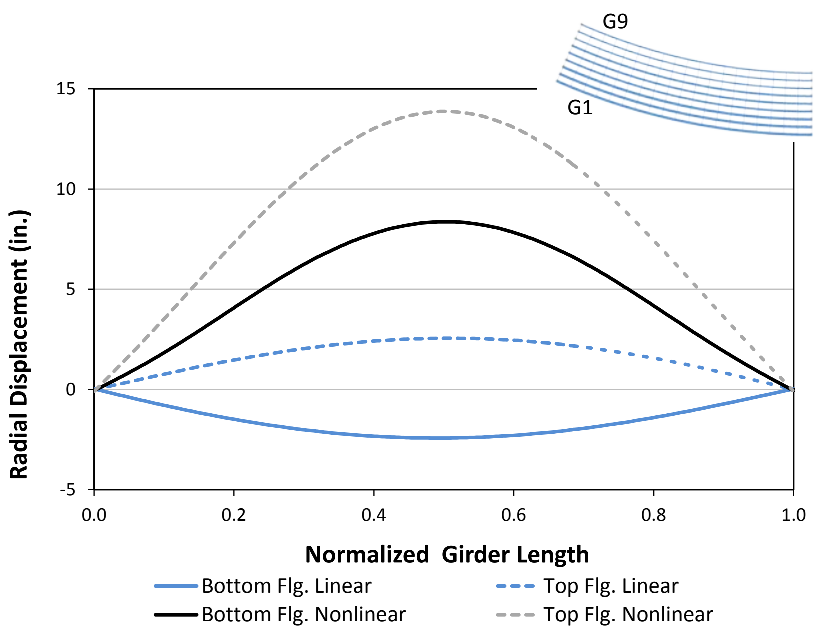

Figure 9.9. NISCR11, Girder G1 total dead load radial displacements from first- and second-order analyses.

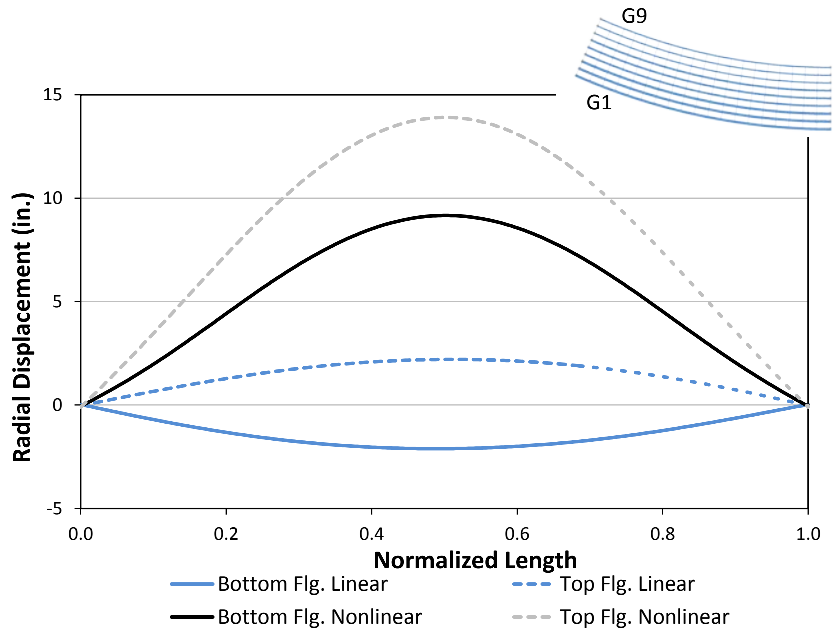

Figure 9.10. NISCR11, Girder G9 total dead load radial displacements from first- and second-order analyses.

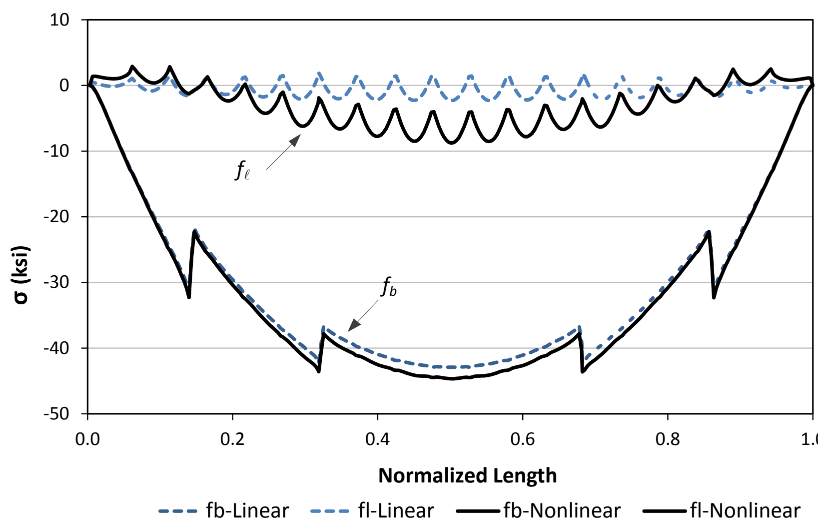

Figure 9.11. NISCR11, Girder G1 top flange stresses under total dead load.

9.6 Partial Depth End Diaphragms (Tub-Girder Bridges)

Partial depth end diaphragms have been used in some of the existing bridges collected but not selected for the analytical studies in NCHRP 12-79. This type of detail should be avoided because it changes the local and global behavior (Helwig et al., 2007). At the local level, the top flange lateral bracing system will lose continuity close to the end diaphragm meaning that the force is redistributed through a different load path to reach the end of the girder. Also, the end panel will experience more deformation with respect to the adjacent panels, having a direct impact in the adjacent elements that control the cross section distortion, such as the internal cross-frames.

The global consequences include a significant increase of the girder deflections and rotations. If both ends of a span experience twist rotations due to diaphragm deformations, the entire span experiences these rotations (essentially as an overall rigid-body rotation of the entire span). Furthermore, significant diaphragm flexibility conflicts with the rigid diaphragm simplification discussed in Section 2.1.5.

9.7 Non-Collinear External Intermediate Cross-frames or Diaphragms in Tub-Girder Bridges

When tub-girder bridges require external intermediate cross-frames or support diaphragms for relative displacement control between the girders or the distribution of reactions to the supports, the internal and external components should be collinear to avoid undesired behavior at the connection locations. Figure 9.12a shows a sketch where the external cross-frame is skewed but the corresponding internal cross-frames are not collinear. In this case, the upper corners of the external cross-frame are aligned with the corresponding elements of the internal components at the connecting points *A* and *B* in the figure. However, the bottom corner of the cross-frame at *C* has an offset along the girder axis. The sloped webs cause the points *C* and *D* to be offset from the bottom corners of the internal cross-frames. This detail could lead to undesired local stresses as the load path between the cross-frames at the lower part of the girder would be interrupted.

One way to avoid this detail is to make the internal and external cross-frames or diaphragms collinear as shown in Figure 9.12b. This detail keeps the main cross-frame forces all in one plane.

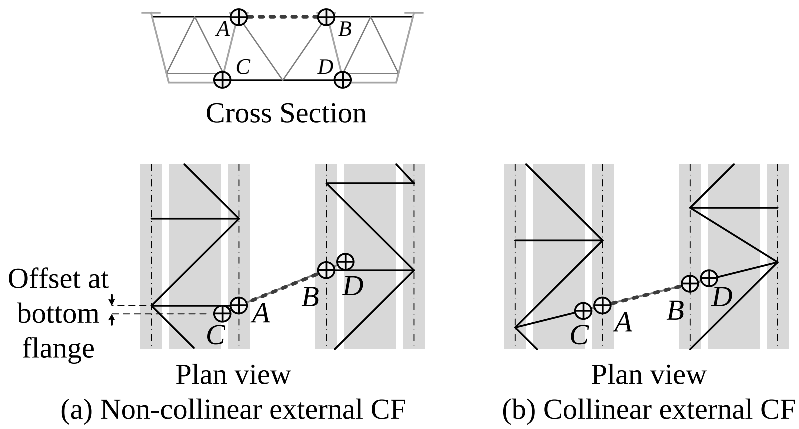

Figure 9.12. Detail of non-collinear and collinear external diaphragms in tub-girder bridges.

9.8 Use of Twin Bearings on Tub-Girders

One possible solution for the tub-girder bearing design is to provide more contact points so that the load taken by each bearing is reduced, thus potentially reducing the associated costs of the bearings. In the case of tub-girder bridges, it is possible to use more than one support bearing at each girder due to the width available at the bottom flange. In straight non-skewed bridges twin bearings are able to share the load equally. However, the reactions on these types of bearings can be very different from one another in curved and/or skewed configurations.

In curved and/or skewed cases, an ideal twin bearing system would transfer a major portion of the girder end torque to the support directly rather than through shear force transfer in the external diaphragms. However, it is common to see uplift at one of the twin supports while the other takes the entire vertical load, potentially exceeding the bearing design force.

In summary, the use of twin bearing on tub-girders creates a situation where the bearing reactions can be sensitive to minor effects potentially causing uplift, and in general, should be avoided for other than straight bridges.

10. Analysis Pitfalls

Chapter 2 provides a detailed description of the analysis methods used in the design of steel girder bridges. Sections 2.1 to 2.8 discuss the characteristics of the 1D, 2D, and 3D models, highlighting their virtues and limitations. In addition, the discussions in Sections 2.12 and 2.13 focus on the structural responses that 1D and 2D models are not able to capture due to the assumptions and simplifications used in the analyses. In this chapter, the analysis methods are revisited to discuss additional aspects that need to be considered when predicting the behavior of steel girder bridges during construction. The following sections discuss practices to avoid when modeling a bridge structure with a given analysis method. In particular, the pitfalls associated with the different analysis methods, which can result in misleading predictions of the structural responses, are presented.

10.1 Line Girder Analysis

- Global second-order amplifications cannot be captured. In general, this analysis method should not be used in cases where the global amplification factor, AF_G, is greater than 1.25 (see Sections 2.9 and 3.1.1).
- With this analysis method, accurate dead load stresses and vertical deflections are obtained in straight-skewed I-girder bridges only when analyzing the dead load condition corresponding to the type of cross-frame detailing. The dead load cross-frame forces and girder flange lateral bending stresses tend to be small in these conditions. However, significantly larger cross-frame forces and flange lateral bending stresses can be encountered at other erection stages.
- Girder cambers predicted by line-girder models may be inaccurate in straight and skewed bridges with large cross-frame forces. Specifically, if the skew index, I_S, is greater than 0.65 (see Sections 3.1.2 and 5.1), the displacements predicted by a line-girder analysis may not be reliable since they do not capture the significant transverse load paths and the correspondingly large forces transferred through the cross-frames.

- In straight and skewed bridges, interactions between the girders via cross-frames and/or diaphragms and/or via the slab generally cannot be captured. If the skew index, I_S, is greater than 0.30, the cross-frame forces and the flange lateral bending stress levels may be significant. In these cases, the results obtained from a line-girder model may be insufficient to predict all the structural responses required to make a complete assessment of the structural behavior.
- Line girder analysis cannot generally account for the influence of a flange level bracing system, and the interaction of the I-girders with this system.
- With this analysis method, the additional vertical deflections in curved I-girders due to substantial coupling between bending and torsion cannot be captured.
- In line-girder analysis, the effects of two bearings under a single tub-girder cannot be directly analyzed. There are cases where the rotations in a tub-girder are sufficiently large to cause uplift at one of the bearings.
- Line-girder analysis is unable to capture the continuity effects associated to the torsional response in continuous-span I-girder bridges.
- Line-girder analysis cannot capture any lateral or radial movement of the structure.
- A 1D analysis is unable to capture dead-load-fit detailing effects since this analysis type does not consider the contributions of cross-frames.

10.2 2D-Grid Analysis

- Global second-order amplifications cannot be captured. In general, it is suggested that this analysis method should not be used in cases where the global amplification factor, AF_G, is greater than 1.25 (see Sections 2.9 and 3.1.1).
- 2D-grid models do not include any depth information in the analysis. Hence, structural responses where the depth information is necessary to obtain accurate predictions cannot be properly captured by this analysis method. Some of the bridge depth attributes generally include:
    - Cross-frame chord depths and positions with respect to the centroid of the girders,
    - Differences between centroidal and shear center axes,

    - Eccentricity between the location of bearings and the girder centroids, and
    - Coupling between axial and bending deformations in cross-frames.
    - Flange-level lateral bracing systems in I-girder bridges and the interaction of these systems with the girders.
- Conventional 2D-grid girder torsion models significantly underestimate the girder torsional stiffnesses, often resulting in an underestimation of cross-frame forces in I-girder bridges. This limitation also can result in a significant over-prediction of the vertical displacements and girder layovers in curved I-girder bridges.
- Conventional 2D-grid cross-frame models cannot represent the physical responses of the cross-frames. This effect can be important in situations such as wide bridges, or bridges containing substantial nuisance stiffness effects causing large cross-frame forces. In straight and skewed I-girder bridges where the skew index, I_S, is greater than 0.30, the cross-frames should be modeled following the recommendations of Chapter 6 to obtain an accurate prediction of the cross-frame forces and of the overall system behavior.
- The response predictions in curved I-girder bridges are sensitive to the level of discretization used in the model. In general, the solutions obtained from a conventional 2D-grid analysis conducted with a refined mesh are less accurate than those obtained from a model with a relatively coarse mesh. This, however, does not necessarily mean that a model with a coarse mesh is the best option to analyze a curved I-girder bridge. The recommendations provided in Chapter 6, which are based on principles of structural mechanics, can be implemented in a 2D-grid analysis to obtain accurate responses, and do not depend on secondary factors such as the level of mesh refinement.
- Conventional 2D-grid models cannot represent the torsional response of I-girders; therefore, they cannot properly predict the responses when the structure has a minimum number of restraints, for example, during lifting.
- Conventional 2D-grid models are not able to capture dead-load-fit cross-frame forces. A more accurate representation of the torsional stiffness and the cross-frame model,

as the discussed in Chapter 6, is required to properly capture the effects of DLF detailing.

10.3 3D-Frame Analysis

- For I-girder bridges, any 3D-frame models that are not a Thin-Walled Open-Section (TWOS) model tend to significantly underpredict the actual girder torsional stiffnesses. Hence, the 3D-Frame models conducted with a poor representation of girder torsional stiffness have essentially the same limitations as the 2D-grid models discussed in the previous section.
- If TWOS 3D-frame elements are tied to a deck model via rigid links, the bottom flange lateral bending displacements can be substantially over-constrained and under-estimated.

10.4 3D Finite Element Analysis

- 3D FEA solutions are generally more sensitive to specific physical details of the structure and to assumptions about the detailed responses. The modeling techniques and methods used to represent the physical characteristics of the structure should be carefully studied before applying them for design purposes. For example, there are several options to model the offset existing between the top flange of the steel girders and the concrete deck centroids. One option is to provide rigid beam elements to simulate this offset. Another option is to include multi-point constraints. The second is not only the most efficient technique in terms of computational resources, but also eliminates any numerical problems that may result from including overly stiff elements in the model.
- Various contributions to flexibility, which may be included implicitly in simpler models, have to be modeled explicitly, with sufficient mesh refinement, to properly capture the effects.
- Large horizontal reactions due to the transverse restraint from guided or fixed bearings may not be present in the physical structure, due to local damage.

- Eigenvalue buckling analysis using 3D FEA generally produces a large number of web buckling modes. Therefore, other types of models are necessary to assess the girder or system overall stability.
- Various contributions to stiffness must be modeled in greater detail in 3D FEA models. For example, connection plates must be modeled properly to avoid false web distortional bending at the cross-frame connections.
- Insufficient refinement of the FEA mesh or discretization of the FEA. For instance, if solid elements are used to model plates, typically more than one element is needed through the thickness. In general the engineer should check convergence of the FEA solution for the key structural responses
- Detailed "incidental" contributions to stiffness, such as the contributions of stay-in-place metal deck forms (which are sensitive to construction practices), are difficult to include in the analysis.
- The orientation of guided or fixed bearings must represent the physical restraints given by the bearings. However, this is a consideration only after the connections to the bearings have been completed and the bearings have been unblocked, etc. In many situations, this is at the end of the steel erection but prior to the placement of the deck concrete.
- Efficient or time productive 3D FEA depends critically on the availability of sophisticated analysis processing capabilities for creation of the models and for synthesis of results; commercial capabilities provided by professional software are becoming increasingly more powerful.
- Locked-in-forces generally need to be included in the 3D FEA of curved I-girder bridges constructed with SDLF or TLDF detailing. They also need to be included in straight-skewed I-girder bridges with large skew indices, to obtain an accurate calculation distribution and magnitude of the cross-frame forces that is not overly conservative.

10.5 All Analysis Methods

- Sources of potential flexibility must be recognized, for example:
    - Flexibility of bent-plates at the connections of skewed cross-frames,
    - Bending of webs due to partial height overhang brackets, and
    - Flexibility of straddle bents, and
    - Sources of flexibility associated within the substructure.

  If it is deemed that these flexibility contributions may have a significant influence on the structural performance, one can generally obtain the best resolution in accounting for their effects by conducting a 3D FEA.
- The engineer must be wary of significant second-order effects in cases such as narrow bridge units, long-span bridges without top-flange lateral bracing systems, and bridges with V-type cross-frames without top chords. Only a nonlinear 3D FEA can capture properly the behavior of structures with these characteristics.
- A good practice always is to check that the sum of reactions is equal to the total applied loads. This includes checking of negative vertical reactions in 2D and 3D models since they are an indication of girder uplift. In 1D analyses, the torsion index, I_T, discussed in Chapter 3 can be used as an indicator of potential girder uplift that may occur due to curvature and/or skew effects.
- Another possible pitfall that is not completely related to the analysis methods, but must be considered when assessing the constructability of a steel girder bridge is the consideration of all critical stages in the partially erected structure. The engineer generally must recognize and analyze specific stages where the structural stability or the control of the deformations in the structure is a concern. The global stability amplifier AF_G discussed in Sections 2.9 and 3.1.1 provides some insight with respect to these considerations.

11. Summary

This chapter provides a summary of the salient guidelines for analysis of curved and/or skewed steel I- and tub-girder bridges, and factors that influence the analysis needs. The chapter is organized into several sections addressing common questions often faced by steel bridge designers and construction engineers.

11.1 When is a Line-Girder Analysis Not Sufficient?

The following are a synthesis of cases when a line-girder analysis is not sufficient:

- Bridges or bridge units where the global amplification of the responses, AF_G, is larger than 1.25 under the nominal (unfactored) total dead load. The global amplification factor AF_G may be estimated as

  $$AF_G = \frac{1}{1 - \frac{M_{\max G}}{M_{crG}}} \tag{2.101}$$

  where M_{maxG} is the maximum total moment supported by the bridge unit for the loading under consideration, equal to the sum of all the girder moments, and

  $$M_{crG} = C_b \frac{\pi^2 sE}{L_s^2} \sqrt{I_{ye} I_x} \tag{2.102}$$

  is the elastic global buckling moment of the bridge unit (Yura et al., 2008). In Eq. (2.102), C_b is the moment gradient modification factor applied to the full bridge cross-section moment diagram, s is the spacing between the two outside girders of the unit, E is the modulus of elasticity of steel,

  $$I_{ye} = I_{yc} + (b/c)I_{yt} \tag{2.103}$$

  is the effective moment of inertia of the individual I-girders about their weak axis, where I_{yc} and I_{yt} are the moments of inertia of the compression and tension flanges about the weak-axis of the girder cross-section respectively, b and c are the distances from the mid-thickness of the tension and compression flanges to the centroidal axis of the cross-section, and I_x is the moment of inertia of the individual girders about their major-axis of bending.

Long and/or narrow I-girder bridge units with two or three I-girders can easily violate this limit. Tub-girder bridge units fabricated with proper internal cross-frames to restrain their cross-section distortions as well as a proper top flange lateral bracing (TFLB) system, which acts as an effective top flange plate creating a pseudo-closed cross-section with the commensurate large torsional stiffness, would rarely violate this limit.

- I-girder bridges or bridge units employing a flange level lateral bracing system. Line-girder analysis generally is not capable of accurately modeling the overall interaction of the girders as a pseudo-box structural system.
- Curved and/or skewed I-girder bridges detailed for NLF, where the tolerable error in any of the response quantities is smaller than that associated with the applicable score provided in Table 5.5. The tolerable error is largely a matter of the engineer's judgment and is generally a function of the magnitude of the construction stresses and displacements as well as various job conditions. The construction stresses and displacements are in turn largely influenced by the bridge span lengths.
- Curved and/or skewed tub-girder bridges, where the tolerable conservative or unconservative error in any of the response quantities is smaller than that associated with the scores provided in Tables 5.13 an 5.14. The tolerable error is largely a matter of the engineer's judgment and is generally a function of the magnitude of the construction stresses and displacements as well as various job conditions. The construction stresses and displacements are in turn largely influenced by the bridge span lengths.
- Straight I-girder bridges with a skew index I_S > 0.30, detailed for SDLF or TDLF. The skew index is defined as

$$I_S = \frac{w_g \tan\theta}{L_s} \tag{3.1}$$

where w_g is the width of the bridge measured between the centerline of the fascia girders, θ is the skew angle (equal to zero for zero skew), and L_s is the span length.

The I-girder major-axis bending stresses and vertical deflections can be estimated with good accuracy for the total dead load condition if TDLF detailing is used, or for the steel dead load condition, if SDLF detailing is used. However, the cross-frame forces and the girder flange lateral bending stresses may be relatively large in the targeted DLF condition, and generally may not be neglected.

- Curved radially-supported I-girder bridges constructed with SDLF or TDLF detailing. For these types of I-girder bridges, the I-girder major-axis bending, flange lateral bending stresses and vertical deflections can be estimated with good accuracy for the total dead load condition if TDLF detailing is used, or for the steel dead load condition, if SDLF detailing is used (assuming adjustment based on the V-Load method). However, a line-girder analysis conducted with the V-load method does not address the locked-in forces generated in the cross-frames under the targeted dead load condition. Therefore, a line-girder (V-Load) analysis is not sufficient to estimate the cross-frame forces in this case. Note that NLF detailing is often a good choice for curved radially-supported bridges.
- Curved and skewed I-girder bridges, detailed for SDLF or TDLF. For these types of bridges, the applicability of the V-Load method tends to break down.

11.2 When is a Traditional 2D-Grid Analysis Not Sufficient?

- Bridges or bridge units where the global amplification of the responses, AF_G, is larger than 1.25 under the nominal (unfactored) total dead load. Long and/or narrow I-girder bridge units with two or three I-girders can easily violate this limit. Practical tub-girder bridge units would rarely violate this limit.
- I-girder bridges or bridge units employing a flange level lateral bracing system. 2D-grid analysis generally is not capable of accurately modeling the overall interaction of the girders as a pseudo-box structural system.

- Curved and/or skewed I-girder and tub-girder bridges, where the tolerable error in any of the response quantities is smaller than that associated with the score provided in Tables 5.5 or Tables 5.13 and 5.14 respectively. The tolerable error is largely a matter of the engineer's judgment and is generally a function of the magnitude of the construction stresses and displacements as well as various job conditions. The construction stresses and displacements are in turn largely influenced by the bridge span lengths.

11.3 When is the Improved 2D-Grid Analysis Method Not Sufficient?

- Bridges or bridge units where the global amplification of the responses, AF_G, is larger than 1.25 under the nominal (unfactored) total dead load. Long and/or narrow I-girder bridge units with two or three I-girders can easily violate this limit. Practical tub-girder bridge units would rarely violate this limit.
- I-girder bridges or bridge units employing a flange level lateral bracing system. Line-girder analysis generally is not capable of accurately modeling the overall interaction of the girders as a pseudo-box structural system.
- Situations where a single I-girder is being analyzed.
- Cases with two or more I-girders connected together but where the connectivity index I_C is greater than or equal to 20. The connectivity index is defined as

$$I_C = \frac{15{,}000}{R(n_{cf}+1)m} \tag{3.2}$$

  where R is the radius of curvature of the bridge centerline in units of ft., n_{cf} is the number of intermediate cross-frames within the span, and m is a constant equal to 1 for simple-span bridges and 2 for continuous-span bridges.

11.4 When does 3D FEA provide the most benefits?

- If the estimated global second-order (stability) effects are significant under any construction configuration, based on AF_G, it is advisable to revise the configuration, or if that is not feasible, perform a second-order 3D FEA of the configuration to better ascertain the physical response. The existence of significant second-order effects indicates that the structure is sensitive to minor variations in its stiffness as well as its loadings. In these circumstances, the higher resolution possible with a well-conceived 3D FEA model can be beneficial and the construction operations should be monitored closely to ensure that the assumed conditions are in place. Although a quality second-order Thin-Walled Open Section (TWOS) 3D Frame model can provide comparable solutions, the 3D FEA modeling approaches discussed in this report are more general and more commonly available. Either of these approaches can be useful for analysis of I-girder stability and second-order deflections and stresses under lifting and early stages of erection.

- In cases where the effects of holding cranes, tie-downs and other rigging need to be assessed, 3D FEA provides the most direct ability to explicitly model the specific boundary conditions. This type of solution may be important in some situations for estimating stresses and deflections regardless of whether second-order effects are significant or not.
- 3D FEA provides the highest resolution for modeling of interactions between a composite slab and the steel I- or tub-girders, including the ability to account for web distortional flexibility, which is an important attribute of the torsional response of composite I-girders. 3D FEA also provides the highest resolution for representation of staged concrete deck placement effects.
- 3D FEA provides the most reliable characterization of the complex interactions between bridge tub-girders and their bracing systems. The various interactions of the diaphragms, cross-frames, and top-flange lateral bracing with the separate tub-girder flanges and webs are difficult to capture using line element (3D frame or 2D grid) models.
- Similarly, I-girder bridge systems with flange-level lateral bracing systems tend to act as pseudo-box structures. In situations where the participation of flange-level lateral bracing is expected to be an important part of the dead load response, direct modeling of the structure by 3D FEA is essential.

- In cases of larger horizontal curvatures and/or skews, where the tolerable error in any of the response quantities is smaller than that associated with the score provided for the simpler methods in Tables 5.5, 5.13 and 5.14 as applicable, 3D FEA provides the best accuracy for a given set of anticipated or idealized construction conditions.
- 3D FEA provides the highest resolution for analysis of SDLF and TDLF detailing effects.

11.5 When Should the Engineer Analyze for Lack-of-Fit Effects due to SLDF or TDLF Detailing?

Curved I-girder bridges constructed using SDLF or TDLF detailing (referred to generally as DLF detailing) always should be analyzed for locked-in force effects. This is because:

- DLF detailing can have a significant impact on the vertical displacements in curved I-girder bridges.
- DLF detailing tends to increase the cross-frame forces in curved I-girder bridges.
- DLF detailing tends to increase the "negative" lateral bending stresses in curved I-girder flanges, i.e., the stresses at the cross-frames, which act like continuous-span beam supports resisting the flange lateral bending.

However, it should be noted that the results of the NCHRP 12-79 studies indicate that NLF detailing is often a good choice for curved radially-supported I-girder bridges.

In addition, in general, lack-of-fit effects need to be included in an accurate 2D-grid or 3D FE analysis to obtain an accurate representation of the physical distribution and magnitude of the cross-frame forces within a straight-skewed I-girder bridge constructed with SDLF or TDLF detailing. As discussed in Section 7.5.3, the cross-frame forces and girder flange lateral bending stresses can be estimated accurately to conservatively, to design a single-size intermediate cross-frame and a separate single size bearing line cross-frame for use throughout a bridge, using an analysis that neglects the lack-of-fit effects. However, for bridges with larger skew indices, the conservatism may be prohibitive. If the single-size cross-frames are judged to be excessively large, an analysis that includes the influence of the lack-of-fit effects generally will produce much more economical results.

11.6 When Should Global Stability Effects Be Considered?

Global stability effects should be considered via a 3D FEA for any construction configuration involving concrete deck placement where AF_G from Eq. (2.101) is greater than 1.25. In addition, I-girder bridges with spans longer than 200 ft.should be checked for global stability under potential critical stages of construction unless a flange level lateral bracing system is employed. In some longer span I-girder bridges without flange level lateral bracing, the overall bridge system can exhibit overall second-order global lateral deflections even with a large number of girders in the bridge cross-section (see the discussion of bridge NISCR11 in Section 9.5). If AF_G from Eq. (2.101) is less than 1.10, it is recommended that the influence of global second-order effects may be neglected.

For intermediate steel erection stages, larger values of AF_G should be acceptable as long as the amplified stresses are sufficiently low. The AASHTO Article 6.10.3 yielding and one-third rule strength checks are expected to provide sufficient constructability limits in these cases, without the need to directly assess the structure's amplified deflections. It is important to note that in typical intermediate erection stages, the girder stresses are well below the AASHTO constructability limits.

11.7 When Should No-Load Fit Cross-Frame Detailing Be Avoided?

- No-Load Fit (NLF) cross-frame detailing should generally be avoided when the bridge experiences layovers at skewed bearings that are larger than the remaining tolerance once the live load rotations are deducted from the bearing torsional rotation capacity.
- At highly-skewed bearing lines in straight or horizontally-curved bridges, NLF detailing can lead to increased fit-up difficulty in the vicinity of the supports. Therefore, for longer-span bridges with highly-skewed bearing lines, NLF should generally be avoided.

11.8 When Should SDLF or TDLF Cross-Frame Detailing Be Avoided?

- The results of the NCHRP 12-79 research suggest that SDLF and TDLF detailing should be avoided in sharply-curved radially-supported bridges unless the girder layovers within the spans are larger than a tolerable value based on the visual appearance of the deflected structure. (Even in this case, the addition of a flange-level lateral bracing system should be considered to stiffen the structure rather than using SDLF or TDLF detailing to control the layover within the spans.) This is because these methods of detailing increase the cross-frame forces and the “negative” flange lateral bending stresses as discussed in Section 11.5. In addition, due to the significant torsional-flexural coupling in horizontally-curved I-girders, and due to the fact that in many bridges, the concrete dead load is substantially larger than the steel dead load, Total Dead Load Fit (TDLF) detailing can potentially lead to large fit-up forces (since the girders may need to be displaced vertically as well as twisted to achieve fit-up). This problem tends to be exacerbated for longer span lengths.
- For curved and skewed bridges, the analytical results of the NCHRP 12-79 research suggest that SDLF and TDLF detailing should be avoided whenever they are not needed to satisfy bearing twist rotation tolerances, and as long as fit-up of the girders at highly skewed bearing lines. If DLF detailing is needed to control the girder layovers and/or reduce fit-up concerns at the bearing lines, SDLF detailing should be considered first. If this is not sufficient to satisfy the bearing twist rotation tolerances, the minimum level of DLF detailing between SDLF and TDLF should be used. This approach balances the use of DLF detailing to control the bearing rotations with the importance of limiting the fit-up forces in the structure. As with the above case, longer spans tend to exacerbate fit-up problems. One can observe from these considerations that SDLF detailing may often be a good “middle of the road” option on these types of bridges.

11.9 When Should No-Load Fit Cross-Frame Detailing be Used?

- The NCHRP 12-79 analytical results indicate the NLF detailing of the cross-frames is commonly a good option for horizontally-curved radially-supported bridges, since this type of detailing tends to minimize the cross-frame forces and corresponding maximum ("negative") girder flange lateral bending stresses due to horizontal curvature effects. However, the experience of some fabricators and erectors is that curved radially-supported bridges are easier to fit-up under unshored SDL erection conditions if SDLF detailing is used. The use of SDLF detailing on curved radially-supported I-girder bridges is a common practice in the industry, although bridges of this type have been detailed and constructed without difficulty using NLF detailing. It is recommended that the expanded use of NLF detailing should be explored and monitored on selected projects to further validate the NCHRP 12-79 findings.
- NLF detailing tends to minimize fit-up forces in the rare situation where the girders and cross-frames may need to be assembled in a shored configuration approximating the theoretical no-load condition. However, erection under other shored or unshored conditions is practically always achievable for straight-skewed bridges.

11.10 When Should Steel Dead Load Fit Cross-Frame Detailing be Used?

- The NCHRP 12-79 analytical results indicate that SDLF cross-frame detailing is a good option for minimizing fit-up forces in the vicinity of sharply-skewed bearing lines during steel erection under unshored or partially-shored conditions. Therefore, particularly for longer spans with a combination of sharp skew of the bearing lines along with horizontal curvature, SDLF detailing is typically a good choice.

11.11 When Should Total Dead Load Fit Cross-Frame Detailing be Used?

- For straight-skewed I-girder bridges, the coupling between the girder torsional response and the girder major-axis bending response is smaller than in curved I-girder bridges. In this case, the use of TDLF detailing gives a bridge in which the webs are approximately plumb under total dead load. Of course, since skewed bridges twist under the application of any vertical loads, the webs will not be plumb under any other loading condition (e.g., they will rotate out-of-plumb under any live load).
- For longer span bridges with large skew, one can have significant differential vertical cambers between adjacent girders. TDLF detailing may still be a viable option for many of these cases, but fit-up of the structural steel during the erection may need to be evaluated. In these situations, the girders may need to be displaced vertically as well as twisted to achieve fit-up. The fit-up can be facilitated by using the girder steel dead load deflections, i.e., allowing the girders to deflect under their self-weight, and detailing the cross-frames for SDLF.

12. References

AASHTO (2010). AASHTO LRFD *Bridge Design Specifications*, 5th Edition, American Association of State Highway and Transportation Officials, Washington, DC.

AASHTO – NSBA (2011). “G13.1-2010, Guidelines for the Analysis of Steel Girder Bridges,” AASHTO – NSBA Steel Bridge Collaboration.

Best Center (2011). “Descus I, Design and Analysis of Curved I-Girder Bridge System” http://best.umd.edu/software/descus-i/

Best Center (2011). “Descus II, Design and Analysis of Curved I-Girder Bridge System” http://best.umd.edu/software/descus-ii/

Bridgesoft, Inc. (2010). “STLBRIDGE, Continuous Steel Bridge Design” http://bridgesoftinc.com/

Chang C.-J. (2006). “Construction Simulation of Curved Steel I-Girder Bridges,” Doctoral Dissertation, School of Civil and Environmental Engineering, Georgia Institute of Technology, Atlanta, GA, 340 pp.

Chang, C.-J., and White, D.W. (2006). “Construction Simulation of Curved I-Girder Bridge Systems,” *Annual Proceedings*, Structural Stability Research Council, San Antonio, TX, 93-114.

Chen, B. (2005). “Top-Flange Lateral Bracing Systems for Trapezoidal Steel Box-Girder Bridges,” Doctoral Dissertation, Department of Civil, Architectural, and Environmental Engineering, University of Texas at Austin, Austin, TX, pp. 134.

Choo, T-W., Linzell, D.G., Lee J.I., Swanson, J.A. (2005). “Response of a Continuous, Skewed, Steel Bridge, during Deck Placement, *Journal of Constructional Steel Research*, Elsevier Ltd., pp. 567-586.

Coletti, D., and Yadlosky, J. (2007). “Analysis of Steel Girder Bridges – New Challenges,” *Proceedings*, World Steel Bridge Symposium, National Steel Bridge Alliance, New Orleans, LA, 21 pp.

Coletti, D.A., Chavel, B.W., and Gatti, W.J. (2009), “The Problems of Skew,” *Proceedings*, World Steel Bridge Symposium, National Steel Bridge Alliance, San Antonio, TX.

Essa, H.S. and Kennedy, D.J.L. (1993). “Distortional Buckling of Steel Beams,” Structural Engineering Report No. 185, Department of Civil Engineering, University of Alberta, Edmonton, Alberta, Canada, pp.356.

Fan, Z.F. and Helwig, T. (1999). “Behavior of Steel Box Girders with Top Flange Bracing”, *Journal of Structural Engineering*, August 1999, ASCE, pp. 829-837.

Fan, Z.F. and Helwig, T. () “Brace Forces Due to Box Girder Distortion,” *ASCE Journal of Structural Engineering*, V. 128, No. 6, June 2002, pp. 710-718.

Fan, Z.F. (1999). “Field and Computational Studies of Steel Trapezoidal Box Girder Bridges,” Doctoral dissertation, Civil and Environmental Engineering Department, University of Houston, 300 pp.

Farris, J.F. (2008). “Behavior of Horizontally Curved I-Girder Bridges during Construction,” M.S. Thesis, Department of Civil, Architectural, and Environmental Engineering, University of Texas at Austin, Austin, TX, pp. 152.

Fisher, S. (2006). “Development of a Simplified Procedure to Predict Dead Load Deflections of Skewed and Non-Skewed Steel Plate Girder Bridges,” M.S. Thesis, School of Civil Engineering, North Carolina State University, Raleigh, NC, 360 pp.

Grubb, M. (1984). “Horizontally Curved I-Girder Bridge Analysis: V-Load Method” Transportation Research Record, No. 289, 1984, pp. 26-36.

Helwig, T., Yura, J., Herman, R., Williamson, E. and Li, D. (2007). “Design Guidelines for Steel Trapezoidal Box Girder Systems,” Technical Report No.

FHWA/TX-07/0-4307-1. Center for Transportation Research, University of Texas at Austin, TX, 84 pp.

Helwig, T., Herman, R. and Zhou, C. (2005). “Lean-On Bracing for Steel Bridge Girders with Skewed Supports,” *Proceedings of the Annual Technical Session and Meeting*, Montreal, Quebec, Structural Stability Research Council, Univ. of Missouri - Rolla, Rolla, MO, 295-306.

Herman, R., Helwig, T., Holt, J., Medlock, R., Romage, M. and Zhou, C. (2005). “Lean-On Cross-Frame Bracing for Steel Girders with Skewed Supports,” *Time for Steel, Steel for Time*, Proceedings, 2005 World Steel Bridge Symposium, National Steel Bridge Alliance, 10 pp.

Huang, W.-H. (1996). “Curved I-Girder Systems,” Ph.D. dissertation, Department of Civil and Environmental Engineering, University of Minnesota, Minneapolis, MN.

Jimenez Chong, J.M. (2012). “Construction Engineering of Steel Tub-Girder Bridge Systems for Skew Effects,” Ph.D. Dissertation, School of Civil and Environmental Engineering, Georgia Institute of Technology, Atlanta, GA, 276 pp.

Kim Roddis, W.M., Kulseth, P., and Liu, Z. (2005). “TAEG 2.0: Torsional Analysis for Exterior Girders,” Kansas Department of Transportation, KS, 81 pp.

Kollbrunner, C. and Basler, K. (1966), “Torsion in Structures”, Springer-Verlag, New York.

Kulicki, J. M., Wassef, W. G., Smith, C., Johns, K. (2005) “AASHTO-LRFD Design Example Horizontally Curved Steel Box Girder Bridge,” NCHRP Project No. NCHRP 12-52, National Cooperative Highway Research Program, Transportation Research Board, National Research Council, 148 pp.

Leon, R., White, D., Dykas, J., Bhuiyan, M., Ozgur, C., Jimenez, J., Sanchez, A., (2011) “Field Monitoring and Computational Studies of a Horizontally Curved Steel Girder Bridge During Construction,” Report to Tennessee Department of

Transportation, School of Civil and Environmental Engineering, Georgia Institute of Technology, Atlanta, GA, September (to appear).

Norton, E.K., Linzell, D.G., Laman, J.A. (2003). "Examination of Response of a Skewed Steel Bridge Superstructure during Deck Placement," *Journal of the Transportation Research Board*, 1845, pp. 66-75.

LARSA (2010). "LARSA 4D, The Complete Software for Bridge Engineering," http://www.larsa4d.com/products/larsa4d.aspx

Li, D. (2004). "Behavior of Trapezoidal Box Girders with Skewed Supports", Doctoral dissertation, Department of Civil and Environmental Engineering, University of Houston, Houston, TX, 251 pp.

MDX (2011). "MDX Software, The Proven Steels Bridge Design Solution" http://www.mdxsoftware.com/

NHI (2007). "Load and Resistance Factor Design (LRFD) for Highway Bridge Superstructures," Design Manual, NHI Course No. 130081, 130081A-130081D, Publication No. FHWA-NHI-07-035, National Highway Institute, Federal Highway Administration, 1982 pp.

NHI (2011). "Analysis and Design of Skewed and Curved Steel Bridges with LRFD, Reference Manual", NHI Course No. 130095, Publication No. FHWA-NHI-10-087, National Highway Institute, Federal Highway Administration, 1476pp.

NSBA (1996). "V-Load Analysis and check (VANCK), User Manual, Version 1.0," National Steel Bridge Alliance and American Institute of Steel Construction.

Ohio DOT Seminar (2008). "Ohio DOT Seminar, Overview of New Practices and Policies," Ohio Department of Transportation, OH. http://www.dot.state.oh.us/

Ozgur, C. (2011), "Influence of Cross-Frame Detailing on Curved and/or Skewed Steel I-Girder Bridges," Ph.D. Dissertation, School of Civil and Environmental Engineering, Georgia Institute of Technology, Atlanta, GA

Ozgur, C. and White, D.W. (2007). “Behavior and Analysis of a Curved and Skewed I-Girder Bridge,” *Proceedings*, World Steel Bridge Symposium, National Steel Bridge Alliance, Chicago, IL, 18 pp

Poellot, W. (1987). “Computer-Aided Design of Horizontally Curved Girders by the V-Load Method.” *Engineering Journal*, AISC, Vol. 24, No. 1, First Quarter 1987, pp. 42-50.

Quadrato, C., Battistini, A., Frank, K, Helwig, T., and Engelhardt, M. (2010). “Improved Cross-Frame Connection Details for Steel Bridges with Skewed Supports,” Transportation Research Record, No. 2200, 2010, pp. 29-35.

Richardson, G. and Associates (1963). “Analysis and Design of Horizontally Curved Steel Bridge Girders,” United States Steel Structural Report, ADUSS 88-6003-01

Sanchez, T.A. (2011), “Influence of Bracing Systems on the Behavior of Steel Curved and/or Skewed I-Girder Bridges during Construction,” Ph.D. Dissertation, School of Civil and Environmental Engineering, Georgia Institute of Technology, Atlanta, GA

Shah, D.M. (2007), “Effective Flange Width Evaluation for Prestressed Concrete Bulb-Tee Girder Bridges,” M.S. Thesis, Department of Civil Engineering, The State University of Buffalo, NY, 131 pp.

Simulia (2010). “Abaqus, Realistic Simulations” http://www.simulia.com

Stith, J.C. (2010). “Predicting the Behavior of Horizontally Curved I-Girders during Construction.” Doctoral Dissertation, Department of Civil, Architectural, and Environmental Engineering, University of Texas at Austin, Austin, TX, pp. 330.

Topkaya, C., and Williamson, E. (2003). “Development of Computational Software for Analysis of Curved Girders under Construction Loads,” *Computers and Structures*, May 2003, Elsevier Ltd., pp. 2087-2098.

Topkaya, C., Williamson, E., and Frank, K. (2004a). “Behavior of Curved Steel Trapezoidal Box-Girders during Construction.” *Engineering Structures*, Elsevier, 26(6), 721-733.

Topkaya, C., Yura, J., and Williamson, E. (2004b). “Composite Shear Stud Strength at Early Concrete Ages,” *Journal of Structural Engineering*, ASCE, pp. 952-959.

Tung, D. and Fountain, R. (1970). “Approximate Torsional Analysis of Curved Box Girders by the M/R-Method,” *AISC Engineering Journal*, July 1970, AISC, pp. 65-74.

United States Steel Corporation (1965), “Highway Structures Design Book,” ADUSS 88-1895-01, Vol. 1.White, D.W., Zureick, A.H., Phoawanich, N.P. and Jung, S.K. (2001). “Development of Unified Equations for Design of Curved and Straight Steel Bridge I Girders,” Final Report to AISI, PSI Inc. and FHWA, October, 547 pp.

Yang, Y.B. and McGuire, W. (1984). “A procedure for analyzing space frames with partial warping restraint”, *International Journal for Numerical Methods in Engineering*. 20 (1984) 1377–1389.

Yura, J., Helwig, T., Herman, R. and Zhou, C. (2008). “Global Lateral Buckling of I-Shaped Girder Systems,” *Journal of Structural Engineering*, 134(9), 1487-1494.

Ziemian, R. (2010). Guide to Stability Design Criteria for Metal Structures, 6th Edition, Wiley, New Jersey.